

Analysis and Numerical Simulations of Epidemic Models on the Example of COVID–19 and Dengue

by

Peter Heidrich
from Idar–Oberstein

Accepted Dissertation thesis for the partial fulfilment of the requirements for a
Doctor of Natural Sciences
Fachbereich 3: Mathematik/Naturwissenschaften
Universität Koblenz–Landau

Reviewer:

Prof. Dr. Thomas Götz
Prof. Dr. Edy Soewono

Examiner:

Prof. Dr. Thomas Götz
Prof. Dr. Michael Hinze
Prof. Dr. Klaus Fischer

Date of the oral examination: March 29, 2021

Abstract

Scientific and public interest in epidemiology and mathematical modelling of disease spread has increased significantly due to the current COVID–19 pandemic. Political action is influenced by forecasts and evaluations of such models and the whole society is affected by the corresponding countermeasures for containment. But how are these models structured? Which methods can be used to apply them to the respective regions, based on real data sets? These questions are certainly not new. Mathematical modelling in epidemiology using differential equations has been researched for quite some time now and can be carried out mainly by means of numerical computer simulations. These models are constantly being refined and adapted to corresponding diseases. However, it should be noted that the more complex a model is, the more unknown parameters are included. A meaningful data adaptation thus becomes very difficult.

The goal of this thesis is to design applicable models using the examples of COVID–19 and dengue, to adapt them adequately to real data sets and thus to perform numerical simulations.

For this purpose, first the mathematical foundations are presented and a theoretical outline of ordinary differential equations and optimization is provided. The parameter estimations shall be performed by means of adjoint functions. This procedure represents a combination of static and dynamical optimization. The objective function corresponds to a least squares method with L^2 norm which depends on the searched parameters. This objective function is coupled to constraints in the form of ordinary differential equations and numerically minimized, using Pontryagin’s maximum (minimum) principle and optimal control theory.

In the case of dengue, due to the transmission path via mosquitoes, a model reduction of an *SIRUV* model to an *SIR* model with time–dependent transmission rate is performed by means of time–scale separation. The *SIRUV* model includes uninfected (*U*) and infected (*V*) mosquito compartments in addition to the susceptible (*S*), infected (*I*) and recovered (*R*) human compartments, known from the *SIR* model. The unknown parameters of the reduced *SIR* model are estimated using data sets from Colombo (Sri Lanka) and Jakarta (Indonesia). Based on this parameter estimation the predictive power of the model is checked and evaluated. In the case of Jakarta, the model is additionally provided with a mobility component between the individual city districts, based on commuter data. The transmission rates of the *SIR* models are also dependent on meteorological data as correlations between these and dengue outbreaks have been demonstrated in previous data analyses.

For the modelling of COVID–19 we use several *SEIRD* models which in comparison to the *SIR* model also take into account the latency period and the number of deaths via exposed (*E*) and deaths (*D*) compartments. Based on these models a parameter estimation with adjoint functions is performed for the location Germany. This is possible because since the beginning of the pandemic, the cumulative number of infected persons and deaths are published daily by Johns Hopkins University and the Robert–Koch–Institute. Here, a *SEIRD* model with a time delay regarding the deaths proves to be particularly suitable. In the next step, this model is used to compare the parameter estimation via adjoint functions with a Metropolis algorithm. Analytical effort, accuracy and calculation speed are taken into account.

In all data fittings, one parameter each is determined to assess the estimated number of unreported cases.

Zusammenfassung

Das wissenschaftliche und öffentliche Interesse an der Epidemiologie und der mathematischen Modellierung von Krankheitsausbreitungen hat aufgrund der aktuellen COVID-19 Pandemie erheblich zugenommen. Das politische Handeln wird von Prognosen und Bewertungen solcher Modelle beeinflusst, und die entsprechenden Gegenmaßnahmen zur Eindämmung sind für die gesamte Gesellschaft spürbar. Doch wie sind diese Modelle aufgebaut? Mittels welcher Methoden lassen sie sich, basierend auf realen Datensätzen, auf die jeweiligen Regionen anwenden? Diese Fragen sind sicher nicht neu, wird die mathematische Modellierung in der Epidemiologie mit Hilfe von Differentialgleichungen schon seit längerem erforscht und kann vor allem in Form von numerischen Computersimulationen durchgeführt werden. Diese Modelle werden ständig verfeinert und an entsprechende Krankheiten angepasst. Hier bleibt jedoch zu beachten, dass je aufwendiger ein Modell ist, umso mehr unbekannte Parameter sind enthalten. Eine sinnvolle Datenanpassung wird somit sehr schwierig.

Das Ziel der vorliegenden Arbeit ist am Beispiel von COVID-19 und Dengue anwendbare Modelle aufzustellen, diese adäquat an reale Datensätze anzupassen und damit numerische Simulationen durchzuführen.

Hierzu werden zunächst die mathematischen Grundlagen geschaffen und ein theoretischer Abriss zu gewöhnlichen Differentialgleichungen und zur Optimierung dargestellt. Die Parameterschätzung soll mittels adjungierter Funktionen durchgeführt werden. Dieses Verfahren stellt eine Kombination aus statischer und dynamischer Optimierung dar. Die Zielfunktion entspricht einer Kleinste-Quadrate-Methode mit L^2 -Norm, welche von den gesuchten Parametern abhängt. Diese Zielfunktion wird gekoppelt an Nebenbedingungen in Form von gewöhnlichen Differentialgleichungen und, unter Verwendung von Pontryagins Maximum- (Minimum-)Prinzip und optimaler Steuerung, numerisch minimiert.

Im Falle von Dengue wird, aufgrund des Übertragungsweges über Mosquitos, eine Modellreduktion eines *SIRUV*-Modells auf ein *SIR*-Modell mit zeitabhängiger Übertragungsrate mittels Zeitskalen-Separation durchgeführt. Das *SIRUV* Modell enthält uninfected (*U*) und infected (*V*) compartments der Mosquitos, zusätzlich zu den aus dem *SIR* Modell bekannten susceptible (*S*), infected (*I*) und recovered (*R*) compartments der Menschen. Die unbekannt Parameter des reduzierten *SIR*-Modells werden unter Verwendung von Datensätzen aus Colombo (Sri Lanka) und Jakarta (Indonesien) geschätzt. Auf Grundlage dieser Parameterschätzung wird dann die Vorhersagekraft des Modells überprüft und bewertet. Im Fall von Jakarta wird das Modell zusätzlich mit einer Mobilitätskomponente zwischen den einzelnen Stadtbezirken, auf der Basis von Pendlerdaten, versehen. Die Übertragungsraten der *SIR*-Modelle sind außerdem abhängig von meteorologischen Daten, da in den vorherigen Datenanalysen Korrelationen zwischen diesen und den Dengueausbrüchen nachgewiesen werden.

Zur Modellierung von COVID-19 verwenden wir mehrere *SEIRD*-Modelle, welche im Vergleich zum *SIR*-Modell auch die Latenzzeit und die Anzahl der Todesfälle mittels exposed (*E*) und deaths (*D*) compartments berücksichtigen. Basierend auf diesen Modellen wird für den Standort Deutschland eine Parameterschätzung mit adjungierten Funktionen durchgeführt. Dies ist möglich, da seit Pandemiebeginn täglich sowohl die kumulierte Anzahl der Infizierten als auch der Todesfälle von der Johns Hopkins Universität und dem Robert-Koch-Institut veröffentlicht werden. Hier erweist sich ein *SEIRD*-Modell mit Zeitverzögerung bezüglich der Todesfälle als besonders geeignet. Dieses wird im nächsten Schritt dazu verwendet die Parameterschätzung via adjungierter Funktionen mit einem Metropolis-Algorithmus zu vergleichen. Hierbei werden analytischer Aufwand, Genauig-

keit und Rechengeschwindigkeit berücksichtigt.

In sämtlichen Datenanpassungen wird jeweils ein Parameter zur Schätzung der Dunkelziffer ermittelt.

Acknowledgements

I would like to thank my doctoral advisor Prof. Dr. Thomas Götz for accepting me as a PhD student and for consulting me in numerous discussions, thus providing significant support for my research. Accepting an external doctoral student who is fully employed also involves risks at times and cannot be taken for granted. Likewise, I would also like to thank the entire research group and especially the coauthors of the individual research papers for productive work.

In particular, I thank my love Elke, who has supported me from the beginning in my project and encouraged. Not only did she help me with the linguistic proofreading of the thesis and had to listen to each of my lectures on a trial basis. She also had to accept a few times in everyday life when my mind wandered off into research and I was not always the most sociable of contemporaries. Her support has been instrumental in the successful completion of this work.

I would also like to thank my parents Heide and Werner, who supported me with all that was necessary throughout my entire education from the beginning and, of course, taught me the first steps. They never spared to show me that they are proud of me. I would also like to thank my sister Julia and her husband Stefan for encouraging me in my plans and always showing interest in my work.

Last but not least, I would like to thank all my friends and colleagues who have also always given me the feeling that I am doing something special and who have also always asked with interest how my research is going.

Contents

1	General Introduction	1
1.1	Epidemiology	1
1.2	Thesis Structure	3
I	Mathematical Foundations	5
2	Basic Definitions, Theorems and Examples	7
2.1	Ordinary differential equations	9
2.2	Solution methods	13
2.2.1	Elementary solution methods	14
2.2.2	Numerical solution methods	16
3	Epidemic Models	19
3.1	Basics in epidemiological modelling	19
3.2	The SIR model including demography	22
3.3	Modelling vector-borne diseases	26
4	Optimization	29
4.1	Static optimization	29
4.1.8	Numerical methods	32
4.2	Dynamical optimization: Optimal control theory	33
4.2.7	Optimal control including constant time delays	39
4.3	Parameter estimation via adjoint functions	43
II	Contributions	47
5	Research Paper I: Modelling Dengue with the SIR-Model	49
5.1	Abstract	49
5.2	Introduction	49
5.3	Data analysis	50
5.4	The SIR model	52
5.5	Results	54
5.6	Acknowledgement	54
	Bibliography	57
6	Research Paper II: Simulation and Prediction of Dengue Outbreaks Based on an SIR Model with Time-Dependent Transmission Rate Including Meteorological Data. An Example for Colombo and Jakarta	59
6.1	Abstract	59
6.2	Introduction	60

Contents

6.3	Data analysis	61
6.4	The SIR model	64
6.4.1	Time-scale separation	65
6.4.2	Alternative derivation of $\beta(t)$	69
6.5	Data fit analysis	69
6.6	Results	73
6.6.1	Numerical results of the parameter fit	73
6.6.2	Prediction quality of the model	77
6.7	Conclusions	78
6.A	Appendix A: Analytical derivation of the parameter fit	83
6.B	Appendix B: Algorithm pseudocode	88
Bibliography		89
7 Research Paper III: Prediction of Dengue Cases Based on Human Mobility and Seasonality. An Example for the City of Jakarta		
		93
7.1	Abstract	93
7.2	Introduction	93
7.3	Data analysis	94
7.4	Model analysis	96
7.4.2	SIR model with mobility	97
7.4.3	SIRUV with mobility	98
7.4.4	Reduction of the SIRUV to a SIR model	101
7.5	Data fit analysis	104
7.6	Results	106
7.6.1	Numerical simulations of the SIR model	106
7.6.2	Prediction quality of the SIR model	107
7.7	Conclusions	110
7.A	Appendix A: Reduction of the SIRUV to a SIR model	111
7.B	Appendix B: Detailed description of solving the optimal control problem in Section 7.5	114
7.C	Appendix C: Numerical findings and predictions with the two models	116
Bibliography		123
8 Research Paper IV: Early Stage COVID–19 Disease Dynamics in Germany: Models and Parameter Identification		
		127
8.1	Abstract	127
8.2	Introduction	127
8.3	Mathematical model	128
8.4	A few analytical considerations	133
8.5	Adjoint equations and optimization	134
8.6	Simulation results	136
8.7	Conclusions and outlook	139
Bibliography		141
9 Research Paper V: The COVID–19 Outbreak in Germany — Models and Parameter Estimation		
		143
9.1	Abstract	143

9.2	Introduction	143
9.3	Model	144
9.4	Parameter estimation	147
9.4.1	Adjoint based approach	148
9.4.2	Metropolis algorithm	152
9.5	Numerical results and comparison of the algorithms	153
9.5.1	Specific results for the adjoint approach	155
9.5.2	Specific results for the Metropolis algorithm approach	156
9.6	Conclusion	158
9.A	Appendix A: Plots for the adjoint approach	161
9.B	Appendix B: Results and plots for Metropolis algorithm	163
	Bibliography	171
	III Closing	173
	10 Conclusions and Outlook	175
10.1	Summary	175
10.2	Outlook	175
	Bibliography	177

1 General Introduction

Due to the outbreak of the COVID–19 pandemic starting at the end of the year 2019 the term (*infectious disease*) *epidemiology* is currently present in all media. The epidemiologists refer to mathematical models which are used to analyze current developments and future prognoses of disease spread and to simulate the effect of possible control measures. However, this presupposes that basic parameter values of these mathematical models can be derived from existing data. At this point we are thematically in the center of this thesis, in which, exemplarily for the diseases *COVID–19* and *dengue*, mathematical models are developed, adapted to real data sets and analyzed to perform several numerical simulations.

First, however, we dedicate ourselves to the concept of epidemiology and give a brief overview of the objects and technical terms behind this science based on the findings in [1, 19, 22, 28].

1.1 Epidemiology

The science of epidemiology is concerned with the causes and associated spread of diseases. At this point, a more differentiated distinction could be made between *infectious*, *communicable* and *transmittable diseases*, whereby we will use these categories synonymously in the following.

Basically, the spread of a disease is called *epidemic* as long as the number of new cases increases. As soon as this number is decreasing, a so-called *regression* is present. If a communicable disease is permanent, relatively constant and present only in a limited territory, it is called *endemic*. On the other hand, if an infectious disease is supra-regional, i.e. even crosses countries or continents, it is called a *pandemic*. For example, the *World Health Organization (WHO)* classifies dengue as endemic in certain subtropical and tropical areas, whereby the disease is subject to seasonal fluctuations. The currently circulating COVID–19 epidemic is classified as a pandemic as every inhabited continent is affected without exception [37].

Table 1.1: Exemplary assignment of different diseases to their pathogens.

Pathogen type	Caused diseases
Bacteria	Tuberculosis, Pneumonia
Viral	HIV, Influenza, Dengue, COVID–19
Fungal	Dermatomycoses
Parasitic	Protozoan infection, Helminthiasis
Prion	Creutzfeldt–Jakob

Since infectious diseases require a *pathogen*, a further distinction is made here between *bacterial*, *viral*, *fungal*, *parasite* or *prion*. An exemplary assignment of different pathogens to corresponding diseases is shown in Table 1.1. The *reservoirs* for such pathogens can be

1 General Introduction

found in *humans, animals* or the *environment*. However, it is possible that the reservoir may be changed by the pathogen across species, e.g. transmission from animals to humans or vice versa is called *zoonosis*.

The mode of disease *transmission* is a central issue in epidemiology. Table 1.2 lists the different types of transmission routes with some examples. Infectious diseases can be caused by *direct contact* or also *indirect*, e.g. if surfaces are contaminated with the corresponding pathogen and this is absorbed into the body.

Table 1.2: List of transmission paths.

Transmission path	Example diseases
Person-to-person	HIV, Syphilis, Influenza, COVID-19
Airbourne transmission	Influenza, COVID-19, Chickenpox, Measles
Vector-borne diseases	ZIKA, Dengue, Malaria
Food- and waterborne diseases	Cholera, Salmonella
Vertical transmitted diseases	HIV, Syphilis

The example of COVID-19 shows that an infection can occur as indirect *person-to-person* transmission, as well as via *airbourne transmission* by inhalation of infectious *droplets* or *aerosols*. Thereby the responsible pathogen *SARS-CoV-2* is transmitted from person to person [29]. In *vector-borne diseases* the so-called *vectors* play the central role. For example, these can be mosquitoes, fleas and lice but also foxes or raccoons. In the case of dengue, the *dengue virus (DENV)* is taken up by a mosquito by blood meal at an infected person and transmitted to another person again by blood meal [35]. *Environmentally transmitted diseases* such as cholera or salmonella result from the uptake of the corresponding pathogen via water or food. *Vertical disease transmission* occurs via the placenta of a mother on her child before or during birth, as for example with HIV or syphilis.

In order to be able to quantify outbreaks of diseases, epidemiology uses certain quantities. For example, the number of newly infected individuals in a given period is called *incidence* and the number of infected individuals at a given time *prevalence*. If diseases can also lead to death, the *case fatality rate (CFR)* also plays an important role. This is calculated with

$$\text{CFR} = \frac{\text{Number of deaths due to the disease}}{\text{Cumulated total number of infected}} .$$

However, since it is unclear during an ongoing epidemic which current infections can lead to death, the CFR can only be determined exactly after an epidemic has ended [29]. Regarding such quantities it is problematic that not all cases have to be registered, because there may be *asymptomatic cases* or cases with mild *symptoms* that are not recognized as such. Another important term in epidemiology is the so-called *incubation period*. This refers to the period of time from when the pathogen enters the body and the first symptoms appear. In contrast, the *latency period* is the time span until the individual becomes *infectious*. It should be noted that incubation and latency period do not have to be congruent because the disease can also be transmitted before the onset of symptoms as the current COVID-19 pandemic shows [29].

Central questions now arise for epidemiologists which one would like to answer with mathematical models, e.g.

- How does the incidence and prevalence of the epidemic behave in a given time interval?
- Which parameters play a role and how can they be identified and influenced?
- How high is the number of unregistered cases?
- How will the pandemic develop in the future?
- Which control methods, e.g. *vaccination*, *isolation* or *vector control*, can be sensibly applied and how can their use be optimally planned?

The motivation for the present thesis is therefore to develop accurate and at the same time practicable models for the diseases COVID–19 and dengue. Furthermore, a suitable method for adapting them to real data sets is examined to be able to provide useful answers to the questions posed in the future by numerical simulations.

1.2 Thesis Structure

Part I: The first part provides a theoretical overview as a basis for the understanding of the presented contributions in Part II. This includes the fundamental definitions, theorems and examples of *ordinary differential equations* and the corresponding solution theory including common numerical methods in Chapter 2. Following this, the basics of mathematical modelling in epidemiology are presented in Chapter 3. An overview is given and especially *SIR* models for the simulation of human–to–human transmission and *SIRUV* models for vector–borne diseases are investigated. Chapter 4 thematizes *static* and *dynamical optimization*, in which basic approaches are presented theoretically and numerically. Based on this we derive a parameter estimation via *adjoint functions*, which is used and evaluated in the following contributions.

Part II: In five research papers, three of which have already been published, the research results are presented. The first three are about modelling dengue, based on real data sets from *Colombo* and *Jakarta*. In Chapter 5 a model reduction via time–scale separation from an *SIRUV* model to an *SIR* model with *time–dependent transmission rate* is applied. Previous data analysis of the dengue and associated rain data shows that these are cross–correlated. Accordingly, the transmission rate is designed to take into account the seasonal effects of the rainy seasons. The model presented in this way is adapted to the data sets with the help of adjoint functions. A more detailed description of this procedure is presented in Chapter 6. In detail, the analysis for the determination of the adjoint equations and the numerical solution using a least squares objective function is pre–calculated. A parameter estimation follows which is now used to investigate the predictive power of the model in the following period. This is done using the already known data sets from Colombo and Jakarta. The latter location is in the focus of Chapter 7 as we have received much more differentiated data on the individual districts in Jakarta and additional data on commuter movements between these districts. This data is analyzed and a reduced *SIR* model is developed, including mobility and again a time–dependent transmission rate which processes meteorological data. Based on this, the parameter estimation with adjoint functions is performed and the predictive power of the model is checked and evaluated in all districts. In the last two contributions an *SEIRD* model is developed to describe the COVID–19 outbreak in Germany. In Chapter 8 the available data sets on the cumulative number of infected persons and deaths are presented. The sensitivity of individual parameters is reviewed and three different variants of the model are tested. The

1 General Introduction

data adaptation is again done by means of adjoint functions. These results are taken up in the last contribution in Chapter 9 and an *SEIRD* model with time delay regarding the death cases is used to simulate the disease spread. A parameter estimation with a more recent data set is performed. The focus is on the numerical comparison of the parameter fitting with adjoint functions compared to the so-called *Metropolis algorithm*. Both are analyzed in detail and also runtimes and accuracy are checked. The bibliographies can be found at the end of the respective contributions.

Part III: In the last part the results of the research contributions are summarized and an outlook on possible future research is given in Chapter 10. The thesis concludes with the bibliography for the entire work, except Part II.

Part I

Mathematical Foundations

2 Basic Definitions, Theorems and Examples

In the following the necessary basic terms for the present thesis are summarized. It is assumed that the reader is familiar with the basic mathematical terms in *calculus*, *(linear) algebra*, *topology*, *measurement and integral theory*, *probability theory* and *statistics*. At this point we refer to the corresponding basic literature [5, 6, 8–10, 13, 26].

Let \mathbb{N} denote the set of the *natural numbers* and \mathbb{R} the *real numbers*. *Vector spaces* are defined over \mathbb{R} , if not stated otherwise. The following contents are based on [9, 11, 17, 34].

Definition 2.0.1. (*Banach space*)

A *normed vector space* $(X, \|\cdot\|_X)$ with corresponding *norm* $\|\cdot\|_X$ and *metric* $\mathbf{d}_X(x, y) := \|x - y\|_X$ for $x, y \in X$ is called *complete*, if each cauchy sequence $(x_n)_{n \in \mathbb{N}}$ with $x_n \in X$ for all $n \in \mathbb{N}$ converges within this space. A complete and normed vector space is also called *Banach space*.

Examples of Banach spaces are

- \mathbb{R}^n with $n \in \mathbb{N}$ as *euclidean space* with *euclidean norm* $\|x\|_2 := \left(\sum_{i=1}^n |x_i|^2\right)^{1/2}$
- $\mathcal{C}(\mathcal{D}) := \{f : \mathbb{R} \supset \mathcal{D} \rightarrow \mathbb{R} \mid f \text{ is continuous}\}$ with the norm $\|f\|_\infty := \sup_{t \in \mathcal{D}} |f(t)|$
- $\mathcal{C}^k(\mathcal{D}) := \{f : \mathbb{R} \supset \mathcal{D} \rightarrow \mathbb{R} \mid f \text{ is } k\text{-times continuously differentiable}\}$ with the norm $\|f\|_{\mathcal{C}^k(\mathcal{D})} := \sum_{i=0}^k \|f^{(i)}\|_\infty$
- Let the *function* f be (Ω, \mathfrak{A}) – $(\mathbb{R}, \mathfrak{B}(\mathbb{R}))$ *measurable* and $|f|$ be p –*times* μ –*integratable* on *measure space* $(\Omega, \mathfrak{A}, \mu)$. The Banach space $L^p(\mu)$ with $1 \leq p < \infty$ denotes the space of *equivalence classes* $[f]$ with

$$f \sim g \quad :\Leftrightarrow \quad f = g \quad \mu\text{-almost everywhere}$$

$$\text{and } L^p\text{-norm } \|[f]\|_{L^p} := \left(\int_\Omega |f|^p d\mu\right)^{1/p}.$$

Definition 2.0.2. (*Operator and functional*)

Let $(X, \|\cdot\|_X), (Y, \|\cdot\|_Y)$ be normed vector spaces and $\mathcal{D} \subset X$. A mapping $\mathcal{T} : \mathcal{D} \rightarrow Y$ is called *operator*. If additional $Y = \mathbb{R}$, we call \mathcal{T} *functional*. An operator \mathcal{T} is called

- *linear*, if \mathcal{D} is a *subspace* of X and $\mathcal{T}(ax_1 + bx_2) = a\mathcal{T}(x_1) + b\mathcal{T}(x_2)$ for all $a, b \in \mathbb{R}, x_1, x_2 \in \mathcal{D}$
- *bounded*, if there exists $C > 0$ with $\|\mathcal{T}(x)\|_Y \leq C\|x\|_X$ for all $x \in \mathcal{D}$.

Furthermore, we need the following definitions for our later investigations:

Definition 2.0.3. (*Gâteaux derivative*)

Let $(X, \|\cdot\|_X), (Y, \|\cdot\|_Y)$ be normed vector spaces, $\mathcal{D} \subset X$ open and $f : \mathcal{D} \rightarrow Y$. The function f is called *Gâteaux differentiable* at $x_0 \in \mathcal{D}$ to the *direction* $h \in X$, if the following limit exists

$$\delta f(x_0, h) := \lim_{\varepsilon \rightarrow 0} \frac{f(x_0 + \varepsilon h) - f(x_0)}{\varepsilon} = \left. \frac{df(x_0 + \varepsilon h)}{d\varepsilon} \right|_{\varepsilon=0}.$$

The function f is called *Gâteaux differentiable* at x_0 , if this holds for all directions $h \in X$ and $\delta f(x_0, \cdot) : X \rightarrow Y, h \rightarrow \delta f(x_0, h)$ is called *Gâteaux derivative of f at x_0* .

2 Basic Definitions, Theorems and Examples

Definition 2.0.4. (Fréchet derivative)

Let $(X, \|\cdot\|_X), (Y, \|\cdot\|_Y)$ be normed vector spaces, $\mathcal{D} \subset X$ open and $f : \mathcal{D} \rightarrow Y$. The function f is called *Fréchet differentiable* at $x_0 \in \mathcal{D}$, if there exists a bounded linear operator $\mathcal{T} : X \rightarrow Y$ with

$$\lim_{\|h\|_X \rightarrow 0} \frac{\|f(x_0 + h) - f(x_0) - \mathcal{T}(h)\|_Y}{\|h\|_X} = 0.$$

Furthermore, $\mathcal{T} : X \rightarrow Y$ is called *Fréchet derivative of f at x_0* .

Remark 2.0.5. It should be noted that Gâteaux differentiable functions generally do not need to be Fréchet differentiable, but the backward direction does apply. If a function f is Fréchet (and consequently also Gâteaux) differentiable at x_0 , the derivatives agree and $\mathcal{T}(h) = \delta f(x_0, h)$ holds true.

If we set $X := Y := \mathbb{R}$ with $\mathcal{D} \subset \mathbb{R}$ open, $\delta f(x_0, 1)$ corresponds to the first *derivative* of a *differentiable* function $f : \mathcal{D} \rightarrow \mathbb{R}$ at $x_0 \in \mathcal{D}$

$$\left. \frac{df}{dx} \right|_{x=x_0} = \lim_{\varepsilon \rightarrow 0} \frac{f(x_0 + \varepsilon) - f(x_0)}{\varepsilon},$$

with linear operator $\mathcal{T}(h) := \delta f(x_0, h) = h \cdot \left. \frac{df}{dt} \right|_{x=x_0}$. We also use f' instead of $\frac{df}{dt}$ and $f'', f''', \dots, f^{(n)}$ for the *n*th *derivation* of an *n*-fold (*continuously*) *differentiable* function.

In the multidimensional case $f : \mathcal{D} \rightarrow \mathbb{R}$ with $\mathcal{D} \subset \mathbb{R}^n$ open, $\delta f(x_0, h)$ denotes the *directional derivative* in direction $h \in \mathbb{R}^n$ at $x_0 \in \mathcal{D}$. If the operator $\mathcal{T}(h) := \delta f(x_0, h)$ is bounded and linear, this derivative can be expressed with the *gradient of f*

$$\nabla f = \begin{pmatrix} \frac{\partial f}{\partial x_1} \\ \vdots \\ \frac{\partial f}{\partial x_n} \end{pmatrix},$$

by $\delta f(x_0, h) = \nabla f(x_0)^T h = \frac{\partial f(x_0)}{\partial x_1} h_1 + \dots + \frac{\partial f(x_0)}{\partial x_n} h_n$. So the gradient is the representing *matrix* for the first derivative and in case of the second derivative the *Hessian matrix of f*

$$\nabla^2 f = \begin{pmatrix} \frac{\partial^2 f}{\partial x_1^2} & \cdots & \frac{\partial^2 f}{\partial x_1 \partial x_n} \\ \vdots & \ddots & \vdots \\ \frac{\partial^2 f}{\partial x_n \partial x_1} & \cdots & \frac{\partial^2 f}{\partial x_n^2} \end{pmatrix} = \left(\frac{\partial^2 f}{\partial x_i \partial x_j} \right)_{i,j=1,\dots,n}.$$

If $f : \mathcal{D} \rightarrow \mathbb{R}^m$, the *Jacobian matrix of f*

$$\mathcal{J}_f = \begin{pmatrix} \frac{\partial f_1}{\partial x_1} & \cdots & \frac{\partial f_1}{\partial x_n} \\ \vdots & \ddots & \vdots \\ \frac{\partial f_m}{\partial x_1} & \cdots & \frac{\partial f_m}{\partial x_n} \end{pmatrix} = \left(\frac{\partial f_i}{\partial x_j} \right)_{\substack{i=1,\dots,m \\ j=1,\dots,n}}$$

is used to express the linear operator $\mathcal{T}(h) := \delta f(x_0, h) = \mathcal{J}_f(x_0) \cdot h$.

Cases in which the set X corresponds to *infinite-dimensional function spaces* are still being investigated in Chapter 4–9.

2.1 Ordinary differential equations

In the following we consider basic research results on *ordinary differential equations*. This includes an outline of the solution theory as well as numerical methods based on [2, 9, 15, 16, 33].

Definition 2.1.1. (*Dynamical system*)

Let \mathcal{D} be a set of discrete time points or a continuous time span, X a non-empty set and let a function be defined by $\Phi : \mathcal{D} \times X \rightarrow X$. The tuple (\mathcal{D}, X, Φ) is called a *dynamical system*, if the following properties are fulfilled for all $x \in X$ and $0, t_1, t_2, t_1 + t_2 \in \mathcal{D}$:

- (i) $\Phi(0, x) = x$,
- (ii) $\Phi(t_2, \Phi(t_1, x)) = \Phi(t_1 + t_2, x)$.

Remark 2.1.2. The mapping $\Phi_x : \mathcal{D} \rightarrow X$ with $\Phi_x(t) := \Phi(t, x)$ is called *flow*, and x is named *initial state*. Furthermore, the set X is designated by *phase space* and the set $O_x := \{\Phi_x(t) \mid t \in \mathcal{D}\}$ is called *orbit* or *trajectory* regarding x .

Autonomous ordinary differential equations represent special cases of such dynamical systems.

Definition 2.1.3. (*Ordinary differential equation (ODE)*)

Let $\Omega \subset \mathbb{R} \times (\mathbb{R}^m)^n$ be an open set and $g : \Omega \rightarrow \mathbb{R}^m$ a (continuous) function, then an *ordinary differential equation of order n* in *explicit notation* is given by the equation

$$x^{(n)}(t) = g\left(t, x(t), x'(t), x''(t), \dots, x^{(n-1)}(t)\right). \quad (2.1)$$

An n -times (continuously) differentiable function $x : \mathcal{D} \rightarrow \mathbb{R}^m$ is called *solution* of the ordinary differential equation, if it satisfies equation (2.1) and

$$\left(t, x(t), x'(t), x''(t), \dots, x^{(n-1)}(t)\right) \in \Omega$$

for all $t \in \mathcal{D}$.

If an ODE is of the form

$$x^{(n)}(t) = g\left(x(t), x'(t), x''(t), \dots, x^{(n-1)}(t)\right), \quad (2.2)$$

one speaks also of an *autonomous* ODE.

Remark 2.1.4. In case of an autonomous ODE the function g does not explicitly depend on the variable t , but only indirectly through the function x .

An ODE can also be specified in *implicit form* for $\Omega \subset \mathbb{R} \times (\mathbb{R}^m)^{n+1}$ by the equation

$$g\left(t, x(t), x'(t), x''(t), \dots, x^{(n)}(t)\right) = 0.$$

Since the functions x and g in the case of $m \geq 2$ represent vector-valued mappings, we also speak of *ODE systems with m equations* in these cases.

An ODE is called *linear*, if it is given by

$$a_n(t)x^{(n)}(t) + a_{n-1}(t)x^{(n-1)}(t) + \dots + a_1(t)x'(t) + a_0(t)x(t) + b(t) = 0,$$

whereby the $m \times m$ -matrix *coefficients* $a_i : \mathcal{D} \rightarrow \mathcal{L}(\mathbb{R}^m)$ with $\mathcal{L}(\mathbb{R}^m) := \{A \mid A : \mathbb{R}^m \rightarrow \mathbb{R}^m \text{ continuous and linear}\}$ are functions depending on t . These can also be constant for all $i = 0, \dots, n$, so that we call the equation *linear with constant coefficients*. If $b(x) = 0$, the ODE is called *homogeneous*, otherwise *inhomogeneous*.

2 Basic Definitions, Theorems and Examples

Furthermore, we will deal exclusively with first-order ODE systems

$$\frac{dx}{dt} = g(t, x(t)), \quad (2.3)$$

since higher-order ODE systems can be traced back to them.

Definition 2.1.5. (*Initial value problem (IVP)*)

Let there be an ODE system as in equation (2.3). It is called *initial value problem*, if additionally an *initial value* satisfying

$$x(t_0) = x_0 \quad (2.4)$$

is given for $(t_0, x_0) \in \Omega$. This is also called *initial condition*.

Example 2.1.6. (Autonomous ODE)

An example of an autonomous IVP is

$$\frac{dx}{dt} = \beta x, \quad x(0) = x_0 > 0.$$

Note, that one can write x instead of $x(t)$ as shorthand in such equations. The function $x : \mathbb{R} \rightarrow \mathbb{R}$ satisfying $x(t) = x_0 e^{\beta t}$ is the solution of this problem, since

$$\frac{dx}{dt} = \beta (x_0 e^{\beta t}) = \beta x.$$

In terms of Definition 2.1.1 we can set

$$\Phi_{x_0}(t) := x_0 e^{\beta t}.$$

This flow meets the conditions of a dynamical system, because

$$\Phi(0, x_0) = x_0 e^0 = x_0$$

and

$$\Phi(t_2, \Phi(t_1, x_0)) = (x_0 e^{\beta t_1}) e^{\beta t_2} = x_0 e^{\beta(t_1+t_2)} = \Phi(t_1 + t_2, x_0)$$

for all $x_0 > 0$ and $t_1, t_2 \in \mathbb{R}$. Figure 2.1 shows the graphs of different example flows, depending on the starting value for x_0 .

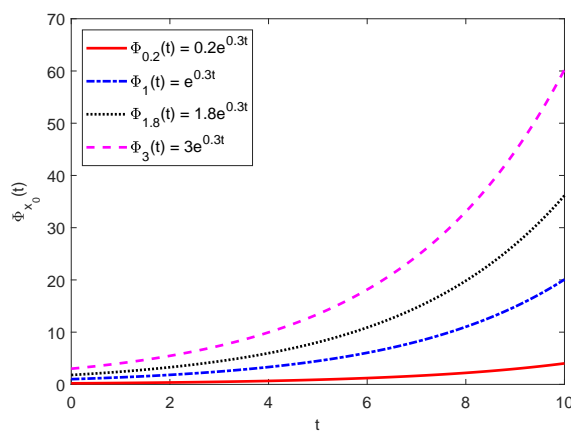


Figure 2.1: *Graphs* defined by the sets $G(\Phi_{x_0}) = \{(t, \Phi_{x_0}(t)) \mid t \in \mathcal{D}\}$ of several examples for $\Phi_{x_0}(t) = x_0 e^{\beta t}$ with $\beta = 0.3$ and $x_0 \in \{0.2, 1, 1.8, 3\}$.

An epidemiological example for such an *exponential growth* would be the initial phase of a disease outbreak, where $x(t)$ indicates the number of infected persons at the time t , the parameter β stands for the so-called *transmission rate* and x_0 for the initial number of infected individuals at time point t_0 .

Example 2.1.7. (Non-autonomous ODE)

If we now assume that the spread of the disease is periodic due to external conditions, such as the weather conditions which influence the immune system, the *instantaneous rate of change* could be described by, e.g.

$$\frac{dx}{dt} = \beta \cos(t)x, \quad x(0) = x_0 > 0.$$

Obviously this IVP explicitly depends on the variable t . The solution of this equation is given by $x : \mathbb{R} \rightarrow \mathbb{R}$ satisfying $x(t) = x_0 e^{\beta \sin(t)}$, because

$$\frac{dx}{dt} = \beta \cos(t) \left(x_0 e^{\beta \sin(t)} \right) = \beta \cos(t)x.$$

If we now define a flow by $\Phi_{x_0}(t) = x_0 e^{\beta \sin(t)}$, this does not meet the requirements of Definition 2.1.1, since

$$\Phi(t_2, \Phi(t_1, x_0)) = \left(x_0 e^{\beta \sin(t_1)} \right) e^{\beta \sin(t_2)} = x_0 e^{\beta(\sin(t_1) + \sin(t_2))}$$

which generally does not correspond to

$$\Phi(t_1 + t_2, x_0) = x_0 e^{\beta \sin(t_1 + t_2)}$$

for all $t_1, t_2 \in \mathbb{R}$.

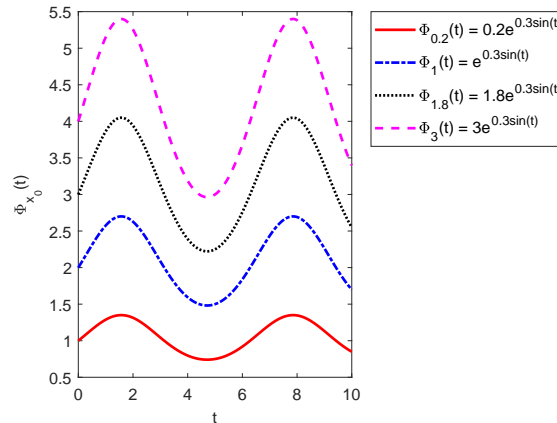


Figure 2.2: Graphs for the examples $\Phi_{x_0}(t) = x_0 e^{\beta \sin(t)}$ with $\beta = 0.3$ and $x_0 \in \{0.2, 1, 1.8, 3\}$.

The solution theory regarding ODEs has been extensively researched. For the purpose of this thesis the most important requirements and theorems are quoted here. Elementary to study the solvability of ordinary differential equations is the concept of *Lipschitz continuity*.

Definition 2.1.8. (Lipschitz continuity)

Let be $\Omega \subset \mathbb{R} \times \mathbb{R}^m$, then we call the function $g : \Omega \rightarrow \mathbb{R}^m$ with $(t, x) \rightarrow g(t, x)$ *Lipschitz continuous* in x , if a constant value $L \geq 0$ exists, so that

$$\|g(t, x) - g(t, y)\|_2 \leq L \|x - y\|_2 \quad (2.5)$$

2 Basic Definitions, Theorems and Examples

for all $(t, x), (t, y) \in \Omega$ applies. The function g is called *locally Lipschitz continuous*, if for each $(t_0, x_0) \in \Omega$ there exists a *neighbourhood* $\hat{\Omega} \subset \Omega$ of (t_0, x_0) , on which g is Lipschitz continuous.

Lipschitz continuity implies locally Lipschitz continuity. A useful tool to examine for the property is the following theorem:

Theorem 2.1.9. *Let $\Omega \subset \mathbb{R} \times \mathbb{R}^m$ be an open set and the function $g : \Omega \rightarrow \mathbb{R}^m$, $(t, x) \rightarrow g(t, x)$ be continuous. If the partial derivatives $\frac{\partial g_i}{\partial x_j}$ for all $i, j = 1, \dots, m$ exist and are continuous on Ω , then g is locally Lipschitz continuous.*

The Lipschitz continuity leads to a central theorem within the solution theory of ordinary differential equations:

Theorem 2.1.10. *(Picard–Lindelöf)*

Let $\Omega \subset \mathbb{R} \times \mathbb{R}^m$ be an open set and the function $g : \Omega \rightarrow \mathbb{R}^m$, $(t, x) \rightarrow g(t, x)$ be continuous in t and locally Lipschitz continuous in x . Then for all $(t_0, x_0) \in \Omega$ with given IVP

$$\frac{dx}{dt} = g(t, x(t)), \quad x(t_0) = x_0, \quad (2.6)$$

there exists

- (i) *an open interval $\hat{\mathcal{D}}$ with $t_0 \in \hat{\mathcal{D}}$ and unique solution $x : \hat{\mathcal{D}} \rightarrow \mathbb{R}^m$ for (2.6),*
- (ii) *a unique maximal solution $x : \mathcal{D} \rightarrow \mathbb{R}^m$ with $t_0 \in \mathcal{D}$ solving (2.6).*

Remark 2.1.11. A solution $x : \mathcal{D} \rightarrow \mathbb{R}^m$ of an IVP is called *maximal*, if for all (local) solutions $\hat{x} : \hat{\mathcal{D}} \rightarrow \mathbb{R}^m$ we have $\hat{\mathcal{D}} \subset \mathcal{D}$ and $x(t) = \hat{x}(t)$ for all $t \in \hat{\mathcal{D}}$.

Various formulations of the theorem can be found in the literature, which is proven with the help of the *Banach fixpoint theorem*.

It can also be shown that, if Ω is a *simply connected domain* and g is continuous in t and Lipschitz continuous in x , then a unique solution exists and can be extended up to the *boundary* of Ω .

Besides the Picard-Lindelöf theorem, with the strong property of Lipschitz continuity, the *Peano theorem* plays an important role. Here, on the basis of weaker assumptions, the existence of a solution is confirmed, but without the unity. The proof is based on the theorem of *Arzelà-Ascoli* and the *Schauder fixpoint theorem*.

Theorem 2.1.12. *(Peano)*

Let $\Omega \subset \mathbb{R} \times \mathbb{R}^m$ be an open set and the function $g : \Omega \rightarrow \mathbb{R}^m$ be continuous. Then for all $(t_0, x_0) \in \Omega$ with given IVP

$$\frac{dx}{dt} = g(t, x(t)), \quad x(t_0) = x_0, \quad (2.7)$$

there exists an open interval \mathcal{D} with $x_0 \in \mathcal{D}$ and solution $x : \mathcal{D} \rightarrow \mathbb{R}^m$ for (2.7).

Example 2.1.13. We consider again the IVP

$$\frac{dx}{dt} = \beta \cos(t)x, \quad x(0) = x_0 > 0,$$

and investigate it concerning Lipschitz continuity

$$\|g(t, x) - g(t, y)\|_2 = \|\beta \cos(t)(x - y)\|_2 = \underbrace{|\beta| |\cos(t)|}_{\leq 1} \|x - y\|_2 \leq \underbrace{|\beta|}_{=L} \|x - y\|_2.$$

Alternatively, one could check

$$\frac{\partial g}{\partial x} = \beta \cos(t),$$

which is continuous. Thus the ODE fulfills the Lipschitz property and can be uniquely solved, as already seen.

Example 2.1.14. In the following example, a function of the form

$$\beta(t) = \begin{cases} \beta_0, & t < c \\ \beta_1, & t \geq c \end{cases}$$

with constants $\beta_0, \beta_1, c > 0$ is integrated in the IVP by

$$\frac{dx}{dt} = \beta(t)x, \quad x(0) = x_0 > 0.$$

Obviously the function $g(t, x) = \beta(t)x$ is discontinuous in the variable t , but a Lipschitz constant $L = \max\{\beta_0, \beta_1\}$ exists. This problem can be solved by

$$x_\alpha(t) = \begin{cases} x_0 e^{\beta_0 t}, & t < c \\ \alpha e^{\beta_1(t-c)}, & t \geq c \end{cases}$$

for all $\alpha \in \mathbb{R}$. Accordingly there are infinitely many solutions as long as there is no additional initial condition for $t \geq c$. To generate a continuous, but at c not differentiable, solution one can choose $\alpha = x_0 e^{\beta_0 c}$, see Figure 2.3.

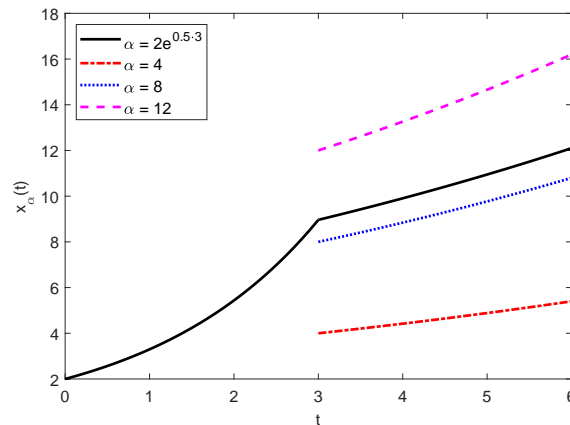


Figure 2.3: Graphs of $x_\alpha(t)$ for $x_0 = 2, \beta_0 = 0.5, \beta_1 = 0.1, c = 3$ and $\alpha \in \{2e^{0.5 \cdot 3}, 4, 8, 12\}$.

To put the example with continuous solution into epidemiological context, let $x(t)$ be the number of infected individuals at time t at the beginning of a disease outbreak. The jump within the function $\beta(t)$ then represents the reduction of the initial transmission rate β_0 to a lower β_1 at time c . This could be caused by, e.g. contact restrictions.

2.2 Solution methods

In the following section elementary and numerically solution methods for ordinary differential equations are presented which are necessary for the present thesis.

2.2.1 Elementary solution methods

Theorem 2.2.1.1. (*Separation of the variables*)

Let $\mathcal{D}_1, \mathcal{D}_2 \subset \mathbb{R}$ be open intervals and the functions $q : \mathcal{D}_1 \rightarrow \mathbb{R}$ and $h : \mathcal{D}_2 \rightarrow \mathbb{R}$ be continuous with given IVP

$$\frac{dx}{dt} = q(t)h(x(t)), \quad x(t_0) = x_0, \quad (2.8)$$

for $t_0 \in \mathcal{D}_1$ and $x_0 \in \mathcal{D}_2$.

(i) If $h(x_0) = 0$ holds true, the constant function $x : \mathcal{D}_1 \rightarrow \mathbb{R}$ satisfying $x(t) = x_0$ is a solution.

(ii) If $h(x_0) \neq 0$ holds true, there exists an open interval \mathcal{D} with $t_0 \in \mathcal{D}$ and a solution $x : \mathcal{D} \rightarrow \mathbb{R}$ which can be achieved by solving the equation

$$\int_{x_0}^x \frac{1}{h(\tau)} d\tau = \int_{t_0}^t q(\xi) d\xi. \quad (2.9)$$

Example 2.2.1.2. Consider the problem

$$\frac{dx}{dt} = \beta x(N - x), \quad x(t_0) = x_0 > 0, \quad (2.10)$$

with $N > x_0$. This problem can be solved by *separation of the variables* choosing $q(t) := \beta$ and $h(x) := x(N - x)$ which leads to a *logistic function*

$$x(t) = \frac{N}{e^{-N\beta(t-t_0)} \left(\frac{N}{x_0} - 1 \right) + 1}. \quad (2.11)$$

Again, in epidemiological context of the spread of a disease, the solution $x(t)$ describes the number of infected persons at time t . In this example, the growth is limited by multiplication with the term $N - x(t)$. This means that as soon as $x(t)$ approaches the *upper limit* N , the growth strives towards 0. In this example, $N - x(t)$ would represent the number of individuals still susceptible to the disease at time t , if the population size is named by N and consists only of susceptible and infected individuals. Figure 2.4 shows the *sigmoid* course of such a solution.

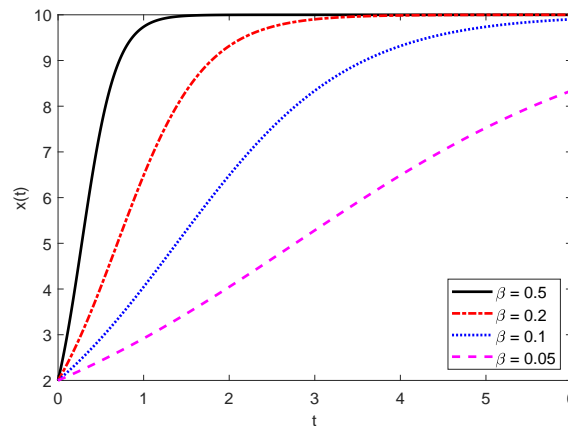


Figure 2.4: Graphs of the logistic solution $x(t)$ for $t_0 = 0, N = 10, x_0 = 2$ and $\beta \in \{0.5, 0.2, 0.1, 0.05\}$.

Theorem 2.2.1.3. Let $\mathcal{D} \subset \mathbb{R}$ be an open interval and the functions $a, b : \mathcal{D} \rightarrow \mathbb{R}$ be continuous with given linear IVP

$$\frac{dx}{dt} = a(t)x(t) + b(t), \quad x(t_0) = x_0, \quad (2.12)$$

for $t_0 \in \mathcal{D}$ and $x_0 \in \mathbb{R}$. Then there exists a unique solution $x : \mathcal{D} \rightarrow \mathbb{R}$ with

$$x(t) = e^{A(t)} \left(x_0 + \int_{t_0}^t e^{-A(\tau)} b(\tau) d\tau \right), \quad (2.13)$$

whereby $A(t) = \int_{t_0}^t a(\xi) d\xi$.

Example 2.2.1.4. In the following we consider the linear IVP with constant coefficients $a, b \in \mathbb{R}$

$$\frac{dx}{dt} = ax + b, \quad x(t_0) = x_0. \quad (2.14)$$

The above theorem leads to the solution

$$x(t) = \left(x_0 + \frac{b}{a} \right) e^{a(t-t_0)} - \frac{b}{a}, \quad (2.15)$$

also shown in Figure 2.5 with some examples.

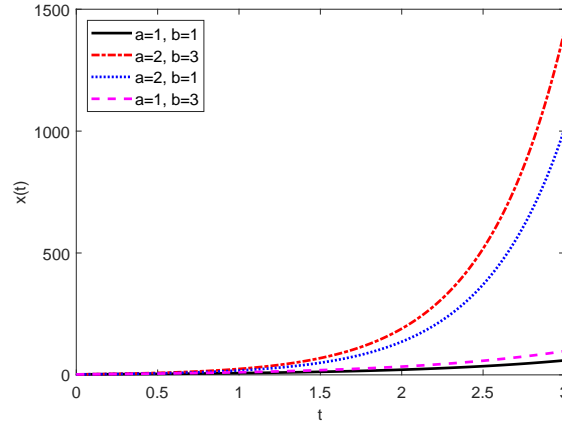


Figure 2.5: Graphs of $x(t)$ for $t_0 = 0, x_0 = 2$ and some combinations for $a, b \in \{1, 2, 3\}$.

Theorem 2.2.1.5. (*Homogeneous linear ODE system with constant coefficient*)

Let $A \in \mathbb{R}^{m \times m}$ be a constant and diagonalizable $m \times m$ -matrix with linear independent eigenvectors $v^{(1)}, \dots, v^{(m)}$ and corresponding eigenvalues z_1, \dots, z_m with given IVP

$$\frac{dx}{dt} = Ax, \quad x(t_0) = x_0. \quad (2.16)$$

Then the function $\Psi : \mathbb{R} \rightarrow \mathbb{R}^{m \times m}$ with

$$\Psi(t) := \begin{pmatrix} e^{z_1(t-t_0)} v_1^{(1)} & e^{z_2(t-t_0)} v_1^{(2)} & \dots & e^{z_m(t-t_0)} v_1^{(m)} \\ \vdots & \vdots & \ddots & \vdots \\ e^{z_1(t-t_0)} v_m^{(1)} & e^{z_2(t-t_0)} v_m^{(2)} & \dots & e^{z_m(t-t_0)} v_m^{(m)} \end{pmatrix}$$

is a fundamental matrix of (2.16).

2 Basic Definitions, Theorems and Examples

Remark 2.2.1.6. A *fundamental matrix* contains *basis vectors* of the *solution space* of a linear ODE system. In Theorem 2.2.1.5 it holds that $\Psi(t_0)$ is *nonsingular*. It can be shown that $\Psi(t)$ is then also nonsingular for all $t \in \mathbb{R}$.

The solution has the form $x(t) = \Psi(t) \cdot k$ with $k \in \mathbb{R}^m$. This vector k can be uniquely determined by solving the equation $x_0 = \Psi(t_0) \cdot k$.

In the present theorem the diagonalizability of the matrix A is provided. For the solution of systems with not diagonalizable matrices, please refer to [16, 33].

2.2.2 Numerical solution methods

Since only a fraction of ODEs can be solved analytically, numerical methods are required. A first approach provides the approximation of the differential equation with a sufficiently small value for $h > 0$ at t using the difference quotient

$$\frac{dx}{dt} \approx \frac{x(t+h) - x(t)}{h}$$

which leads from

$$\frac{dx}{dt} = g(t, x(t))$$

to the approximation

$$\frac{x(t+h) - x(t)}{h} \approx g(t, x(t))$$

and finally

$$x(t+h) \approx x(t) + hg(t, x(t)).$$

If we now set

$$\begin{aligned} t_i &= t, & t_{i+1} &= t + h, \\ x_i &= x(t), & x_{i+1} &= x(t + h), \end{aligned}$$

we get the iteration rule of the so-called *explicit Euler* procedure

$$x_{i+1} = x_i + hg(t_i, x_i) \tag{2.17}$$

or as *implicit Euler*

$$x_{i+1} = x_i + hg(t_{i+1}, x_{i+1}). \tag{2.18}$$

The initial condition $x(t_0) = x_0$ of an IVP thus provides the start value of the algorithm. In every iteration step an *error* occurs. This error depends directly on the selected *step size* h . A much more precise method is therefore, e.g. the *explicit classical Runge-Kutta* method with

$$\begin{aligned} k_1 &= g(t_i, x_i), \\ k_2 &= g\left(t_i + \frac{h}{2}, x_i + \frac{h}{2}k_1\right), \\ k_3 &= g\left(t_i + \frac{h}{2}, x_i + \frac{h}{2}k_2\right), \\ k_4 &= g(t_i + h, x_i + hk_3), \end{aligned}$$

leading to

$$x_{i+1} = x_i + \frac{h}{6}(k_1 + 2k_2 + 2k_3 + k_4).$$

For detailed informations regarding the errors of this procedures, please refer to [15].

2 *Basic Definitions, Theorems and Examples*

3 Epidemic Models

In the following sections basic models of mathematical epidemiology are presented. Using the example of the *SIR* model for human-to-human transmitted diseases, basic disciplines of analysis are demonstrated. In addition, the *SIRUV* model for modelling vector-borne diseases is introduced. The explanations in this chapter are based on the research in [1, 19, 21, 22, 31].

3.1 Basics in epidemiological modelling

In the present examples the following *compartments* are classified which indicate the number of corresponding persons at time t :

- *Susceptibles* $S(t)$: individuals who are susceptible to the disease and can be infected by infectious persons
- *Exposed* $E(t)$: persons who have already been infected but are not yet infectious, e.g. because they are still in the latent period
- *Infected* $I(t)$: infectious individuals who can transmit the disease on contact
- *Recovered* $R(t)$: people who have recovered from the disease and/or are immune
- *Total Population* $N(t)$: total number of affected individuals.

A selection of basic models including these compartments is shown in the Tables 3.1 and 3.2 on the pages 20 and 21. The differential equations are based on the respective instantaneous rates of change. The core of all models is the so-called *incidence term* $\frac{\beta}{N}SI$ which indicates the number of individuals per time step that pass from the susceptibles S to the exposed E or directly to the infected I due to an infection. The so-called *transmission rate* β consists of the product of the per capita *contact rate* c with the *probability* p that a contact with an infectious individual leads to an infection, thus $\beta = cp$. This is multiplied by the current number of susceptible persons S and the probability $\frac{I}{N}$, that a contact person is infectious.

In the model with exposed E they enter the infected compartment I at a rate of κ . The I compartment is left with a *recovery rate* γ either to the recovered R or directly to the susceptibles S . If there is a transition in the models from the recovered R back to the S compartment, this is done at the rate α . All the rates mentioned are positive and have the unit $[\text{time unit}]^{-1}$, e.g. $[\text{days}]^{-1}$, $[\text{years}]^{-1}$ etc. so that on both sides of the ODE systems we have the unit $[\text{number of individuals}] \cdot [\text{time unit}]^{-1}$.

A challenge in modelling with these ODE systems is the choice of the parameters. It can be shown that an infected individual spends on average $\frac{1}{\gamma}$ time units in the I compartment. The same applies to $\frac{1}{\kappa}$ in E and $\frac{1}{\alpha}$ in R . This insight enables us to determine these variables, if statistical data are available. For example, one can choose for a disease with a latent period of three days $\kappa = \frac{1}{3}$, a recovery period of 14 days $\gamma = \frac{1}{14}$ and a loss of immunity after six months $\alpha = \frac{1}{180}$.

3 Epidemic Models

Table 3.1: Basic examples of epidemiological models with flow chart and ODE system.

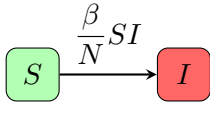
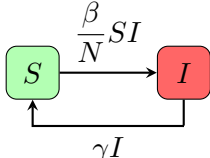
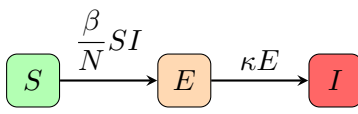
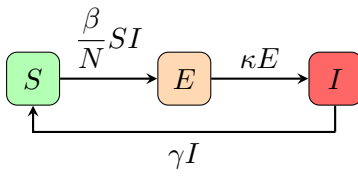
Model	Structure	ODE System
SI		$\frac{dS}{dt} = -\frac{\beta}{N}SI$ $\frac{dI}{dt} = \frac{\beta}{N}SI$
SIS		$\frac{dS}{dt} = -\frac{\beta}{N}SI + \gamma I$ $\frac{dI}{dt} = \frac{\beta}{N}SI - \gamma I$
SEI		$\frac{dS}{dt} = -\frac{\beta}{N}SI$ $\frac{dE}{dt} = \frac{\beta}{N}SI - \kappa E$ $\frac{dI}{dt} = \kappa E$
$SEIS$		$\frac{dS}{dt} = -\frac{\beta}{N}SI + \gamma I$ $\frac{dE}{dt} = \frac{\beta}{N}SI - \kappa E$ $\frac{dI}{dt} = \kappa E - \gamma I$

Table 3.2: Basic examples of epidemiological models with flow chart and ODE system.

Model	Structure	ODE System
<i>SIR</i>	<pre> graph LR S[S] -- "β/N * SI" --> I[I] I -- "γ * I" --> R[R] </pre>	$\frac{dS}{dt} = -\frac{\beta}{N}SI$ $\frac{dI}{dt} = \frac{\beta}{N}SI - \gamma I$ $\frac{dR}{dt} = \gamma I$
<i>SIRS</i>	<pre> graph LR S[S] -- "β/N * SI" --> I[I] I -- "γ * I" --> R[R] R -- "α * R" --> S </pre>	$\frac{dS}{dt} = -\frac{\beta}{N}SI + \alpha R$ $\frac{dI}{dt} = \frac{\beta}{N}SI - \gamma I$ $\frac{dR}{dt} = \gamma I - \alpha R$
<i>SEIR</i>	<pre> graph LR S[S] -- "β/N * SI" --> E[E] E -- "κ * E" --> I[I] I -- "γ * I" --> R[R] </pre>	$\frac{dS}{dt} = -\frac{\beta}{N}SI$ $\frac{dE}{dt} = \frac{\beta}{N}SI - \kappa E$ $\frac{dI}{dt} = \kappa E - \gamma I$ $\frac{dR}{dt} = \gamma I$
<i>SEIRS</i>	<pre> graph LR S[S] -- "β/N * SI" --> E[E] E -- "κ * E" --> I[I] I -- "γ * I" --> R[R] R -- "α * R" --> S </pre>	$\frac{dS}{dt} = -\frac{\beta}{N}SI + \alpha R$ $\frac{dE}{dt} = \frac{\beta}{N}SI - \kappa E$ $\frac{dI}{dt} = \kappa E - \gamma I$ $\frac{dR}{dt} = \gamma I - \alpha R$

3 Epidemic Models

All rates in this examples are set according to the time unit [days]⁻¹. The transmission rate on the other hand cannot generally be derived in this way, which requires a parameter estimation.

By applying Theorem 2.1.9 and 2.1.10 it can be concluded that these systems can be solved uniquely on *compact* intervals $[t_0, t_1] \subset [0, +\infty)$ with (continuously) differentiable functions $S, E, I, R : [t_0, t_1] \rightarrow \mathbb{R}$. The initial conditions are given by $S(t_0) = S_0 \geq 0$, $I(t_0) = I_0 \geq 0$ etc..

In these models we assume that the total population N at time t consists of the sum of the given compartments, e.g. in the case of the *SEIR* or *SEIRS* model

$$N(t) = S(t) + E(t) + I(t) + R(t).$$

It applies that

$$\frac{dN}{dt} = \frac{dS}{dt} + \frac{dE}{dt} + \frac{dI}{dt} + \frac{dR}{dt} = 0$$

and thus that N is constant for all t with $N = S_0 + E_0 + I_0 + R_0$.

Of these basic models, only the *SI* and *SIS* can be solved analytically using the substitution $S = N - I$. In case of the *SIS* model this leads to the equation

$$\frac{dI}{dt} = \frac{\beta}{N}(N - I)I - \gamma I = \frac{\beta}{N} \left(N \left(1 - \frac{\gamma}{\beta} \right) - I \right) I, \quad I_0 \geq 0$$

which can be solved by using the separation of the variables, see 2.2.1.1 and 2.2.1.2. All other systems, despite possible substitutions, need to be solved with numerical methods.

3.2 The SIR model including demography

In the case of disease courses that extend over longer periods of time, it can also make sense to take demographic developments within the population into account. These demographic elements can be integrated into the systems in the Tables 3.1 and 3.2. We consider this using the example of the *SIR* model, see Figure 3.1.

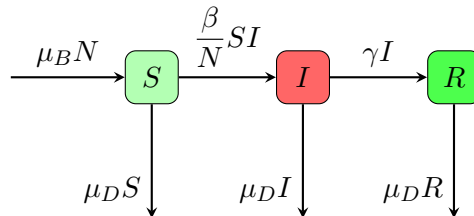


Figure 3.1: Flow chart of the *SIR* model with demography (3.1).

If we assume, for example, that the population has a birth rate of μ_B and a natural death rate of μ_D and that all newborns are born susceptible, the S compartment increases by $\mu_B N$ newborns and decreases by $\mu_D S$ naturally deceased in each time step. Analogously, the other compartments decrease by the respective number of deceased $\mu_D E, \mu_D I$ etc.

which leads to the ODE system

$$\frac{dS}{dt} = \mu_B N - \mu_D S - \frac{\beta}{N} SI, \quad S_0 \geq 0, \quad (3.1a)$$

$$\frac{dI}{dt} = \frac{\beta}{N} SI - (\gamma + \mu_D) I, \quad I_0 \geq 0, \quad (3.1b)$$

$$\frac{dR}{dt} = \gamma I - \mu_D R, \quad R_0 \geq 0. \quad (3.1c)$$

The derivation of the death rate also corresponds to those for γ , κ etc.. For example, if one assumes an average life expectancy of 70 years, one can choose $\mu_D = \frac{1}{70 \cdot 360}$. The birth rate can usually be read from statistics. For the total population N at time t we assume that $N(t) = S(t) + I(t) + R(t)$ holds true. This leads to

$$\frac{dN}{dt} = \frac{dS}{dt} + \frac{dI}{dt} + \frac{dR}{dt} = (\mu_B - \mu_D) N,$$

which means that for N an ODE has to be solved with initial value $N_0 := S_0 + I_0 + R_0$. In this case, this can be done by $N(t) = N_0 e^{(\mu_B - \mu_D)(t - t_0)}$.

For simplicity, however, we assume that birth and death rates are the same and can therefore be replaced by $\mu := \mu_B = \mu_D$. Thus, we receive

$$\frac{dS}{dt} = \mu(N - S) - \frac{\beta}{N} SI, \quad S_0 \geq 0, \quad (3.2a)$$

$$\frac{dI}{dt} = \frac{\beta}{N} SI - (\gamma + \mu) I, \quad I_0 \geq 0, \quad (3.2b)$$

$$\frac{dR}{dt} = \gamma I - \mu R, \quad R_0 \geq 0. \quad (3.2c)$$

Since in (3.2) we have $\frac{dN}{dt} = 0$, it follows that N is constant with $N = S_0 + I_0 + R_0$. If we substitute $R = N - S - I$ the system is reduced to a two-dimensional system

$$\frac{dS}{dt} = \mu(N - S) - \frac{\beta}{N} SI, \quad S_0 \geq 0,$$

$$\frac{dI}{dt} = \frac{\beta}{N} SI - (\gamma + \mu) I, \quad I_0 \geq 0,$$

which must be solved numerically. However, a further analysis allows to extract more precise properties of this system. For this purpose we rescale both sides of the equations and divide them by N and obtain for $\hat{x}_1 := \frac{S}{N}$ and $\hat{x}_2 := \frac{I}{N}$

$$\frac{d\hat{x}_1}{dt} = \mu(1 - \hat{x}_1) - \beta \hat{x}_1 \hat{x}_2, \quad \hat{x}_{10} = \hat{x}_1(t_0) \geq 0,$$

$$\frac{d\hat{x}_2}{dt} = (\beta \hat{x}_1 - (\gamma + \mu)) \hat{x}_2, \quad \hat{x}_{20} = \hat{x}_2(t_0) \geq 0.$$

It should be noted that the new variables \hat{x}_1 and \hat{x}_2 no longer have units. The next step is to do the same for the time variable by introducing $\tau := (\gamma + \mu)t$. This variable has no unit and leads to, e.g. $x_1(\tau) := \hat{x}_1\left(\frac{\tau}{\gamma + \mu}\right) = \hat{x}_1(t)$ with $\frac{d\hat{x}_1}{d\tau} = \frac{1}{\gamma + \mu} \frac{d\hat{x}_1}{dt}$ and finally to the *dimensionless ODE system*

$$\frac{dx_1}{d\tau} = \rho(1 - x_1) - \mathcal{R}_0 x_1 x_2, \quad x_{10} = x_1(\tau_0) \geq 0, \quad (3.3a)$$

$$\frac{dx_2}{d\tau} = (\mathcal{R}_0 x_1 - 1) x_2, \quad x_{20} = x_2(\tau_0) \geq 0, \quad (3.3b)$$

including the substitutions $\rho := \frac{\mu}{\gamma + \mu}$ and $\mathcal{R}_0 := \frac{\beta}{\gamma + \mu}$.

For further analysis we need the following definition:

3 Epidemic Models

Definition 3.2.1. (Equilibrium points)

Consider a given autonomous IVP with continuous $g : \mathbb{R}^m \rightarrow \mathbb{R}^m$

$$\frac{dx}{dt} = g(x(t)), \quad x(t_0) = x_0. \quad (3.4)$$

Then a *constant solution* $x^* : [t_0, +\infty) \rightarrow \mathbb{R}^m$ of (3.4) satisfying

$$g(x^*) = 0$$

is called *equilibrium* or *singular point*. An equilibrium x^* is called *locally asymptotically stable*, if a neighbourhood $\mathcal{X} \subset \mathbb{R}^m$ of x^* exists such that

$$\lim_{t \rightarrow +\infty} x(t) = x^*$$

holds true for all solutions $x : [t_0, +\infty) \rightarrow \mathbb{R}^m$ of (3.4) with $x(t_0) \in \mathcal{X}$.

So in our case we have to solve the equations

$$\begin{aligned} 0 &= \rho(1 - x_1^*) - \mathcal{R}_0 x_1^* x_2^*, \\ 0 &= (\mathcal{R}_0 x_1^* - 1) x_2^* \end{aligned}$$

and find the so-called *disease-free equilibrium* $x_{DE}^* = (1, 0)$ and the *endemic equilibrium* $x_{EE}^* = \left(\frac{1}{\mathcal{R}_0}, \rho \left(1 - \frac{1}{\mathcal{R}_0}\right)\right)$. The former occurs when the entire population is susceptible and no infected persons are present. In the second case, a fixed proportion of the population is always infected with the disease, i.e. endemic.

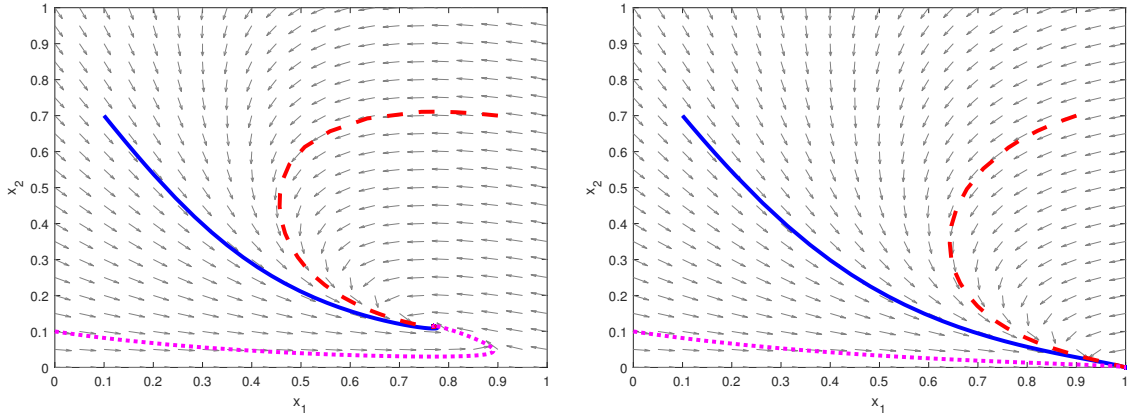


Figure 3.2: Direction fields of the dimensionless ODE system (3.3) with $\rho := 0.5$ and initial conditions $x_0^{(1)} := (0.1, 0.7)$ (blue/solid), $x_0^{(2)} := (0.9, 0.7)$ (red/dashed) and $x_0^{(3)} := (0, 0.1)$ (magenta/dotted). On the left we have $\mathcal{R}_0 = 1.3$ and on the right $\mathcal{R}_0 = 0.8$.

The direction field in Figure 3.2 shows that the trajectories of the system with $\mathcal{R}_0 > 1$ tend towards the endemic equilibrium x_{EE}^* . On the other hand, in the case $\mathcal{R}_0 < 1$ the solutions tend to the disease free equilibrium x_{DE}^* . These observations are no coincidence. The following theorem helps to investigate the stability of the present equilibria in more detail.

Theorem 3.2.2. (*Local stability of equilibria*)

Consider a given autonomous IVP with continuous $g : \mathbb{R}^m \rightarrow \mathbb{R}^m$

$$\frac{dx}{dt} = g(x(t)), \quad x(t_0) = x_0,$$

and equilibrium point x^* . If the eigenvalues of the Jacobian matrix

$$\mathcal{J}_g(x^*) = \left(\frac{\partial g_i(x^*)}{\partial x_j} \right)_{i,j=1,\dots,m}$$

have only negative real parts, then the equilibrium point x^* is locally asymptotically stable.

The explanation for this theorem is based on *linearizing* the ODE system for solutions sufficiently close to the equilibrium.

In our example the following applies to the Jacobian matrix

$$\mathcal{J}_g(x) = \begin{pmatrix} -\rho - \mathcal{R}_0 x_2 & -\mathcal{R}_0 x_1 \\ \mathcal{R}_0 x_2 & \mathcal{R}_0 x_1 - 1 \end{pmatrix}.$$

Inserting the disease-free equilibrium $(1, 0)$ into \mathcal{J}_g leads to

$$\mathcal{J}_g(x^*) = \begin{pmatrix} -\rho & -\mathcal{R}_0 \\ 0 & \mathcal{R}_0 - 1 \end{pmatrix}.$$

In this case the eigenvalues can be read directly from the diagonal and we get

$$\begin{aligned} z_1 &= -\rho < 0, \\ z_2 &= \mathcal{R}_0 - 1 < 0, \quad \text{if and only if } \mathcal{R}_0 < 1. \end{aligned} \tag{3.5}$$

Analogously, the local stability of the endemic equilibrium is examined and the following result is obtained:

- If $\mathcal{R}_0 < 1$, there exists a unique disease-free equilibrium $x_{DE}^* = (1, 0)$ which is locally asymptotically stable.
- If $\mathcal{R}_0 > 1$, there exist a disease-free equilibrium $x_{DE}^* = (1, 0)$ which is unstable, and an endemic equilibrium $x_{EE}^* = \left(\frac{1}{\mathcal{R}_0}, \rho \left(1 - \frac{1}{\mathcal{R}_0} \right) \right)$ which is locally asymptotically stable.

It can even be shown that

- If $\mathcal{R}_0 < 1$, the disease-free equilibrium $x_{DE}^* = (1, 0)$ is *globally stable*.
- If $\mathcal{R}_0 > 1$ and $x_{20} > 0$, the endemic equilibrium $x_{EE}^* = \left(\frac{1}{\mathcal{R}_0}, \rho \left(1 - \frac{1}{\mathcal{R}_0} \right) \right)$ is *globally stable*.

Global stability here means that the initial values do not have to be chosen near the equilibrium, but only have to meet certain conditions, e.g. $x_{20} > 0$ in the second case.

Mathematically, the meaning of

$$\mathcal{R}_0 = \frac{\beta}{\gamma + \mu} \tag{3.6}$$

becomes clear at this point since this value represents a threshold for the stability of the two equilibria. Biologically, this value corresponds to the so-called *Basic Reproduction Number*. This is the average number of new infections that an infected individual causes during the course of its disease in an otherwise susceptible population. It therefore seems logical that the disease "dies out" if an individual infects less than one other person with the disease. In our derivation, we have already used a method to determine this Basic Reproduction Number using the Jacobian matrix, also called the *Jacobian approach*. This is done by inserting the disease-free equilibrium in \mathcal{J}_g and checking for which threshold this equilibrium becomes stable, see equation (3.5). Since this approach does not always work, there are also alternative ways, such as the *Next-Generation approach*.

3.3 Modelling vector-borne diseases

So far we have looked at diseases caused by human-to-human transmission. However, many diseases are transmitted to humans by so-called *vectors*, such as dengue or malaria. The carrier animals for vector-borne diseases can be, e.g. mosquitoes, fleas, flies or also foxes and primates which have received the pathogen from a human or another animal before or carry it in themselves.

In the following we focus on diseases such as dengue which are transmitted from mosquitoes to humans. For this, the female mosquito must already have bitten an infected person in order to absorb the pathogen before it can transmit the disease via a second bite to another human. The modelling includes the already known groups within the human compartments susceptibles S , infected I and recovered R . Additionally, the mosquito population with uninfected U and infected V vectors is now also considered which leads to an $SIRUV$ model.

$$\frac{dS}{dt} = \mu(N - S) - \frac{\beta}{M}SV, \quad S_0 \geq 0, \quad (3.7a)$$

$$\frac{dI}{dt} = \frac{\beta}{M}SV - (\gamma + \mu)I, \quad I_0 \geq 0, \quad (3.7b)$$

$$\frac{dR}{dt} = \gamma I - \mu R, \quad R_0 \geq 0, \quad (3.7c)$$

$$\frac{dU}{dt} = \psi(t) - \frac{\vartheta}{N}UI - \nu U, \quad U_0 \geq 0, \quad (3.7d)$$

$$\frac{dV}{dt} = \frac{\vartheta}{N}UI - \nu V, \quad V_0 \geq 0. \quad (3.7e)$$

For the total human population we assume that $N(t) = S(t) + I(t) + R(t)$. It follows that

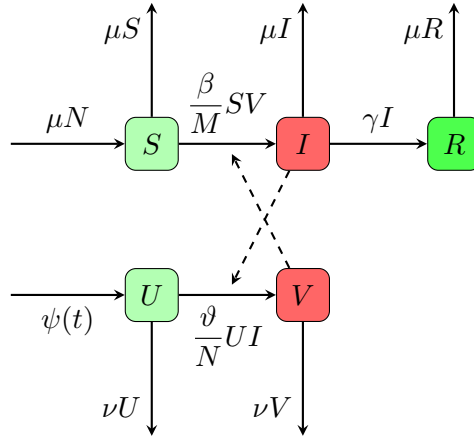
$$\frac{dN}{dt} = \frac{dS}{dt} + \frac{dI}{dt} + \frac{dR}{dt} = 0,$$

which in (3.7) leads to a constant $N = S_0 + I_0 + R_0$. The rates γ and μ again stand for the human recovery and birth/death rate.

Concerning the mosquito population M at time t , we have $M(t) = U(t) + V(t)$ and receive

$$\frac{dM}{dt} = \frac{dU}{dt} + \frac{dV}{dt} = \psi(t) - \nu M,$$

whereby ν indicates the death rate of the vectors. Usually, such a population is subject to seasonal fluctuations, as the reproduction depends directly on meteorological conditions. In order to provide a first easy access, we assume for the following consideration that $\psi(t) = \nu M$ and thus $\frac{dM}{dt} = 0$. The parameter ν corresponds, as already known in human

Figure 3.3: Flow chart of the $SIRUV$ model with demography (3.7).

dynamics, to the reciprocal value of the average life expectancy of the corresponding vector, e.g. at 10 days we have $\nu = \frac{1}{10}$ [days] $^{-1}$.

The incidence term $\frac{\beta}{M}SV$ is derived similar to the SIR model. The transmission rate β is the product of the per capita contact rate between a human and vectors and the probability that contact with an infected vector will lead to infection of the human. This is multiplied by the current number of susceptible humans S and the probability $\frac{V}{M}$, that a vector is infected. The second incidence term $\frac{\vartheta}{N}UI$ is derived analogously from the point of view of the vectors. It should be noted that the transmission rates β and ϑ generally do not have the same values. The difficulty in modelling is, that both parameters must be derived from data. However, in Chapter 5–7 techniques are presented to solve this problem in a practicable way. Using the substitutions $R = N - S - I$ and $U = M - V$ leads to a three-dimensional system

$$\begin{aligned} \frac{dS}{dt} &= \mu(N - S) - \frac{\beta}{M}SV, & S_0 &\geq 0, \\ \frac{dI}{dt} &= \frac{\beta}{M}SV - (\gamma + \mu)I, & I_0 &\geq 0, \\ \frac{dV}{dt} &= \frac{\vartheta}{N}(M - V)I - \nu V, & V_0 &\geq 0, \end{aligned}$$

which can be transformed to

$$\begin{aligned} \frac{d\hat{x}_1}{dt} &= \mu(1 - \hat{x}_1) - \beta\hat{x}_1\hat{x}_3, & \hat{x}_{10} &\geq 0, \\ \frac{d\hat{x}_2}{dt} &= \beta\hat{x}_1\hat{x}_3 - (\gamma + \mu)\hat{x}_2, & \hat{x}_{20} &\geq 0, \\ \frac{d\hat{x}_3}{dt} &= \vartheta(1 - \hat{x}_3)\hat{x}_2 - \nu\hat{x}_3, & \hat{x}_{30} &\geq 0, \end{aligned}$$

with $\hat{x}_1 := \frac{S}{N}$, $\hat{x}_2 := \frac{I}{N}$ and $\hat{x}_3 := \frac{V}{M}$. Again, we define $\tau := (\gamma + \mu)t$ and receive analogous

3 Epidemic Models

to (3.2)

$$\frac{dx_1}{d\tau} = \rho_H(1 - x_1) - \mathcal{R}_H x_1 x_3, \quad x_{10} \geq 0, \quad (3.8a)$$

$$\frac{dx_2}{d\tau} = \mathcal{R}_H x_1 x_3 - x_2, \quad x_{20} \geq 0, \quad (3.8b)$$

$$\frac{dx_3}{d\tau} = \rho_V (\mathcal{R}_V (1 - x_3) x_2 - x_3), \quad x_{30} \geq 0, \quad (3.8c)$$

including the values $\rho_H := \frac{\mu}{\gamma + \mu}$, $\rho_V := \frac{\nu}{\gamma + \mu}$, $\mathcal{R}_H := \frac{\beta}{\gamma + \mu}$ and $\mathcal{R}_V := \frac{\vartheta}{\nu}$. Applying the Jacobian approach leads to the Basic Reproduction Number

$$\mathcal{R}_0 = \mathcal{R}_H \mathcal{R}_V = \frac{\beta \vartheta}{(\gamma + \mu) \nu}$$

and by computation one can find the disease-free equilibrium $x_{DE}^* = (1, 0, 0)$ and the endemic equilibrium

$$x_{EE}^* = \left(\frac{\mathcal{R}_V \rho_H + 1}{\mathcal{R}_V (\rho_H + \mathcal{R}_H)}, \frac{\rho_H (\mathcal{R}_H \mathcal{R}_V - 1)}{\mathcal{R}_V (\rho_H + \mathcal{R}_H)}, \frac{\rho_H (\mathcal{R}_H \mathcal{R}_V - 1)}{\mathcal{R}_H (\mathcal{R}_V \rho_H + 1)} \right).$$

The vector dynamics can also be coupled to other models as required, resulting in *SISUV*, *SEIRUV* etc..

The basic models presented here can be modified to simulate even more complex processes. In the case of dengue, for example, a so-called *multistrain model* can be set up to incorporate the different serotypes of the virus in the infection process. Models in which the different age groups are taken into account with the help of *partial differential equations (PDE)* are also conceivable. PDEs can also be used to simulate the *spatial* spreading of a diseases. Introductory examples can be found in [19, 22].

In the presented models of human-to-human transmitted diseases and vector-borne diseases, it can be seen that the transmission rates β and ϑ play a prominent role in the transmission dynamics. Control methods can therefore aim to reduce contact rates and transmission probabilities, e.g. through contact restrictions, wearing masks and hygiene measures in the case of COVID-19 or long-sleeved clothing, mosquito nets, and sprays in the case of dengue. These measures have a direct influence on the corresponding transmission paths. In addition, vaccinations can be used for COVID-19 [27]. In the case of dengue, the control of the vector itself, e.g. by pesticides, plays a decisive role [36]. The optimal use of such means is therefore of great interest.

4 Optimization

In this chapter a parameter estimation via adjoint functions is derived. Prerequisite for this are methods of static and dynamical optimization, based on the research in [4, 7, 11, 12, 14, 15, 17, 18, 20, 23–25, 30, 32].

4.1 Static optimization

In the following our goal is to find a *minimum* $u_* \in \mathcal{U} \subset \mathbb{R}^m$ of a twice continuously differentiable function $J : \mathbb{R}^m \rightarrow \mathbb{R}$. The set \mathcal{U} is also called *feasible set* and the function J *objective function*. A common notation for such a *minimization problem* is

$$\min_{u \in \mathcal{U}} J(u) \quad (4.1a)$$

with

$$\mathcal{U} = \{u \in \mathbb{R}^m \mid h_i(u) = 0 \text{ and } k_j(u) \leq 0 \text{ for all } i = 1, \dots, l_1, j = 1, \dots, l_2\}. \quad (4.1b)$$

Alternatively, the problem can be formulated as

$$\min_u J(u) \quad (4.2a)$$

subject to (s.t.)

$$h_i(u) = 0, \quad i = 1, \dots, l_1, \quad (4.2b)$$

$$k_j(u) \leq 0, \quad j = 1, \dots, l_2. \quad (4.2c)$$

The *equality* (4.2b) and *inequality* (4.2c) *constraints* including twice continuously differentiable functions $h_i, k_j : \mathbb{R}^m \rightarrow \mathbb{R}$ must therefore be fulfilled at the minimum point u_* . The searched solution can also be expressed with the following notation

$$u_* = \arg \min_{u \in \mathcal{U}} J(u), \quad (4.3)$$

where "arg" stands for *argument*. Within optimization, a distinction is made between different types of minima.

Definition 4.1.1. (*Minimum*)

Consider an optimization problem as given in (4.1). A *feasible solution* $u_* \in \mathcal{U}$ is called

- (i) *local minimum*, if $J(u_*) \leq J(u)$ for all u in a neighbourhood $\hat{\mathcal{U}} \subset \mathcal{U}$ of u_* ,
- (ii) *strict local minimum*, if $J(u_*) < J(u)$ for all u in a neighbourhood $\hat{\mathcal{U}} \subset \mathcal{U}$ of u_* ,
- (iii) *global minimum*, if $J(u_*) \leq J(u)$ for all $u \in \mathcal{U}$,
- (iv) *unique global minimum*, if $J(u_*) < J(u)$ for all $u \in \mathcal{U}$.

4 Optimization

In optimization one distinguishes between so-called *necessary* and *sufficient conditions* for a minimum. In a first step, we assume an optimization problem without constraints ($\mathcal{U} = \mathbb{R}^m$) which is also called *unconstrained minimization problem*.

Theorem 4.1.2. (*Necessary optimality conditions*)
Consider an unconstrained minimization problem

$$\min_{u \in \mathbb{R}^m} J(u).$$

The objective function $J : \mathbb{R}^m \rightarrow \mathbb{R}$ is assumed to be twice continuously differentiable with local minimum $u_* \in \mathbb{R}^m$. Then the Necessary Optimality Conditions of First and Second Order hold true

- (i) $\nabla J(u_*) = 0$,
- (ii) $\nabla^2 J(u_*)$ is positive semi-definit.

Theorem 4.1.3. (*Sufficient optimality conditions*)
Consider an unconstrained minimization problem

$$\min_{u \in \mathbb{R}^m} J(u).$$

The objective function $J : \mathbb{R}^m \rightarrow \mathbb{R}$ is assumed to be twice continuously differentiable. If there exists $u_* \in \mathbb{R}^m$ so that the Sufficient Optimality Conditions

- (i) $\nabla J(u_*) = 0$,
- (ii) $\nabla^2 J(u_*)$ is positive definit

are satisfied, then u_* is a strict local minimum for J .

Example 4.1.4. As example we solve the unconstrained minimization problem

$$\begin{aligned} u_* &= \arg \min_{u \in \mathbb{R}^2} J(u), \\ J(u) &= u_1^2 + (u_2 - 3)^2. \end{aligned}$$

As gradient we receive

$$\nabla J(u) = \begin{pmatrix} 2u_1 \\ 2u_2 - 6 \end{pmatrix},$$

with

$$u_* = (0, 3),$$

since $\nabla J(u_*) = 0$. The respective Hessian matrix reads as

$$\nabla^2 J(u_*) = \begin{pmatrix} 2 & 0 \\ 0 & 2 \end{pmatrix}$$

which is obviously positive definit. Consequently, u_* is a strict local minimum, in this case even a unique global minimum, since J is a *strict convex* objective function.

With the addition of constraints *Lagrange multipliers* are used to solve the minimization problem. Here, we only turn to the procedure for equality constraints as in (4.2b), of the type $h_i(u) = 0$. With the addition of inequality constraints, the so-called *Karush–Kuhn–Tucker conditions* have to be checked.

Definition 4.1.5. (*Lagrange function and multipliers*)

Consider a constrained minimization problem

$$\min_{u \in \mathcal{U}} J(u) \quad (4.4a)$$

with

$$\mathcal{U} = \{u \in \mathbb{R}^m \mid h_i(u) = 0 \text{ for all } i = 1, \dots, l\} \quad (4.4b)$$

and $J, h_i : \mathbb{R}^m \rightarrow \mathbb{R}$ twice continuously differentiable for all $i = 1, \dots, l$.

A twice continuously differentiable function defined by

$$\mathcal{L}(u, \lambda) := J(u) + \sum_{i=1}^l \lambda_i h_i(u) \quad (4.5)$$

is called *Lagrange function*, whereby $\lambda := (\lambda_1, \dots, \lambda_l)^T \in \mathbb{R}^l$ are called *Lagrange multipliers*.

Note, that $\mathcal{L}(u, \lambda) = J(u)$ for $u \in \mathcal{U}$. One uses the minimization problem

$$\min_{(u, \lambda) \in \mathbb{R}^m \times \mathbb{R}^l} \mathcal{L}(u, \lambda) \quad (4.6)$$

to receive the solutions of the original problem (4.4). Thus, the Lagrange function is examined for the necessary and sufficient conditions in (4.1.2) and (4.1.3) instead. However, the requirements for the sufficient conditions can be weakened to the following theorem:

Theorem 4.1.6. (*Sufficient optimality conditions for constrained minimization*)

Consider a constrained minimization problem with Lagrange function \mathcal{L} as given in (4.4)–(4.5). If there exists $(u_*, \lambda_*) \in \mathbb{R}^m \times \mathbb{R}^l$ so that the gradients $\nabla h_i(u_*)$ are linearly independent for all $i = 1, \dots, l$ (LICQ) and the Sufficient Optimality Conditions

$$(i) \quad \nabla \mathcal{L}(u_*, \lambda_*) = 0,$$

$$(ii) \quad s^T \nabla_{uu}^2 \mathcal{L}(u_*, \lambda_*) s > 0, \\ \text{for all } s \in \mathbb{R}^m \text{ satisfying } \nabla h_i(u_*)^T s = 0 \text{ for all } i = 1, \dots, l \text{ and } s \neq 0$$

are satisfied, then $u_* \in \mathcal{U}$ is a strict local minimum for J in (4.4).

The expression

$$\nabla_{uu}^2 \mathcal{L} := \begin{pmatrix} \frac{\partial^2 \mathcal{L}}{\partial u_1^2} & \cdots & \frac{\partial^2 \mathcal{L}}{\partial u_1 \partial u_m} \\ \vdots & \ddots & \vdots \\ \frac{\partial^2 \mathcal{L}}{\partial u_m \partial u_1} & \cdots & \frac{\partial^2 \mathcal{L}}{\partial u_m^2} \end{pmatrix}$$

means the Hessian matrix of \mathcal{L} with respect to the directions of u .

Note, that (ii) is met, if $\nabla_{uu}^2 \mathcal{L}$ is positive definit.

4 Optimization

Example 4.1.7. Consider the constrained minimization problem

$$\begin{aligned} u_* &= \arg \min_{u \in \mathcal{U}} J(u), \\ J(u) &= u_1^2 + (u_2 - 3)^2 \end{aligned}$$

with

$$\mathcal{U} = \{u \in \mathbb{R}^2 \mid u_1 + u_2 - 1 = 0\}.$$

Now we have $h(u) = u_1 + u_2 - 1$ and obtain the Lagrange function

$$\mathcal{L}(u, \lambda) = u_1^2 + (u_2 - 3)^2 + \lambda(u_1 + u_2 - 1)$$

which leads to the gradient of \mathcal{L}

$$\nabla \mathcal{L}(u, \lambda) = \begin{pmatrix} 2u_1 + \lambda \\ 2u_2 - 6 + \lambda \\ u_1 + u_2 - 1 \end{pmatrix}.$$

Solving the equation $\nabla \mathcal{L} = 0$ we receive

$$(u_*, \lambda_*) = (-1, 2, 2)$$

and the respective Hessian matrix is given by

$$\nabla_{uu}^2 \mathcal{L}(u_*, \lambda_*) = \begin{pmatrix} 2 & 0 \\ 0 & 2 \end{pmatrix}$$

which is positive definite at the point $u_* = (-1, 2)$. Consequently, $u_* \in \mathcal{U}$ is a strict local minimum of J .

4.1.8 Numerical methods

To derive iterative methods for determining local minima, one expands the objective function J around a value $u \in \mathcal{U} \subset \mathbb{R}^m$ for $s \in \mathbb{R}^m$ and $\delta > 0$ sufficiently small as *Taylor series*

$$J(u + \delta s) = J(u) + \nabla J(u)^T \delta s + \frac{1}{2} \delta s^T \nabla^2 J(u) \delta s + \mathcal{O}(\|\delta s\|_2^3). \quad (4.7)$$

So in case of minimization one wants to receive $J(u + \delta s) \leq J(u)$, which leads to

$$\nabla J(u)^T s \leq 0 \quad (4.8)$$

for sufficiently small $\delta > 0$. Condition (4.8) must therefore be fulfilled by a possible *direction of descent* s . Based on these findings, an iteration of the form

$$u^{(i+1)} = u^{(i)} + \delta^{(i)} s^{(i)} \quad (4.9)$$

is used. The value $\delta^{(i)} > 0$ is called *step size*. The most intuitive direction of descent would simply be the negative gradient

$$s^{(i)} = -\nabla J(u^{(i)}), \quad (4.10)$$

since $\nabla J(u^{(i)})^T (-\nabla J(u^{(i)})) = -\|\nabla J(u^{(i)})\| \leq 0$. This is geometrically seen even the *steepest descent direction* at point $u^{(i)}$ and called *Gradient method*. But since this procedure often approaches the minimum in a kind of zigzag motion with many iterations, one usually uses other search directions. Another example is the *Conjugated Gradient method*

$$s^{(0)} = -\nabla J(u^{(0)}), \quad (4.11a)$$

$$s^{(i)} = -\nabla J(u^{(i)}) + \xi^{(i)} s^{(i-1)}, \quad (4.11b)$$

whereby $\xi^{(i)}$ can be defined in different ways, e.g. according to *Fletcher-Reeves*

$$\xi^{(i)} := \frac{\nabla J(u^{(i)})^T \nabla J(u^{(i)})}{\nabla J(u^{(i-1)})^T \nabla J(u^{(i-1)})}.$$

Another well-known application is the *Newton method* with the search direction

$$s^{(i)} = - \left[\nabla^2 J(u^{(i)}) \right]^{-1} \nabla J(u^{(i)}). \quad (4.12)$$

This is based on the idea that the Hessian matrix should be positive definite in the case of minimization. The problem here is that the Hessian matrix and its inverse must be determined at the corresponding point which can be very elaborate. From this approach, so-called *Quasi-Newton methods* have developed, e.g. from *Broyden*, *Fletcher*, *Goldfarb and Shanno (BFGS)*, to approximate the inverse of the Hessian matrix by

$$B^{(i)} = \left[\mathbf{I} - \frac{\Delta u^{(i)} (\Delta y^{(i)})^T}{(\Delta y^{(i)})^T \Delta u^{(i)}} \right] B^{(i-1)} \left[\mathbf{I} - \frac{\Delta y^{(i)} (\Delta u^{(i)})^T}{(\Delta y^{(i)})^T \Delta u^{(i)}} \right] + \frac{\Delta u^{(i)} (\Delta u^{(i)})^T}{(\Delta y^{(i)})^T \Delta u^{(i)}}, \quad (4.13)$$

with $\Delta u^{(i)} = u^{(i)} - u^{(i-1)}$ and $\Delta y^{(i)} = \nabla J(u^{(i)}) - \nabla J(u^{(i-1)})$. As starting value for B one can choose simply $B^{(0)} = \mathbf{I}$, which stands for the $m \times m$ *identity matrix*. Finally, we receive the search direction

$$s^{(i)} = -B^{(i)} \nabla J(u^{(i)}). \quad (4.14)$$

With regard to the exact derivations and the different convergence rates of the procedures, please refer to [23].

Regarding the step size, the following minimization problem must be solved in each iteration step

$$\delta^{(i)} = \arg \min_{\tau > 0} \psi(\tau) \quad \text{with} \quad \psi(\tau) := J(u^{(i)} + \tau s^{(i)}). \quad (4.15)$$

Generally, this cannot be done analytically which means the so-called *linesearch* has to be solved iteratively in the best possible way. This problem is addressed in Chapter 6 and 9.

4.2 Dynamical optimization: Optimal control theory

At the beginning of this section we provide a central tool for the following investigations:

Theorem 4.2.1. (*Fundamental lemma of calculus of variations*)

Let be $f : [t_0, t_1] \rightarrow \mathbb{R}$ a continuous function. If for all continuous differentiable functions $h : [t_0, t_1] \rightarrow \mathbb{R}$ with $h(t_0) = h(t_1) = 0$ the following is given

$$\int_{t_0}^{t_1} f(t) h(t) dt = 0,$$

then $f(t) = 0$ for all $t \in [t_0, t_1]$ holds true.

4 Optimization

It should be noted that there are different versions of this lemma but for the purpose of this thesis this simple form is sufficient. In the previous section we have dealt with static optimization. In the following, however, we will deal with how to find entire optimal functions, based on *Pontryagin's maximum (minimum) principle*. An initial example is given by

$$\min_u \int_{t_0}^{t_1} \omega_1 x(t)^2 + \omega_2 u(t)^2 dt \quad (4.16a)$$

subject to (s.t.)

$$\frac{dx}{dt} = \beta x(t) - \alpha u(t), \quad x(t_0) = x_0 \text{ and } x(t_1) \text{ free.} \quad (4.16b)$$

We want to find a continuously differentiable function $u : [t_0, t_1] \rightarrow \mathbb{R}$, so that the ODE with the continuously differentiable solution $x : [t_0, t_1] \rightarrow \mathbb{R}$ is fulfilled and the *objective functional*

$$J(u) := \int_{t_0}^{t_1} \omega_1 x(t)^2 + \omega_2 u(t)^2 dt$$

is minimized with respect to u . The functional J now depends on the *control variable* u . It should be noted that the solution of the ODE for the *state variable* x depends directly on u , which can also be expressed symbolically by $x(t, u(t))$.

If we relate to Example 2.1.6, where the ODE simulates the exponential growth of newly infected people at the beginning of a disease outbreak, then in this new situation the incidence would be influenced at each time step by the use of u control units with an efficiency $\alpha \geq 0$. For example, this can be done with vaccinations. At the same time, the overall number of control measures and infections should be kept as low as possible. A weighting between these can be done using $\omega_1, \omega_2 > 0$. Generally speaking, such a problem can be defined as follows

$$\min_u \int_{t_0}^{t_1} f(t, x(t), u(t)) dt \quad (4.17a)$$

subject to (s.t.)

$$\frac{dx}{dt} = g(t, x(t), u(t)), \quad x(t_0) = x_0 \text{ and } x(t_1) \text{ free,} \quad (4.17b)$$

including the continuously differentiable functions $f, g : \mathbb{R}^3 \rightarrow \mathbb{R}$ which are chained with $(t, x(t), u(t))$ for $t \in [t_0, t_1]$. In the following we also briefly write $f(t, x, u)$ and $g(t, x, u)$, instead of $f(t, x(t), u(t))$ and $g(t, x(t), u(t))$.

Similar to the approach with Lagrange multipliers in static optimization, a continuously differentiable *adjoint function* $\lambda : [t_0, t_1] \rightarrow \mathbb{R}$ is introduced, resulting in the following Lagrange function

$$\mathcal{L}(x, u, \lambda) := \int_{t_0}^{t_1} f(t, x, u) dt + \int_{t_0}^{t_1} \lambda(t) \left(g(t, x, u) - \frac{dx}{dt} \right) dt. \quad (4.18)$$

The latter term can be transformed using *partial integration* into

$$\begin{aligned} & \int_{t_0}^{t_1} \lambda(t) g(t, x, u) dt - \int_{t_0}^{t_1} \lambda(t) \frac{dx}{dt} dt \\ &= \int_{t_0}^{t_1} \lambda(t) g(t, x, u) dt + \int_{t_0}^{t_1} \frac{d\lambda}{dt} x(t) dt + \lambda(t_0)x(t_0) - \lambda(t_1)x(t_1) \end{aligned}$$

which leads to

$$\begin{aligned} \mathcal{L}(x, u, \lambda) &= \int_{t_0}^{t_1} f(t, x, u) + \lambda(t)g(t, x, u) + \frac{d\lambda}{dt}x(t) dt \\ &\quad + \lambda(t_0)x(t_0) - \lambda(t_1)x(t_1). \end{aligned}$$

Similar to the approach in the previous section, we look at how the directional derivatives of the Lagrange function \mathcal{L} should behave at a minimum (x_*, u_*, λ_*) . For this we introduce an arbitrary continuously differentiable function $h : [t_0, t_1] \rightarrow \mathbb{R}$ with $h(t_0) = 0$ and define in the sense of the Gâteaux derivative in Definition 2.0.3, e.g.

$$\frac{\partial \mathcal{L}}{\partial x} := \lim_{\varepsilon \rightarrow 0} \frac{\mathcal{L}(x + \varepsilon h, u, \lambda) - \mathcal{L}(x, u, \lambda)}{\varepsilon} = \left. \frac{d\mathcal{L}(x + \varepsilon h, u, \lambda)}{d\varepsilon} \right|_{\varepsilon=0}. \quad (4.19)$$

This has to take the value 0 at a minimum, which also applies to analogously defined $\frac{\partial \mathcal{L}}{\partial u}$ and $\frac{\partial \mathcal{L}}{\partial \lambda}$. Furthermore, e.g. we obtain

$$\left. \frac{d(x + \varepsilon h)}{d\varepsilon} \right|_{\varepsilon=0} = h. \quad (4.20)$$

Using the *majorized convergence by Lebesgue* and *chain rule* delivers

$$\begin{aligned} &\left. \frac{d\mathcal{L}(x + \varepsilon h, u, \lambda)}{d\varepsilon} \right|_{\varepsilon=0} \\ &= \int_{t_0}^{t_1} \left. \frac{df(t, x + \varepsilon h, u)}{d\varepsilon} \right|_{\varepsilon=0} + \lambda(t) \left. \frac{dg(t, x + \varepsilon h, u)}{d\varepsilon} \right|_{\varepsilon=0} + \left. \frac{d\lambda}{dt} \frac{d(x + \varepsilon h)}{d\varepsilon} \right|_{\varepsilon=0} dt \\ &\quad - \left. \lambda(t_1) \frac{d(x(t_1) + \varepsilon h(t_1))}{d\varepsilon} \right|_{\varepsilon=0} \\ &= \int_{t_0}^{t_1} h(t) \left(\frac{\partial f(t, x, u)}{\partial x} + \lambda(t) \frac{\partial g(t, x, u)}{\partial x} + \frac{d\lambda}{dt} \right) dt - \lambda(t_1)h(t_1) \end{aligned}$$

and finally at (x_*, u_*, λ_*) we obtain

$$0 = \int_{t_0}^{t_1} h(t) \left(\frac{\partial f}{\partial x} + \lambda(t) \frac{\partial g}{\partial x} + \frac{d\lambda}{dt} \right) dt - \lambda(t_1)h(t_1). \quad (4.21)$$

Since this equation applies to any h and especially to all with $h(t_0) = h(t_1) = 0$, the *fundamental lemma of calculus of variations* 4.2.1 now returns

$$0 = \frac{\partial f}{\partial x} + \lambda(t) \frac{\partial g}{\partial x} + \frac{d\lambda}{dt} \quad (4.22)$$

at (x_*, u_*, λ_*) and thus one receives the *adjoint equation*

$$\frac{d\lambda}{dt} = - \left(\frac{\partial f}{\partial x} + \lambda(t) \frac{\partial g}{\partial x} \right). \quad (4.23)$$

In addition, (4.21) leads for any h with $h(t_1) \neq 0$ in combination with (4.22) to the so-called *transversality condition*

$$\lambda(t_1) = 0. \quad (4.24)$$

Regarding $\frac{\partial \mathcal{L}}{\partial u}$ we get with analogous approach

$$\begin{aligned} \left. \frac{d\mathcal{L}(x, u + \varepsilon h, \lambda)}{d\varepsilon} \right|_{\varepsilon=0} &= \int_{t_0}^{t_1} \left. \frac{df(t, x, u + \varepsilon h)}{d\varepsilon} \right|_{\varepsilon=0} + \lambda(t) \left. \frac{dg(t, x, u + \varepsilon h)}{d\varepsilon} \right|_{\varepsilon=0} dt \\ &= \int_{t_0}^{t_1} h(t) \left(\frac{\partial f(t, x, u)}{\partial u} + \lambda(t) \frac{\partial g(t, x, u)}{\partial u} \right) dt \end{aligned}$$

4 Optimization

and recognize that at a minimum (x_*, u_*, λ_*) the *optimality condition* applies

$$0 = \frac{\partial f}{\partial u} + \lambda(t) \frac{\partial g}{\partial u}. \quad (4.25)$$

The same procedure regarding $\frac{\partial \mathcal{L}}{\partial \lambda}$ provides at (x_*, u_*, λ_*) the ODE constraint

$$\frac{dx}{dt} = g(t, x, u), \quad (4.26)$$

since

$$\begin{aligned} \left. \frac{d\mathcal{L}(x, u, \lambda + \varepsilon h)}{d\varepsilon} \right|_{\varepsilon=0} &= \int_{t_0}^{t_1} \left. \frac{d(\lambda + \varepsilon h)}{d\varepsilon} \right|_{\varepsilon=0} \left(g(t, x, u) - \frac{dx}{dt} \right) dt \\ &= \int_{t_0}^{t_1} h(t) \left(g(t, x, u) - \frac{dx}{dt} \right) dt \end{aligned}$$

and finally

$$0 = g(t, x, u) - \frac{dx}{dt}.$$

This leads to the following definitions and theorems:

Definition 4.2.2. (*Hamiltonian*)

Consider an optimal control problem as given in (4.17), then

$$H(t, x, u, \lambda) := f(t, x, u) + \lambda(t)g(t, x, u) \quad (4.27)$$

is called *Hamiltonian*.

Theorem 4.2.3. (*Pontryagin's maximum (minimum) principle*)

Consider an optimal control problem as given in (4.17) with corresponding *Hamiltonian*

$$H(t, x, u, \lambda) = f(t, x, u) + \lambda(t)g(t, x, u).$$

If u_* with corresponding x_* is a minimum for (4.17), then there exists an adjoint function λ_* such that

$$(i) \quad 0 = \frac{\partial H}{\partial u},$$

$$(ii) \quad \frac{d\lambda}{dt} = -\frac{\partial H}{\partial x}, \quad \lambda(t_1) = 0,$$

$$(iii) \quad \frac{dx}{dt} = g(t, x, u), \quad x(t_0) = x_0$$

is satisfied for all $t \in [t_0, t_1]$ at (x_*, u_*, λ_*) . Furthermore, we have

$$H(t, x_*, u_*, \lambda_*) \leq H(t, x_*, u, \lambda_*)$$

for all controls u at $t \in [t_0, t_1]$.

Remark 4.2.4. It should be noted that we have made strong assumptions about u and λ by assuming that they are continuously differentiable. However, this method can also be used with much weaker properties such as u and h *piecewise continuous* and λ *piecewise differentiable*.

Furthermore, one can check with

$$\frac{\partial^2 H}{\partial u^2} > 0$$

at (x_*, u_*, λ_*) , if the problem is a minimization problem for H .

Example 4.2.5. We consider the example

$$\min_u \int_0^1 \omega_1 x(t)^2 + \omega_2 u(t)^2 dt$$

s.t.

$$\frac{dx}{dt} = \beta x(t) - \alpha u(t), \quad x(0) = 5 \text{ and } x(1) \text{ free},$$

with $\omega_1, \omega_2, \beta, \alpha > 0$. Defining $f(t, x, u) := \omega_1 x^2 + \omega_2 u^2$ and $g(t, x, u) := \beta x - \alpha u$ delivers the Hamiltonian

$$H(t, x, u, \lambda) := \omega_1 x^2 + \omega_2 u^2 + \lambda(\beta x - \alpha u),$$

with

$$\begin{aligned} \frac{\partial H}{\partial u} &= 2\omega_2 u - \alpha\lambda, \\ \frac{\partial^2 H}{\partial u^2} &= 2\omega_2 > 0, \\ \frac{\partial H}{\partial x} &= 2\omega_1 x + \beta\lambda. \end{aligned}$$

The necessary conditions lead to

$$\begin{aligned} u &= \frac{\alpha}{2\omega_2} \lambda, \\ \frac{d\lambda}{dt} &= -2\omega_1 x - \beta\lambda, \quad \lambda(1) = 0, \\ \frac{dx}{dt} &= \beta x - \alpha u = \beta x - \frac{\alpha^2}{2\omega_2} \lambda, \quad x(0) = 5. \end{aligned} \tag{4.28}$$

One obtains the vector-valued linear ODE with constant coefficients

$$\frac{d}{dt} \begin{pmatrix} x \\ \lambda \end{pmatrix} = \begin{pmatrix} \beta & -\frac{\alpha^2}{2\omega_2} \\ -2\omega_1 & -\beta \end{pmatrix} \begin{pmatrix} x \\ \lambda \end{pmatrix}, \quad x(0) = 5, \lambda(1) = 0.$$

The determination of the eigenvalues provides

$$0 = \det \begin{pmatrix} \beta - z & -\frac{\alpha^2}{2\omega_2} \\ -2\omega_1 & -\beta - z \end{pmatrix} = -(\beta - z)(\beta + z) - \frac{\omega_1}{\omega_2} \alpha^2 = z^2 - \beta^2 - \frac{\omega_1}{\omega_2} \alpha^2$$

which leads to two real-valued eigenvalues

$$z_{1,2} = \pm \sqrt{\beta^2 + \frac{\omega_1}{\omega_2} \alpha^2}.$$

Thus, applying 2.2.1.5 the solution has the form

$$\begin{pmatrix} x \\ \lambda \end{pmatrix} (t) = c_1 e^{z_1 t} v_1 + c_2 e^{z_2 t} v_2,$$

whereby v_1, v_2 stand for respective eigenvectors for z_1 and z_2 . We obtain the coefficients c_1 and c_2 using the initial and end conditions for x and λ respectively. In our example we now set $\omega_1, \omega_2 := \frac{1}{2}$ and $\beta, \alpha := 1$. Consequently we get

$$u_* = \lambda_*$$

4 Optimization

and

$$z_1 = \sqrt{2}, \quad v_1 = \begin{pmatrix} \frac{1}{1-\sqrt{2}} \\ 1 \end{pmatrix},$$

$$z_2 = -\sqrt{2}, \quad v_2 = \begin{pmatrix} \frac{1}{1+\sqrt{2}} \\ 1 \end{pmatrix},$$

and solving the equation system for $x(0) = 5$ and $\lambda(1) = 0$

$$5 = c_1 \frac{1}{1-\sqrt{2}} + c_2 \frac{1}{1+\sqrt{2}},$$

$$0 = c_1 e^{\sqrt{2}} + c_2 e^{-\sqrt{2}},$$

delivers

$$c_1 = \frac{5e^{-2\sqrt{2}}}{1-\sqrt{2} - (1+\sqrt{2})e^{-2\sqrt{2}}} \quad \text{and} \quad c_2 = \frac{-5}{1-\sqrt{2} - (1+\sqrt{2})e^{-2\sqrt{2}}}.$$

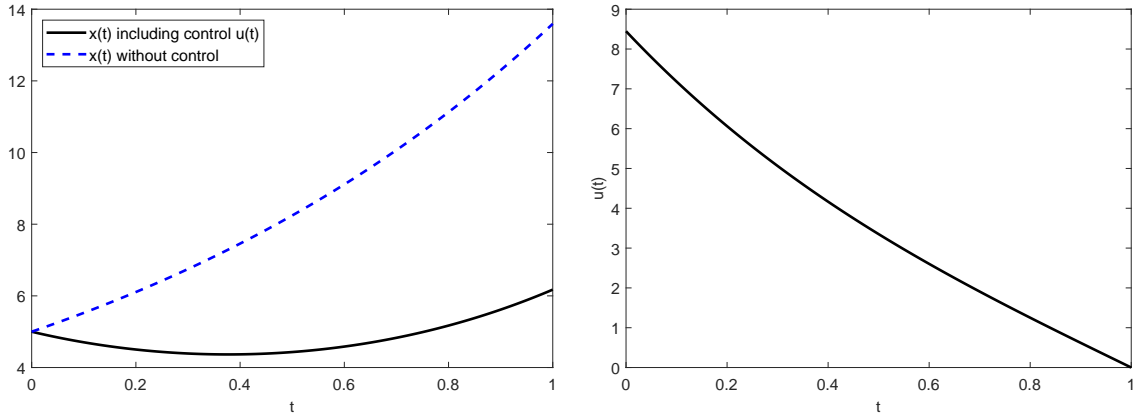


Figure 4.1: Optimal solution for Example 4.2.5. In the left graphs one can see the significant difference between controlled and uncontrolled state variable. On the right hand side the optimal control strategy is mapped, with initially high values which decrease monotonically. In this example u corresponds to the adjoint function λ .

Remark 4.2.6. The available results of the optimal control theory can now be extended further. There are applications in which a so-called *pay-off term* $\varphi(x(t_1))$ is integrated in the objective function

$$J(u) := \varphi(x(t_1)) + \int_{t_0}^{t_1} f(t, x(t), u(t)) dt.$$

In applications this can mean that the state variable should have a value as low as possible at the end time. In the medical field, this would be the case with optimal medication u to reduce disease triggers x at the end of the treatment. In this case, the analytical procedure is analogous which only leads to a change in the transversality condition

$$\lambda(t_1) = \left. \frac{d\varphi}{dx} \right|_{x=x(t_1)}. \quad (4.29)$$

Furthermore, the control variable u can be provided with upper and lower limits $l_1, l_2 \in \mathbb{R}$ so that $l_1 \leq u(t) \leq l_2$ for all $t \in [t_0, t_1]$. These results can be transferred analogously to the multidimensional case, so that entire ODE systems can be examined.

Unfortunately, optimal control problems can generally not be solved analytically, so that again a numerical method must be applied. One such algorithm is the *forward-backward sweep method*. At the beginning the necessary condition $0 = \frac{\partial H}{\partial u}$ has to be solved by hand as in Example 4.2.5 in equation (4.28). If this is not possible, suitable numerical methods like the *Newton's method* or *secant method* are necessary. We denote the solution of the necessary condition by \hat{u} in Algorithm 1.

Algorithm 1 Pseudocode Forward-Backward Sweep Method

- 1: $u \leftarrow$ startvalue, e.g. $u \equiv 0$
 - 2: **repeat**
 - 3: $u_{old} \leftarrow u$
 - 4: $x \leftarrow$ compute state variable depending on u and x_0
 - 5: $\lambda \leftarrow$ compute adjoint function depending on x , u and $\lambda(t_1)$
 - 6: $u \leftarrow$ update depending on u_{old} , x and by hand/numerically computed \hat{u}
 - 7: **until** $\|u_{old} - u\| < \text{TOL}$
-

The functions are discretized. Choosing the start value $u \equiv 0$ means that the system is solved first without control variable. The corresponding state variable is solved forward on time scale because of its start condition, whereas the adjoint function is solved backward on time scale due to its end condition. Possible numerical solution methods have already been presented in Section 2.2.2. It should be noted that for the backward solutions of an ODE, e.g. the explicit Euler changes to

$$x_{i-1} = x_i - hg(t_i, x_i, u_i),$$

with $h := t_i - t_{i-1}$.

The update of the new u depends on the previous u_{old} , x , λ and the calculated \hat{u} . Since x as well as λ cannot yet be assumed to be optimal, it is advisable to move only a part of u_{old} towards \hat{u} . This can be done by using a convex combination between these two

$$u := (1 - \iota)u_{old} + \iota\hat{u}$$

with $\iota \in (0, 1)$. Regarding the choice of a norm for the termination condition there are also several possibilities. In case of a fixed end value for the state variable $x(t_1) := x_{end}$ the transversality condition is omitted in the presented procedure and $\lambda(t_1)$ is unknown. In this case, numerical *shooting methods* can be used to solve the corresponding optimal control problem. Another special case occurs when both $f(t, x, u)$ and $g(t, x, u)$ depend linearly on u in (4.17). In this case, a so-called *bang-bang control* can be applied.

4.2.7 Optimal control including constant time delays

In the next step we investigate optimal control problems where one constant time delay $\tau > 0$ in the state variable plays a role. For this we consider for example

$$\min_u \int_{t_0}^{t_1} \omega_1 x(t)^2 + \omega_2 u(t)^2 dt \tag{4.30a}$$

4 Optimization

subject to (s.t.)

$$\frac{dx}{dt} = \beta x(t) - \alpha u(t)x(t - \tau), \quad (4.30b)$$

$$x(s) = \psi(s) \text{ for } s \in [t_0 - \tau, t_0], \quad (4.30c)$$

$$x(t_1) \text{ free.} \quad (4.30d)$$

In this case one needs a continuously differentiable (*initial*) *history function* $\psi : [t_0 - \tau, t_0] \rightarrow \mathbb{R}$ because of the time delay τ which describes the course of the state variable x before the time t_0 . In this example the quantitative reduction αu depends proportionally on the state of x at time $t - \tau$. Such a system could be written more generally as follows

$$\min_u \int_{t_0}^{t_1} f(t, x, x_\tau, u) dt \quad (4.31a)$$

subject to (s.t.)

$$\frac{dx}{dt} = g(t, x, x_\tau, u), \quad (4.31b)$$

$$x(s) = \psi(s) \text{ for } s \in [t_0 - \tau, t_0], \quad (4.31c)$$

$$x(t_1) \text{ free,} \quad (4.31d)$$

including $x_\tau(t) := x(t - \tau)$. The continuously differentiable functions $f, g : \mathbb{R}^4 \rightarrow \mathbb{R}$ are now chained with $(t, x(t), x_\tau(t), u(t))$ for $t \in [t_0, t_1]$. The respective Lagrange function reads as

$$\begin{aligned} \mathcal{L}(x, x_\tau, u, \lambda) &:= \int_{t_0}^{t_1} f(t, x, x_\tau, u) dt \\ &+ \int_{t_0}^{t_1} \lambda(t) \left(g(t, x, x_\tau, u) - \frac{dx}{dt} \right) dt. \end{aligned}$$

Slightly modified regarding the previous derivation, we introduce an arbitrary continuously differentiable function $h : [t_0 - \tau, t_1] \rightarrow \mathbb{R}$ with $h(t_0) = 0$ and set $h_\tau(t) := h(t - \tau)$. The look at the Gâteaux derivation with respect to x delivers

$$\begin{aligned} \frac{\partial \mathcal{L}}{\partial x} &:= \lim_{\varepsilon \rightarrow 0} \frac{\mathcal{L}(x + \varepsilon h, x_\tau + \varepsilon h_\tau, u) - \mathcal{L}(x, x_\tau, u)}{\varepsilon} \\ &= \left. \frac{d\mathcal{L}(x + \varepsilon h, x_\tau + \varepsilon h_\tau, u)}{d\varepsilon} \right|_{\varepsilon=0}. \end{aligned}$$

Consequently, at a minimum $(x_*, x_{\tau*}, u_*, \lambda_*)$ one finds

$$0 = \left. \frac{d\mathcal{L}(x + \varepsilon h, x_\tau + \varepsilon h_\tau, u)}{d\varepsilon} \right|_{\varepsilon=0} \quad (4.32a)$$

$$= \int_{t_0}^{t_1} h(t) \left(\frac{\partial f(t, x, x_\tau, u)}{\partial x} + \lambda(t) \frac{\partial g(t, x, x_\tau, u)}{\partial x} + \frac{d\lambda}{dt} \right) dt \quad (4.32b)$$

$$+ \int_{t_0}^{t_1} h(t - \tau) \left(\frac{\partial f(t, x, x_\tau, u)}{\partial x_\tau} + \lambda(t) \frac{\partial g(t, x, x_\tau, u)}{\partial x_\tau} \right) dt \quad (4.32c)$$

$$- \lambda(t_1)h(t_1). \quad (4.32d)$$

The second integral (4.32c) can be transformed using the *substitution* $\hat{t} := t - \tau$ into

$$\int_{t_0 - \tau}^{t_1 - \tau} h(\hat{t}) \left(\frac{\partial f(\hat{t} + \tau, x, x_\tau, u)}{\partial x_\tau} + \lambda(\hat{t} + \tau) \frac{\partial g(\hat{t} + \tau, x, x_\tau, u)}{\partial x_\tau} \right) d\hat{t}. \quad (4.33)$$

4.2 Dynamical optimization: Optimal control theory

Note that in (4.33) all functions in f and g depend on $t+\tau$ and that we have $x_\tau(t+\tau) = x(t)$.

Let us now assume an arbitrary continuously differentiable h with $h \equiv 0$ for all $t \notin (t_1 - \tau, t_1)$, then we obtain with the *fundamental lemma of calculus of variations*

$$0 = \frac{\partial f}{\partial x} + \lambda(t) \frac{\partial g}{\partial x} + \frac{d\lambda}{dt} \quad (4.34)$$

and finally the adjoint equation for $t \in (t_1 - \tau, t_1)$

$$\frac{d\lambda}{dt} = - \left(\frac{\partial f}{\partial x} + \lambda(t) \frac{\partial g}{\partial x} \right). \quad (4.35)$$

The same procedure with $h \equiv 0$ for $t \notin (t_0, t_1 - \tau)$ returns

$$0 = \frac{\partial f}{\partial x} + \lambda(t) \frac{\partial g}{\partial x} + \frac{d\lambda}{dt} + \frac{\partial f}{\partial x_\tau} \Big|_{t=t+\tau} + \lambda(t+\tau) \frac{\partial g}{\partial x_\tau} \Big|_{t=t+\tau} \quad (4.36)$$

and for the adjoint function on $(t_0, t_1 - \tau)$

$$\frac{d\lambda}{dt} = - \left(\frac{\partial f}{\partial x} + \lambda(t) \frac{\partial g}{\partial x} \right) - \left(\frac{\partial f}{\partial x_\tau} \Big|_{t=t+\tau} + \lambda(t+\tau) \frac{\partial g}{\partial x_\tau} \Big|_{t=t+\tau} \right). \quad (4.37)$$

In summary, this results for the adjoint equation over the entire interval $[t_0, t_1]$ in the expression

$$\frac{d\lambda}{dt} = - \left(\frac{\partial f}{\partial x} + \lambda(t) \frac{\partial g}{\partial x} \right) - \left(\frac{\partial f}{\partial x_\tau} \Big|_{t=t+\tau} + \lambda(t+\tau) \frac{\partial g}{\partial x_\tau} \Big|_{t=t+\tau} \right) \chi_{[t_0, t_1 - \tau]}(t). \quad (4.38)$$

Here, $\chi_{[a,b]} : \mathbb{R} \rightarrow \{0, 1\}$ stands for the so-called *characteristic function*

$$\chi_{[a,b]}(t) := \begin{cases} 1, & t \in [a, b] \\ 0, & t \notin [a, b]. \end{cases}$$

If we use an arbitrary continuously differentiable h with $h \equiv 0$ for $t \notin (t_0 - \tau, t_0)$, we obtain

$$0 = \frac{\partial f}{\partial x_\tau} \Big|_{t=t+\tau} + \lambda(t+\tau) \frac{\partial g}{\partial x_\tau} \Big|_{t=t+\tau}$$

on $(t_0 - \tau, t_0)$. Analogous to the procedure without time delay, we receive the transversality condition $\lambda(t_1) = 0$ for the adjoint equation (4.38).

If we define, based on the previous investigations, a Hamiltonian such as

$$H(t, x, x_\tau, u, \lambda) := f(t, x, x_\tau, u) + \lambda(t)g(t, x, x_\tau, u), \quad (4.39)$$

the adjoint equation at a minimum $(x_*, x_{\tau*}, u_*, \lambda_*)$ reads as

$$\frac{d\lambda}{dt} = - \frac{\partial H}{\partial x} - \frac{\partial H}{\partial x_\tau} \Big|_{t=t+\tau} \chi_{[t_0, t_1 - \tau]}(t), \quad \lambda(t_1) = 0. \quad (4.40)$$

It should be noted that in our approach we assumed exactly one constant time delay τ for the state variable. This derivation can be done in a similar way for the control variable u and with different constant time delays $0 < \tau_1 < \tau_2 < \dots < \tau_k$.

4 Optimization

Example 4.2.8. Consider the input example

$$\min_u \int_0^1 \omega_1 x(t)^2 + \omega_2 u(t)^2 dt$$

s.t.

$$\begin{aligned} \frac{dx}{dt} &= \beta x(t) - \alpha u(t)x(t - \tau), \\ x(s) &\equiv 5 \text{ for } s \in [-\tau, 0] \text{ and } x(1) \text{ free,} \end{aligned}$$

with $J(u) := \int_0^1 \omega_1 x(t)^2 + \omega_2 u(t)^2 dt$ and $\omega_1, \omega_2, \beta, \alpha, \tau > 0$. The Hamiltonian reads as

$$H(t, x, x_\tau, u, \lambda) := \omega_1 x^2 + \omega_2 u^2 + \lambda (\beta x - \alpha u x_\tau).$$

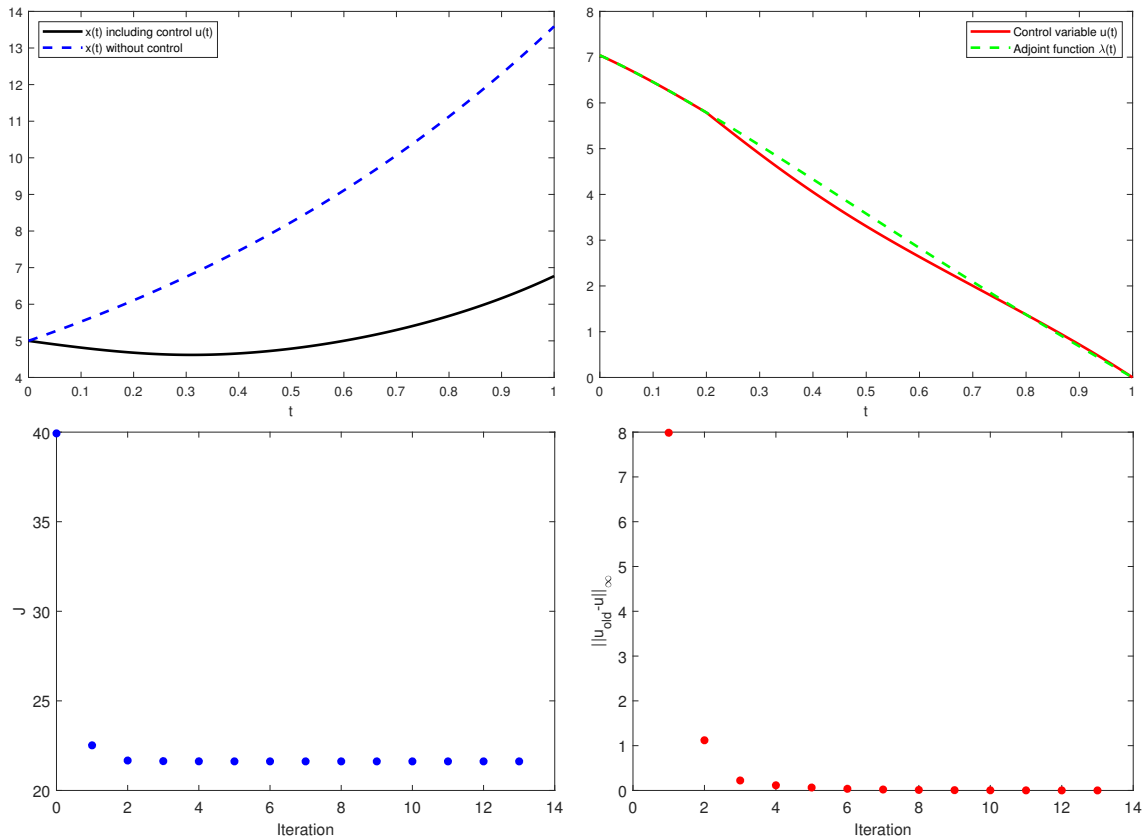


Figure 4.2: Graphical results for Example 4.2.8 with $\omega_1, \omega_2 := \frac{1}{2}$, $\beta := 1$ and $\alpha, \tau := 0.2$. In the upper left corner the influence of the control variable u on the state variable x is clearly visible. To the right of it one can see the control variable u and the corresponding adjoint λ . In comparison to Example 4.2.5 the deviation of u from λ can be seen. This begins at the time $\hat{t} := 0.2$ which corresponds exactly to the time delay τ and demonstrates its influence. The lower graphs show on the left side the development of the objective function J and on the right side the error $\|u_{\text{old}} - u\|_\infty$ depending on the respective iteration. As initial value $u \equiv 0$ is chosen and Algorithm 1 stops, when $\|u_{\text{old}} - u\|_\infty < 10^{-3}$ holds true.

Further we receive

$$\begin{aligned} 0 &= \frac{\partial H}{\partial u} \\ &= 2\omega_2 u - \lambda \alpha x(t - \tau), \end{aligned}$$

leading to

$$u_* = \frac{\alpha}{2\omega_2} \lambda x(t - \tau)$$

and

$$\frac{\partial^2 H}{\partial u^2} = 2\omega_2 > 0.$$

Concerning the adjoint equation we find

$$\begin{aligned} \frac{d\lambda}{dt} &= -\frac{\partial H}{\partial x} - \frac{\partial H}{\partial x_\tau} \Big|_{t=t+\tau} \chi_{[0,1-\tau]}(t) \\ &= -2\omega_1 x - \lambda\beta + \alpha\lambda(t + \tau)u(t + \tau)\chi_{[0,1-\tau]}(t), \end{aligned}$$

with transversality condition $\lambda(1) = 0$. Due to the included time delay, one can see that in this example a numerical method is necessary.

4.3 Parameter estimation via adjoint functions

In the following section it is now a matter of combining the presented techniques for static and dynamical optimization in order to derive unknown model parameters by data fitting. For this we suppose that a discrete data set (t_i, d_i) is present in which $t_0 < t_1 < \dots < t_n$ represent measurement time points and d_i the corresponding data. The data points are interpolated so that we receive a continuous function $x^{\text{data}} : [t_0, t_n] \rightarrow \mathbb{R}$ with $x^{\text{data}}(t_i) = d_i$. This function x^{data} is to be approximated by a model, e.g.

$$\frac{dx}{dt} = \beta x(1 - x), \quad x(t_0) = x_0. \quad (4.41)$$

We assume that the model parameters β and x_0 are unknown. A first approach would be a kind of least squares method by solving the minimization problem

$$\min_{u \in \mathbb{R}^k} \int_{t_0}^{t_n} (x(t) - x^{\text{data}}(t))^2 dt, \quad (4.42)$$

with constraint (4.41). The target variable $u \in \mathbb{R}^k$ contains the unknown parameters, e.g. β and x_0 . The objective function

$$J(u) := \int_{t_0}^{t_n} (x(t) - x^{\text{data}}(t))^2 dt$$

becomes minimal, if the model best represents the *data function* x^{data} . Generally we formulate this problem by

$$\min_{u \in \mathbb{R}^k} \int_{t_0}^{t_n} f(t, x, u) dt + \psi(u) \quad (4.43a)$$

subject to (s.t.)

$$\frac{dx}{dt} = g(t, x, u), \quad x(t_0) = x_0, \quad (4.43b)$$

4 Optimization

with twice continuously differentiable functions $x : [t_0, t_n] \rightarrow \mathbb{R}$ and $f, g : \mathbb{R}^{k+2} \rightarrow \mathbb{R}$ chained with (t, x, u) for all $t \in [t_0, t_n]$. Note, that x depends on t . The objective function $J : \mathbb{R}^k \rightarrow \mathbb{R}$

$$J(u) := \int_{t_0}^{t_n} f(t, x, u) dt + \psi(u) \quad (4.44)$$

contains an additional twice differentiable *regularization term* $\psi : \mathbb{R}^k \rightarrow [0, +\infty)$. The regularization term is presumed to be convex and *radially unbounded*, which means that $\psi(u) \rightarrow +\infty$ for $\|u\|_2 \rightarrow +\infty$. We form the Lagrange function

$$\mathcal{L}(x, u, \lambda) := \int_{t_0}^{t_n} f(t, x, u) dt + \psi(u) + \int_{t_0}^{t_n} \lambda(t) \left(g(t, x, u) - \frac{dx}{dt} \right) dt \quad (4.45a)$$

$$= \int_{t_0}^{t_n} f(t, x, u) + \lambda(t)g(t, x, u) + \frac{d\lambda}{dt}x(t) dt \quad (4.45b)$$

$$+ \lambda(t_0)x_0 - \lambda(t_n)x(t_n) + \psi(u) \quad (4.45c)$$

and the Hamiltonian

$$H(t, x, u, \lambda) := f(t, x, u) + \lambda(t)g(t, x, u). \quad (4.46)$$

Based on analogous investigations to the previous sections, we receive necessary optimality conditions at a minimum (x_*, u_*, λ_*) by

- (i) $0 = \frac{\partial \mathcal{L}}{\partial u_j}, \quad j = 1, \dots, k,$
- (ii) $\frac{d\lambda}{dt} = -\frac{\partial H}{\partial x}, \quad \lambda(t_n) = 0,$
- (iii) $\frac{dx}{dt} = g(t, x, u), \quad x(t_0) = x_0.$

Example 4.3.1. In this example, we want to test the presented method using an artificially generated data set (t_i, d_i) . For this purpose we consider a model of the form

$$\frac{dx}{dt} = \beta x(1 - x), \quad x(0) = x_0, \quad (4.47)$$

and solve the ODE for $\beta := 0.3$ and $x_0 := 0.1$ on the interval $[0, 20]$. This leads with Example 2.2.1.2 to the logistic function

$$\tilde{x}(t) := \frac{1}{1 + e^{-0.3t} \left(\frac{1}{0.1} - 1 \right)}.$$

Furthermore, we produce equidistant time points

$$0 =: t_0 < t_1 < \dots < t_{200} := 20$$

with corresponding data points

$$d_i := \max(\tilde{x}(t_i) + 0.1\hat{n}_i, 0)$$

which include *standard normally distributed* noise $\hat{n}_i \sim \mathcal{N}(0, 1)$. The resulting data set (t_i, d_i) is shown in Figure 4.3 on page 46. The corresponding data function x^{data} is generated by *spline* interpolation with $x^{\text{data}}(t_i) = d_i$.

4.3 Parameter estimation via adjoint functions

To test the adjoint approach, we now assume the model in (4.47) is to be fitted to x^{data} with unknown parameters β and x_0 , so $u := (\beta, x_0)$. The objective function reads as

$$J(u) := \omega_1 \int_0^{20} (x(t) - x^{\text{data}}(t))^2 dt + \omega_2 \|u\|_2^2,$$

with corresponding minimization problem

$$\min_{u \in \mathbb{R}^2} \omega_1 \int_0^{20} (x(t) - x^{\text{data}}(t))^2 dt + \omega_2 \|u\|_2^2.$$

In this example weights ω_1 and ω_2 are used. We set

$$\omega_1 := \frac{1}{\int_0^{20} x^{\text{data}}(t)^2 dt},$$

to normalize the least squares term concerning the data function. To let the regularization term $\psi(u) = \omega_2 \|u\|_2^2 = \omega_2(\beta^2 + x_0^2)$ have as little influence as possible on the numerical solution we choose, e.g. $\omega_2 := 10^{-9}$. The effects of this weight ω_2 will be discussed in more detail in Chapter 9, e.g. also in the case $\omega_2 = 0$.

In the first step we form the gradient of the Lagrange function

$$\begin{aligned} \mathcal{L}(x, u, \lambda) := & \omega_1 \int_0^{20} (x(t) - x^{\text{data}}(t))^2 dt + \omega_2(\beta^2 + x_0^2) \\ & + \int_0^{20} \lambda(t) \left(\beta x(t) (1 - x(t)) - \frac{dx}{dt} \right) dt \end{aligned}$$

with respect to u

$$\nabla_u \mathcal{L} = \begin{pmatrix} 2\omega_2\beta + \int_0^{20} \lambda(t)x(t)(1-x(t)) dt \\ 2\omega_2x_0 + \lambda(t_0) \end{pmatrix}.$$

The Hamiltonian reads as

$$H(t, x, u, \lambda) := \omega_1 (x - x^{\text{data}})^2 + \lambda(t)\beta x (1 - x)$$

which leads to the adjoint equation

$$\frac{d\lambda}{dt} = -2\omega_1 (x - x^{\text{data}}) + (2x - 1)\beta\lambda, \quad \lambda(20) = 0.$$

The evaluation of the Hessian matrix of the Lagrange function with respect to u delivers

$$\nabla_{uu}^2 \mathcal{L} = \begin{pmatrix} 2\omega_2 & 0 \\ 0 & 2\omega_2 \end{pmatrix} = 2\omega_2 \begin{pmatrix} 1 & 0 \\ 0 & 1 \end{pmatrix}$$

and shows the direct influence of the regularization term on its positive definiteness.

In our example, we choose $s := \nabla_u \mathcal{L}$ as search direction and thus apply the gradient method. Furthermore, we choose $u^{(0)} := (0.5, 0.5)$ as start value. The pseudo code shows that we now use the already known numerical optimization methods with respect to u , paired with the forward-backward sweep method, because in each iteration the ODEs of the state and adjoint variable must be solved with the current $u^{(i)}$.

4 Optimization

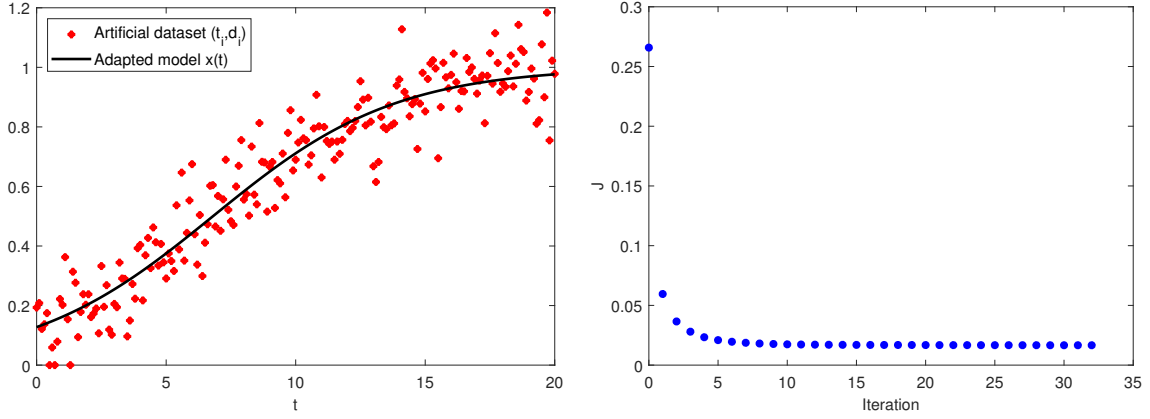


Figure 4.3: Solution for Example 4.3.1. Algorithm 2 returns $u = (0.28, 0.13)$ as numerical solution. It stops after 32 iterations at an accuracy of $|J - J_{old}| < 10^{-9}$ with $J = 0.0167$. The artificial data set (t_i, d_i) was created with $\tilde{u} := (0.3, 0.1)$.

Algorithm 2 Pseudocode for the adjoint approach.

- 1: $u, x^{\text{data}} \leftarrow$ load initial values for u and data (t_i, d_i)
 - 2: $x, \lambda \leftarrow$ solve ODE for state variable and adjoint function
 - 3: $J, \nabla_u \mathcal{L} \leftarrow$ compute objective function and gradient regarding u
 - 4: $s \leftarrow$ compute search direction
 - 5: **repeat**
 - 6: $J_{old} \leftarrow J$
 - 7: $\vartheta \leftarrow \operatorname{argmin}_{\vartheta > 0} \psi(\vartheta)$ with $\psi(\vartheta) := J(u + \vartheta s)$
 - 8: $u \leftarrow u + \vartheta s$
 - 9: $x, \lambda, J, \nabla_u \mathcal{L}, s \leftarrow$ update depending on u
 - 10: **until** $|J - J_{old}| < \text{TOL}$
 - 11: $u_*, x_*, \lambda_*, J_* \leftarrow u, x, \lambda, J$
-

In our example, we choose as linesearch algorithm in step 7 a backtracking algorithm with Armijo step size rule, see [3] and Section 6.B.

The adjoint approach is examined in more detail in the research papers, see Chapter 5–9. Due to the complexity of the diseases COVID–19 and dengue, extensions of the necessary conditions to ODE systems with and without time delay are necessary.

Part II

Contributions

5 Research Paper I: Modelling Dengue with the SIR–Model

Peter Heidrich Thomas Götz

The paper *Modelling Dengue with the SIR–Model* was written by Peter Heidrich and Thomas Götz. The theoretical elaboration, formulation and calculations were done by Peter Heidrich. Thomas Götz advised him on this and took over the linguistic revision of the article. The layout of the paper is adapted to the present thesis.

The contribution is based on a lecture held on 19 June 2018 at the *ECMI 2018 Conference in Budapest (18–22 June 2018)* and was published as proceeding in *Faragó I.; Izsák F.; Simon P.: Progress in Industrial Mathematics at ECMI 2018. Mathematics in Industry, Vol. 30, Springer, pp 175–182, 2019* (https://doi.org/10.1007/978-3-030-27550-1_22).

5.1 Abstract

Severe dengue outbreaks and their consequences point out the need for prognosis and control methods which can be derived by epidemiological mathematical models. In this article we develop a model to describe observed data on hospitalized dengue cases in Colombo (Sri Lanka) and Jakarta (Indonesia). Usually, the disease is epidemiologically modelled with the *SIRUV* model consisting of the susceptible (*S*), infected (*I*) and recovered humans (*R*) and the uninfected (*U*) and infected (*V*) female mosquitos. Because we do not have any information about the mosquito population we reduce the model to a *SIR* model which depends on a time–dependent transmission rate $\beta(t)$ and fit it to the received data sets. To solve this, optimal control theory constructed on Pontryagin’s maximum (minimum) principle is applied in order to reach the solution with numerical optimization methods. The results serve as a basis for different simulations.

Keywords: Dengue, Modelling, *SIR* model, Epidemiology, Numerical simulation, Parameter fit

5.2 Introduction

Severe dengue outbreaks and their consequences point out the need for prognosis and control methods which can be derived by epidemiological mathematical models. Dengue is classified as a fast emerging viral disease which occurs in over 100 tropical and subtropical endemic countries every year – especially in South East Asia, Latin America and the Western Pacific. The dengue virus is categorized in four distinct serotypes (DEN 1 – 4). Once infected with the virus a severe flu–like infection or in some cases a severe dengue (dengue haemorrhagic fever) may occur. In severe course of the disease dengue fever can lead to death. The disease is a mosquito–borne viral infection which is transmitted by vectors like the *Aedes aegypti*. The female mosquito absorbs the virus while feeding on the

blood of an infected human. When the infected mosquito bites an uninfected human the virus can be transmitted. Thus, the human functions as a carrier and multiplier of the virus. A transmission is followed by an incubation time of 4–10 days. Once infected, the virus is located 2–7 days in the blood. Meanwhile the patient shows the symptoms and can transmit the virus in a period of maximum 12 days to an uninfected mosquito. The recovery from the infection caused by one serotype of the virus provides lifelong immunity against this specific serotype. However, a subsequent infection with another serotype increases the risk of a severe dengue. The transmission of the disease depends on the living conditions for the vectors which are influenced by regional rainfall, temperature, humidity and the degree of urbanization. The *World Health Organisation (WHO)* hypothesizes that approximately 50–100 million infections occur every year whereby latest estimates are at 390 million infected humans of which only approximately one fourth is hospitalized or registered [6].

By private communication we received data sets of dengue cases in *Colombo (Sri Lanka)* and *Jakarta (Indonesia)* from the local *Departments of Mathematics* [2, 4]. Usually, the disease is modelled with the *SIRUV* model consisting of the *susceptible (S)*, *infected (I)* and *recovered (R) humans* and the *uninfected (U)* and *infected (V) female mosquitos*. Because we do not have any information about the mosquito population we reduce the model to a *SIR* model applying the findings of *Rocha et al.* [1]

$$\begin{aligned}\frac{dS}{dt} &= \mu(N - S) - \frac{\beta(t)}{N}SI, \\ \frac{dI}{dt} &= \frac{\beta(t)}{N}SI - (\alpha + \mu)I, \\ \frac{dR}{dt} &= \alpha I - \mu R.\end{aligned}$$

The system is reduced from five to three ordinary differential equations (ODEs) and depends on a time dependent *transmission rate* $\beta(t)$. In order to fit the parameters of the model to the received data sets we implement an objective function

$$J(u) = \int_0^T (I(t) - I^d(t))^2 dt + \frac{\|u\|^2}{N^2}$$

which shall be minimized with respect to u . The results serve as a basis for two numerical simulations concerning the behaviour of the dengue outbreaks.

5.3 Data analysis

The available data consists of the weekly hospitalized dengue cases in the *Colombo City District* and the *Special Capital Region of Jakarta*. To reduce the noise in the data we smoothen it with a moving average. Each data point d_i is replaced by $\bar{d}_i = \frac{1}{4} \sum_{k=0}^3 d_{i-k}$ for all $i \geq 3$. In both cases a periodical behaviour with varying intensities concerning the peaks can be recognized. In Colombo we observe half-yearly repeating outbreaks in the midyear and at the turn of the year, the dengue outbreaks in Jakarta appear yearly in the first quarter. The results of the fast Fourier transform (FFT) underpin these observations since significant high values at two frequencies per year in Colombo and one frequency per year in Jakarta can be noticed. It is assumed that this behaviour relates to the weather conditions especially the precipitation, because the vectors of the disease need small amounts of standing water to lay their eggs in. We apply the FFT on the appropriate rainfall data sets and recognize that their periodical behaviour fit to the dengue data.

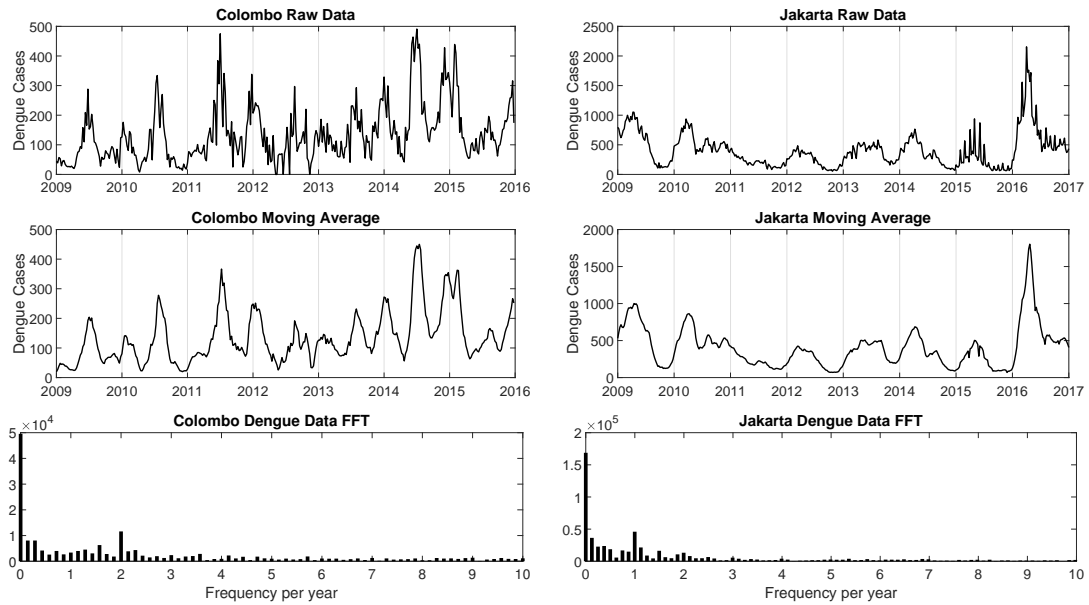


Figure 5.1: Dengue raw data, moving average and FFT for Colombo and Jakarta.

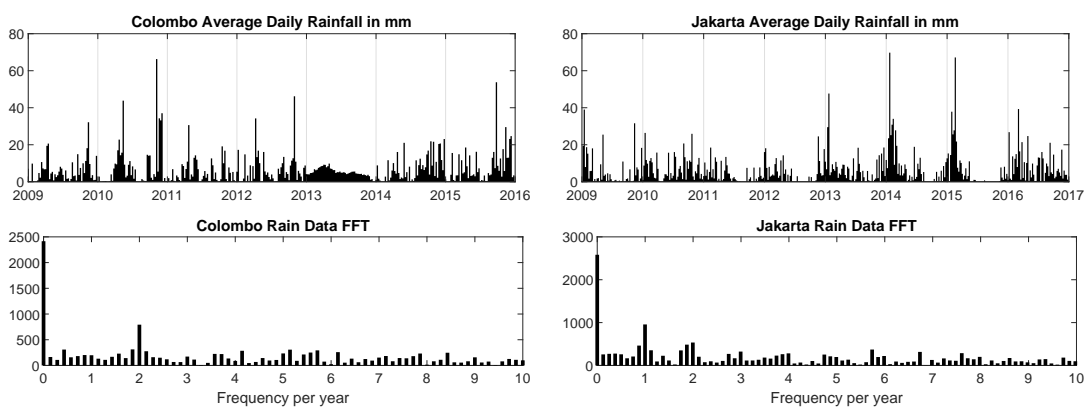


Figure 5.2: Rain data and their FFT analysis for Colombo and Jakarta.

To substantiate the relation between rainfall and dengue data we use a cross-correlation and finally receive significant high values at time lags between 6 to 10 weeks. Consequently, this means that after an intensive rain period it takes approximately two months until the dengue cases significantly rise in the cases of Colombo and Jakarta.

The clusters between precipitation and dengue data additionally show that if the average daily rainfall is stronger than approximately 15mm to 20mm a day, less dengue data points appear. Thus, we assume that in periods of very strong rainfall the eggs of the mosquitos are destroyed or washed away so that the reproduction of the vectors is restricted. In the following this border will be called *cut-off*.

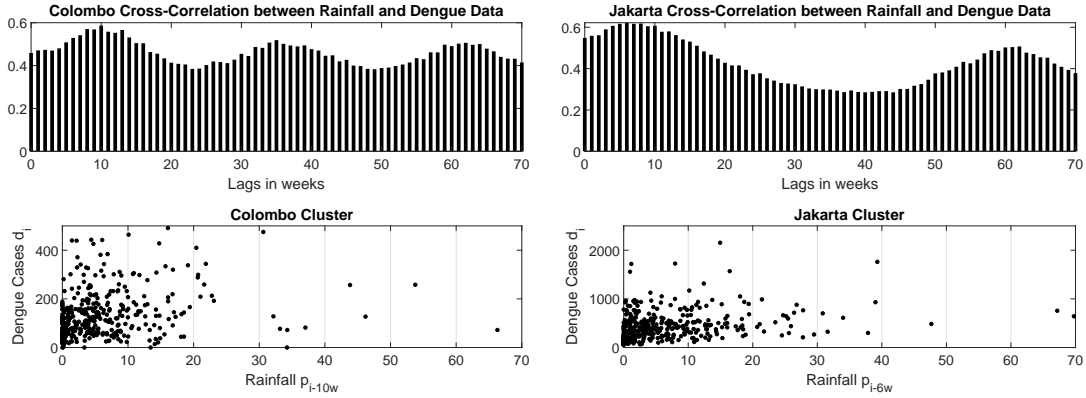


Figure 5.3: Cross-correlation and cluster between dengue and rain data in Colombo and Jakarta.

5.4 The SIR model

The present *SIR* Model includes the three usual groups of *susceptible* (S), *infected* (I) and *recovered* (R) individuals:

$$\frac{dS}{dt} = \mu(N - S) - \frac{\beta(t)}{N}SI, \quad S(t_0) = S_0 \geq 0, \quad (5.1a)$$

$$\frac{dI}{dt} = \frac{\beta(t)}{N}SI - (\alpha + \mu)I, \quad I(t_0) = I_0 \geq 0, \quad (5.1b)$$

$$\frac{dR}{dt} = \alpha I - \mu R, \quad R(t_0) = R_0 \geq 0, \quad (5.1c)$$

$$N = S_0 + I_0 + R_0. \quad (5.1d)$$

The *total population* N is assumed to be constant because of the short time period. Consequently, the *birth* and *death rate* are equal and named with μ . The transition from infected to recovered individuals depends on the *recovery rate* α . We omit the explicit mosquito dynamics of *uninfected* (U) and *infected* (V) vectors and use a time-dependent *transmission rate* $\beta(t)$ instead, see Table 5.1.

Here β_0 stands for the *average transmission rate* and β_1 for the *degree of periodical variation*. In simulation 2 a *phase-shift* φ is additionally included and β_1 is multiplied with an integral of the precipitation function p_c . It is defined by

$$p_c(\xi) = \begin{cases} p(\xi), & p(\xi) < c \\ 0, & p(\xi) \geq c. \end{cases} \quad (5.2)$$

Table 5.1: Examined transmission rates $\beta(t)$ for Simulation 1 and 2.

Simulation 1	Simulation 2
$\beta(t) = \beta_0 + \beta_1 \cos(\omega t)$	$\beta(t) = \beta_0 + \beta_1 \int_{t-\tau_2/52}^{t-\tau_1/52} p_c(\xi) d\xi \cdot \sin\left(\omega\left(t + \frac{\varphi}{52}\right)\right)$

The continuously differentiable function $p(\xi)$ includes the rainfall data points p_i and c represents the *cut-off*. The interval $[t - \frac{\tau_2}{52}, t - \frac{\tau_1}{52}]$ is set around the time lag between precipitation and dengue data. In the case of Colombo the time lag is 10 weeks, therefore $[t - \frac{12}{52}, t - \frac{8}{52}]$ is a possible choice.

To fit the model to the dengue data we solve the optimization problem

$$\min_u J(u) = \min_u \int_0^T (\gamma I(t) - I^d(t))^2 dt + \frac{\|u\|^2}{N^2} \quad (5.3)$$

subject to (5.1). Because it is assumed that only a fraction of infected individuals are hospitalized we establish γ as *hospitalization rate*. The continuous function $I^d(t)$ includes the dengue data points \bar{d}_i and u consists of the parameters that shall be fitted.

Table 5.2: Fitted and fixed parameters in Simulation 1 and 2.

	Fitted Parameters	Fixed Parameters
Simulation 1	$u = (\beta_0, \beta_1, S_0, I_0, R_0)'$	$N, \mu, \alpha, \omega, \gamma$
Simulation 2	$u = (\beta_0, \beta_1, c, \tau_2, \varphi, \gamma, S_0, I_0, R_0)'$	$N, \mu, \alpha, \omega, \tau_1$

The integral in $J(u)$ is based on a L^2 norm so that its minimization corresponds to a least squares method. Additionally we add a *regularization term* $\frac{\|u\|^2}{N^2}$. Its size is much smaller than the size of the integral therefore $\int_0^T (\gamma I(t) - I^d(t))^2 dt$ dominates the minimization algorithm which is decisive for the biological context. The addition with this convex and radially unbounded regularization term has an analytical background because otherwise some parameters would disappear in the *gradient* and consequently the corresponding columns and rows in the *Hessian matrix* would be equal to zero. Thus, it would be difficult to calculate and categorize *critical points*. In a way this corresponds to a *Tikhonov regularization* [5]. The division by the size of the total population N is caused by the fact that the transmission rate $\beta(t)$ is divided by N in the *SIR* model and the investigation of the initial conditions S_0, I_0 and R_0 in relation to N is useful.

In order to optimize (5.3) with *Pontryagin's maximum (minimum) principle* we introduce a *Lagrange function*

$$\mathcal{L}(u, x, \lambda) = \int_0^T (\gamma I(t) - I^d(t))^2 dt + \frac{\|u\|^2}{N^2} + \int_0^T \left\langle \lambda(t), g(u, x(t), t) - \frac{dx(t)}{dt} \right\rangle dt,$$

where $\lambda = (\lambda_S, \lambda_I, \lambda_R)'$ includes the *adjoint functions*, $x = (S, I, R)'$ consists of the *state variables*, $g = (g_S, g_I, g_R)'$ symbolizes the right terms of the ODEs in (5.1) and $\langle \cdot, \cdot \rangle$ stands for the scalar product. The *necessary optimality condition* for a minimum (u^*, x^*, λ^*) is fulfilled if $\nabla \mathcal{L}(u^*, x^*, \lambda^*) = 0$ holds.

Solving $\frac{\partial \mathcal{L}}{\partial x_i} = 0$ via Gâteaux derivative delivers the adjoint ODEs

$$\begin{aligned}\frac{d\lambda_S}{dt} &= \left(\mu + \frac{\beta(t)}{N} I \right) \lambda_S - \frac{\beta(t)}{N} I \lambda_I, \\ \frac{d\lambda_I}{dt} &= \frac{\beta(t)}{N} S \lambda_S + \left((\alpha + \mu) - \frac{\beta(t)}{N} S \right) \lambda_I - \alpha \lambda_R - 2\gamma (\gamma I - I^d), \\ \frac{d\lambda_R}{dt} &= \mu \lambda_R, \\ 0 &= \lambda_S(T), \lambda_I(T), \lambda_R(T),\end{aligned}$$

and $\frac{\partial \mathcal{L}}{\partial \lambda_i} = 0$ leads to the ODEs in (5.1). In Simulation 2 the gradient of \mathcal{L} respect to u is given by

$$\begin{aligned}\frac{\partial \mathcal{L}}{\partial u_i} &= u_i \frac{2}{N^2} + \frac{1}{N} \int_0^T \frac{\partial \beta(t)}{\partial u_i} (\lambda_I(t) - \lambda_S(t)) S(t) I(t) dt, \quad i \in \{1, \dots, 5\}, \\ \frac{\partial \mathcal{L}}{\partial u_6} &= \gamma \frac{2}{N^2} + 2 \int_0^T I(t) (\gamma I(t) - I^d(t)) dt, \\ \frac{\partial \mathcal{L}}{\partial u_7} &= S_0 \frac{4}{N^2} + R_0 \frac{2}{N^2} - \frac{2}{N} + \lambda_S(0) - \lambda_I(0), \\ \frac{\partial \mathcal{L}}{\partial u_9} &= R_0 \frac{4}{N^2} + S_0 \frac{2}{N^2} - \frac{2}{N} + \lambda_R(0) - \lambda_I(0).\end{aligned}$$

u_8 is calculated by the substitution $I_0 = N - S_0 - R_0$. The *conjugate gradient method* combined with the *forward-backward sweep method* is applied to solve the optimization problem numerically until $\|J(u_{i+1}) - J(u_i)\| < 10^{-9}$ holds [3].

5.5 Results

In both simulations a time-scale t in years is applied, see Table 5.3. The values of the fixed parameters N, μ and α are extracted from statistics of the *WHO* [6].

The timing of the peaks fits to the behaviour in the data sets especially in Simulation 2 because of the phase shift φ . In Jakarta the model maps the relation between the yearly peaks whereby the inclusion of the rain data allows a more accurate dynamical behaviour. In Colombo the half-yearly varying oscillation proves more difficult to be reproduced though, the adding of the precipitation again improves the dynamics of the model. Comparing the absolute values of the fitted parameters in both locations we determine that similar results are achieved.

5.6 Acknowledgement

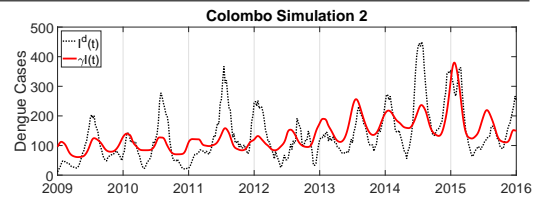
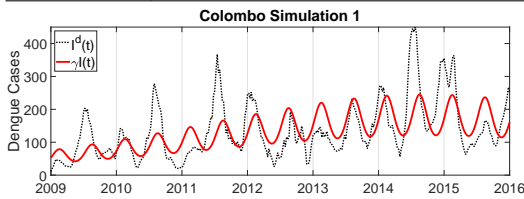
Peter Heidrich wants to thank the research fund of the University Koblenz–Landau for supporting the participation in the ECMI 2018 conference.

Table 5.3: Numerical and graphical results for Simulation 1 and 2 in Colombo and Jakarta.

Jakarta	β_0	β_1	c	τ_2	γ	φ	S_0	I_0	R_0
Sim. 1	38,6	6,0	/	/	1	/	$6,6 \cdot 10^6$	$6,0 \cdot 10^2$	$3,4 \cdot 10^6$
Sim. 2	51,6	14,7	17,0	9,0	0,45	9,2	$4,8 \cdot 10^6$	$1,2 \cdot 10^3$	$5,2 \cdot 10^6$
	N	μ	α	τ_1	ω				
Sim. 1	10^7	1/69	26	/	2π				
Sim. 2	10^7	1/69	26	4	2π				



Colombo	β_0	β_1	c	τ_2	γ	φ	S_0	I_0
Sim. 1	26,7	4,6	/	/	1	/	$1,3 \cdot 10^6$	$5,0 \cdot 10^1$
Sim. 2	37,2	-10,0	15,0	14,00	0,44	-4,0	$9,1 \cdot 10^5$	$2,1 \cdot 10^2$
	R_0	N	μ	α	τ_1	ω		
Sim. 1	$1,5 \cdot 10^4$	$1,3 \cdot 10^6$	1/75	26	/	4π		
Sim. 2	$3,9 \cdot 10^5$	$1,3 \cdot 10^6$	1/75	26	8	4π		



Bibliography

- [1] Aguiar, M.; Rocha, F.; Souza, M.; Stollenwerk, N.: *Time-scale separation and center manifold analysis describing vector-borne disease dynamics*. International Journal of Computer Mathematics, Vol. 90, pp 2105–2125, 2013
<https://doi.org/10.1080/00207160.2013.783208>
- [2] Aldila, D.: *Private Communication*. Department of Mathematics – University of Indonesia, Jakarta, 2017
- [3] Lenhart, S.; Workman, J.T.: *Optimal Control Applied to Biological Models*. CRC Press, 2007
- [4] Perrera, S.: *Private Communication*. Department of Mathematics – University of Colombo, Sri Lanka, 2016
- [5] Tikhonov, A.N.; Goncharsky, A.; Stepanov, V.V.; Yagola, A.G.: *Numerical Methods for the Solution of Ill-Posed Problems*. Springer Amsterdam, 2013
- [6] World Health Organization (WHO). Accessed 31 Aug 2018
<http://who.int>

Bibliography

6 Research Paper II: Simulation and Prediction of Dengue Outbreaks Based on an SIR Model with Time–Dependent Transmission Rate Including Meteorological Data. An Example for Colombo and Jakarta

Peter Heidrich Thomas Götz

The paper *Simulation and Prediction of Dengue Outbreaks Based on an SIR Model with Time–Dependent Transmission Rate Including Meteorological Data. An Example for Colombo and Jakarta* was accepted for publication on 31 January 2021 by *International Journal of Biomathematics, World Scientific*. It is a theoretical deepening of the proceeding presented in Chapter 5 and reviews the usability of the model for prediction. The layout of the paper is adapted to the present thesis.

The theoretical elaboration, calculations and writing were carried out by Peter Heidrich. Thomas Götz provided the ideas for the article and took over the linguistic revision of the text.

6.1 Abstract

Vector–borne diseases can usually be examined with a vector–host model like the *SIRUV* model. This, however, depends on parameters that contain detailed information about the mosquito population that we usually do not know. For this reason, in this article we reduce the *SIRUV* model to an *SIR* model with a time–dependent and periodic transmission rate $\beta(t)$. Since the living conditions of the mosquitos depend on the local weather conditions, meteorological data sets flow into the model in order to achieve a more realistic behaviour. The developed *SIR* model is adapted to existing data sets of hospitalized dengue cases in Jakarta (Indonesia) and Colombo (Sri Lanka) using numerical optimization based on Pontryagin’s maximum principle. A previous data analysis shows that the results of this parameter fit are within a realistic range and thus allow further investigations. Based on this, various simulations are carried out and the prediction quality of the model is examined.

Keywords: Dengue, Modelling, *SIR* model, Epidemiology, Numerical simulation, Parameter fit

6.2 Introduction

In 2017 a severe dengue outbreak was reported in Sri Lanka. According to the *World Health Organisation (WHO)* approximately 81.000 dengue fever cases are registered between 1 January and 30 June – more than 4 times the numbers compared to the same time period of the previous seven years [31].

Dengue is a mosquito–borne disease and a risk to approximately half the world’s population and we face between 100 to 400 million cases every year in more than 100 tropical and subtropical countries. First species of *Aedes* mosquitoes have been found to overwinter even in Central Europe [7]. The four serotypes of the dengue virus (DEN–1 to DEN–4) cause mostly just mild symptoms, however some cases progress to a severe dengue case (haemorrhagic fever) and may have lethal complications. Mosquitoes like the *Aedes aegypti* act as vectors for the disease. Female mosquitoes feed on human blood and may transfer the virus to a prior virus–free human or vice–versa. Once the virus enters into a human organism, it can be located in the blood for a period of up to one week. The incubation period ranges between 4 to 10 days [30]. During this period the patients develop first symptoms and the virus can be re–transmitted to other mosquitoes that feed on the blood of the infected human. Life long immunity against a single serotype is acquired, but cross–infections with another serotypes can increase the risk of a severe dengue progression.

The life–cycle of the vector mosquitoes depends on climatic conditions since spawning requires the availability of stagnant water or small puddles of water. Thus, regional rainfall, temperature and humidity are important factors. The progressing urbanization enhances the increase of impervious surfaces and hence dengue transmission on a larger scale. In our investigations we focus on the impact of meteorological factors for the two model regions *Colombo (Sri Lanka)* and *Jakarta (Indonesia)*. Thanks to private communication with local colleagues, we received data sets on recorded dengue cases in the local hospitals [1, 17]. Unfortunately, these data do not provide information on whether these cases are mild or severe, nor on the percentage of these hospitalized cases compared to unregistered cases. In order to take this fact into account, a *hospitalization rate* γ will be introduced in the following studies. The data sets are used to develop a mathematical model concerning dengue fever in order to use the results for prognosis or to integrate control variables such as vaccination.

Usually, vector–borne diseases are epidemiologically investigated with a vector–host model like the *SIRUV* model

$$\begin{aligned}\frac{dS}{dt} &= \mu(N - S) - \frac{\hat{\beta}}{M}SV, \\ \frac{dI}{dt} &= \frac{\hat{\beta}}{M}SV - (\alpha + \mu)I, \\ \frac{dR}{dt} &= \alpha I - \mu R, \\ \frac{dU}{dt} &= \psi - \nu U - \frac{\vartheta}{N}UI, \\ \frac{dV}{dt} &= \frac{\vartheta}{N}UI - \nu V,\end{aligned}$$

consisting of the *susceptible (S)*, *infected (I)* and *recovered humans (R)* and the *uninfected (U)* and *infected (V)* female mosquitos [15, 23, 24]. Since in our case there is no detailed

information about the mosquito population we reduce the model to an *SIR* model

$$\begin{aligned}\frac{dS}{dt} &= \mu(N - S) - \frac{\beta(t)}{N}SI, \\ \frac{dI}{dt} &= \frac{\beta(t)}{N}SI - (\alpha + \mu)I, \\ \frac{dR}{dt} &= \alpha I - \mu R.\end{aligned}$$

The system is reduced from five to three *ordinary differential equations (ODEs)* via time-scale separation and includes a time-dependent *transmission rate* $\beta(t)$. In order to fit the parameters of the model to the received data sets, we implement an *objective function*

$$J(u) = \int_{t_0}^{t_1} (\gamma I(t) - I^d(t))^2 dt + \frac{\|u\|^2}{N^2},$$

which shall be minimized. This optimization problem depends on $u \in \mathbb{R}^l$ – which includes the parameters that shall be fitted – and on the *ODEs* of the *SIR* model. To solve this *optimal control theory* constructed on *Pontryagin's maximum principle* is applied [14, 19] in order to reach the solution with numerical optimization methods. The results serve as a basis for different simulations concerning the behaviour of the dengue outbreaks. The parameter fit is also used to test the prediction quality of the model.

Also conceivable would be the addition of *exposed (E)* and *deaths (D) compartments* to the reduced *SIR* model. The latter would be particularly useful, if death records were available to fit a *lethality rate* within the model, see the example of COVID-19 in [11]. Especially in connection with a *multistrain model*, this would be profitable. A multistrain model takes into account the infections with the different virus strains and thus also the more severe course of the disease with repeated infections [29].

However, the aim of this paper is to simplify this process by using a reduced *SIR* model based on the *SIRUV* model to investigate the methods presented as a first step.

6.3 Data analysis

The available data consists of the weekly hospitalized dengue cases in *Colombo* (2009 – 2016) and the *Special Capital Region of Jakarta* (2009 – 2017) [1, 17].

According to the data sets in Jakarta, a total population $N_J = 10154584$ is assumed. With regard to the Colombo data, there is no information available whether the dengue cases refer only to the city or to the entire district. Therefore, we assume $N_C = 1538671$ as the mean value [3]. To reduce the noise in the data we smoothen it with a *moving average*. Each data point d_i is replaced by $\bar{d}_i = \frac{1}{4} \sum_{k=0}^3 d_{i-k}$ for all $i \geq 3$. In both cases a periodical behaviour with varying intensities concerning the peaks can be recognized. In Colombo we observe half-yearly repeating outbreaks in the midyear and at the turn of the year. The intensities of the peaks at midyear double from 2009 to 2011. In the time period between 2012 and 2014 we notice a similar behaviour. Compared to the middle of the year the peaks at the turn of the year irregularly vary. The dengue outbreaks in Jakarta appear yearly in the first quarter. The intensities of the peaks halve from 2009 to 2012, approximately remain on that level until 2015 and finally quadruple in 2016. The results of the *fast Fourier transform (FFT)* underpin the observed periodicities since significant high values at two frequencies per year in Colombo and one frequency per year in Jakarta can be noticed.

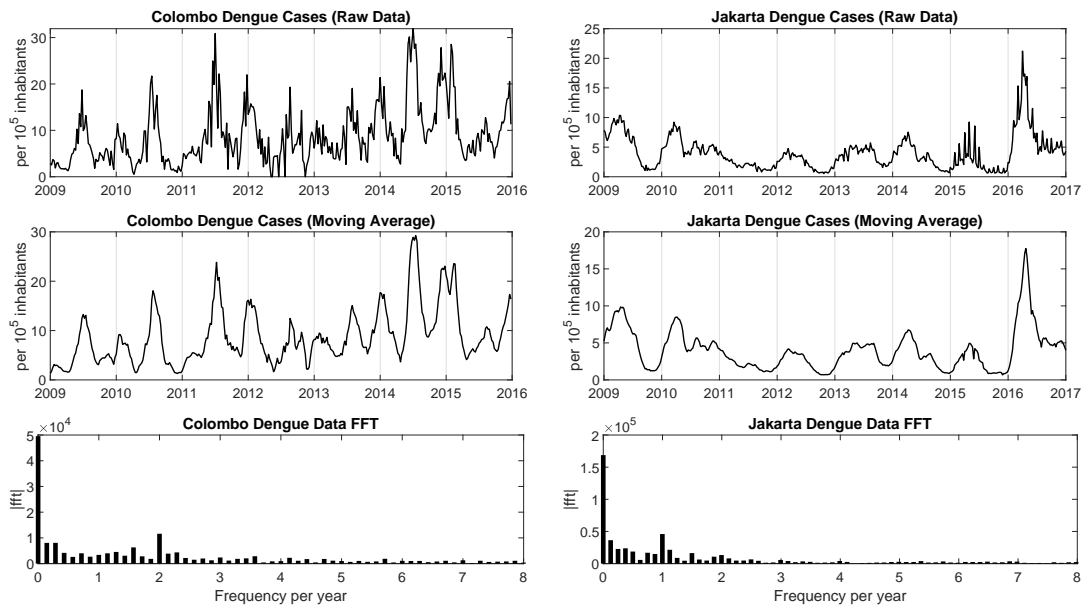


Figure 6.1: Dengue data from Colombo and Jakarta and results of the fast Fourier transform [20, 21]. The data sets are displayed per 100,000 inhabitants.

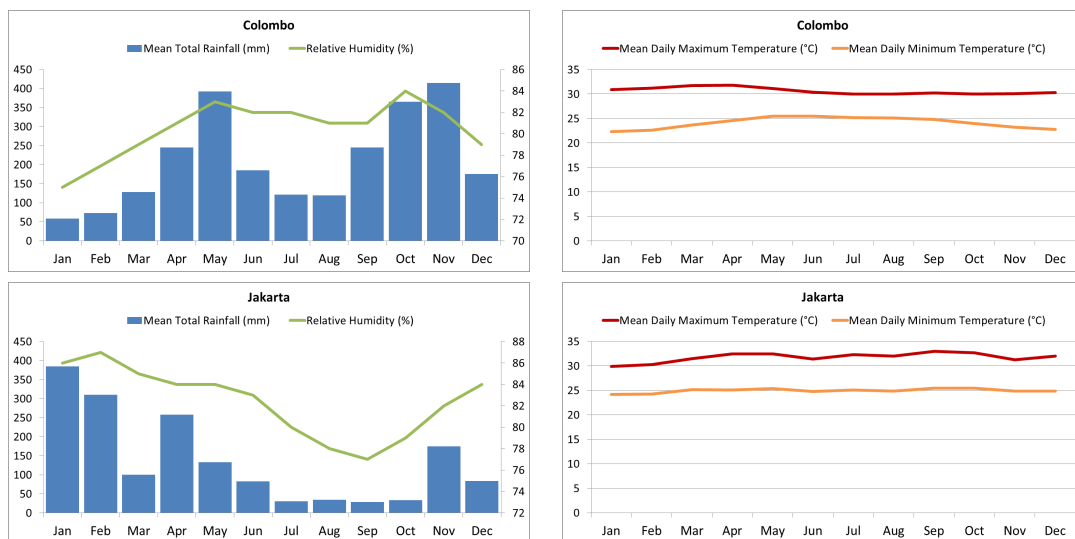


Figure 6.2: Annual weather data from Colombo and Jakarta [28, 33].

It is assumed that the periodical behaviour in the dengue data relates to the weather conditions especially to precipitation [10, 12]. The reproduction of the vectors depends on it since the mosquitos need small amounts of standing water to lay their eggs in. The annual weather data show similar periodicities for rainfall and humidity whereas the temperature is relative constant. In addition to the dengue data we received rainfall data sets p_i from Colombo and Jakarta in the appropriate time spans which are also smoothed using a moving average $\bar{p}_i = \frac{1}{4} \sum_{k=0}^3 p_{i-k}$. Likewise, here the *FFT* shows significant high values at two frequencies per year in Colombo and one frequency per year in Jakarta.

To substantiate the relation between rainfall and dengue data we use a cross-correlation and determine time lags around 6 weeks in Jakarta and 10 weeks in Colombo. Consequently, this means that after an intensive rain period it takes approximately two months until the dengue cases significantly rise. The *clusters* between precipitation and dengue data additionally show that if the average daily rainfall is stronger than approximately 10mm to 20mm a day, less dengue data points appear. Thus, we assume that in periods of very strong rainfall the eggs of the mosquitos are destroyed or washed away so that the reproduction of the vectors is restricted. In the following this border will be called *cut-off*.

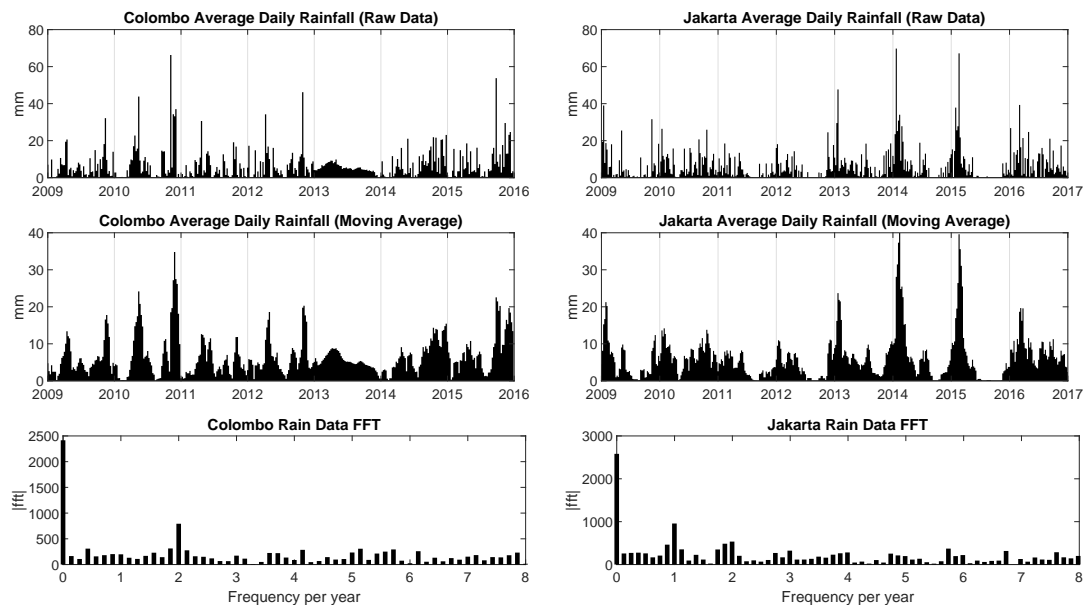


Figure 6.3: Rain data from Colombo and Jakarta and results of the fast Fourier transform.

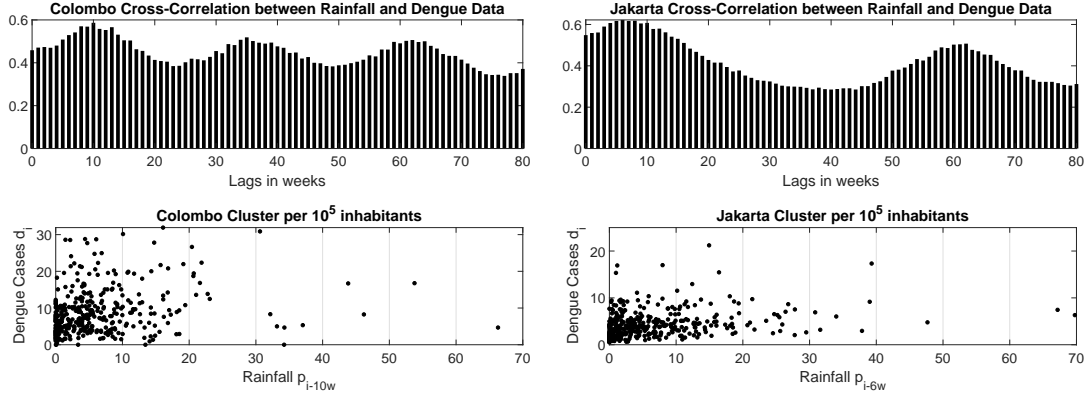


Figure 6.4: Cross-correlation and cluster between rain and dengue data.

6.4 The SIR model

The focus of this paper is an *SIR* model consisting of *susceptible* (S), *infected* (I) and *recovered* (R) humans

$$\frac{dS}{dt} = \mu(N - S) - \frac{\beta(t)}{N}SI, \quad S(t_0) = S_0 \geq 0, \quad (6.1a)$$

$$\frac{dI}{dt} = \frac{\beta(t)}{N}SI - (\alpha + \mu)I, \quad I(t_0) = I_0 \geq 0, \quad (6.1b)$$

$$\frac{dR}{dt} = \alpha I - \mu R, \quad R(t_0) = R_0 \geq 0, \quad (6.1c)$$

$$N = S + I + R. \quad (6.1d)$$

It applies that $S, I, R \in \mathcal{C}^1(\mathcal{D}, \mathbb{R})$ with $\mathcal{C}^n(X, Y) = \{f : X \rightarrow Y \mid f \text{ is } n \text{ times continuously differentiable in } X\}$ for $X, Y \subset \mathbb{R}$. In the following we set $\mathcal{D} = [t_0, t_1]$ and all investigations are performed for t in years. Since the *birth* and *death rate* μ are assumed to be equal and $\frac{dN}{dt} = 0$ applies, the total human population N is constant. The transition from infected to recovered individuals depends on the *recovery rate* α . The *incidence term* $\frac{\beta(t)}{N}SI$ describes the number of new infections at time t depending on a time-dependent *transmission rate* $\beta \in \mathcal{C}^1(\mathcal{D}, \mathbb{R})$. It is evident that explicit mosquito dynamics are not included although a vector-borne disease is modelled. A time-scale separation – as shown in Rocha et al. [23] – serves as theoretical principle, which shall be illustrated in the following section.

6.4.1 Time-scale separation

As approach we choose the present $SIRUV$ model

$$\frac{dS}{dt} = \mu(N - S) - \frac{\hat{\beta}}{M_0}SV, \quad S(t_0) = S_0 \geq 0, \quad (6.2a)$$

$$\frac{dI}{dt} = \frac{\hat{\beta}}{M_0}SV - (\alpha + \mu)I, \quad I(t_0) = I_0 \geq 0, \quad (6.2b)$$

$$\frac{dR}{dt} = \alpha I - \mu R, \quad R(t_0) = R_0 \geq 0, \quad (6.2c)$$

$$\frac{dU}{dt} = \psi(t) - \nu U - \frac{\vartheta}{N}UI, \quad U(t_0) = U_0 \geq 0, \quad (6.2d)$$

$$\frac{dV}{dt} = \frac{\vartheta}{N}UI - \nu V, \quad V(t_0) = V_0 \geq 0, \quad (6.2e)$$

$$N = S + I + R. \quad (6.2f)$$

In addition to human dynamics this ODE includes *uninfected* (U) and *infected* (V) mosquitos with $U, V, \psi \in \mathcal{C}^1(\mathcal{D}, \mathbb{R})$. Here, the function

$$\psi(t) = \nu M(t) + \chi \cos(\omega(t - t_M)) M(t)$$

describes the seasonal growth of the vector population whereby $M \in \mathcal{C}^1(\mathcal{D}, \mathbb{R})$ stands for the size of the mosquito population at time t . In addition, the equation $M(t) = U(t) + V(t)$ provides

$$\frac{dM}{dt} = \chi \cos(\omega(t - t_M)) M, \quad (6.3)$$

since $\frac{dM(t)}{dt} = \frac{dU(t)}{dt} + \frac{dV(t)}{dt} = \nu M(t) + \chi \cos(\omega(t - t_M)) M(t) - \nu U(t) - \nu V(t)$.

The ODE (6.3) can explicitly be solved by

$$M(t) = M_0 e^{\frac{\chi}{\omega} \sin(\omega(t - t_M))}, \quad (6.4)$$

whereby $M_0 = M(t_M) \geq 0$ stands for the initial condition. Furthermore, M_0 is related to the average size of the mosquito population given by

$$\bar{M} = M_0 \cdot \frac{1}{\omega} \int_0^\omega e^{\frac{\chi}{\omega} \sin(\tau)} d\tau. \quad (6.5)$$

Due to the periodicity, equation (6.5) is valid if time periods are considered over whole years. By adding (6.3) and using the substitutions $R(t) = N - S(t) - I(t)$ and $U(t) = M(t) - V(t)$ in (6.2) we receive an $SIVM$ model

$$\frac{dS}{dt} = \mu(N - S) - \frac{\hat{\beta}}{M_0}SV, \quad (6.6a)$$

$$\frac{dI}{dt} = \frac{\hat{\beta}}{M_0}SV - (\alpha + \mu)I, \quad (6.6b)$$

$$\frac{dV}{dt} = \frac{\vartheta}{N}(M - V)I - \nu V, \quad (6.6c)$$

$$\frac{dM}{dt} = \chi \cos(\omega(t - t_M)) M. \quad (6.6d)$$

Table 6.1: Assumed parameters of the *SIVM* model with t in years. For the constants c_k a magnitude of 10^0 is assumed, e.g. $c_k = 2$ for $k = 1, 2$.

Parameter	Meaning
$\mu = \frac{1}{70}$	Human death and birth rate (average life expectancy ≈ 70 years)
$\alpha = 26$	Human recovery rate (≈ 2 weeks)
$\hat{\beta} = c_1\alpha$	Transmission rate between infected vector and human (unknown)
$\nu = 26$	Mosquito death and birth rate (average life expectancy ≈ 2 weeks)
$\vartheta = c_2\nu$	Transmission rate between infected human and uninfected vector (unknown)
$N = 10^6$	Human population size (depends on investigated region)
$M_0 = 10N$	Average mosquito population size (unknown)
$\omega \in \{2\pi, 4\pi\}$	Periodical frequency of vector population
$\chi < \ln(2)\omega$	Intensity of periodical variation within mosquito population ($< 100\%$)

The magnitude of χ is assumed to be smaller than $\ln(2)\omega$ since

$$\max_{t \in \mathbb{R}} e^{\frac{\chi}{\omega} \sin(\omega(t-t_M))} = e^{\frac{\chi}{\omega}}$$

holds true and $\chi = \ln(2)\omega$ solves the equation

$$2M_0 = M_0 e^{\frac{\chi}{\omega}}.$$

Table 6.1 describes the parameters adopted for our research which are derived from statistics [4, 30]. In order to perform the time-scale separation we convert the *SIVM* model (6.6) into an *IVM* model

$$\frac{dI}{dt} = \frac{\hat{\beta}}{M_0} (N - I) V - (\alpha + \mu) I, \quad (6.7a)$$

$$\frac{dV}{dt} = \frac{\vartheta}{N} (M - V) I - \nu V, \quad (6.7b)$$

$$\frac{dM}{dt} = \chi \cos(\omega(t - t_M)) M. \quad (6.7c)$$

This is based on the functionality of an *SISUV* model in which the class of recovered individuals R is missing. Instead infected individuals I go directly into the class of susceptible individuals S . The recovery rate α now describes a much longer time period compared to the *SIRUV* model. Consequently, α changes in its order of magnitude and with it the transmission rate $\hat{\beta}$. At this point it should be noted that the investigation of a time-scale separation based on an *SISUV* model is presented here only for simplification and has the character of a toy problem. The much more complicated procedure with an *SIRUV* model, which is necessary for our approach, can be read in [26]. In our new system (6.7) a possible value for the recovery rate would be $\alpha = \frac{1}{10}$ [23]. After this adjustment the parameters of the human dynamics are now in a similar magnitude of 10^{-1} and the vector dynamics of 10^1 . Because of this the vector dynamic V acts much faster on the time-scale t compared to the human dynamics I . We consider the size ratio between the parameters of human and mosquito dynamics which can be expressed e.g. by

$$\varepsilon = \frac{\mu}{\nu} = \frac{1}{70 \cdot 26} = 5.5 \cdot 10^{-4}.$$

In addition, we define $\nu = \frac{\bar{\nu}}{\varepsilon}$ and $\vartheta = \frac{\bar{\vartheta}}{\varepsilon}$ which delivers $\bar{\vartheta} = \vartheta\varepsilon = \vartheta\frac{\bar{\nu}}{\nu}$ and provides

$$\frac{dI}{dt} = \frac{\hat{\beta}}{M_0} (N - I) V - (\alpha + \mu) I, \quad (6.8a)$$

$$\frac{dV}{dt} = \frac{1}{\varepsilon} \left(\frac{\bar{\vartheta}}{N} (M - V) I - \bar{\nu} V \right), \quad (6.8b)$$

$$\frac{dM}{dt} = \chi \cos(\omega(t - t_M)) M. \quad (6.8c)$$

This system depends not only on the time t , but also on the parameters and in particular ε . Consequently, the behavior of the solutions $I(t, \varepsilon)$ and $V(t, \varepsilon)$ must be investigated in dependence on very small ε . Therefore, we develop a power series around $\varepsilon = 0$ similar to the structure of a Taylor series with $I(t, 0) = I^{(0)}$ and $V(t, 0) = V^{(0)}$ as follows

$$\begin{aligned} I(t, \varepsilon) &= I^{(0)} + I^{(1)}\varepsilon + I^{(2)}\varepsilon^2 + \mathcal{O}(\varepsilon^3), \\ V(t, \varepsilon) &= V^{(0)} + V^{(1)}\varepsilon + V^{(2)}\varepsilon^2 + \mathcal{O}(\varepsilon^3). \end{aligned}$$

The derivations with respect to t deliver

$$\begin{aligned} \frac{dI(t, \varepsilon)}{dt} &= \frac{dI^{(0)}}{dt} + \frac{dI^{(1)}}{dt}\varepsilon + \mathcal{O}(\varepsilon^2), \\ \frac{dV(t, \varepsilon)}{dt} &= \frac{dV^{(0)}}{dt} + \frac{dV^{(1)}}{dt}\varepsilon + \mathcal{O}(\varepsilon^2), \end{aligned}$$

and we receive

$$\frac{dI(t, \varepsilon)}{dt} = \frac{\hat{\beta}}{M_0} (N - I^{(0)}) V^{(0)} - (\alpha + \mu) I^{(0)} + \mathcal{O}(\varepsilon^1), \quad (6.9a)$$

$$\frac{dV(t, \varepsilon)}{dt} = \frac{1}{\varepsilon} \left(\frac{\bar{\vartheta}}{N} (M - V^{(0)}) I^{(0)} - \bar{\nu} V^{(0)} \right) + \mathcal{O}(\varepsilon^0), \quad (6.9b)$$

$$\frac{dM}{dt} = \chi \cos(\omega(t - t_M)) M. \quad (6.9c)$$

Furthermore, we define a fast (mosquito) time-scale by $\tilde{t} = \frac{t}{\varepsilon}$ and calculate the derivations with respect to \tilde{t}

$$\frac{dI(t, \varepsilon)}{d\tilde{t}} = \varepsilon \frac{dI(t, \varepsilon)}{dt} = \varepsilon \underbrace{\left(\frac{\hat{\beta}}{M_0} (N - I^{(0)}) V^{(0)} - (\alpha + \mu) I^{(0)} \right)}_{\frac{dI^{(0)}}{d\tilde{t}}} + \mathcal{O}(\varepsilon^2), \quad (6.10a)$$

$$\frac{dV(t, \varepsilon)}{d\tilde{t}} = \varepsilon \frac{dV(t, \varepsilon)}{dt} = \underbrace{\left(\frac{\bar{\vartheta}}{N} (M - V^{(0)}) I^{(0)} - \bar{\nu} V^{(0)} \right)}_{\frac{dV^{(0)}}{d\tilde{t}}} + \mathcal{O}(\varepsilon^1), \quad (6.10b)$$

$$\frac{dM}{d\tilde{t}} = \varepsilon \chi \cos(\omega(t - t_M)) M. \quad (6.10c)$$

Comparing equal orders of ε in (6.10) in leading order $\mathcal{O}(\varepsilon^0)$ delivers

$$\begin{aligned} \frac{dI^{(0)}}{d\tilde{t}} &= 0, \\ \frac{dV^{(0)}}{d\tilde{t}} &= \frac{\bar{\vartheta}}{N} (M - V^{(0)}) I^{(0)} - \bar{\nu} V^{(0)}, \\ \frac{dM}{d\tilde{t}} &= 0. \end{aligned}$$

We conclude that $I^{(0)} \equiv I^{(0)}(\tilde{t}_0)$ and $M \equiv M(\tilde{t}_0)$ are approximately constant for very small values of ε on the fast time-scale \tilde{t} . From this we get the inhomogeneous ODE

$$\frac{dV^{(0)}}{d\tilde{t}} = - \underbrace{\left(\frac{\bar{\vartheta}}{N} I^{(0)}(\tilde{t}_0) + \bar{\nu} \right)}_a V^{(0)} + \underbrace{\frac{\bar{\vartheta}}{N} M(\tilde{t}_0) I^{(0)}(\tilde{t}_0)}_b,$$

which can explicitly be solved with $V_0 = V(\tilde{t}_0)$ by

$$V(t) = \exp\left(-a \frac{t - t_0}{\varepsilon}\right) \cdot \left(V_0 - \frac{b}{a}\right) + \frac{b}{a},$$

where \tilde{t} is replaced by $\frac{t}{\varepsilon}$ again. For $t \rightarrow \infty$ the solution achieves exponentially fast its *equilibrium* V^* because $\frac{a}{\varepsilon} \gg 1$

$$V^* = \frac{\frac{\bar{\vartheta}}{N} M(\tilde{t}_0) I^{(0)}(\tilde{t}_0)}{\frac{\bar{\vartheta}}{N} I^{(0)}(\tilde{t}_0) + \bar{\nu}}.$$

On the slow time-scale t we use $I^{(0)}(t_0) = I^{(0)}(\tilde{t}_0)$, $M(t_0) = M(\tilde{t}_0)$ and $V^{(0)}(t_0) = V^*$ as initial conditions. In equation (6.9b) the comparison of equal orders of ε in leading order $\mathcal{O}(\varepsilon^{-1})$ provides

$$0 = \frac{\bar{\vartheta}}{N} \left(M - V^{(0)} \right) I^{(0)} - \bar{\nu} V^{(0)}$$

and finally

$$V^{(0)} = \frac{\frac{\bar{\vartheta}}{N} M I^{(0)}}{\frac{\bar{\vartheta}}{N} I^{(0)} + \bar{\nu}}. \quad (6.11)$$

Consequently, in the human dynamics the expression $V^{(0)}$ can be substituted by (6.11) for small values of ε and we obtain

$$\frac{dI^{(0)}}{dt} = \frac{\hat{\beta}}{M_0} \left(N - I^{(0)} \right) \frac{\frac{\bar{\vartheta}}{N} M I^{(0)}}{\frac{\bar{\vartheta}}{N} I^{(0)} + \bar{\nu}} - (\alpha + \mu) I^{(0)}.$$

Since $I^{(0)} \ll N$ and $\bar{\vartheta} \ll 1$ the expression $\frac{\bar{\vartheta}}{N} I^{(0)}$ can be neglected in the denominator which means that

$$\frac{\frac{\bar{\vartheta}}{N} M I^{(0)}}{\frac{\bar{\vartheta}}{N} I^{(0)} + \bar{\nu}} \approx \frac{\frac{\bar{\vartheta}}{N} M I^{(0)}}{\bar{\nu}}.$$

We define a time-dependent transmission rate

$$\beta(t) = \hat{\beta} \frac{\bar{\vartheta}}{M_0 \bar{\nu}} M(t) = \frac{\hat{\beta} \bar{\vartheta}}{\nu} e^{\frac{\chi}{\omega} \sin(\omega(t-t_M))}$$

and finally obtain

$$\frac{dI^{(0)}}{dt} = \frac{\beta(t)}{N} \left(N - I^{(0)} \right) I^{(0)} - (\alpha + \mu) I^{(0)}. \quad (6.12)$$

Using the substitutions $\beta_0 = \frac{\hat{\beta} \bar{\vartheta}}{\nu}$ and $\beta_1 = \frac{\chi}{\omega}$ delivers

$$\beta(t) = \beta_0 e^{\beta_1 \sin(\omega(t-t_M))} \approx \beta_0 (1 + \beta_1 \sin(\omega(t-t_M))). \quad (6.13)$$

The procedure shown illustrates the idea of the incidence term in our *SIR* model in (6.1). It should be noted that we reduced the number of the four unknown parameters M_0 , $\hat{\beta}$, χ and ϑ to β_0 and β_1 .

6.4.2 Alternative derivation of $\beta(t)$

In the following, an alternative derivation of the incidence term is outlined based on considerations using probabilities [15]. Again we assume that the size of the mosquito population at time t can be approximated with $M(t) = M_0 e^{\frac{\chi}{\omega} \sin(\omega(t-t_M))}$. Let κ be the per capita *contact rate* per unit of time between a human individual and mosquitos. If we assume that the number of contacts until time t behaves proportional to the size of the mosquito population, then $\kappa \int_{t_0}^t M(\tau) d\tau$ describes the number of contacts a human individual had with vectors until time t and $\frac{d}{dt} \kappa \int_{t_0}^t M(\tau) d\tau = \kappa M(t)$ the number of contacts per unit of time. For example with a constant vector population M_0 the number of contacts until time t is described by $\kappa M_0(t - t_0)$ and the number of contacts per unit of time by κM_0 . If we use the probabilities in Table 6.2 as a basis the incidence term of

Table 6.2: Probabilities to transmit the disease when a human comes into contact with a mosquito.

Value	Meaning
ρ_1	Probability that a vector had a blood meal from a human
$\frac{I}{N}$	Probability that the blood meal was from an infected human
ρ_2	Probability that the disease was transmitted to the vector
ρ_3	Probability that a contact with an infected vector leads to a transmission
$\rho = \rho_1 \frac{I}{N} \rho_2 \rho_3$	Probability of disease transmission in contact with a vector

new infections per unit of time with S susceptible individuals can be expressed by

$$\kappa M(t) \cdot \rho \cdot S = \frac{\kappa M(t) \rho_1 \rho_2 \rho_3}{N} S I.$$

Here, $\kappa M(t) \rho$ stands for the expected number of transmissions at $\kappa M(t)$ contacts per unit of time for one human individual.

The time-dependent transmission rate is described by

$$\beta(t) = \kappa M(t) \rho_1 \rho_2 \rho_3 = \kappa M_0 \rho_1 \rho_2 \rho_3 e^{\frac{\chi}{\omega} \sin(\omega(t-t_M))},$$

which complies with

$$\beta(t) = \beta_0 e^{\beta_1 \sin(\omega(t-t_M))} \approx \beta_0 (1 + \beta_1 \sin(\omega(t-t_M))), \quad (6.14)$$

using the substitutions $\beta_0 = \kappa M_0 \rho_1 \rho_2 \rho_3$ and $\beta_1 = \frac{\chi}{\omega}$. Again we receive an approach for the incidence term of our *SIR* model in (6.1).

6.5 Data fit analysis

Let be $I^C, I^J \in \mathcal{C}^1(\mathcal{D}, \mathbb{R})$ whereby I^C includes the smoothed dataset from Colombo and I^J from Jakarta. In order to fit the number of infected individuals I to the dengue data set $I^d \in \{I^C, I^J\}$, we analyze an *objective function* $J \in \mathcal{C}^1(\mathbb{R}^l, \mathbb{R})$ and the *minimization problem*

$$\min_u J(u) = \min_u \int_{t_0}^{t_1} (\gamma I(t) - I^d(t))^2 dt + \frac{\|u\|^2}{N^2} \quad (6.15a)$$

subject to

$$\frac{dS}{dt} = \mu(N - S) - \frac{\beta(t)}{N}SI, \quad S(t_0) = S_0 \geq 0, \quad (6.15b)$$

$$\frac{dI}{dt} = \frac{\beta(t)}{N}SI - (\alpha + \mu)I, \quad I(t_0) = I_0 \geq 0, \quad (6.15c)$$

$$\frac{dR}{dt} = \alpha I - \mu R, \quad R(t_0) = R_0 \geq 0, \quad (6.15d)$$

$$N = S + I + R. \quad (6.15e)$$

It is assumed that only a fraction of infected individuals is registered or hospitalized, therefore we implement γ as *hospitalization rate* [30]. Although γ is independent of units, in the following we refer to this as a rate. The term $\int_{t_0}^{t_1} (\gamma I(t) - I^d(t))^2 dt \geq 0$ becomes small, if γI is fitted to I^d .

In (6.15) we consider a least squares method, based on a L^2 norm. The convex and radially unbounded *control term* $\|u\|^2/N^2$ has direct influence on the definiteness of the *Hessian matrix* and represents a kind of *Tikhonov regularization* [27]. Due to the weighting with $1/N^2$ its influence on the minimization is negligible compared to the integral $\int_{t_0}^{t_1} (\gamma I(t) - I^d(t))^2 dt$.

The vector $u \in \mathbb{R}^l$ includes the initial conditions of the ODE S_0 and R_0 the hospitalization rate γ and the unknown parameters of the transmission rates $\beta(t)$, see Table 6.3.

Table 6.3: Utilized transmission rates $\beta(t)$ and corresponding parameters in Simulation 1 and 2.

Simulation 1	Simulation 2
$\beta(t) = \beta_0 + \beta_1 \sin(\omega(t + \varphi/52))$	$\beta(t) = \beta_0 + \beta_1 \int_{t-\eta_2/52}^{t-\eta_1/52} p_c(\tau) d\tau \cdot \sin(\omega(t + \varphi/52))$
$u = (\beta_0, \beta_1, \varphi, \gamma, S_0, R_0)^T$	$u = (\beta_0, \beta_1, c, \eta_2, \varphi, \gamma, S_0, R_0)^T$

Here β_0 stands for the *average transmission rate* and $\beta_1 \int_{t-\eta_2/52}^{t-\eta_1/52} p_c(\tau) d\tau$ in Simulation 2, respectively β_1 in Simulation 1, for the *degree of periodical variation*. A *phase-shift* φ in weeks is included which corresponds to $-t_M$ in (6.4). The precipitation function $p_c(\tau)$ is defined by

$$p_c(\tau) = \begin{cases} p(\tau), & p(\tau) < c \\ 0, & p(\tau) \geq c. \end{cases} \quad (6.16)$$

Here, $p(\tau) \in \mathcal{C}^1(\mathcal{D}, \mathbb{R})$ includes the smoothed rainfall data points \bar{p}_i and c represents the *cut-off*. As described in Section 6.3, it is assumed that extremely heavy rainfall destroys the mosquito eggs and disrupts population growth. For this reason, p_c is set to zero in this case, so that $\beta(t) = \beta_0$ applies at this time point. The interval $[t - \eta_2/52, t - \eta_1/52]$ is set around the time lag between precipitation and dengue data. Thus, in Colombo $[t - 11/52, t - 9/52]$ is a possible choice, due to the corresponding time lag of 10 weeks.

The transmission rate $\beta(t)$ directly influences the so-called *Basic Reproduction Number*

$$\mathcal{R}_0(t) = \frac{\beta(t)}{\alpha + \mu}, \quad (6.17)$$

which indicates how many new infections an infected person causes on average during his illness in an otherwise susceptible population. It should be noted that in our case this is time-dependent due to the transmission rate.

To solve the optimization problem with a *Lagrange function* $\mathcal{L} : \mathbb{R}^l \times \mathcal{C}^1(\mathcal{D}, \mathbb{R}^6) \rightarrow \mathbb{R}$ we implement *adjoint functions* $\lambda_S, \lambda_I, \lambda_R \in \mathcal{C}^1(\mathcal{D}, \mathbb{R})$ as *Lagrange multipliers*. In order to simplify the notation we define the functions $x, \lambda \in \mathcal{C}^1(\mathcal{D}, \mathbb{R}^3)$ with $x = (S, I, R)^T$, $\lambda = (\lambda_S, \lambda_I, \lambda_R)^T$ and $g : \mathcal{D} \times \mathcal{C}^1(\mathcal{D}, \mathbb{R}^3) \times \mathbb{R}^l \rightarrow \mathbb{R}$ with $g = (g_S, g_I, g_R)^T$ whereby g_S, g_I and g_R symbolize the right sides of the ODEs in (6.15). Finally, the Lagrange function is defined by

$$\mathcal{L}(u, x, \lambda) = \int_{t_0}^{t_1} (\gamma I(t) - I^d(t))^2 dt + \frac{\|u\|^2}{N^2} + \int_{t_0}^{t_1} \lambda(t)^T \left(g(t, x(t), u) - \frac{dx(t)}{dt} \right) dt. \quad (6.18)$$

The *necessary optimality condition* for a *critical point* (u^*, x^*, λ^*) is fulfilled if

$$\nabla \mathcal{L}(u^*, x^*, \lambda^*) = 0. \quad (6.19)$$

Here, x^* and λ^* represent the *state* and *adjoint functions* which belong to u^* .

In the following, the results refer to $\beta(t)$ in Simulation 2, see Table 6.3. The analysis in this regard can be found in the Appendix 6.A. From there we get the gradient

$$\nabla_u \mathcal{L}(u, x, \lambda) = \nabla J(u)$$

of the Lagrange function with respect to the directions of u

$$\begin{aligned} \frac{\partial \mathcal{L}(u, x, \lambda)}{\partial u_i} &= u_i \frac{2}{N^2} + \frac{1}{N} \int_{t_0}^{t_1} \frac{\partial \beta(t)}{\partial u_i} (\lambda_I(t) - q \lambda_S(t)) S(t) I(t) dt, \\ &\quad i = 1, \dots, 5, \\ \frac{\partial \mathcal{L}(u, x, \lambda)}{\partial u_6} &= \gamma \frac{2}{N^2} + 2 \int_{t_0}^{t_1} I(t) (\gamma I(t) - I^d(t)) dt, \\ \frac{\partial \mathcal{L}(u, x, \lambda)}{\partial u_7} &= S_0 \frac{2}{N^2} + \lambda_S(t_0) - \lambda_I(t_0), \\ \frac{\partial \mathcal{L}(u, x, \lambda)}{\partial u_8} &= R_0 \frac{2}{N^2} + \lambda_R(t_0) - \lambda_I(t_0). \end{aligned}$$

The partial derivatives of $\beta(t) = \beta_0 + \beta_1 \int_{t-\eta_2/52}^{t-\eta_1/52} p_c(\tau) d\tau \sin(\omega(t + \varphi/52))$ are given by

$$\begin{aligned} \frac{\partial \beta(t)}{\partial \beta_0} &= 1, \\ \frac{\partial \beta(t)}{\partial \beta_1} &= \int_{t-\eta_2/52}^{t-\eta_1/52} p_c(\tau) d\tau \sin(\omega(t + \varphi/52)), \\ \frac{\partial \beta(t)}{\partial c} &= \begin{cases} 0, & \text{if } p(\tau) < c \text{ or } p(\tau) \geq c \text{ for all } \tau \in [t - \eta_2/52, t - \eta_1/52] \\ c \left(\sum_{i=0}^n \frac{1}{\frac{dp(b_i)}{d\tau}} - \sum_{i=0}^m \frac{1}{\frac{dp(a_i)}{d\tau}} \right) \beta_1 \sin(\omega(t + \varphi/52)), & \text{else,} \end{cases} \\ &\quad a_i < b_i < a_{i+1} < b_{i+1} \text{ with } a_i, b_i \in p^{-1}(c), \\ \frac{\partial \beta(t)}{\partial \eta_2} &= \frac{p_c(t - \eta_2/52)}{52} \beta_1 \sin(\omega(t + \varphi/52)), \\ \frac{\partial \beta(t)}{\partial \varphi} &= \frac{\omega \cos(\omega(t + \varphi/52))}{52} \beta_1 \int_{t-\eta_2/52}^{t-\eta_1/52} p_c(\tau) d\tau. \end{aligned}$$

Equation (6.19) is solved respect to the directions of x using *Gâteaux derivatives* [8]. This leads to the ODEs of the adjoint functions

$$\frac{d\lambda_S}{dt} = \left(\mu + \frac{\beta(t)}{N}I \right) \lambda_S - \frac{\beta(t)}{N}I\lambda_I, \quad (6.20a)$$

$$\frac{d\lambda_I}{dt} = \frac{\beta(t)}{N}S\lambda_S + \left((\alpha + \mu) - \frac{\beta(t)}{N}S \right) \lambda_I - \alpha\lambda_R - 2\gamma(\gamma I - I^d), \quad (6.20b)$$

$$\frac{d\lambda_R}{dt} = \mu\lambda_R. \quad (6.20c)$$

Additionally, we receive the so-called *transversality conditions*, known from Pontryagin's maximum principle [19]

$$\begin{aligned} \lambda_S(t_1) &= 0, \\ \lambda_I(t_1) &= 0, \\ \lambda_R(t_1) &= 0. \end{aligned}$$

Since the optimization problem depends on the adjoint functions these ODEs need to be calculated. In the case of $\lambda_R(t)$ this can be done analytically by

$$\lambda_R(t) = \lambda_R(t_0)e^{\mu t}.$$

As $\lambda_R(t_1) = 0$ it follows that

$$0 = \lambda_R(t_1) = \lambda_R(t_0)e^{\mu t_1}$$

and thus $\lambda_R(t_0) = 0$ because $e^{\mu t_1} \neq 0$. Consequently we obtain

$$\lambda_R(t) \equiv 0.$$

Solving (6.19) respect to the directions of λ via Gâteaux derivatives delivers the state variable ODEs

$$\frac{dS}{dt} = \mu(N - S) - \frac{\beta(t)}{N}SI, \quad (6.21a)$$

$$\frac{dI}{dt} = \frac{\beta(t)}{N}SI - (\alpha + \mu)I, \quad (6.21b)$$

$$\frac{dR}{dt} = \alpha I - \mu R. \quad (6.21c)$$

If (u^*, x^*, λ^*) is a minimum of $\mathcal{L}(u, x, \lambda)$, it follows that

$$J(u^*) = \mathcal{L}(u^*, x^*, \lambda^*) \leq \mathcal{L}(u, x, \lambda) = J(u)$$

for all admissible solutions (u, x, λ) which preoccupy the state variable ODEs in (6.21). Examining whether the *sufficient condition* is satisfied in (u^*, x^*, λ^*) is extensive because the *Hessian matrix* of $\mathcal{L}(u, x, \lambda)$ needs to be investigated. However, at this point it is noted that for (u^*, x^*, λ^*) a maximum of the objective function is excluded since $J(u)$ is bounded from below and unbounded from above.

6.6 Results

The optimization can be solved numerically using the *forward-backward sweep method* combined with a *Quasi-Newton (BFGS)* or (*Conjugate*) *Gradient* algorithm. The step size determination is performed with a *backtracking* method using the *Armijo* rule [2, 5, 6, 9, 14, 16, 18, 25]. The procedure stops when $\|J_{n+1} - J_n\|_2 < \text{TOL}$ is fulfilled. The detailed procedures of the algorithm used are shown in the pseudocode in Appendix 6.B. Compared to (6.15), a slightly modified objective function J is used in the program

$$J(u) = \frac{1}{\max_{t \in \mathcal{D}} I^d} \int_{t_0}^{t_1} (\gamma I(t) - I^d(t))^2 dt + \frac{\|u\|^2}{N^2}.$$

Fixed parameters like the recovery rate, average human life expectancy and total population sizes in the respective regions are derived from statistics and the received data sets [1, 3, 17, 30, 32].

6.6.1 Numerical results of the parameter fit

In the following section the data fit without direct influence of rain data is called Simulation 1 and Simulation 2 includes the rain data. The results of the parameter fit are presented in Tables 6.6 and 6.7.

First we compare the results of the simulations in the respective locations. All parameters except β_1 can be compared directly. In both cases the order of magnitude of the fitted parameters is the same, i.e. the addition of the weather data in Simulation 2 does not fundamentally change the results. In Jakarta and Colombo this addition causes an optimization of the objective function J by about 11–13%. Due to the adjustment of the phase shift φ the timing of the extrema and turning points in γI fits in most cases to the corresponding peaks in the data sets I^d . For example, this can be seen in Jakarta 2012 and 2017 and in Colombo 2013–14. The addition of the rain data causes an increase of the dynamics within the model whereby detailed fluctuations are reflected within the respective seasons, e.g. in Jakarta in 2009 and 2013 or Colombo in 2012 and 2014. Especially in Jakarta, the ratio of the peaks to each other is well reflected. Concerning Colombo, this only applies to certain years. The reason for this could be that due to the very large fluctuations, a shorter period of time would be more effective for the parameter fit.

In the following we compare the results between Jakarta and Colombo. In Simulation 1 the fitted parameters hardly differ from each other in both locations. In Simulation 2 the values are also in a similar order of magnitude but slightly larger deviations can be detected. This is caused by the different weather conditions which influence the development of the local mosquito populations and thus the spread of the disease. The size of the cut-off parameter c is in a realistic range with about 16mm in Jakarta and 10mm in Colombo. The same applies to the adjustment of the integration limit depending on η_2 whose values with 7 weeks in Jakarta and 10 weeks in Colombo match the corresponding timelags between rain and dengue dates, see Figure 6.4. The hospitalization rate γ is also in a realistic range with about 30% in both regions. To compare the degree of periodical variation we examine the size of the term

$$\beta_1 \int_{t-\frac{\eta_2}{52}}^{t-\frac{\eta_1}{52}} p_c(\tau) d\tau < \beta_1 \cdot \frac{\eta_2 - \eta_1}{52} \cdot c =: \tilde{\beta}_1. \quad (6.22)$$

We get $\tilde{\beta}_1 = 24.91$ for Jakarta and $\tilde{\beta}_1 = 14.49$ for Colombo.

Table 6.4: Relation between the degree of periodical variation and average transmission rate in Simulation 1 and 2.

	Jakarta	Colombo
Simulation 1: β_1/β_0	0.16	0.22
Simulation 2: $\tilde{\beta}_1/\beta_0$	0.46	0.44

Table 6.4 shows that the relationship between periodical variation and the average transmission rate leads to similar results in Jakarta and Colombo. These also allow conclusions about the behavior of the mosquito population. Provided the size of the vector population can be modeled by $M(t) = M_0 e^{\frac{\chi}{\omega} \sin(\omega(t+\varphi/52))}$, the term

$$e^{\frac{\chi}{\omega} \sin(\omega(t+\frac{\varphi}{52}))} \approx 1 + \frac{\chi}{\omega} \sin\left(\omega\left(t + \frac{\varphi}{52}\right)\right)$$

describes the seasonal variation of the mosquito population. As shown in Section 6.4 in Simulation 1 the fraction $\frac{\beta_1}{\beta_0}$ approximately corresponds to the size of the expression $\frac{\chi}{\omega}$. Since $|\frac{\chi}{\omega} \sin(\omega(t+\varphi/52))| \leq 0.22$ applies for $\frac{\chi}{\omega} = \frac{\beta_1}{\beta_0}$, we can conclude that the size of the mosquito population varies by a maximum of approximately 25%. In Simulation 2 the term

$$\frac{\beta_1}{\beta_0} \int_{t-\frac{\eta_2}{52}}^{t-\frac{\eta_1}{52}} p_c(\tau) d\tau < \frac{\tilde{\beta}_1}{\beta_0}$$

corresponds to a time-dependent expression $\frac{\chi(t)}{\omega}$ with $\chi: \mathcal{D} \rightarrow \mathbb{R}_0^+$. Using the result from Table 6.4 we get $|\frac{\chi(t)}{\omega} \sin(\omega(t+\varphi/52))| < 0.46$ and consequently a variation of at most about 50%.

The transmission rate graphs show the periodicity associated with the dynamics within disease transmission, see Tables 6.6–6.7. The influence of the cut-off parameter c is clearly visible. Using the values for β_0 and β_1 respectively $\tilde{\beta}_1$, restricting intervals for the Basic Reproduction Number $\mathcal{R}_0(t)$ can now be determined from equation (6.17), see Table 6.5.

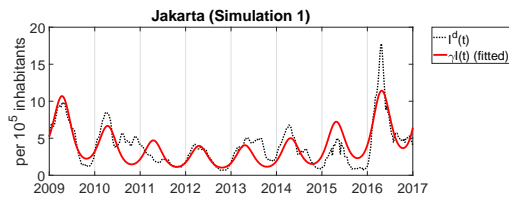
Table 6.5: Limiting intervals to the order of magnitude of the Basic Reproduction Number $\mathcal{R}_0(t) = \beta(t)/\alpha + \mu$ in Jakarta and Colombo.

	Jakarta	Colombo
Simulation 1	[1.5, 2.1]	[1.4, 2.2]
Simulation 2	[1.1, 3.0]	[0.7, 1.8]

It can be seen that in Simulation 1 very similar limits exist for both locations. However, there are larger differences in the second simulation. It is also noticeable here that in Colombo the value can temporarily fall below the barrier $\mathcal{R}_0 = 1$ with maximum fluctuations.

Table 6.6: Results of Simulation 1 and 2 based on the data sets from Jakarta. The total population size is assumed to be $N = 10154584$. The following parameters are fixed: $\alpha, \mu, \omega, \eta_1$.

Parameters	β_0	β_1	c	η_2	φ	γ	α	μ	ω	η_1
Simulation1	46.71	7.47	/	/	10.41	0.26	26	1/69	2π	/
Simulation2	54.01	84.69	15.77	6.97	9.12	0.34	26	1/69	2π	6



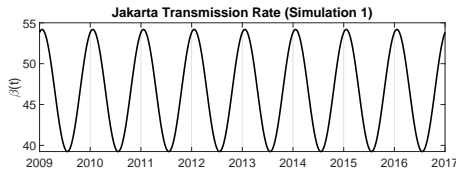
$$S_0 = 5552245 \quad I_0 = 2079$$

$$R_0 = 4600260 \quad J = 114.13$$

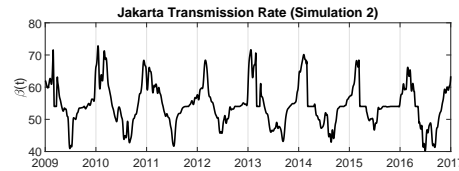


$$S_0 = 4652792 \quad I_0 = 1772$$

$$R_0 = 5500020 \quad J = 102.63$$



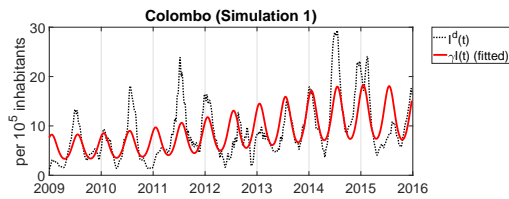
$$\beta(t) = \beta_0 + \beta_1 \sin(\omega(t + \varphi/52))$$



$$\beta(t) = \beta_0 + \beta_1 \int_{t-\frac{\eta_2}{52}}^{t-\frac{\eta_1}{52}} p_c(\tau) d\tau \sin(\omega(t + \frac{\varphi}{52}))$$

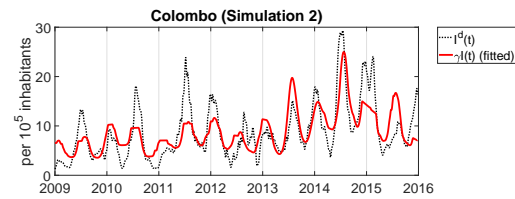
Table 6.7: Results of Simulation 1 and 2 based on the data sets from Colombo. The total population size is assumed to be $N = 1538671$. The following parameters are fixed: $\alpha, \mu, \omega, \eta_1$.

Parameters	β_0	β_1	c	η_2	φ	γ	α	μ	ω	η_1
Simulation1	47.71	10.39	/	/	10.60	0.37	26	$1/75$	4π	/
Simulation2	32.54	99.64	9.45	9.80	9.35	0.33	26	$1/75$	4π	9



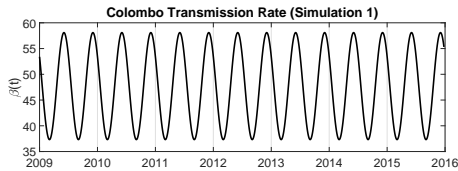
$$S_0 = 838311 \quad I_0 = 321$$

$$R_0 = 700039 \quad J = 63.80$$

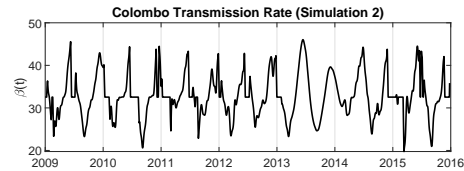


$$S_0 = 1238470 \quad I_0 = 302$$

$$R_0 = 299899 \quad J = 55.44$$



$$\beta(t) = \beta_0 + \beta_1 \sin(\omega(t + \varphi/52))$$



$$\beta(t) = \beta_0 + \beta_1 \int_{t-\frac{\eta_2}{52}}^{t-\frac{\eta_1}{52}} p_c(\tau) d\tau \sin(\omega(t + \frac{\varphi}{52}))$$

6.6.2 Prediction quality of the model

With regard to the intention to use control methods to reduce the spread of disease, the predictive quality of the model plays a major role. In the following, the parameters included in $u = (\beta_0, \beta_1, c, \eta_2, \varphi, \gamma, S_0, R_0)^T$ are fitted up to a time $\hat{t} \in \mathcal{D}$. The model subsequently uses these parameters and makes a prediction to the end time t_1 . In Simulation 3 we use the available rain data and in Simulation 4 the average rainfall data of previous years within the prognosis interval, see Tables 6.9 and 6.10. To give more weight to current than to past data we introduce a weight function $H : \mathcal{D} \rightarrow \mathbb{R}^+$ with

$$H(t) = w \cdot \exp\left(-\frac{(t - \hat{t})^2}{2\sigma^2}\right) + z.$$

The parameters $w = 50$, $\sigma = \frac{4}{52}$ and $z = 1$ are selected so that the period of the last four weeks before \hat{t} is weighted considerably more strongly. Hence, we solve the minimization problem

$$\min_u J(u) = \min_u \frac{1}{\max_{t \in \mathcal{D}} I^d} \int_{t_0}^{\hat{t}} H(t) (\gamma I(t) - I^d(t))^2 dt + \left(\frac{\|u\|}{N}\right)^2.$$

In the following simulations the end time \hat{t} of the parameter fit is chosen so that in the previous 4–8 weeks the number of dengue cases increased significantly. In practice, this optimization should be constantly updated. Additionally we calculate based on the L^1 norm

$$\mathcal{E}_1 = \int_{\hat{t}}^{\hat{t}+1} \frac{|\gamma I(t) - I^d(t)|}{\max_{t \in [\hat{t}, \hat{t}+1]} I^d(t)} dt \quad \text{and} \quad \mathcal{E}_2 = \frac{1}{t_1 - \hat{t}} \int_{\hat{t}}^{t_1} \frac{|\gamma I(t) - I^d(t)|}{\max_{t \in [\hat{t}, t_1]} I^d(t)} dt$$

and additionally in Colombo

$$\mathcal{E}_3 = 2 \int_{\hat{t}}^{\hat{t}+1/2} \frac{|\gamma I(t) - I^d(t)|}{\max_{t \in [\hat{t}, \hat{t}+1/2]} I^d(t)} dt.$$

These values are used to determine the deviation of the model in relation to the corresponding maximum value within the data. Although the forecast for the coming season is in the foreground, the model also reveals tendencies in the following years.

In Jakarta, the respective forecasts for the following year apply well to both simulations. The relation of the predicted peak to the previous one is accurately reflected. The course of the following years is also determined by the model. In some years the forecasts for the coming season are slightly better with the average rain data of the previous years in Simulation 4 than with the actual ones. However, the long-term predictions clearly show better results with the real rain data, see Tables 6.8 and 6.9. In comparison, the simulations in Colombo show greater difficulties in making accurate forecasts. It is noticeable that the model in the shortened time periods $[t_0, \hat{t}]$ of the parameter fit can be better adapted to the dengue data than over the full time scale \mathcal{D} , e.g. for $\hat{t} = 2013 - 1\text{week}$. Due to the half-yearly frequency of the peaks and their strongly fluctuating intensities, the forecasts for the coming half-year are much better than for the entire following year or even the following years. The half-yearly short-term predictions provide useful values which reflect the correct relation to the previous dengue eruptions. Beyond this period, the model becomes inaccurate, e.g. for $\hat{t} = 2012 - 1\text{week}$. In terms of short-term forecasting, the actual rainfall data in Simulation 3 delivers better results. In contrast, the long-term prediction is better with the averaged rain data in Simulation 4, see Tables 6.8 and 6.10. The t -test concerning the residuals $r = \gamma I - I^d$ shows in Jakarta as well as in Colombo that r is not normally distributed $\mathcal{N}(0, \sigma^2)$ in most cases [22].

Table 6.8: Medians of the numerical deviations between model and dengue data.

	Simulation 3		Simulation 4	
	Jakarta	Colombo	Jakarta	Colombo
$\tilde{\mathcal{E}}_1$	0.22	0.26	0.22	0.19
$\tilde{\mathcal{E}}_2$	0.24	0.27	0.63	0.23
$\tilde{\mathcal{E}}_3$	/	0.23	/	0.24

6.7 Conclusions

The present paper shows that an *SIR* model with a time-dependent transmission rate represents a practicable alternative to the usual *SIRUV* model. Especially with regard to the adaptation of unknown parameters based on real data sets, the strength of this reduced system is evident, since missing information on the corresponding mosquito population is no longer an obstacle. However, the results obtained do allow conclusions to be drawn about the periodic fluctuations within the vector populations. The parameter fit depends strongly on the quality of the collected data sets. The addition of weather data shows that the local precipitation has a considerable influence on the periodic outbreaks of dengue. It has also been shown that the *SIR* model is particularly suitable for short-term forecasts, in the case of Jakarta even for longer periods. A useful application is when the system is constantly updated with data to adjust the parameters perpetually. In return, the fitting period should not be too long, as the spread of the disease can only be simulated meaningfully over short periods of time with such a model. The prediction of the intensity of the next dengue outbreak offers the possibility to apply possible control methods like vector control or information campaigns for prevention. To optimize the degree of control Pontryagin's maximum principle can be used with the optimal control theory. Here it was shown that this can also be used to adapt the model parameters to the real data. Due to similar structures with regard to the transmission pathways of the disease, an application of the model to other vector-borne diseases such as Malaria or ZIKA is also conceivable. With regard to dengue, the development of a much more complex *SIR* multistrain model with a time-dependent transmission rate is desirable in order to represent the dynamics of the disease even more realistically. Furthermore, the addition of *exposed (E)* or *deaths (D) compartments* is also preferable, provided that appropriate data sets are available for the latter.

Acknowledgement

At this point we would like to thank our colleagues D. Aldila and S. N. N. Perera for the provided data sets which served as the basis for the present research.

Table 6.9: Simulation 3 and 4 for Jakarta. Simulation 3 is based on the actual rainfall data whereas Simulation 4 is run with the average rainfall data of the previous years. The parameter fit is executed in the interval $[t_0, \hat{t}]$ (red). The prediction follows for $[\hat{t}, t_1]$ (blue).

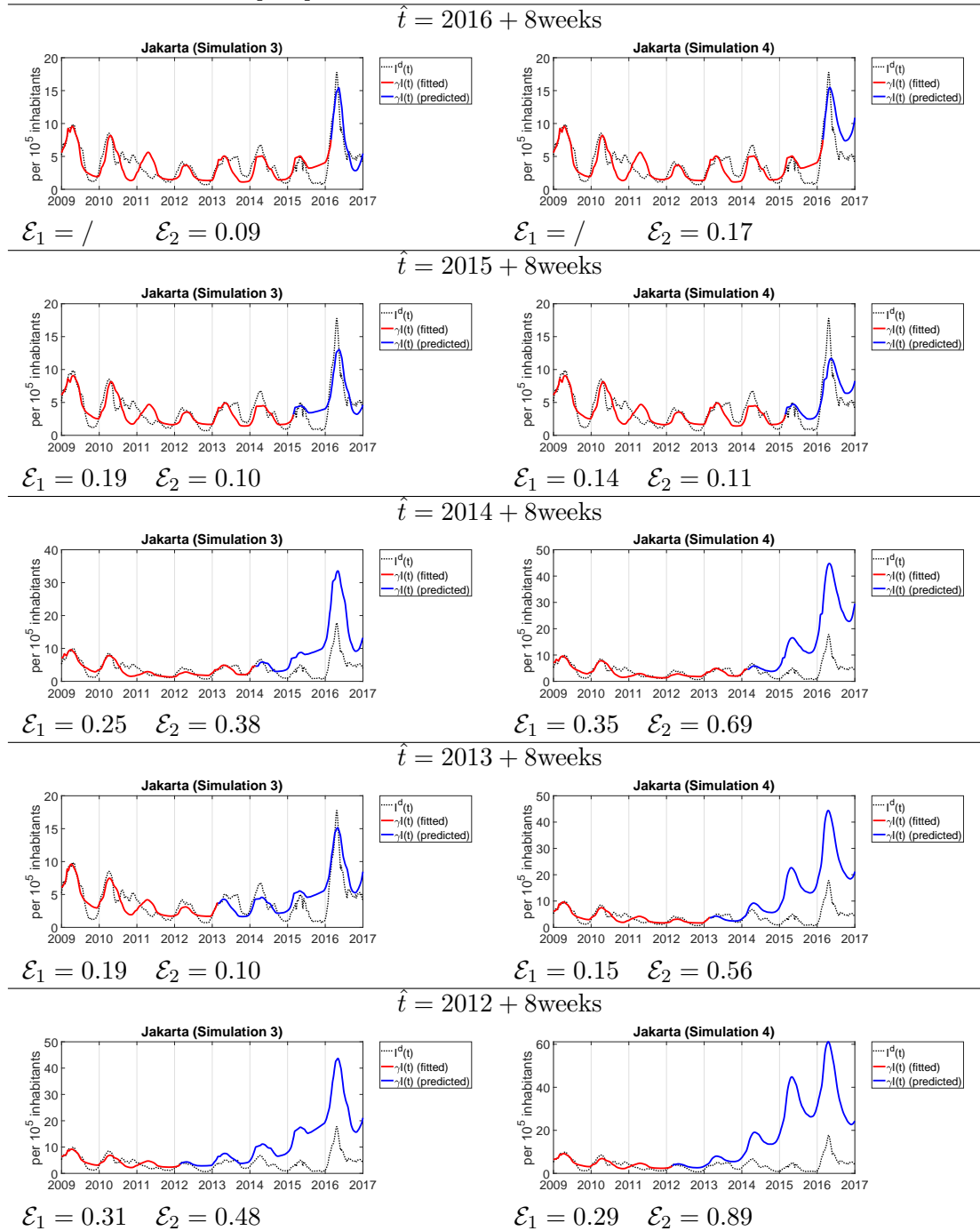
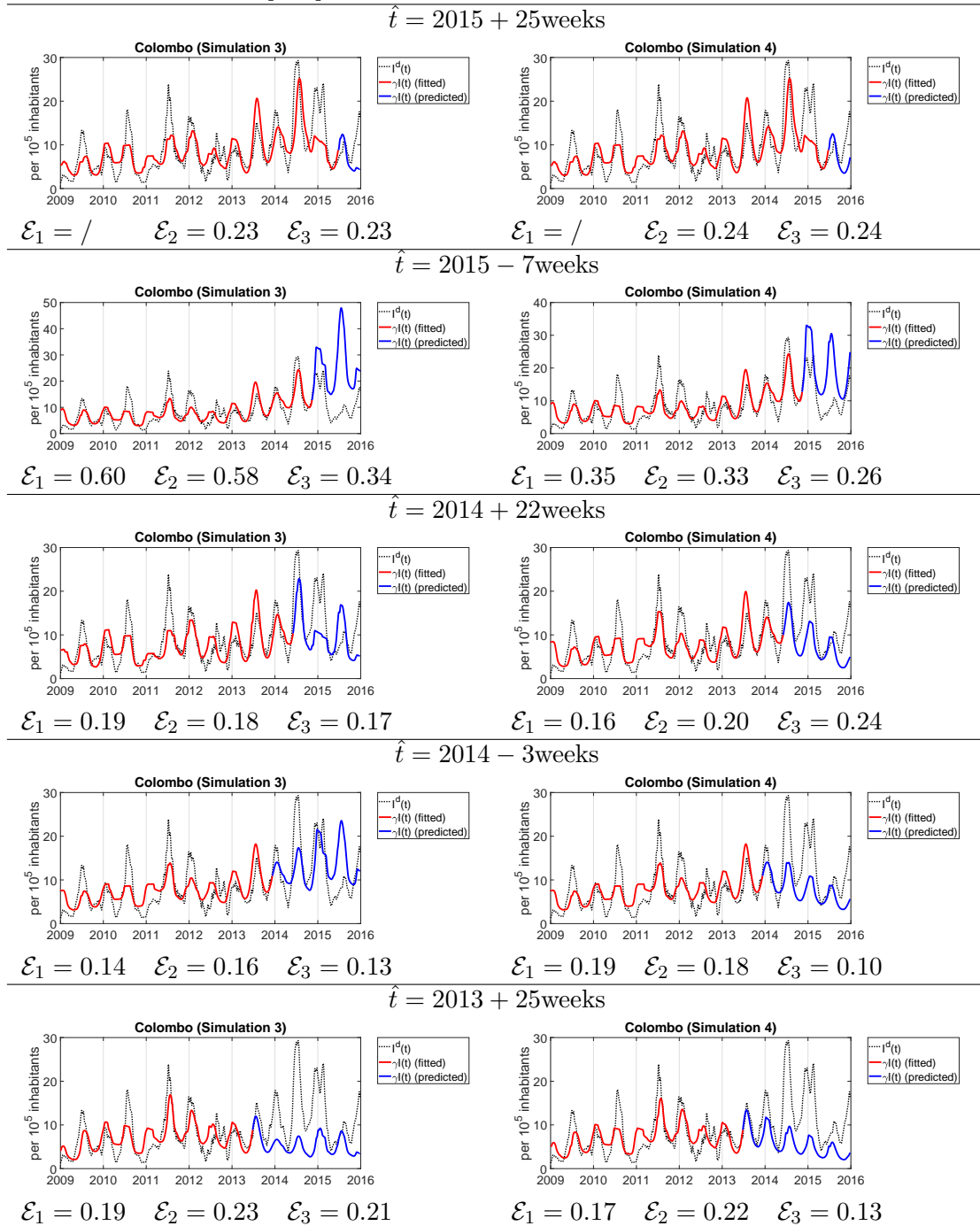
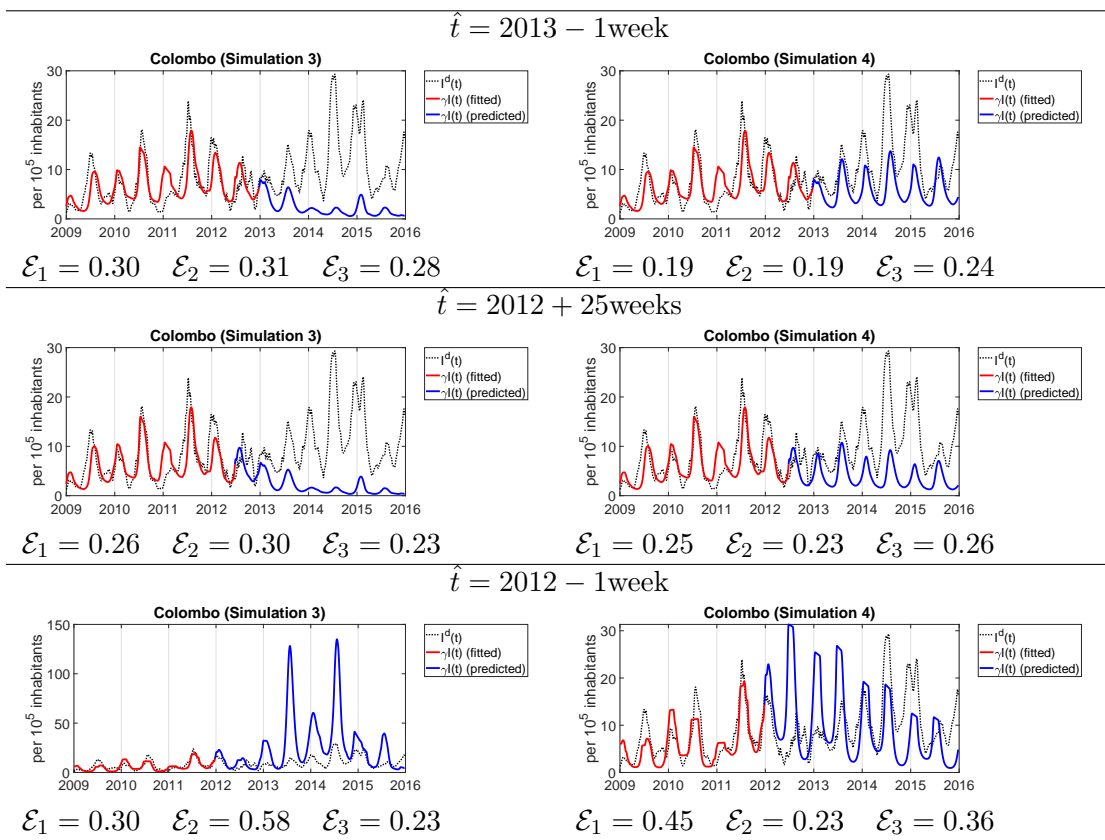


Table 6.10: Simulation 3 and 4 for Colombo. Simulation 3 is based on the actual rainfall data whereas Simulation 4 is run with the average rainfall data of the previous years. The parameter fit is executed in the interval $[t_0, \hat{t}]$ (red). The prediction follows for $[\hat{t}, t_1]$ (blue).





Appendix

6.A Appendix A: Analytical derivation of the parameter fit

We consider the Lagrange function

$$\mathcal{L}(u, x, \lambda) = \int_{t_0}^{t_1} (\gamma I(t) - I^d(t))^2 dt + \frac{\|u\|^2}{N^2} + \int_{t_0}^{t_1} \lambda(t)^T \left(g(t, x(t), u) - \frac{dx(t)}{dt} \right) dt. \quad (6.23)$$

The last summand in (6.23) corresponds to

$$\begin{aligned} \int_{t_0}^{t_1} \lambda(t)^T \left(g(t, x(t), u) - \frac{dx(t)}{dt} \right) dt &= \int_{t_0}^{t_1} \lambda_S(t) \left(g_S(t, x(t), u) - \frac{dS(t)}{dt} \right) dt, \\ &+ \int_{t_0}^{t_1} \lambda_I(t) \left(g_I(t, x(t), u) - \frac{dI(t)}{dt} \right) dt, \\ &+ \int_{t_0}^{t_1} \lambda_R(t) \left(g_R(t, x(t), u) - \frac{dR(t)}{dt} \right) dt. \end{aligned}$$

We exemplarily examine

$$\int_{t_0}^{t_1} \lambda_I(t) \left(g_I(t, x(t), u) - \frac{dI(t)}{dt} \right) dt = \int_{t_0}^{t_1} \lambda_I(t) g_I(t, x(t), u) dt - \int_{t_0}^{t_1} \lambda_I(t) \frac{dI(t)}{dt} dt,$$

which leads to

$$\int_{t_0}^{t_1} \lambda_I(t) g_I(t, x(t), u) dt + \int_{t_0}^{t_1} \frac{d\lambda_I(t)}{dt} I(t) dt + \lambda_I(t_0) I_0 - \lambda_I(t_1) I(t_1),$$

by applying *partial integration*. Furthermore, by substituting $I_0 = N - S_0 - R_0$ and $g_I(t, x(t), u)$ we obtain

$$\begin{aligned} \int_{t_0}^{t_1} \lambda_I(t) \left(g_I(t, x(t), u) - \frac{dI(t)}{dt} \right) dt &= \int_{t_0}^{t_1} \lambda_I(t) \left(\frac{\beta(t)}{N} S(t) I(t) - (\alpha + \mu) I(t) \right) dt \\ &+ \int_{t_0}^{t_1} \frac{d\lambda_I(t)}{dt} I(t) dt \\ &+ \lambda_I(t_0) (N - S_0 - R_0) - \lambda_I(t_1) I(t_1). \end{aligned}$$

Analogously, we receive for the other summands

$$\begin{aligned} \int_{t_0}^{t_1} \lambda_S(t) \left(g_S(t, x(t), u) - \frac{dS(t)}{dt} \right) dt &= \int_{t_0}^{t_1} \lambda_S(t) \left(\mu (N - S(t)) - \frac{\beta(t)}{N} S(t) I(t) \right) dt \\ &+ \int_{t_0}^{t_1} \frac{d\lambda_S(t)}{dt} S(t) dt \\ &+ \lambda_S(t_0) S_0 - \lambda_S(t_1) S(t_1) \end{aligned}$$

6 Appendix

and

$$\begin{aligned} \int_{t_0}^{t_1} \lambda_R(t) \left(g_R(t, x(t), u) - \frac{dR(t)}{dt} \right) dt &= \int_{t_0}^{t_1} \lambda_R(t) \left(\alpha I(t) - \mu R(t) \right) dt \\ &+ \int_{t_0}^{t_1} \frac{d\lambda_R(t)}{dt} R(t) dt \\ &+ \lambda_R(t_0) R_0 - \lambda_R(t_1) R(t_1). \end{aligned}$$

The *necessary optimality condition* for a *critical point* (u^*, x^*, λ^*) is fulfilled if

$$\nabla \mathcal{L}(u^*, x^*, \lambda^*) = 0.$$

We compute the partial derivatives of $\mathcal{L}(u, x, \lambda)$ with respect to u_i for $i = 1, \dots, 5$

$$\begin{aligned} \frac{\partial \mathcal{L}(u, x, \lambda)}{\partial u_i} &= \frac{\partial}{\partial u_i} \frac{\|u\|^2}{N^2} + \frac{\partial}{\partial u_i} \int_{t_0}^{t_1} \lambda_S(t) \left(\mu(N - S(t)) - \frac{\beta(t)}{N} S(t) I(t) \right) dt \\ &+ \frac{\partial}{\partial u_i} \int_{t_0}^{t_1} \lambda_I(t) \left(\frac{\beta(t)}{N} S(t) I(t) - (\alpha + \mu) I(t) \right) dt \end{aligned}$$

and obtain

$$\frac{\partial \mathcal{L}(u, x, \lambda)}{\partial u_i} = u_i \frac{2}{N^2} + \frac{1}{N} \int_{t_0}^{t_1} \frac{\partial \beta(t)}{\partial u_i} \left(\lambda_I(t) - \lambda_S(t) \right) S(t) I(t) dt.$$

The partial derivative with respect to $\gamma = u_6$ is calculated with the chain rule

$$\begin{aligned} \frac{\partial \mathcal{L}(u, x, \lambda)}{\partial u_6} &= \frac{\partial}{\partial \gamma} \frac{\|u\|^2}{N^2} + \frac{\partial}{\partial \gamma} \int_{t_0}^{t_1} (\gamma I(t) - I^d(t))^2 dt \\ &= \gamma \frac{2}{N^2} + 2 \int_{t_0}^{t_1} I(t) (\gamma I(t) - I^d(t)) dt. \end{aligned}$$

In addition, we exemplarily compute the partial derivative with respect to $S_0 = u_7$

$$\begin{aligned} \frac{\partial \mathcal{L}(u, x, \lambda)}{\partial u_7} &= \frac{\partial}{\partial S_0} \frac{\|u\|^2}{N^2} + \frac{\partial}{\partial S_0} \lambda_S(t_0) S_0 + \frac{\partial}{\partial S_0} \lambda_I(t_0) (N - S_0 - R_0) \\ &= S_0 \frac{2}{N^2} + \lambda_S(t_0) - \lambda_I(t_0), \end{aligned}$$

which can be done analogously for $R_0 = u_8$. In summary, we receive the gradient

$$\nabla_u \mathcal{L}(u, x, \lambda) = \nabla J(u)$$

of the Lagrange function with respect to the directions of u

$$\begin{aligned} \frac{\partial \mathcal{L}(u, x, \lambda)}{\partial u_i} &= u_i \frac{2}{N^2} + \frac{1}{N} \int_{t_0}^{t_1} \frac{\partial \beta(t)}{\partial u_i} \left(\lambda_I(t) - \lambda_S(t) \right) S(t) I(t) dt, \\ &i = 1, \dots, 5, \\ \frac{\partial \mathcal{L}(u, x, \lambda)}{\partial u_6} &= \gamma \frac{2}{N^2} + 2 \int_{t_0}^{t_1} I(t) (\gamma I(t) - I^d(t)) dt, \\ \frac{\partial \mathcal{L}(u, x, \lambda)}{\partial u_7} &= S_0 \frac{2}{N^2} + \lambda_S(t_0) - \lambda_I(t_0), \\ \frac{\partial \mathcal{L}(u, x, \lambda)}{\partial u_8} &= R_0 \frac{2}{N^2} + \lambda_R(t_0) - \lambda_I(t_0). \end{aligned}$$

6.A Appendix A: Analytical derivation of the parameter fit

The partial derivatives of $\beta(t) = \beta_0 + \beta_1 \int_{t-\eta_2/52}^{t-\eta_1/52} p_c(\tau) d\tau \sin(\omega(t + \varphi/52))$ are given by

$$\begin{aligned} \frac{\partial \beta(t)}{\partial \beta_0} &= 1, \\ \frac{\partial \beta(t)}{\partial \beta_1} &= \int_{t-\eta_2/52}^{t-\eta_1/52} p_c(\tau) d\tau \sin(\omega(t + \varphi/52)), \\ \frac{\partial \beta(t)}{\partial c} &= \begin{cases} 0, & \text{if } p(\tau) < c \text{ or } p(\tau) \geq c \text{ for all } \tau \in [t - \eta_2/52, t - \eta_1/52] \\ c \left(\sum_{i=0}^n \frac{1}{\frac{dp(b_i)}{d\tau}} - \sum_{i=0}^m \frac{1}{\frac{dp(a_i)}{d\tau}} \right) \beta_1 \sin(\omega(t + \varphi/52)), & \text{else,} \\ a_i < b_i < a_{i+1} < b_{i+1} \text{ with } a_i, b_i \in p^{-1}(c), \end{cases} \\ \frac{\partial \beta(t)}{\partial \eta_2} &= \frac{p_c(t - \eta_2/52)}{52} \beta_1 \sin(\omega(t + \varphi/52)), \\ \frac{\partial \beta(t)}{\partial \varphi} &= \frac{\omega \cos(\omega(t + \varphi/52))}{52} \beta_1 \int_{t-\eta_2/52}^{t-\eta_1/52} p_c(\tau) d\tau. \end{aligned}$$

In the cases of c and η_2 we have to take a closer look at the function $G : \mathbb{R}^2 \rightarrow \mathbb{R}$ with $G(c, \eta_2) = \int_a^b p_c(\tau) d\tau$ whereby in our application $[a, b] = [t - \eta_2/52, t - \eta_1/52]$ holds true. Since $p(\tau)$ is a continuous function $p^{-1}((-\infty, c)) = \{\tau \in \mathbb{R} : p(\tau) < c\}$ is a open set. If we define $D_c = \{\tau \in \mathbb{R} : p(\tau) < c\} \cap [a, b]$ four cases can occur.

1. $D_c = (a_1, b_1) \cup (a_2, b_2) \cup \dots \cup (a_{n-1}, b_{n-1})$, if $p(a), p(b) \geq c$,
2. $D_c = [a, b_0) \cup (a_1, b_1) \cup \dots \cup (a_{n-1}, b_{n-1})$, if $p(a) < c, p(b) \geq c$,
3. $D_c = (a_1, b_1) \cup (a_2, b_2) \cup \dots \cup (a_{n-1}, b_{n-1}) \cup (a_n, b]$, if $p(a) \geq c, p(b) < c$,
4. $D_c = [a, b_0) \cup (a_1, b_1) \cup \dots \cup (a_{n-1}, b_{n-1}) \cup (a_n, b]$, if $p(a), p(b) < c$,

with $a < b_0 < a_1 < b_1 < \dots < a_{n-1} < b_{n-1} < a_n < b$. In the following we will investigate case 4, the other cases can be calculated analogously. Since $p(\tau)$ is continuous we obtain

$$\begin{aligned} G(c, \eta_2) &= \int_a^b p_c(\tau) d\tau = \int_{D_c} p(\tau) d\tau \\ &= \int_a^{b_0} p(\tau) d\tau + \sum_{i=1}^{n-1} \int_{a_i}^{b_i} p(\tau) d\tau + \int_{a_n}^b p(\tau) d\tau \\ &= F(b_0) - F(a) + \sum_{i=1}^{n-1} (F(b_i) - F(a_i)) + F(b) - F(a_n), \end{aligned} \quad (6.24)$$

whereby $p(a_i) = c = p(b_i)$ without change of sign in $\frac{dp(\tau)}{d\tau}$ and $\frac{dF(\tau)}{d\tau} = p(\tau)$. Provided that the derivation of the inverse function can locally be formed by $\frac{dp^{-1}(c)}{dc} = \frac{1}{\frac{dp(\tau)}{d\tau}}$ and by using the chain rule we receive

$$\frac{\partial G}{\partial c} = c \left(\frac{1}{\frac{dp(b_0)}{d\tau}} + \sum_{i=1}^{n-1} \left(\frac{1}{\frac{dp(b_i)}{d\tau}} - \frac{1}{\frac{dp(a_i)}{d\tau}} \right) - \frac{1}{\frac{dp(a_n)}{d\tau}} \right).$$

6 Appendix

Additionally, we receive $\frac{\partial G}{\partial c} = 0$ in the cases of

$$G(c, \eta_2) = \begin{cases} \int_a^b p(\tau) d\tau, & p(\tau) < c \text{ for all } \tau \in [a, b] \\ 0, & p(\tau) \geq c \text{ for all } \tau \in [a, b]. \end{cases}$$

The substitution $a = t - \eta_2/52$ in (6.24) delivers $\frac{\partial G}{\partial \eta_2} = \frac{p_c(t - \eta_2/52)}{52}$ since

$$\frac{\partial G}{\partial \eta_2} = \begin{cases} \frac{p(t - \eta_2/52)}{52}, & p(t - \eta_2/52) < c \\ 0, & p(t - \eta_2/52) \geq c. \end{cases}$$

In order to compute the *Gâteaux derivatives* of $\mathcal{L}(u, x, \lambda)$ respect to x an arbitrary function $h \in \mathcal{C}^1(\mathcal{D}, \mathbb{R})$ satisfying $h(t_0) = 0$ is implemented. We define $I_\varepsilon : \mathcal{D} \rightarrow \mathbb{R}$ with $I_\varepsilon(t) = I(t) + \varepsilon h(t)$. It follows that $I_\varepsilon(t_0) = I(t_0)$ for all $\varepsilon \in \mathbb{R}$. Furthermore, let $x_\varepsilon : \mathcal{D} \rightarrow \mathbb{R}^3$ be defined by $x_\varepsilon = (S, I_\varepsilon, R)^T$. It is valid that $I_\varepsilon(t) \rightarrow I(t)$ and $x_\varepsilon(t) \rightarrow x(t)$ for $\varepsilon \rightarrow 0$ and all $t \in \mathcal{D}$. We receive

$$\left. \frac{dI_\varepsilon(t)}{d\varepsilon} \right|_{\varepsilon=0} = h(t)$$

and

$$\frac{\partial \mathcal{L}(u, x, \lambda)}{\partial I} = \lim_{\varepsilon \rightarrow 0} \frac{\mathcal{L}(u, x_\varepsilon, \lambda) - \mathcal{L}(u, x, \lambda)}{\varepsilon} = \left. \frac{d\mathcal{L}(u, x_\varepsilon, \lambda)}{d\varepsilon} \right|_{\varepsilon=0}.$$

At a critical point (u^*, x^*, λ^*) we have

$$\begin{aligned} 0 &= \frac{\partial \mathcal{L}(u, x, \lambda)}{\partial I} = \left. \frac{d\mathcal{L}(u, x_\varepsilon, \lambda)}{d\varepsilon} \right|_{\varepsilon=0} \\ &= \int_{t_0}^{t_1} \frac{d}{d\varepsilon} \left(\gamma I_\varepsilon(t) - I^d(t) \right)^2 \Big|_{\varepsilon=0} dt \\ &\quad + \int_{t_0}^{t_1} \lambda_S(t) \frac{d}{d\varepsilon} \left(\mu(N - S(t)) - \frac{\beta(t)}{N} S(t) I_\varepsilon(t) \right) \Big|_{\varepsilon=0} dt \\ &\quad + \int_{t_0}^{t_1} \lambda_I(t) \frac{d}{d\varepsilon} \left(\frac{\beta(t)}{N} S(t) I_\varepsilon(t) - (\alpha + \mu) I_\varepsilon(t) \right) \Big|_{\varepsilon=0} dt \\ &\quad + \int_{t_0}^{t_1} \frac{d\lambda_I(t)}{dt} \cdot \left. \frac{dI_\varepsilon(t)}{d\varepsilon} \right|_{\varepsilon=0} dt - \lambda_I(t_1) \left. \frac{dI_\varepsilon(t_1)}{d\varepsilon} \right|_{\varepsilon=0} \\ &\quad + \int_{t_0}^{t_1} \lambda_R(t) \frac{d}{d\varepsilon} \left(\alpha I_\varepsilon(t) - \mu R(t) \right) \Big|_{\varepsilon=0} dt \\ &= \int_{t_0}^{t_1} 2\gamma h(t) \left(\gamma I(t) - I^d(t) \right) dt + \int_{t_0}^{t_1} \lambda_S(t) \left(-\frac{\beta(t)}{N} S(t) h(t) \right) dt \\ &\quad + \int_{t_0}^{t_1} \lambda_I(t) \left(\frac{\beta(t)}{N} S(t) h(t) - (\alpha + \mu) h(t) \right) dt + \int_{t_0}^{t_1} \frac{d\lambda_I(t)}{dt} h(t) dt \\ &\quad - \lambda_I(t_1) h(t_1) + \int_{t_0}^{t_1} \lambda_R(t) \alpha h(t) dt. \end{aligned}$$

Summing up the integrals and excluding $h(t)$ delivers

$$0 = \int_{t_0}^{t_1} h(t) f(t) dt - \lambda_I(t_1) h(t_1), \quad (6.25)$$

whereby $f \in \mathcal{C}^1(\mathcal{D}, \mathbb{R})$ is defined by

$$f(t) = 2\gamma \left(\gamma I(t) - I^d(t) \right) - \frac{\beta(t)}{N} S(t) \lambda_S(t) + \left(\frac{\beta(t)}{N} S(t) - (\alpha + \mu) \right) \lambda_I(t) + \frac{d\lambda_I(t)}{dt} + \alpha \lambda_R(t).$$

6.A Appendix A: Analytical derivation of the parameter fit

Since equation (6.25) has to be fulfilled for arbitrary $h(t)$ it is particularly satisfied for all $h(t)$ with $h(t_0) = h(t_1) = 0$. Thus, the *fundamental lemma of calculus of variations* delivers that $f(t) = 0$ on \mathcal{D} , see [13]. Furthermore, if we chose an arbitrary $h(t)$ with $h(t_1) \neq 0$ we conclude that $\lambda_I(t_1) = 0$ because $f(t) = 0$. Applying this procedure concerning $0 = \frac{\partial \mathcal{L}}{\partial S}$ and $0 = \frac{\partial \mathcal{L}}{\partial R}$ delivers ODEs for the adjoint functions

$$\begin{aligned}\frac{d\lambda_S}{dt} &= \left(\mu + \frac{\beta(t)}{N} I \right) \lambda_S - \frac{\beta(t)}{N} I \lambda_I, \\ \frac{d\lambda_I}{dt} &= \frac{\beta(t)}{N} S \lambda_S + \left((\alpha + \mu) - \frac{\beta(t)}{N} S \right) \lambda_I - \alpha \lambda_R - 2\gamma (\gamma I - I^d), \\ \frac{d\lambda_R}{dt} &= \mu \lambda_R,\end{aligned}$$

and the transversality conditions

$$\begin{aligned}\lambda_S(t_1) &= 0, \\ \lambda_I(t_1) &= 0, \\ \lambda_R(t_1) &= 0.\end{aligned}$$

The partial derivatives of $\mathcal{L}(u, x, \lambda)$ respect to the directions of λ are computed again with Gâteaux derivatives which delivers in (u^*, x^*, λ^*)

$$\begin{aligned}0 &= \frac{\partial \mathcal{L}(u, x, \lambda)}{\partial \lambda_S} = \mu (N - S(t)) - \frac{\beta(t)}{N} S(t) I(t) - \frac{dS(t)}{dt}, \\ 0 &= \frac{\partial \mathcal{L}(u, x, \lambda)}{\partial \lambda_I} = \frac{\beta(t)}{N} S(t) I(t) - (\alpha + \mu) I(t) - \frac{dI(t)}{dt}, \\ 0 &= \frac{\partial \mathcal{L}(u, x, \lambda)}{\partial \lambda_R} = \alpha I(t) - \mu R(t) - \frac{dR(t)}{dt},\end{aligned}$$

and consequently we reobtain the state variable ODEs

$$\begin{aligned}\frac{dS}{dt} &= \mu (N - S) - \frac{\beta(t)}{N} S I, \\ \frac{dI}{dt} &= \frac{\beta(t)}{N} S I - (\alpha + \mu) I, \\ \frac{dR}{dt} &= \alpha I - \mu R.\end{aligned}$$

6.B Appendix B: Algorithm pseudocode

Algorithm 3 Pseudocode for parameter adjustment using adjoint functions.

- 1: $u, I^{\text{DATA}}, \rho, \iota \leftarrow$ load initial values for u , respective dengue and rain data and $\rho, \iota \in (0, 1)$
 - 2: $x, \lambda \leftarrow$ solve ODE for state variable (forward) and adjoint function (backward) on $[t_0, t_1]$
 - 3: $J, \nabla J \leftarrow$ compute objective function and gradient regarding u
 - 4: $s \leftarrow$ compute search direction
 - 5: **repeat**
 - 6: $J_{old} \leftarrow J$
 - 7: $\vartheta \leftarrow 1$
 - 8: **repeat**
 - 9: $\vartheta \leftarrow \rho\vartheta$
 - 10: $x \leftarrow$ update depending on $u + \vartheta s$
 - 11: **until** $J(u + \vartheta s) \leq J + \iota\vartheta s^T \nabla J$ (Armijo Rule)
 - 12: $u \leftarrow u + \vartheta s$
 - 13: $x, \lambda, J, \nabla J, s \leftarrow$ update depending on u
 - 14: **until** $\|J - J_{old}\|_2 < \text{TOL}$
 - 15: $u^*, x^*, \lambda^*, J^* \leftarrow u, x, \lambda, J$
-

Bibliography

- [1] Aldila, D.: *Private communication*. Department of Mathematics, University of Indonesia – Jakarta, 2017
- [2] Broyden, C.G.: *The Convergence of a Class of Double-rank Minimization Algorithms 1. General Considerations*. IMA Journal of Applied Mathematics, Vol. 6, No. 1, pp 76–90, 1970
<https://doi.org/10.1093/imamat/6.1.76>
- [3] Department of Census and Statistics – Sri Lanka: *Census of Population and Housing 2001 and 2012*. Accessed 17 Dec 2020
<http://www.statistics.gov.lk>
- [4] Ernst, K.; Walker, K. et al.: *Aedes aegypti (Diptera: Culicidae) Longevity and Differential Emergence of Dengue Fever in Two Cities in Sonora, Mexico*. Journal of Medical Entomology, Vol. 54, No.1, pp 204–211, 2017
<https://doi.org/10.1093/jme/tjw141>
- [5] Fletcher, R.: *A new approach to variable metric algorithms*. The Computer Journal, Vol. 13, No. 3, pp 317–322, 1970
- [6] Fletcher, R.; Reeves, C.: *Function minimization by conjugate gradients*. The Computer Journal, Vol. 7, No. 2, pp 149–154, 1964
- [7] Fuehrer, H.-P.; Schoener, E.; Weiler, S.: *Monitoring of alien mosquitoes in Western Austria (Tyrol, Austria, 2018)*. PLOS Neglected Tropical Diseases, Vol. 14, No. 6, pp 1–10, 2020
<https://doi.org/10.1371/journal.pntd.0008433>
- [8] Gâteaux, R.: *Fonctions d'une infinité de variables indépendantes*. Bulletin de la Société Mathématique de France, Vol. 47, pp 70–96, 1919
- [9] Goldfarb, D.: *A Family of Variable Metric Updates Derived by Variational Means*. Mathematics of Computation, Vol. 24, No. 109, pp 23–26, 1970
- [10] Götz, T.; Altmeier, N.; Bock, W.; Rockenfeller, R.; Wijaya, K. P.: *Modeling dengue data from Semarang, Indonesia*. Ecological Complexity, Vol. 30, pp 57–62, 2016
<https://doi.org/10.1016/j.ecocom.2016.12.010>
- [11] Götz, T.; Heidrich, P.: *Early stage COVID-19 disease dynamics in Germany: Models and parameter identification*. Journal of Mathematics in Industry, Vol. 10, No. 20, Springer Open, 2020
<https://doi.org/10.1186/s13362-020-00088-y>
- [12] Heidrich, P.; Götz, T.: *Modelling Dengue with the SIR model*. Progress in Industrial Mathematics at ECMI 2018, Vol. 30, Springer Switzerland, pp 175–182, 2019
https://doi.org/10.1007/978-3-030-27550-1_22

Bibliography

- [13] Jost, J.; Li–Jost, X.: *Calculus of Variations*. Cambridge University Press, 1998
- [14] Lenhart, S.; Workman, J.T.: *Optimal control applied to biological models*. CRC Press, 2007
- [15] Martcheva, M.: *An introduction to mathematical epidemiology*. Springer US, 2015
- [16] Nocedal, J.; Wright, S.: *Numerical Optimization*. Springer New York, 2006
- [17] Perera, S.: *Private communication*. Department of Mathematics, University of Colombo – Sri Lanka, 2016
- [18] Polak, E.; Ribiere, G.: *Note sur la convergence de méthodes de directions conjuguées*. ESAIM: Mathematical Modelling and Numerical Analysis – Modélisation Mathématique et Analyse Numérique, Vol. 3, pp 35–43, 1969
- [19] Pontryagin, L.: *Mathematical Theory of Optimal Processes*. CRC Press, 2018
- [20] Rabiner, L.; Schafer, R.: *Theory and Applications of Digital Speech Processing*. Pearson, 2011
- [21] Rao, K.; Kim, N.; Stepanov, V.; Hwang, J.: *Fast Fourier Transform – Algorithms and Applications*. Springer Netherlands, 2011
- [22] Rice, J.: *Mathematical Statistics and Data Analysis*. Cengage Learning, 2006
- [23] Rocha, F.; Aguiar, M.; Souza, M.; Stollenwerk, N.: *Time–scale separation and centre manifold analysis describing vector–borne disease dynamics*. International Journal of Computer Mathematics, Vol. 90, No. 10, pp 2105–2125, 2013
<https://doi.org/10.1080/00207160.2013.783208>
- [24] Rocha, F.; Mateus, L.; Skwara, U.; Aguiar, M.; Stollenwerk, N.: *Understanding Dengue fever dynamics: a study of seasonality in vector–borne disease models*. International Journal of Computer Mathematics, Vol. 93, No. 8, pp 1405–1422, 2016
<https://doi.org/10.1080/00207160.2015.1050961>
- [25] Shanno, D.: *Conditioning of Quasi–Newton Methods for Function Minimization*. Mathematics of Computation, Vol. 24, No. 111, pp 647–656, 1970
- [26] Souza, M.: *Multiscale analysis for a vector–borne epidemic model*. Journal of Mathematical Biology, Vol. 68, pp 1269–1293, 2014
<https://doi.org/10.1007/s00285-013-0666-6>
- [27] Tikhonov, A.N.; Goncharsky, A.; Stepanov, V.V.; Yagola, A.G.: *Numerical Methods for the Solution of Ill–Posed Problems*. Springer Amsterdam, 2013
- [28] WetterKontor: *Weather data for Colombo and Jakarta*. Accessed 17 Dec 2020
<https://www.wetterkontor.de>
- [29] Wikramaratna, P.; Simmons, C.; Gupta, S.; Recker, M.: *The Effects of Tertiary and Quaternary Infections on the Epidemiology of Dengue*. PLOS ONE, Vol. 5, No. 8, pp 1–8, 2010
<https://doi.org/10.1371/journal.pone.0012347>

- [30] World Health Organization (WHO): *Dengue and severe dengue*. Accessed 17 Dec 2020
<https://www.who.int/news-room/fact-sheets/detail/dengue-and-severe-dengue>
- [31] World Health Organization (WHO): *Dengue fever — Sri Lanka*. Accessed 17 Dec 2020
<https://www.who.int/csr/don/19-july-2017-dengue-sri-lanka/en/>
- [32] World Life Expectancy: *Average life expectancy in Indonesia and Sri Lanka*. Accessed 17 Dec 2020
<https://www.worldlifeexpectancy.com>
- [33] World Meteorological Organization: *Meteorological data for Colombo and Jakarta*. Accessed 17 Dec 2020
<https://worldweather.wmo.int>

Bibliography

7 Research Paper III: Prediction of Dengue Cases Based on Human Mobility and Seasonality. An Example for the City of Jakarta

Peter Heidrich Yashika Jayathunga Wolfgang Bock Thomas Götz

The paper *Prediction of Dengue Cases Based on Human Mobility and Seasonality. An Example for the City of Jakarta* by Peter Heidrich, Yashika Jayathunga, Wolfgang Bock and Thomas Götz is currently being reviewed by the journal *Mathematical Methods in the Applied Sciences, Wiley Online Library*. The layout of the paper is adapted to the present thesis.

Peter Heidrich contributed the section to *Data analysis*, parts of *Model analysis* the *Data fit analysis* and the programming and presentation of the *Results*. Yashika Jayathunga supplemented the above sections and contributed significantly to the analysis of mobility in the *Model analysis* section. Wolfgang Bock wrote the *Introduction* and took over the complete revision and organization of this paper. Thomas Götz worked with him on the idea for the article and provided advice.

7.1 Abstract

In this article we combine a multipatch *SIRUV* model with seasonal mosquito breeding rate in order to develop a seasonal *SIR* model via a time-scale separation. The model is applied to commuting and dengue incident data in Jakarta to forecast dengue outbreaks. Qualitatively the analysis is in good agreement with the actual outbreaks.

Keywords: Dengue model, Seasonality models, Multipatch models, Prediction model, Time-scale separation, Numerical optimization

7.2 Introduction

Dengue is a very old disease, described for the first time in Chinese history books from the 10th century. Already in that time, the disease was spread via ships to the neighbouring areas. However before 1970 just 9 countries worldwide experienced severe dengue cases [49]. Due to urbanization, globalization and the accessibility to long distance flights, the disease nowadays is spread over the whole subtropics and tropics causing around 12,000 deaths per year, threatening half of the human population [18, 40]. The infection cycle of dengue makes use of mosquitos of the type *Aedes* [1, 5, 20, 23] as carrier of the disease. For dengue disease, there exist four strains of the virus DENV-1 to DENV-4 [11, 19, 41, 42]. Recently there is a intensive on-going discussion about the existence of a fifth strain, which is however not confirmed yet up to the authors knowledge, see e.g. [33, 43, 46].

The modelling of the disease hence goes from simple *SIR* (susceptible–infected–recovered) to complex multistrain models and models incorporating partial differential equations for the human mobility. There are too many approaches to give a comprehensive overview, hence we refer to the publications [2–4, 8, 9, 13–17, 24, 38, 39] and the monograph [27] and the references therein. The modelling of human mobility itself is already a challenging task. An interesting model has been proposed by Brockmann et.al. [7] which is based on the Dollar bill tracking in USA resulting in a power law distribution for a fractional partial differential equation. In general for particular examples, it is not possible to predict the trajectory of a single particle. It is more reasonable to consider commuting data of certain districts. In that case instead of using a partial differential equation one considers a system of ordinary differential equations, matching to the commuting data. Such multipatch models have recently become a useful tool to describe the mobility between certain hospital areas, see e.g. [6]. Although humans and their mobility are one core ingredient of the disease spread, in the case of dengue, one has to consider also the mosquito population. It is reasonable to consider the mosquito populations between patches as non–moving due to their small action radius. But since mosquitos breed in standing water see [48], it is important to consider seasons of rainfall. The seasonality of rainfall can be directly correlated to the seasonality in dengue outbreaks, see e.g. [13, 22].

In this paper we use a metapopulation multipatch *SIRUV* model combined with a seasonality in the number of mosquitos to predict dengue outbreaks in the city of Jakarta. For this we derive a residence budgeting time matrix from the commuting data for the five districts of Jakarta. Based on a fast Fourier transform we study the seasonality of the dengue cases for the region. We derive a multipatch *SIR* model from the multipatch *SIRUV* model studied in [6] via a time–scale separation as in [37]. Via an optimal control approach based on Pontryagin’s maximum principle we fit the data to the multipatch model in Section 7.4. Based on this we both simulate the seasonal mutipatch model with the obtained parameters and give a prediction analysis based on that model. The outbreaks seen in the real data are qualitatively in good agreement and are quantitatively sound. We want to point out that here the combination of human mobility data and seasonal rainfall and dengue data lead to a good prediction of dengue cases.

Remark 7.2.1. Note that it is clear, that in order to obtain a quantitative accurate prediction also multi–strain effects have to be taken into account. Especially in describing severe dengue cases the secondary infections play a crucial role. On the other hand, data of the distribution of the strains was not available in our data sets. We thank the anonymous referee very much for pointing this out. A multi–strain consideration will be subject of our further studies.

7.3 Data analysis

The available data consists of the weekly hospitalized dengue cases in the five administrative cities of the *Special Capital Region of Jakarta* (2009 – 2017). We received this data through private communication with the *Department of Mathematics* of the *University of Indonesia*. To reduce the noise the data was processed using a *moving average*. In each patch the data point d_ι is replaced by $\bar{d}_\iota = \frac{1}{4} \sum_{k=0}^3 d_{\iota-k}$ for all $\iota \geq 3$.

In all regions a similar behavior can be observed since the periodical behavior is almost identical. In most cases the dengue outbreaks appear in the first quarter of each year. The intensities of the outbreak peaks decrease from 2009 to 2012 up to 50%, approximately remain on that level until 2015 and finally drastically increase in 2016 (see Figure 7.1). The results of the *fast Fourier transform (FFT)* underpin the observed periodicities since

significant high values at one frequency per year can be noticed in all patches (see Figure 7.2).

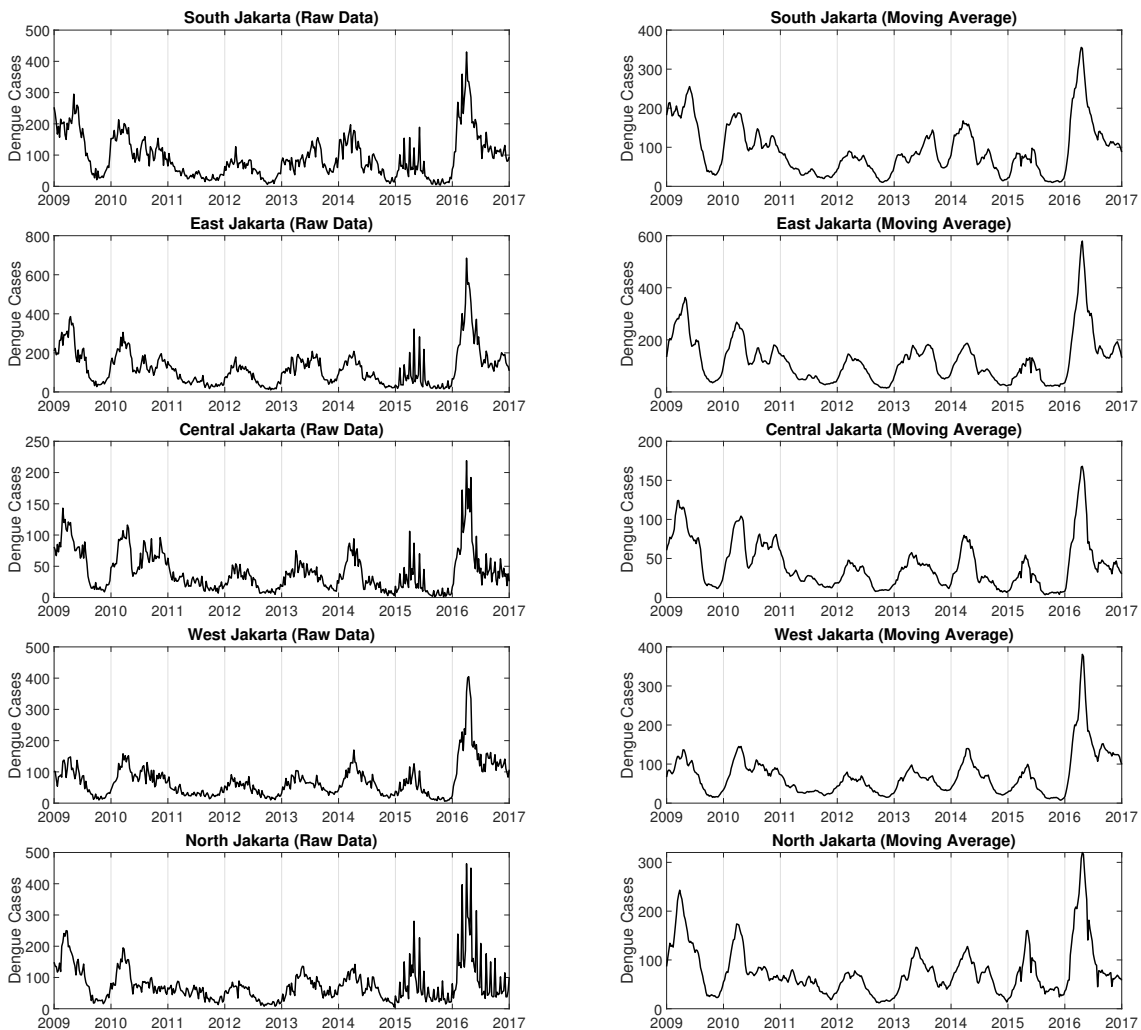


Figure 7.1: Raw data and moving average for the dengue cases in the five domains South, East, Central, West and North Jakarta.

It is assumed that the periodical behavior in the dengue data relates to the weather conditions especially to precipitation. This is due to the fact, that mosquitos breed in standing water, see e.g. [48]. The annual weather data show similar periodicities for rainfall and humidity whereas the temperature remains relatively constant. In addition to the dengue data we received rainfall data sets from Jakarta in the appropriate timespans which are also smoothed with the moving average $\bar{p}_\iota = \frac{1}{4} \sum_{k=0}^3 p_{\iota-k}$ for all $\iota \geq 3$. The *FFT* shows significant high values at one frequency per year (see Figure 7.2 and 7.3). To manifest the relation between rainfall and dengue data we use a cross-correlation and determine time lags around 6 – 8 weeks in all regions except South Jakarta with 4 – 6 weeks. Consequently, this means that after an intensive rain period it takes approximately two months until the dengue cases significantly rise. The *clusters* between precipitation and dengue data additionally show that if the average daily rainfall is stronger than approximately 15mm to 20mm a day, less dengue data points appear (see Figure 7.4). Thus, we assume that in periods of very strong rainfall the eggs of mosquitos are destroyed or washed away and thus the reproduction of the vectors is reduced, see e.g. [13].

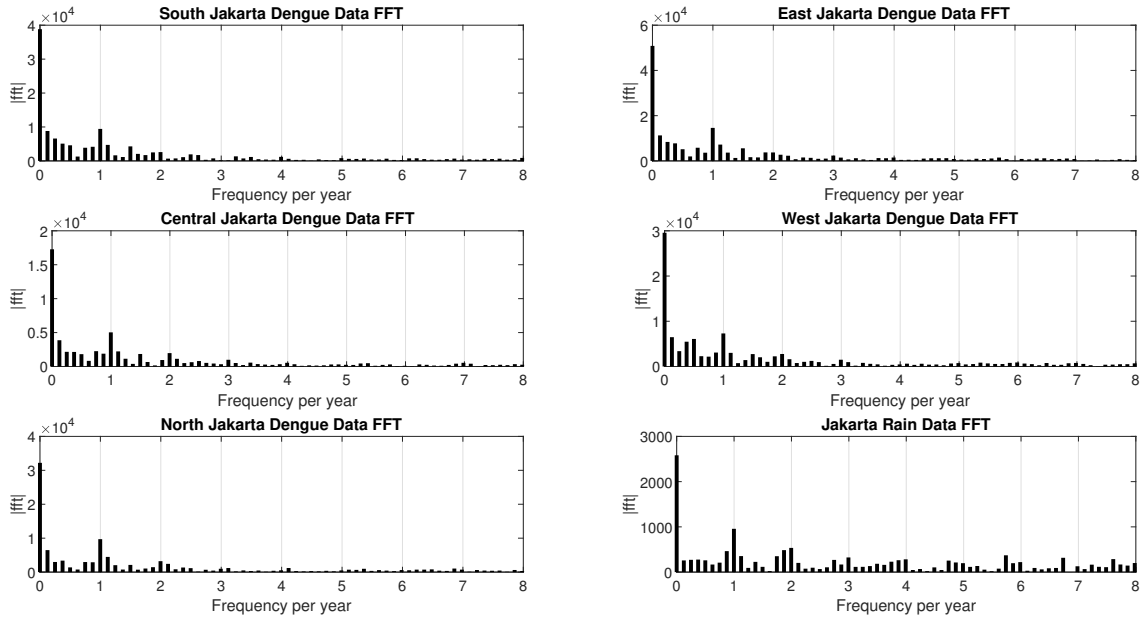


Figure 7.2: Fast Fourier transform (FFT) of the dengue and rain data from Jakarta [35].

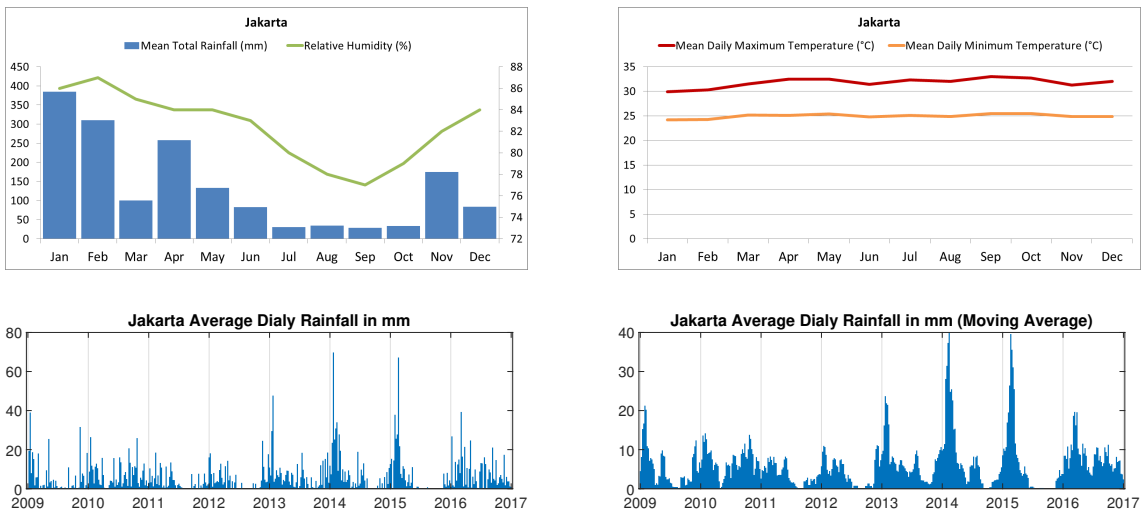


Figure 7.3: Annual weather data, raw data and moving average of the weekly rain data [47, 51].

7.4 Model analysis

Usually vector-borne diseases like dengue are studied with vector-host models such as the *SIRUV* model. This can be converted to a *SIR* model with the help of a time-scale separation. In the following section, for sake of simplicity, we first introduce an *SIR* model with mobility. We show that indeed it can be obtained from an *SIRUV* model with mobility, including the *residence budgeting time matrix* P . This is presented subsequently and more detailed in the Appendix 7.A.

Remark 7.4.1. For the sake of simplicity we chose an *SIRUV* or *SIR* model rather than an *SEIRUV* or *SEIR* model. The latter would take also exposed humans. By this choice we neglect the influence of intrinsic and extrinsic incubation periods. Comparing to [27, 37, 38] however for dengue, *SIR* and *SIRUV* models give a reasonable qualitative

dynamical behaviour.

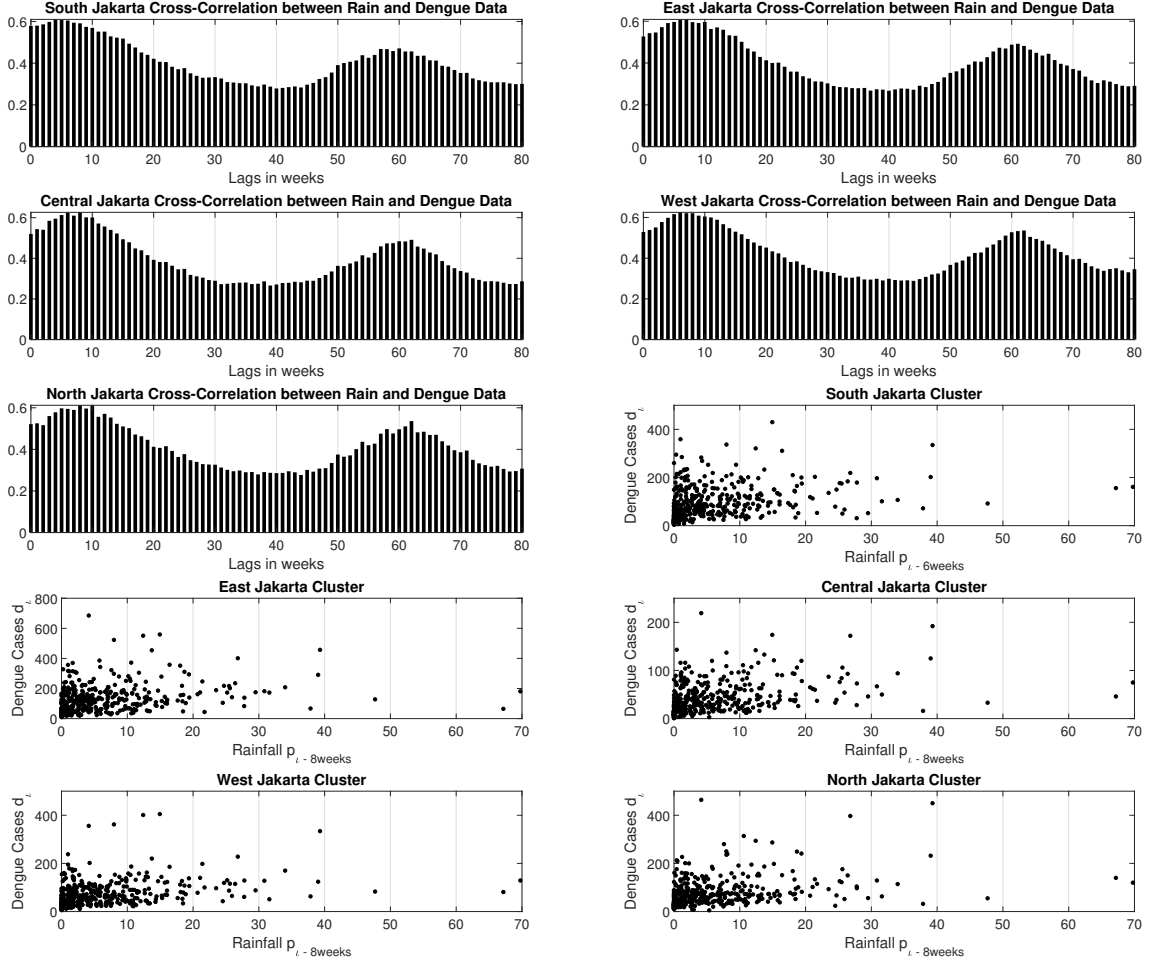


Figure 7.4: Cross-correlation and cluster between rain and dengue data in the respective districts [34].

7.4.2 SIR model with mobility

The following *SIR* model includes the three usual groups of *susceptible* (S_i), *infected* (I_i) and *recovered* (R_i) human individuals of the patches $i = 1, \dots, n$

$$\frac{dS_i}{dt} = \mu(N_i - S_i) - S_i \sum_{j=1}^n \left(p_{ij} \frac{\beta_j(t)}{N_j} \sum_{k=1}^n p_{kj} I_k \right), \quad S_i(t_0) = S_{i0} \geq 0, \quad (7.1a)$$

$$\frac{dI_i}{dt} = S_i \sum_{j=1}^n \left(p_{ij} \frac{\beta_j(t)}{N_j} \sum_{k=1}^n p_{kj} I_k \right) - (\alpha + \mu) I_i, \quad I_i(t_0) = I_{i0} \geq 0, \quad (7.1b)$$

$$\frac{dR_i}{dt} = \alpha I_i - \mu R_i, \quad R_i(t_0) = R_{i0} \geq 0, \quad (7.1c)$$

$$N_i = S_i + I_i + R_i. \quad (7.1d)$$

Let be $S_i, I_i, R_i \in \mathcal{C}^1(\mathbb{D}, \mathbb{R})$ with $\mathcal{C}^n(X, Y) = \{f : X \rightarrow Y \mid f \text{ is } n \text{ times continuously differentiable in } X\}$ for $X, Y \subset \mathbb{R}$. In the following we set $\mathbb{D} = [t_0, t_1]$. The *birth* and *death*

rate μ are assumed to be equal and the transition from infected to recovered is given by the recovery rate α . We assume that birth, death and recovery rate is the same over all patches. This is reasonable for the concrete application, which is considering data from different city districts of Jakarta, Indonesia. The *incidence term*

$$S_i \sum_{j=1}^n \left(p_{ij} \frac{\beta_j(t)}{N_j} \sum_{k=1}^n p_{kj} I_k \right) \quad (7.2)$$

describes the number of new infections in patch i at time t depending on time-dependent transmission rates $\beta_j \in \mathcal{C}^1(\mathbb{D}, \mathbb{R})$. The residence budgeting time matrix $P = (p_{ij})_{i,j=1,\dots,n}$ includes the commuting rates between the patches i and j . If $i = j$ applies, then the fraction of the individuals is meant that remains in its patch and does not commute. Consequently, the sum $\sum_{k=1}^n p_{kj} I_k$ stands for the number of infected individuals in patch j at time t . The population size of patch i is described by N_i . From

$$\frac{dN_i}{dt} = \frac{dS_i}{dt} + \frac{dI_i}{dt} + \frac{dR_i}{dt} = 0$$

it follows that these are constant. This is due to the fact that we investigate a commuter model in which some of the individuals leave their patch to work and then return. The changes in the size of the individual patches caused by long-term movements within the total population are therefore not taken into account. In addition, the following applies

$$0 = \frac{dN_i}{dt} = - \underbrace{\sum_{j=1}^n p_{ij} N_i}_1 + \sum_{j=1}^n p_{ji} N_j + \underbrace{\mu (N_i - N_i)}_0,$$

from which we receive

$$N_i = \sum_{j=1}^n p_{ji} N_j. \quad (7.3)$$

The total population is then given by $N = \sum_{i=1}^n N_i$.

7.4.3 SIRUV with mobility

A multi-patch vector-host mathematical model is defined in this section to describe the human and mosquito interactions which will cause disease spread. In addition to human dynamics as in equation (7.1) this system of ODEs includes *uninfected* (U_i) and *infected* (V_i) mosquitoes with $U_i, V_i, \in \mathcal{C}^1(\mathbb{D}, \mathbb{R})$. Dengue fever is assumed to be transmitted by two means of interactions between host and vector: susceptible mosquitoes (U_i) may interact with infected human (I_i) individuals at a rate of $\frac{\vartheta_i}{N_i}$ and infected mosquitoes (V_i) may interact with susceptible humans (S_i) at a rate of $\frac{\hat{\beta}_i}{M_{i0}}$. The incidence rates at which humans and mosquitoes get infected are $\frac{\hat{\beta}_i}{M_{i0}} S_i V_i$ and $\frac{\vartheta_i}{N_i} U_i I_i$, respectively. Here we assume that vectors do not move between the patches [28, 29, 48] and the movements between the patches are coupled by a residence budgeting time matrix $P = (p_{ij})_{i,j=1,\dots,n}$ for [25]. The complete system of nonlinear ordinary differential equations for the n patches reads

as follows:

$$\frac{dS_i}{dt} = \mu(N_i - S_i) - S_i \sum_{j=1}^n p_{ij} \frac{\hat{\beta}_j}{M_{j0}} V_j, \quad S_i(t_0) = S_{i0} \geq 0, \quad (7.4a)$$

$$\frac{dI_i}{dt} = S_i \sum_{j=1}^n p_{ij} \frac{\hat{\beta}_j}{M_{j0}} V_j - (\alpha + \mu) I_i, \quad I_i(t_0) = I_{i0} \geq 0, \quad (7.4b)$$

$$\frac{dR_i}{dt} = \alpha I_i - \mu R_i, \quad R_i(t_0) = R_{i0} \geq 0, \quad (7.4c)$$

$$\frac{dU_i}{dt} = \psi_i(t) - \nu U_i - \frac{\vartheta_i}{N_i} U_i \sum_{j=1}^n p_{ji} I_j, \quad U_i(t_0) = U_{i0} \geq 0, \quad (7.4d)$$

$$\frac{dV_i}{dt} = \frac{\vartheta_i}{N_i} U_i \sum_{j=1}^n p_{ji} I_j - \nu V_i, \quad V_i(t_0) = V_{i0} \geq 0, \quad (7.4e)$$

$$N_i = S_i + I_i + R_i. \quad (7.4f)$$

Here, the functions $\psi_i \in \mathcal{C}^1(\mathbb{D}, \mathbb{R})$ with $\psi_i(t) = \nu M_i(t) + \chi_i \cos(\omega(t - t_M)) M_i(t)$ describe the seasonal growth of the vector populations in the patches i , where $M_i \in \mathcal{C}^1(\mathbb{D}, \mathbb{R})$ stands for the size of the mosquito population at time t . Furthermore, the equation $M_i(t) = U_i(t) + V_i(t)$ provides

$$\frac{dM_i}{dt} = \chi_i \cos(\omega(t - t_M)) M_i, \quad (7.5)$$

since

$$\frac{dM_i(t)}{dt} = \frac{dU_i(t)}{dt} + \frac{dV_i(t)}{dt} = \nu M_i(t) + \chi_i \cos(\omega(t - t_M)) M_i(t) - \nu U_i(t) - \nu V_i(t).$$

The ODE (7.5) has the explicit solution

$$M_i(t) = M_{i0} e^{\frac{\chi_i}{\omega} \sin(\omega(t - t_M))}, \quad (7.6)$$

where $M_{i0} = M_i(t_M) \geq 0$ stands for the initial condition of (7.5) at the time t_M . Additionally M_{i0} represents the amplitude in (7.6) and is directly related to the average population size of the mosquitos since

$$\bar{M}_i = M_{i0} \cdot \frac{1}{\omega} \int_0^\omega e^{\frac{\chi_i}{\omega} \sin(\tau)} d\tau.$$

Figure (7.5) shows the seasonal growth of the vector populations in the patches $i = 1, \dots, 5$ for a time period of 10 years. We use the substitutions $R_i(t) = N_i - S_i(t) - I_i(t)$ and $U_i(t) = M_i(t) - V_i(t)$ to reduce (7.4) to

$$\frac{dS_i}{dt} = \mu(N_i - S_i) - S_i \sum_{j=1}^n p_{ij} \frac{\hat{\beta}_j}{M_{j0}} V_j, \quad S_{i0} \geq 0, \quad (7.7a)$$

$$\frac{dI_i}{dt} = S_i \sum_{j=1}^n p_{ij} \frac{\hat{\beta}_j}{M_{j0}} V_j - (\alpha + \mu) I_i, \quad I_{i0} \geq 0, \quad (7.7b)$$

$$\frac{dV_i}{dt} = \frac{\vartheta_i}{N_i} (M_i - V_i) \sum_{j=1}^n p_{ji} I_j - \nu V_i, \quad V_{i0} \geq 0. \quad (7.7c)$$

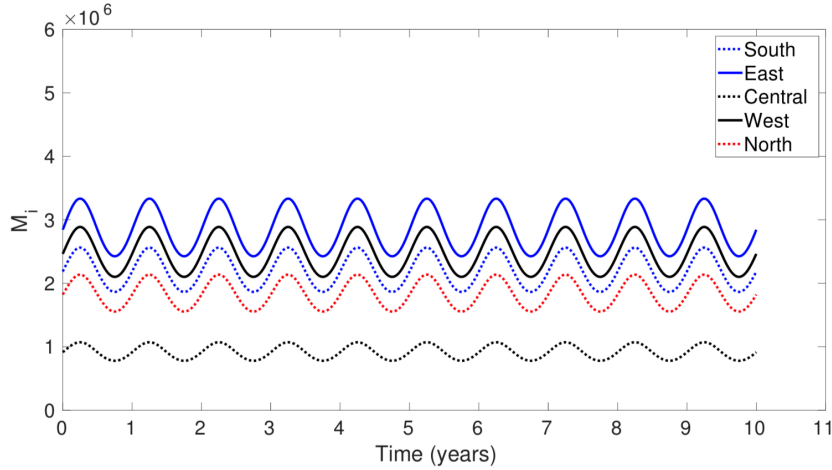


Figure 7.5: Seasonal growth of the vector populations. The initial conditions of the five patches are given as $M_{i0} = 10N_i$. The respective initial conditions for the hosts are $N = [2185711, 2843816, 914182, 2463560, 1747315]$, $t_M = 0$ and $\omega = 2\pi$.

The model (7.7) is simulated for an example with five patches. Note that a highly populated area will have a higher risk of infection see e.g. [21, 36, 45]. Here, the residence budgeting time matrix P is created using annual commuting data collected from five administrative districts of Jakarta, Indonesia (South, East, Central, West and North). Data is gained from the private communications of the authors with Dipo Aldila and Edy Soewono. The rates of annual travel data within the five areas of Jakarta are given by the Table 7.1.

Table 7.1: Rates of annual travel data within areas. The entries of the matrix are given per every 100 individuals.

from \ to	South	East	Central	West	North
South	0	4.68	9.51	3.79	1.98
East	10.82	0	9.45	3.29	6.77
Central	3.7	1.74	0	3.46	2.44
West	5.38	0.92	9.41	0	8.49
North	1.75	2.33	6.42	3.68	0

The entries of the residence budgeting time matrix P were computed from the data in Table 7.1 under the assumption that a host will stay in the patch where it is residing for 16hours and will perform short-time movements to the other patches for the remaining one third of the day. The corresponding residence budgeting time matrix based on the travel rates are computed as in Table 7.2.

Comparing the dynamics of the infected host compartment the maximum of infected hosts can be found in East Jakarta, while the minimum occurs in Central Jakarta. A higher host movement hence results in more infected hosts in the respective areas. Also, with the seasonal parameters used in simulating the model a seasonal pattern of the disease outbreak can be seen, see Figure 7.6.

Table 7.2: Residence budgeting time matrix P in %.

from \ to	South	East	Central	West	North
South	93.35	1.56	3.17	1.26	0.66
East	3.61	89.89	3.15	1.10	2.26
Central	1.23	0.58	96.22	1.15	0.81
West	1.79	0.31	3.14	91.93	2.83
North	0.58	0.78	2.14	1.23	95.27

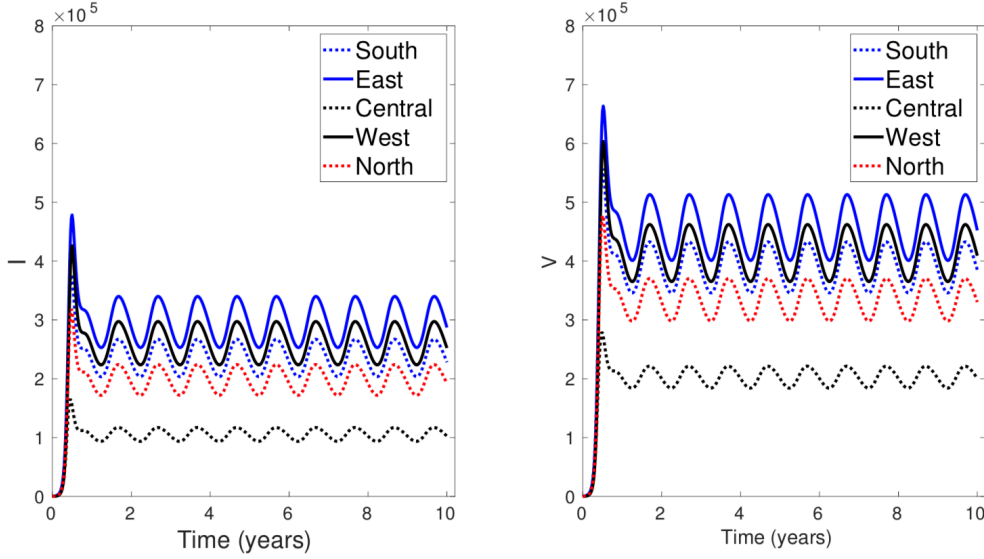


Figure 7.6: Plots in the left-hand side illustrate the dynamics of the infected host population of the five administrative districts for 10 years. Plots in the right-hand side illustrate the dynamics of the infected vector population of the five administrative districts for 10 years. The parameters used in the simulations are given by Table 7.3, where $c_1 = 2$, $c_2 = 2$, and $c_4 = 1$. In addition, $N = [2185711, 2843816, 914182, 2463560, 1747315]$.

7.4.4 Reduction of the SIRUV to a SIR model

The $SIRUV$ model given by equation (7.4) serves as basis for the development of the reduced SIR model. The procedure is based on the research on time-scale separation by Rocha et al. [37]. We present the detailed calculation in the Appendix 7.A.

Remark 7.4.5. The parameters chosen throughout our study are those from [37]. Since our model is based on the model in this paper, to have a comparable setting it is in our opinion reasonable to use the same parameter set. Compare for other parameters as e.g. life expectancy also [10, 50].

For χ_i it is assumed to be less than 5 to generate a maximally doubling of the mosquito population sizes since

$$\max_{t \in \mathbb{R}} e^{\frac{\chi_i}{\omega} \sin(\omega(t-t_M))} = e^{\frac{\chi_i}{\omega}}$$

and $\chi_i = \ln(2)\omega = 4.36$ solves the equation

$$2M_{i0} = M_{i0} e^{\frac{\chi_i}{\omega}}.$$

Table 7.3: Assumed parameter sizes of the *SIRUV* model with t in years. The expressions c_k are expected to be constant in the time-scale separation [10, 50].

Parameter	Meaning
$\mu = \frac{1}{69}$	Human death and birth rate (average life expectancy ≈ 69 years)
$\alpha = 26$	Human recovery rate (\approx two weeks)
$\hat{\beta}_i = c_1 \alpha$	Transmission rate between infected vector and human (unknown)
$\nu = 26$	Mosquito death and birth rate (average life expectancy ≈ 2 weeks)
$\vartheta_i = c_2 \nu$	Transmission rate between infected human and uninfected vector (unknown)
$N_{i0} = c_3 10^6$	Human population size (depends on investigated region)
$M_{i0} = c_4 N_{i0}$	Average mosquito population size (unknown)
$\omega = 2\pi$	Periodical frequency of vector population size
$\chi_i < 5$	Intensity of periodical variation within the mosquito population ($< 100\%$)

To be able to perform time-scale separation the model (7.7) is simplified by an *IVM* model with adapted parameters.

$$\frac{dI_i}{dt} = (N_i - I_i) \sum_{j=1}^n p_{ij} \frac{\hat{\beta}_j}{M_{j0}} V_j - (\alpha + \mu) I_i, \quad I_{i0} \geq 0, \quad (7.8a)$$

$$\frac{dV_i}{dt} = \frac{\vartheta_i}{N_i} (M_i - V_i) \sum_{j=1}^n p_{ji} I_j - \nu V_i, \quad V_{i0} \geq 0, \quad (7.8b)$$

$$\frac{dM_i}{dt} = \chi_i \cos(\omega(t - t_M)) M_i, \quad M_{i0} \geq 0. \quad (7.8c)$$

The vector dynamics V_i act much faster on the time-scale t compared to the human dynamics I_i . The size ratio between the parameters in the human and vector dynamics is exploited as follows

$$\varepsilon = \frac{\mu}{\nu} = \frac{1}{69 \cdot 26} = 5.6 \cdot 10^{-4}.$$

We define $\nu = \frac{\bar{\nu}}{\varepsilon}$ and $\vartheta_i = \frac{\bar{\vartheta}_i}{\varepsilon}$ which delivers $\bar{\vartheta}_i = \vartheta_i \varepsilon = \vartheta_i \frac{\bar{\nu}}{\nu}$ and develop (7.8) into a power series similar to the structure of a Taylor series

$$\begin{aligned} I_i(t, \varepsilon) &= I_i^{(0)} + \varepsilon I_i^{(1)} + \mathcal{O}(\varepsilon^2), \\ V_i(t, \varepsilon) &= V_i^{(0)} + \varepsilon V_i^{(1)} + \mathcal{O}(\varepsilon^2), \end{aligned} \quad (7.9)$$

with $I_i(t, 0) = I_i^{(0)}$ and $V_i(t, 0) = V_i^{(0)}$. The derivatives of (7.9) with respect to t provide

$$\frac{dI_i(t, \varepsilon)}{dt} = (N_i - I_i^{(0)}) \sum_{j=1}^n p_{ij} \frac{\hat{\beta}_j}{M_{j0}} V_j^{(0)} - (\alpha + \mu) I_i^{(0)} + \mathcal{O}(\varepsilon^1), \quad (7.10a)$$

$$\frac{dV_i(t, \varepsilon)}{dt} = \frac{1}{\varepsilon} \left(\frac{\bar{\vartheta}_i}{N_i} (M_i - V_i^{(0)}) \sum_{j=1}^n p_{ji} I_j^{(0)} - \bar{\nu} V_i^{(0)} \right) + \mathcal{O}(\varepsilon^0), \quad (7.10b)$$

$$\frac{dM_i}{dt} = \chi_i \cos(\omega(t - t_M)) M_i. \quad (7.10c)$$

In addition, we define a fast (mosquito) time-scale by $\tilde{t} = \frac{t}{\varepsilon}$ and compute the derivatives of the ODE system with respect to \tilde{t} . Indeed we get in leading order $\mathcal{O}(\varepsilon^0)$

$$\begin{aligned}\frac{dI_i^{(0)}}{d\tilde{t}} &= 0, \\ \frac{dV_i^{(0)}}{d\tilde{t}} &= \frac{\bar{\vartheta}_i}{N_i} \left(M_i - V_i^{(0)} \right) \sum_{j=1}^n p_{ji} I_j^{(0)} - \bar{\nu} V_i^{(0)}, \\ \frac{dM_i}{d\tilde{t}} &= 0.\end{aligned}$$

Hence, $I_i^{(0)}$ and M_i are independent of \tilde{t} and for $V_i^{(0)}$ we get an inhomogeneous ODE

$$\frac{dV_i^{(0)}}{d\tilde{t}} = - \underbrace{\left(\frac{\bar{\vartheta}_i}{N_i} \sum_{j=1}^n p_{ji} I_j^{(0)}(\tilde{t}_0) + \bar{\nu} \right)}_{=a_i} V_i^{(0)}(t) + \underbrace{\frac{\bar{\vartheta}_i}{N_i} M_i(\tilde{t}_0) \sum_{j=1}^n p_{ji} I_j^{(0)}(\tilde{t}_0)}_{=b_i}$$

which can explicitly be solved for $V_{i0} = V_i^{(0)}(\tilde{t}_0)$ by

$$V_i^{(0)}(t) = \exp\left(-a_i \frac{t - t_0}{\varepsilon}\right) \cdot \left(V_{i0} - \frac{b_i}{a_i} \right) + \frac{b_i}{a_i},$$

where we replaced \tilde{t} again by $\frac{t}{\varepsilon}$. For $t \rightarrow \infty$ the function $V_i^{(0)}(t)$ achieves exponentially fast its equilibrium V_i^* since $\frac{a_i}{\varepsilon} \gg 1$

$$V_i^* = \frac{b_i}{a_i} = \frac{\frac{\bar{\vartheta}_i}{N_i} M_i(\tilde{t}_0) \sum_{j=1}^n p_{ji} I_j^{(0)}(\tilde{t}_0)}{\frac{\bar{\vartheta}_i}{N_i} \sum_{j=1}^n p_{ji} I_j^{(0)}(\tilde{t}_0) + \bar{\nu}}.$$

On the slow time-scale t we use $I_i^{(0)}(t_0) = I_i^{(0)}(\tilde{t}_0)$ and $V_i^{(0)}(t_0) = V_i^*$ as initial conditions and equation (7.10b) in leading order $\mathcal{O}(\varepsilon^{-1})$ provides

$$V_i^{(0)}(t) = \frac{\frac{\bar{\vartheta}_i}{N_i} M_i(t) \sum_{j=1}^n p_{ji} I_j^{(0)}(t)}{\frac{\bar{\vartheta}_i}{N_i} \sum_{j=1}^n p_{ji} I_j^{(0)}(t) + \bar{\nu}}.$$

By using this expression for $V_i^{(0)}$ in (7.10a) we obtain again in leading order $\mathcal{O}(\varepsilon^0)$

$$\begin{aligned}\frac{dI_i^{(0)}}{dt} &= \left(N_i - I_i^{(0)} \right) \sum_{j=1}^n \left(p_{ij} \frac{\hat{\beta}_j \bar{\vartheta}_j M_j(t)}{M_{j0} \bar{N}_j} \sum_{k=1}^n p_{kj} I_k^{(0)}(t) \right) \\ &\quad - (\alpha + \mu) I_i^{(0)}.\end{aligned}$$

We define time-dependent transmission rates by

$$\beta_j(t) = \frac{\hat{\beta}_j \bar{\vartheta}_j}{\bar{\nu}} \cdot \frac{M_j(t)}{M_{j0}} = \frac{\hat{\beta}_j \bar{\vartheta}_j}{\bar{\nu}} e^{\frac{\chi_j}{\omega} \sin(\omega(t-t_M))}$$

and finally obtain

$$\frac{dI_i^{(0)}}{dt} = \left(N_i - I_i^{(0)} \right) \sum_{j=1}^n \left(p_{ij} \frac{\beta_j(t)}{N_j} \sum_{k=1}^n p_{kj} I_k^{(0)}(t) \right) - (\alpha + \mu) I_i^{(0)}.$$

This result provides the approach to the incidence term of our *SIR* model in (7.1). Using the substitutions $\beta_{j0} = \frac{\hat{\beta}_j \vartheta_j}{\nu}$ and $\beta_{j1} = \frac{\chi_j}{\omega}$ delivers

$$\beta_j(t) = \beta_{j0} e^{\beta_{j1} \sin(\omega(t-t_M))} \approx \beta_{j0} (1 + \beta_{j1} \sin(\omega(t-t_M))) . \quad (7.11)$$

It should be noted that we reduced the number of the $4n$ unknown parameters $\hat{\beta}_j$, ϑ_j , χ_j and M_{j0} to the $2n$ parameters β_{j0} and β_{j1} . Additionally, we forego explicit mosquito dynamics.

Remark 7.4.6. The time scale separation results in a Holling–type II functional response for $V(I)$ as a function of the infected humans. This can be reduced further to a linear relation in human *SIR* models on which the following analysis of data is based. The last reduction, i.e. $V(I) \rightarrow I$ however holds just in reasonable parameter regions in the *SIRUV* model. Indeed it holds when the endemic stationary state is in order of the small parameter μ . In an *SISUV* model, where the stationary state is of order one this is not the case.

7.5 Data fit analysis

In this section we will determine the seasonality and the hospitalization rate according to the underlying data set. The seasonality will be encoded in the transmission function $\beta(t)$ as a frequency and a phase shift in a sine–function. All the selected and fixed parameters we use throughout this section are given in Table 7.3.

In order to add seasonality and hospitalization rate in the patches, we formulate an optimal control problem and solve it using a conjugate gradient method combined with a forward–backward sweep method. Details of this procedure are presented in Appendix 7.B. For the computational reasons we add a quadratic penalization term which ensures the convexity of the cost functional and hence the existence of a minimizer. Statistically we hence use a form of weighted least squares to fit the data. Of course other statistical methods could be used, however, since we want to obtain a functional dependence of the infection rate on time, methods from optimal control are directly available and straightforward. The numerical simulations for the predictions show that the results are in good agreement with the underlying data. A sensitivity analysis will be part of a forthcoming publication.

In order to fit $I_i(t)$ with t in years to the dengue data from Jakarta we analyze an objective function $J \in \mathcal{C}^1(\mathbb{R}^l, \mathbb{R})$ and the corresponding minimization problem

$$\min_u J(u) = \min_u \sum_{i=1}^n \int_{t_0}^{t_1} \frac{(\gamma_i I_i(t) - I_i^d(t))^2}{\max_{t \in \mathbb{D}} I_i^d(t)} dt + \left(\frac{\|u\|}{N} \right)^2 \quad (7.12a)$$

subject to

$$\frac{dS_i}{dt} = \mu(N_i - S_i) - S_i \sum_{j=1}^n \left(p_{ij} \frac{\beta_j(t)}{N_j} \sum_{k=1}^n p_{kj} I_k \right), \quad S_{i0} \geq 0, \quad (7.12b)$$

$$\frac{dI_i}{dt} = S_i \sum_{j=1}^n \left(p_{ij} \frac{\beta_j(t)}{N_j} \sum_{k=1}^n p_{kj} I_k \right) - (\alpha + \mu) I_i, \quad I_{i0} \geq 0, \quad (7.12c)$$

$$\frac{dR_i}{dt} = \alpha I_i - \mu R_i, \quad R_{i0} \geq 0, \quad (7.12d)$$

$$N_i = S_i + I_i + R_i. \quad (7.12e)$$

It is assumed that only a fraction of infected individuals is registered or hospitalized, therefore γ_i is implemented as *hospitalization rate* in patch i [48]. Let $I_i^d \in \mathcal{C}^1(\mathbb{D}, \mathbb{R})$ be the cubic spline interpolation through the moving average points \bar{d}_i . Then $\int_{t_0}^{t_1} (\gamma_i I_i(t) - I_i^d(t))^2 dt \geq 0$ becomes small, if $\gamma_i I_i$ is fitted to I_i^d . The particular integral is divided by $\max_{t \in \mathbb{D}} I_i^d(t)$ to exclude imbalances between the fitting of the patches, since they have different sizes of populations. The integrals in $J(u)$ are based on a L^2 norm so that its minimization corresponds to a least squares method.

Additionally, we add the convex and radially unbounded *regularization term* $(\|u\|/N)^2$, which is similar to a *Tikhonov regularization* [44]. We use as a weight for the penalization term $1/N^2$, where $N = \sum_{i=1}^n N_i$. Thus, its influence on the result of the minimization is vanishingly small, however, it directly affects the convexity of the minimization problem.

The vector $u \in \mathbb{R}^l$ includes the initial conditions of the ODE S_{i0} and R_{i0} the hospitalization rates γ_i and the unknown parameters of the transmission rates $\beta_j(t)$, see Table 7.4. The initial values of the infected individuals I_i are calculated using the substitution $I_{i0} = N_i - S_{i0} - R_{i0}$. In the following simulations we assume the same transmission and hospitalization rate $\beta(t)$ and γ in all patches.

Table 7.4: Simulations with the corresponding transmission rates $\beta(t)$ and parameters in u . On the basis of statistics, we assume that the average human lifespan is 69 years, so that $\mu = \frac{1}{69}$, see [50]. The recovery rate is estimated at two weeks, leading to $\alpha = 26$, see [48].

Simulation	$\beta(t), u$
1	$\beta(t) = \beta_0 + \beta_1 \sin(\omega(t + \varphi/52))$ $u = (\beta_0, \beta_1, \varphi, \gamma, S_{10}, \dots, S_{n0}, R_{10}, \dots, R_{n0})^T$
2	$\beta(t) = \beta_0 + \beta_1 \int_{t-\eta_2/52}^{t-\eta_1/52} p_c(\tau) d\tau \sin(\omega(t + \varphi/52))$ $u = (\beta_0, \beta_1, c, \eta_2, \varphi, \gamma, S_{10}, \dots, S_{n0}, R_{10}, \dots, R_{n0})^T$

We have that the parameter β_0 stands for the *average transmission rate* and β_1 respectively $\beta_1 \int_{t-\eta_2/52}^{t-\eta_1/52} p_c(\tau) d\tau$ for the *degree of periodical variation*. A *phase-shift* φ in weeks is additionally included and β_1 is multiplied with an integral of the precipitation function $p_c(\tau)$ in Simulation 2. It is defined by

$$p_c(\tau) = \begin{cases} p(\tau), & p(\tau) < c \\ 0, & p(\tau) \geq c. \end{cases} \quad (7.13)$$

The function $p(\tau) \in \mathcal{C}^1(\mathbb{D}, \mathbb{R})$ includes the smoothed rainfall data points \bar{p}_i and c represents the *cut-off*. The cut-off is due to the fact that for large rainfalls eggs are destroyed or washed away [13]. As described already in Section 7.3, this can also be seen from the clusters in precipitation and dengue data. Here one sees a drastical decrease of dengue cases in the average rainfall is higher than around 15mm per day. One could also use a more mollified function for the cut-off of p_c . It is however not to expect that this would change the result remarkably. The interval $[t - \eta_2/52; t - \eta_1/52]$ is set around the lag between precipitation and dengue data.

Table 7.5: Numerical results of the parameter fit in Simulation 1 and 2. All other parameters are according to Table 7.3.

Parameters	β_0	β_1	c	η_2	φ	γ	α	μ	ω	η_1
Simulation 1	47.31	7.53	/	/	10.48	0.24	26	$\frac{1}{69}$	2π	/
Simulation 2	57.43	45.50	16	7.80	9.00	0.25	26	$\frac{1}{69}$	2π	6

7.6 Results

7.6.1 Numerical simulations of the SIR model

In the following section the data fit without direct influence of rain data is called Simulation 1 and Simulation 2 includes the rain data. The numerical and graphical results of these simulations are represented in Table 7.5 and 7.7. The magnitude of the parameters β_0 , γ and φ is the same whereby Simulation 2 shows a higher average transmission rate for β_0 . To compare the degree of periodic variation we examine the size of the term

$$\beta_1 \int_{t-\frac{\eta_2}{52}}^{t-\frac{\eta_1}{52}} p_c(\tau) d\tau < \beta_1 \cdot \frac{\eta_2 - \eta_1}{52} \cdot c = 45.50 \cdot \frac{1.8}{52} \cdot 16 = 25.20. \quad (7.14)$$

In Simulation 2 this term fluctuates between 0 and 25.20 whereas in Simulation 1 we obtain $\beta_1 = 7.53$. The cut-off c and the interval limits $[t - \eta_2/52; t - \eta_1/52]$ fit to the assumptions in Section 7.3 since $15mm \leq c \leq 20mm$ and $\eta_2 = 7.80$ are sensible values in terms of the cluster and cross-correlation between the moving average of rainfall and dengue data. The hospitalization rate γ is in the expected range of 25%. Due to the optimization of the phase shift φ , the timing of the model fits well to the dengue peaks in the data set. When comparing the respective graphs, it is noticeable that a more realistic dynamic can be recognized by adding the rain data. This is particularly noticeable because certain fluctuations during the individual periods are reflected, such as in 2009. It is also striking that between 2015 and 2016 Simulation 2 does not reproduce the very low values in contrast to Simulation 1. The rain data indicate that the longest period with very low precipitation was before 2015 which is reflected in the dengue data but not in the model. On the one hand side *SIR* models are only suitable for short periods of time and the start time of the data fit should be set later. But this would be also true for Simulation 1. A possible explanation is that 2016 was an El Nino year which could lead to outliers since then the functional form for the seasonality could be wrong. Further deviations can be found in various patches in 2010, 2013 and 2014 because in these cases the timing of the peaks differs from other years. Overall, it should be noted that the different intensities of the dengue peaks and their relation to each other are well represented by the *SIR* model. The results also allow conclusions about the behavior of the mosquito population. Provided the size of the vector population can be modeled by $M_i(t) = M_{i0} e^{\frac{\chi}{\omega} \sin(\omega(t+\varphi/52))}$, the term

$$e^{\frac{\chi}{\omega} \sin(\omega(t+\frac{\varphi}{52}))} \approx 1 + \frac{\chi}{\omega} \sin\left(\omega\left(t + \frac{\varphi}{52}\right)\right)$$

describes the seasonal variation of the mosquito population. As shown in Section 7.4 in Simulation 1 the fraction $\frac{\beta_1}{\beta_0}$ approximately corresponds to the size of the expression $\frac{\chi}{\omega}$. Since $|\frac{\chi}{\omega} \sin(\omega(t+\varphi/52))| \leq 0.16$ applies for $\frac{\chi}{\omega} = \frac{\beta_1}{\beta_0}$ we can conclude that the size of the mosquito population varies by a maximum of approximately 20%. In Simulation 2 the

term $\frac{\beta_1}{\beta_0} \int_{t-\eta_2/52}^{t-\eta_1/52} p_c(\tau) d\tau$ corresponds to a time-dependent expression $\frac{\chi(t)}{\omega}$ with $\chi : \mathbb{D} \rightarrow \mathbb{R}_0^+$. Using the result from (7.14) we get $\left| \frac{\chi(t)}{\omega} \sin(\omega(t + \varphi/52)) \right| \leq 0.44$ and consequently a variation of at most about 50%. The graph of the transmission rate $\beta(t)$ in the second simulation reflects the dynamic processes within the model. For example, the effects of the cut-off are visible in the years 2014–2015, when $\beta(t)$ assumes the value β_0 over longer periods of time. In contrast, the very dry time at the end of 2015 is clearly shown in $\beta(t)$ in the same way.

Table 7.6: Results of the parameter fit and $\beta(t)$ in Simulation 1 and 2.

Parameters	β_0	β_1	c	η_2	φ	γ	α	μ	ω	η_1
Simulation 1	47.31	7.53	/	/	10.48	0.24	26	$\frac{1}{69}$	2π	/

Transmission Rate

$$\beta(t) = \beta_0 + \beta_1 \sin(\omega(t + \varphi/52)) \quad \beta(t) \in [39.74; 54.84]$$

Parameters	β_0	β_1	c	η_2	φ	γ	α	μ	ω	η_1
Simulation 2	57.43	45.50	16	7.80	9.00	0.25	26	$\frac{1}{69}$	2π	6

Transmission Rate

$$\beta(t) = \beta_0 + \beta_1 \int_{t-\eta_2/52}^{t-\eta_1/52} p_c(\tau) d\tau \sin(\omega(t + \varphi/52)) \quad \beta(t) \in [43.83; 75.28]$$

7.6.2 Prediction quality of the SIR model

The prediction quality of the model is the basis for further application with regard to various control methods. For this reason, we test the presented model using the available data sets. In the following, the parameters in $u = (\beta_0, \beta_1, c, \eta_2, \varphi, \gamma, S_0, R_0)^T$ are fitted up to a time $\hat{t} \in [t_0; t_1]$. Then the model continues with these findings and makes a prediction to the end time 2017. In Simulation 3 we use the available rain data and in Simulation 4 the average rainfall data of previous years within the prognosis interval (see Tables 7.10 and 7.11). To give more weight to current than to past data we introduce a weight function $H : \mathbb{D} \rightarrow \mathbb{R}^+$ with

$$H(t) = w \cdot \exp\left(-\frac{(t - \hat{t})^2}{2\sigma^2}\right) + z.$$

The parameters $w = 50$, $\sigma = \frac{4}{52}$ and $z = 1$ are selected so that the period of the last four weeks before \hat{t} is weighted considerably more strongly. Consequently, we obtain the

Table 7.7: Results of the parameter fit in Simulation 1 and 2.

Simulation 1				Simulation 2			
S_{i0}	I_{i0}	R_{i0}	N_i	S_{i0}	I_{i0}	R_{i0}	N_i
1166192	612	1018908	2185711	935017	658	1250036	2185711
1664665	632	1178518	2843816	1343231	627	1499958	2843816
404974	313	508895	914182	313890	340	599952	914182
1279767	112	1183681	2463560	1013347	158	1450055	2463560
922332	479	824504	1747315	746904	466	999945	1747315

minimization problem

$$\min_u J(u) = \min_u \sum_{i=1}^n \int_{t_0}^{\hat{t}} H(t) \frac{(\gamma I_i(t) - I_i^d(t))^2}{\max_{t \in \mathbb{D}} I_i^d(t)} dt + \left(\frac{\|u\|}{N} \right)^2.$$

In practice, the optimization up to \hat{t} should be constantly updated. In our simulations we have optimized in most cases until eight weeks after the turn of the year. The reason for this is that in Jakarta the number of dengue cases increases significantly every year during this period and the model is to be tested for its prediction quality for the following season. Additionally we calculate based on the L^1 norm

$$\mathcal{E}_1 = \int_{\hat{t}}^{\hat{t}+1} \frac{|\gamma I_i(t) - I_i^d(t)|}{\max_{t \in [\hat{t}, \hat{t}+1]} I_i^d(t)} dt \quad \text{and} \quad \mathcal{E}_2 = \frac{1}{t_1 - \hat{t}} \int_{\hat{t}}^{t_1} \frac{|\gamma I_i(t) - I_i^d(t)|}{\max_{t \in [\hat{t}, t_1]} I_i^d(t)} dt.$$

These values are used to determine the deviation of the model in relation to the corresponding maximum value within the data. Although the forecast for the coming season is in the foreground, the model also reveals tendencies in the following years. For example, the relatively high increase of registered cases in 2016 is indicated not only in the direct forecast of the corresponding year, but also in the long-term forecasts. In most cases, the model provides information about the expected size of dengue cases in the coming season. It is noticeable that in most cases the relation of the forthcoming peak to the previous peaks is quite realistic. With regard to the short-term forecast, it makes no significant difference whether the model continues to calculate with the actual or average rain data. Large deviations between Simulation 3 and 4 arise only with the long-term forecast until 2017.

Remark 7.6.3. Note that, although the model is very homogeneous among the regions, due to the same hospitality rate and the same ratio of mosquito to humans and other parameters, the fitting results for the model are in good agreement with the data. This is also an effect of the mobility matrix, which introduces a spatial-inhomogeneity into the system. In a forthcoming study this particular role of the mobility matrix will be considered.

Table 7.8: Quantitative comparison of the prediction error for South Jakarta.

Simulation 3: The parameter fit is executed in the interval $[2009; \hat{t}]$. The forecast based on this is carried out with the actual rain data for the period $[\hat{t}; 2017]$.

Simulation 4: The forecast in $[\hat{t}; 2017]$ is done with the average rain data from the period $[2009; \hat{t}]$.

	$\hat{t} = 2016 + 8\text{weeks}$		$\hat{t} = 2015 + 8\text{weeks}$		$\hat{t} = 2014 + 8\text{weeks}$	
	\mathcal{E}_1	\mathcal{E}_2	\mathcal{E}_1	\mathcal{E}_2	\mathcal{E}_1	\mathcal{E}_2
Simulation 3	0.12	0.12	0.21	0.12	0.3	0.41
Simulation 4	0.26	0.26	0.17	0.15	0.39	0.67

	$\hat{t} = 2013 + 8\text{weeks}$		$\hat{t} = 2012 + 8\text{weeks}$		$\hat{t} = 2015 + 24\text{weeks}$	
	\mathcal{E}_1	\mathcal{E}_2	\mathcal{E}_1	\mathcal{E}_2	\mathcal{E}_1	\mathcal{E}_2
Simulation 3	0.22	0.18	0.33	0.36	0.17	0.13
Simulation 4	0.19	0.68	0.30	0.56	0.14	0.17

From Table 7.8, and the numerical findings in Appendix 7.C we see that the Simulation 3 has always smaller prediction errors. Of course this is to expect, since more detailed information about the rainfall in the forecasted period is incorporated. Although the error is slightly higher, it is remarkable, that peaks of the prediction of Simulation 4 are in a very good agreement with the peaks in the dengue data, although just average rainfall data from the past timeset was taken. It is clear that the errors are the higher the more time has to be predicted or vice versa the less information is used for a prediction.

Remark 7.6.4. Of course for an exact prediction in practice one has to update the data sets during the time. The model used here is due to several reductions just in a good

agreement for a short time horizon. Moreover as one can see e.g. in the prediction of the years 2015 and 2016 in Table 7.7 the peaks of the outbreak can not be seen clearly. Another reason here could be an uncertainty in the climatic input.

7.7 Conclusions

Modelling dengue using a multi-patch *SIR* model with a time-dependent transmission rate has proven to be practical for predicting the intensity of future outbreaks using realistic data sets. Compared to the *SIRUV* model, this model does not require explicit mosquito dynamics and is therefore subject to only a few unknown variables. The parameters to be adjusted allow conclusions about the periodic behavior of the vector population size and the associated influence of precipitation on the number of dengue cases. In addition, we obtain information on realistic estimates of the number of unreported cases and the influence of precipitation on the reproduction of mosquitoes. Obviously, this application is strongly dependent on the quality of the available disease, weather and commuting data sets. This underlines the importance of a complete and accurate collection of valid data in order to make accurate forecasts. It should also be noted that the application of a *SIR* model is only suitable for short-term applications, which is why in practice the data should always be updated and the model continuously adapted for a short previous period of time. Due to the similarities to other vector-borne diseases, an application of the model to Malaria or ZIKA is conceivable. Pontryagin's maximum principle proved to be quite suitable to fit the parameters of the model to the data. In further research, this optimal control methods should be used to derive optimal vector control or information campaigns within the population to contain future dengue outbreaks. In this context, the multi-patch *SIR* model provides the basis for optimizing these control methods in the individual districts. Especially the commuter movements between the patches can be investigated regarding their influence on control methods and the spread of the disease with the aim to plan and implement feasible and affordable control campaigns.

Acknowledgment

We gratefully thank the anonymous reviewers for giving very valueable hints to enhance the quality of the manuscript. We want to thank Dipo Aldila and Edy Soewono for the discussions and providing the data sets for Jakarta which are used throughout this work.

Appendix

7.A Appendix A: Reduction of the SIRUV to a SIR model

The *SIRUV* model given by equation (7.4) serves as basis for the development of the reduced *SIR* model. The following procedure is based on the research on time-scale separation by Rocha et al. [37].

Table 7.9: Assumed parameter sizes of the *SIRUV* model with t in years. The expressions c_k are expected to be constant in the time-scale separation [10, 50].

Parameter	Meaning
$\mu = \frac{1}{69}$	Human death and birth rate (average life expectancy ≈ 69 years)
$\alpha = 26$	Human recovery rate (\approx two weeks)
$\hat{\beta}_i = c_1\alpha$	Transmission rate between infected vector and human (unknown)
$\nu = 26$	Mosquito death and birth rate (average life expectancy ≈ 2 weeks)
$\vartheta_i = c_2\nu$	Transmission rate between infected human and uninfected vector (unknown)
$N_{i0} = c_310^6$	Human population size (depends on investigated region)
$M_{i0} = c_4N_{i0}$	Average mosquito population size (unknown)
$\omega = 2\pi$	Periodical frequency of vector population size
$\chi_i < 5$	Intensity of periodical variation within the mosquito population ($< 100\%$)

Remark 7.A.1. The parameters chosen throughout our study are those from [37]. Since our model is based on the model in this paper, to have a comparable setting it is in our opinion reasonable to use the same parameter set. Compare for other parameters as e.g. life expectancy also [10, 50].

For χ_i it is assumed to be less than 5 to generate a maximally doubling of the mosquito population sizes since

$$\max_{t \in \mathbb{R}} e^{\frac{\chi_i}{\omega} \sin(\omega(t-t_M))} = e^{\frac{\chi_i}{\omega}}$$

and $\chi_i = \ln(2)\omega = 4.36$ solves the equation

$$2M_{i0} = M_{i0}e^{\frac{\chi_i}{\omega}}.$$

To be able to perform time-scale separation the model (7.7) is simplified by an *IVM* model with adapted parameters.

$$\frac{dI_i}{dt} = (N_i - I_i) \sum_{j=1}^n p_{ij} \frac{\hat{\beta}_j}{M_{j0}} V_j - (\alpha + \mu) I_i, \quad I_{i0} \geq 0, \quad (7.15a)$$

$$\frac{dV_i}{dt} = \frac{\vartheta_i}{N_i} (M_i - V_i) \sum_{j=1}^n p_{ji} I_j - \nu V_i, \quad V_{i0} \geq 0, \quad (7.15b)$$

$$\frac{dM_i}{dt} = \chi_i \cos(\omega(t - t_M)) M_i, \quad M_{i0} \geq 0. \quad (7.15c)$$

7 Appendix

In this new system, the assumed recovery rate lies in the range of years, e.g. $\alpha = \frac{1}{10}$. Supposing that the parameters of the human dynamics are now in a similar magnitude of 10^{-1} and the vector dynamics of 10^1 , we conclude that the vector dynamics V_i act much faster on the time-scale t compared to the human dynamics I_i . The size ratio between the parameters in the human and vector dynamics is exploited as follows

$$\varepsilon = \frac{\mu}{\nu} = \frac{1}{69 \cdot 26} = 5.6 \cdot 10^{-4}.$$

We define $\nu = \frac{\bar{\nu}_i}{\varepsilon}$ and $\vartheta_i = \frac{\bar{\vartheta}_i}{\varepsilon}$ which delivers $\bar{\vartheta}_i = \vartheta_i \varepsilon = \vartheta_i \frac{\bar{\nu}_i}{\nu}$. Consequently, equation (7.15) can be expressed using

$$\frac{dI_i}{dt} = (N_i - I_i) \sum_{j=1}^n p_{ij} \frac{\hat{\beta}_j}{M_{j0}} V_j - (\alpha + \mu) I_i, \quad (7.16a)$$

$$\frac{dV_i}{dt} = \frac{1}{\varepsilon} \left(\frac{\bar{\vartheta}_i}{N_i} (M_i - V_i) \sum_{j=1}^n p_{ji} I_j - \bar{\nu} V_i \right), \quad (7.16b)$$

$$\frac{dM_i}{dt} = \chi_i \cos(\omega(t - t_M)) M_i. \quad (7.16c)$$

The solutions $I_i(t)$ and $V_i(t)$ depend not only on the time variable t but also on the parameters and explicitly on ε . Thus the behavior of $I_i(t, \varepsilon)$ and $V_i(t, \varepsilon)$ for small ε has to be examined around $\varepsilon = 0$. We develop a power series similar to the structure of a Taylor series

$$I_i(t, \varepsilon) = I_i^{(0)} + \varepsilon I_i^{(1)} + \mathcal{O}(\varepsilon^2), \quad (7.17a)$$

$$V_i(t, \varepsilon) = V_i^{(0)} + \varepsilon V_i^{(1)} + \mathcal{O}(\varepsilon^2), \quad (7.17b)$$

with $I_i(t, 0) = I_i^{(0)}$ and $V_i(t, 0) = V_i^{(0)}$. The derivatives of (7.17) with respect to t provide

$$\frac{dI_i(t, \varepsilon)}{dt} = \frac{dI_i^{(0)}}{dt} + \varepsilon \frac{dI_i^{(1)}}{dt} + \mathcal{O}(\varepsilon^2), \quad (7.18a)$$

$$\frac{dV_i(t, \varepsilon)}{dt} = \frac{dV_i^{(0)}}{dt} + \varepsilon \frac{dV_i^{(1)}}{dt} + \mathcal{O}(\varepsilon^2), \quad (7.18b)$$

and by combining equations (7.16), (7.17) and (7.18) we get with [37]

$$\frac{dI_i(t, \varepsilon)}{dt} = (N_i - I_i^{(0)}) \sum_{j=1}^n p_{ij} \frac{\hat{\beta}_j}{M_{j0}} V_j^{(0)} - (\alpha + \mu) I_i^{(0)} + \mathcal{O}(\varepsilon^1), \quad (7.19a)$$

$$\frac{dV_i(t, \varepsilon)}{dt} = \frac{1}{\varepsilon} \left(\frac{\bar{\vartheta}_i}{N_i} (M_i - V_i^{(0)}) \sum_{j=1}^n p_{ji} I_j^{(0)} - \bar{\nu} V_i^{(0)} \right) + \mathcal{O}(\varepsilon^0), \quad (7.19b)$$

$$\frac{dM_i}{dt} = \chi_i \cos(\omega(t - t_M)) M_i. \quad (7.19c)$$

In addition, we define a fast (mosquito) time-scale by $\tilde{t} = \frac{t}{\varepsilon}$ and calculate the derivations

with respect to \tilde{t}

$$\begin{aligned} \frac{dI_i(t, \varepsilon)}{d\tilde{t}} &= \varepsilon \frac{dI_i(t, \varepsilon)}{dt} \\ &= \varepsilon \left((N_i - I_i^{(0)}) \sum_{j=1}^n p_{ij} \frac{\hat{\beta}_j}{M_{j0}} V_j^{(0)} - (\alpha + \mu) I_i^{(0)} \right) + \mathcal{O}(\varepsilon^2), \end{aligned} \quad (7.20a)$$

$$\frac{dV_i(t, \varepsilon)}{d\tilde{t}} = \varepsilon \frac{dV_i(t, \varepsilon)}{dt} = \frac{\bar{\vartheta}_i}{N_i} (M_i - V_i^{(0)}) \sum_{j=1}^n p_{ji} I_j^{(0)} - \bar{\nu} V_i^{(0)} + \mathcal{O}(\varepsilon^1), \quad (7.20b)$$

$$\frac{dM_i}{d\tilde{t}} = \varepsilon \frac{dM_i}{dt} = \varepsilon \chi_i \cos(\omega(t - t_M)) M(t). \quad (7.20c)$$

Comparing equal orders of ε in (7.20) we get in leading order $\mathcal{O}(\varepsilon^0)$

$$\begin{aligned} \frac{dI_i^{(0)}}{d\tilde{t}} &= 0, \\ \frac{dV_i^{(0)}}{d\tilde{t}} &= \frac{\bar{\vartheta}_i}{N_i} (M_i - V_i^{(0)}) \sum_{j=1}^n p_{ji} I_j^{(0)} - \bar{\nu} V_i^{(0)}, \\ \frac{dM_i}{d\tilde{t}} &= 0. \end{aligned}$$

Hence, $I_i^{(0)}$ and M_i are independent of \tilde{t} and for $V_i^{(0)}$ we get an inhomogeneous ODE

$$\frac{dV_i^{(0)}}{d\tilde{t}} = - \underbrace{\left(\frac{\bar{\vartheta}_i}{N_i} \sum_{j=1}^n p_{ji} I_j^{(0)}(\tilde{t}_0) + \bar{\nu} \right)}_{=a_i} V_i^{(0)}(t) + \underbrace{\frac{\bar{\vartheta}_i}{N_i} M_i(\tilde{t}_0) \sum_{j=1}^n p_{ji} I_j^{(0)}(\tilde{t}_0)}_{=b_i}$$

which can explicitly be solved for $V_{i0} = V_i^{(0)}(\tilde{t}_0)$ by

$$V_i^{(0)}(t) = \exp\left(-a_i \frac{t - t_0}{\varepsilon}\right) \cdot \left(V_{i0} - \frac{b_i}{a_i}\right) + \frac{b_i}{a_i},$$

where we replaced \tilde{t} again by $\frac{t}{\varepsilon}$. For $t \rightarrow \infty$ the function $V_i^{(0)}(t)$ achieves exponentially fast its equilibrium V_i^* since $\frac{a_i}{\varepsilon} \gg 1$

$$V_i^* = \frac{b_i}{a_i} = \frac{\bar{\vartheta}_i M_i(\tilde{t}_0) \sum_{j=1}^n p_{ji} I_j^{(0)}(\tilde{t}_0)}{\frac{\bar{\vartheta}_i}{N_i} \sum_{j=1}^n p_{ji} I_j^{(0)}(\tilde{t}_0) + \bar{\nu}}.$$

On the slow time-scale t we use $I_i^{(0)}(t_0) = I_i^{(0)}(\tilde{t}_0)$ and $V_i^{(0)}(t_0) = V_i^*$ as initial conditions and equation (7.19b) in leading order $\mathcal{O}(\varepsilon^{-1})$ provides

$$0 = \frac{\bar{\vartheta}_i}{N_i} (M_i - V_i^{(0)}) \sum_{j=1}^n p_{ji} I_j^{(0)} - \bar{\nu} V_i^{(0)}$$

and hence

$$V_i^{(0)}(t) = \frac{\frac{\bar{\vartheta}_i}{N_i} M_i(t) \sum_{j=1}^n p_{ji} I_j^{(0)}(t)}{\frac{\bar{\vartheta}_i}{N_i} \sum_{j=1}^n p_{ji} I_j^{(0)}(t) + \bar{\nu}}.$$

7 Appendix

By using this expression for $V_i^{(0)}$ in (7.19a) we obtain again in leading order $\mathcal{O}(\varepsilon^0)$

$$\begin{aligned} \frac{dI_i^{(0)}}{dt} &= \left(N_i - I_i^{(0)} \right) \sum_{j=1}^n \left(p_{ij} \frac{\hat{\beta}_j \bar{\vartheta}_j M_j(t)}{M_{j0} \bar{N}_j} \frac{\sum_{k=1}^n p_{kj} I_k^{(0)}(t)}{\sum_{k=1}^n p_{kj} I_k^{(0)}(t) + \bar{\nu}} \right) \\ &\quad - (\alpha + \mu) I_i^{(0)}. \end{aligned}$$

Since $\sum_{k=1}^n p_{kj} I_k^{(0)}(t) \ll N_j$ and $\bar{\vartheta}_j \ll 1$ the expression $\frac{\bar{\vartheta}_j}{N_j} \sum_{k=1}^n p_{kj} I_k^{(0)}(t)$ can be neglected in the denominator which means that

$$\frac{\hat{\beta}_j \bar{\vartheta}_j M_j(t)}{M_{j0} \bar{N}_j} \approx \frac{\hat{\beta}_j \bar{\vartheta}_j M_j(t)}{M_{j0} \bar{\nu}} = \frac{1}{N_j} \cdot \frac{\hat{\beta}_j \bar{\vartheta}_j}{\bar{\nu}} \cdot \frac{M_j(t)}{M_{j0}}.$$

We define time-dependent transmission rates by

$$\beta_j(t) = \frac{\hat{\beta}_j \bar{\vartheta}_j}{\bar{\nu}} \cdot \frac{M_j(t)}{M_{j0}} = \frac{\hat{\beta}_j \bar{\vartheta}_j}{\bar{\nu}} e^{\frac{\chi_j}{\omega} \sin(\omega(t-t_M))}$$

and finally obtain

$$\frac{dI_i^{(0)}}{dt} = \left(N_i - I_i^{(0)} \right) \sum_{j=1}^n \left(p_{ij} \frac{\beta_j(t)}{N_j} \sum_{k=1}^n p_{kj} I_k^{(0)}(t) \right) - (\alpha + \mu) I_i^{(0)}.$$

This result provides the approach to the incidence term of our *SIR* model in (7.1). Using the substitutions $\beta_{j0} = \frac{\hat{\beta}_j \bar{\vartheta}_j}{\bar{\nu}}$ and $\beta_{j1} = \frac{\chi_j}{\omega}$ delivers

$$\beta_j(t) = \beta_{j0} e^{\beta_{j1} \sin(\omega(t-t_M))} \approx \beta_{j0} (1 + \beta_{j1} \sin(\omega(t-t_M))). \quad (7.21)$$

It should be noted that we reduced the number of the $4n$ unknown parameters $\hat{\beta}_j$, ϑ_j , χ_j and M_{j0} to the $2n$ parameters β_{j0} and β_{j1} . Additionally, we forego explicit mosquito dynamics.

Remark 7.A.2. The time scale separation results in a Holling-type II functional response for $V(I)$ as a function of the infected humans. This can be reduced further to a linear relation in human *SIR* models on which the following analysis of data is based. The last reduction, i.e. $V(I) \rightarrow I$ however holds just in reasonable parameter regions in the *SIRUV* model. Indeed it holds when the endemic stationary state is in order of the small parameter μ . In an *SISUV* model, where the stationary state is of order one this is not the case.

7.B Appendix B: Detailed description of solving the optimal control problem in Section 7.5

To solve the optimization problem with a *Lagrange function* $\mathcal{L} : \mathbb{R}^l \times \mathcal{C}^1(\mathbb{D}, \mathbb{R}^{6n}) \rightarrow \mathbb{R}$ we implement *adjoint functions* $\lambda_{S_i}, \lambda_{I_i}, \lambda_{R_i} \in \mathcal{C}^1(\mathbb{D}, \mathbb{R})$ as *Lagrange multipliers*. In order to simplify the notation we define the functions $x, \lambda \in \mathcal{C}^1(\mathbb{D}, \mathbb{R}^{3n})$ and $g : \mathbb{D} \times \mathcal{C}^1(\mathbb{D}, \mathbb{R}^{3n}) \times \mathbb{R}^l \rightarrow \mathbb{R}^{3n}$ with

$$\begin{aligned} x &= (S_1, \dots, S_n, I_1, \dots, I_n, R_1, \dots, R_n)^T, \\ \lambda &= (\lambda_{S_1}, \dots, \lambda_{S_n}, \lambda_{I_1}, \dots, \lambda_{I_n}, \lambda_{R_1}, \dots, \lambda_{R_n})^T, \\ g &= (g_{S_1}, \dots, g_{S_n}, g_{I_1}, \dots, g_{I_n}, g_{R_1}, \dots, g_{R_n})^T, \end{aligned}$$

7.B Appendix B: Detailed description of solving the optimal control problem in Section 7.5

whereby g_{S_i}, g_{I_i} and g_{R_i} symbolize the right sides of the ODEs in (7.12). Finally, the Lagrange function is defined by

$$\begin{aligned} \mathcal{L}(u, x, \lambda) &= \sum_{i=1}^n \int_{t_0}^{t_1} \frac{(\gamma I_i(t) - I_i^d(t))^2}{\max_{t \in \mathbb{D}} I_i^d(t)} dt + \left(\frac{\|u\|}{N} \right)^2 \\ &\quad + \int_{t_0}^{t_1} \lambda(t)^T \left(g(t, x(t), u) - \frac{dx(t)}{dt} \right) dt. \end{aligned} \quad (7.22)$$

The *first order necessary optimality condition* for a minimum (u^*, x^*, λ^*) is fulfilled if

$$\nabla \mathcal{L}(u^*, x^*, \lambda^*) = 0$$

holds true. Solving $\frac{\partial \mathcal{L}}{\partial x_\nu} = 0$ via *Gâteaux derivative* delivers the adjoint ODEs

$$\begin{aligned} \frac{d\lambda_{S_i}}{dt} &= \mu \lambda_{S_i} + \left(\sum_{j=1}^n \left(p_{ij} \frac{\beta(t)}{N_j} \sum_{k=1}^n p_{kj} I_k \right) \right) \lambda_{S_i} - \left(\sum_{j=1}^n \left(p_{ij} \frac{\beta(t)}{N_j} \sum_{k=1}^n p_{kj} I_k \right) \right) \lambda_{I_i}, \\ \frac{d\lambda_{I_i}}{dt} &= \sum_{j=1}^n \left(p_{ij} \frac{\beta(t)}{N_j} \sum_{k=1}^n p_{kj} S_k \lambda_{S_k} \right) - \sum_{j=1}^n \left(p_{ij} \frac{\beta(t)}{N_j} \sum_{k=1}^n p_{kj} S_k \lambda_{I_k} \right) \\ &\quad + (\alpha + \mu) \lambda_{I_i} - \alpha \lambda_{R_i} - \frac{2\gamma (\gamma I_i - I_i^d)}{\max_{t \in [t_0, t_1]} I_i^d(t)}, \\ \frac{d\lambda_{R_i}}{dt} &= \mu \lambda_{R_i}, \\ 0 &= \lambda_{S_i}(t_1), \lambda_{I_i}(t_1), \lambda_{R_i}(t_1), \end{aligned} \quad (7.23)$$

and through the *optimal conditions* based on Pontryagin's maximum principle we obtain the *transversality conditions* in (7.23), see [26, 32]. Furthermore, $\frac{\partial \mathcal{L}}{\partial \lambda_\nu} = 0$ leads to the ODEs in (7.12). The gradient of \mathcal{L} respect to u is given by

$$\begin{aligned} \frac{\partial \mathcal{L}}{\partial u_\iota} &= u_\iota \frac{2}{N^2} + \int_{t_0}^{t_1} \frac{\partial \beta(t)}{\partial u_\iota} \sum_{i=1}^n (\lambda_{I_i}(t) - \lambda_{S_i}(t)) S_i(t) \left(\sum_{j=1}^n \frac{p_{ij}}{N_j} \sum_{k=1}^n p_{kj} I_k(t) \right) dt \\ &\quad \text{for } \iota = 1, \dots, 5, \\ \frac{\partial \mathcal{L}}{\partial \gamma} &= \gamma \frac{2}{N^2} + \sum_{i=1}^n \int_{t_0}^{t_1} \frac{2I_i (\gamma I_i - I_i^d)}{\max_{t \in \mathbb{D}} I_i^d(t)} dt, \\ \frac{\partial \mathcal{L}}{\partial S_{i0}} &= S_{i0} \frac{2}{N^2} + \lambda_{S_i}(t_0) - \lambda_{I_i}(t_0), \\ \frac{\partial \mathcal{L}}{\partial R_{i0}} &= R_{i0} \frac{2}{N^2} + \lambda_{R_i}(t_0) - \lambda_{I_i}(t_0) \quad \text{for } i = 1, \dots, n. \end{aligned}$$

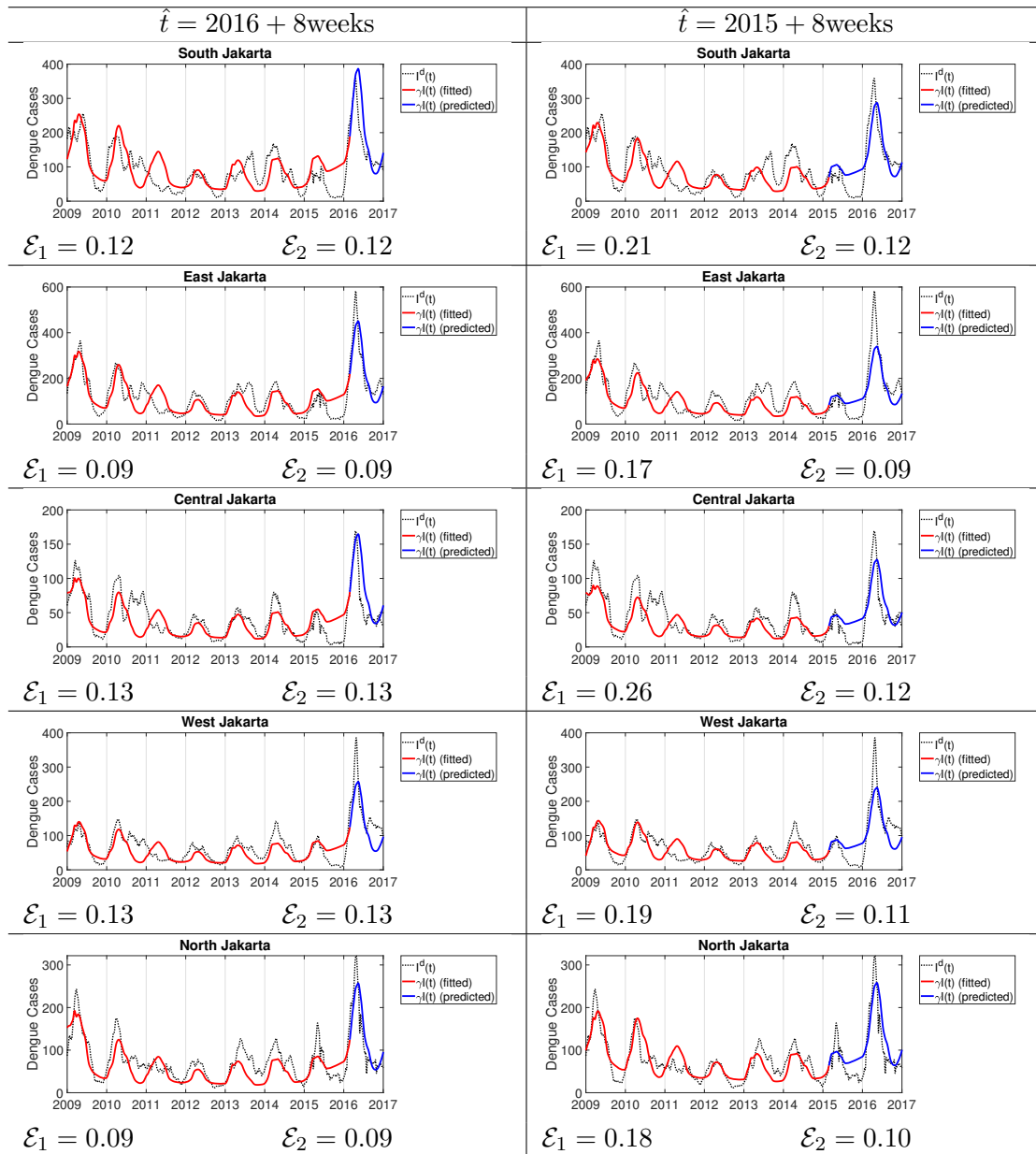
The *conjugate gradient method* combined with the *forward-backward sweep method* is applied to solve the optimization problem numerically until

$$\|J(u_{i+1}) - J(u_i)\| < \text{TOL}$$

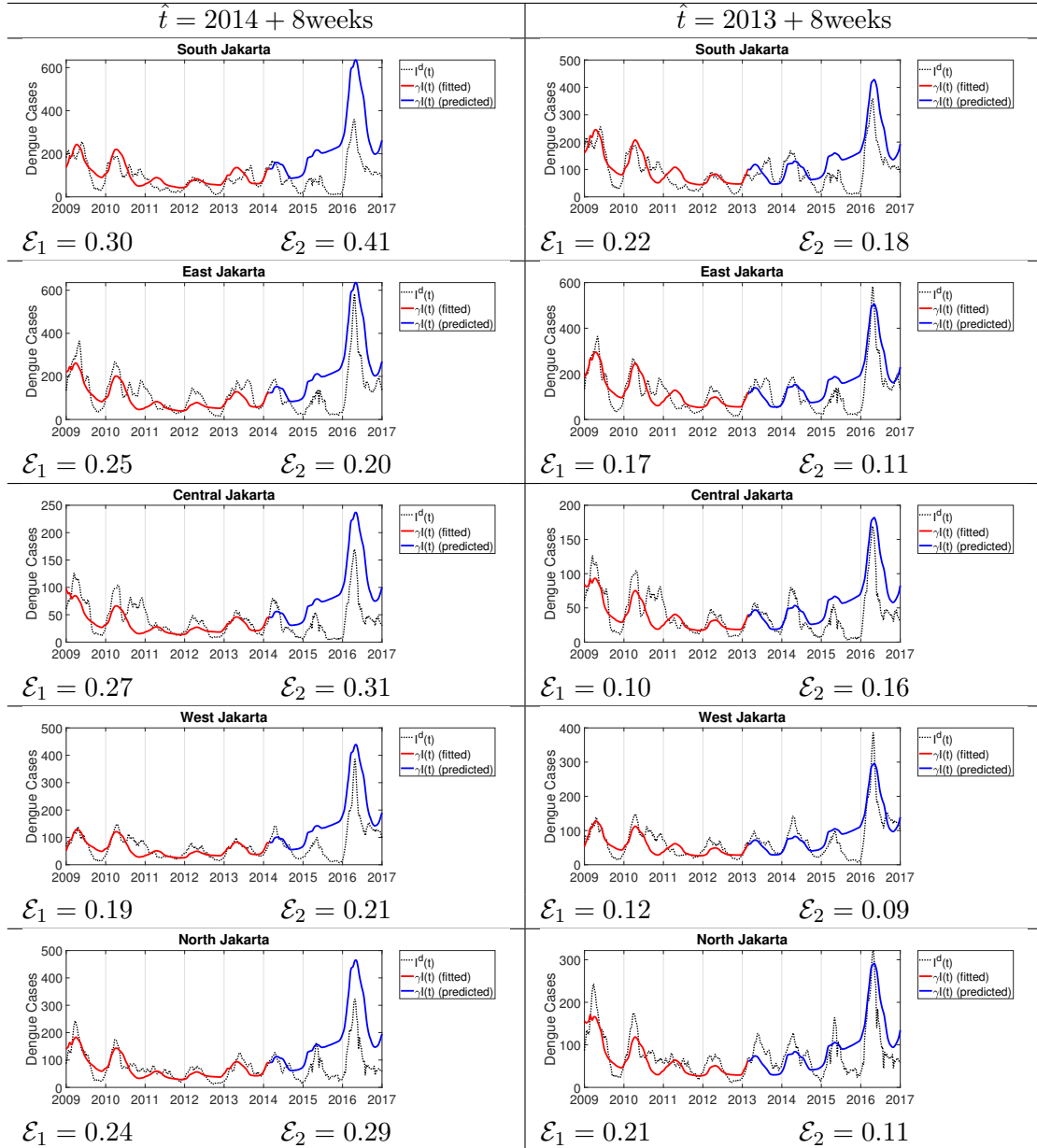
holds true, see e.g. [12, 26, 30, 31].

7.C Appendix C: Numerical findings and predictions with the two models

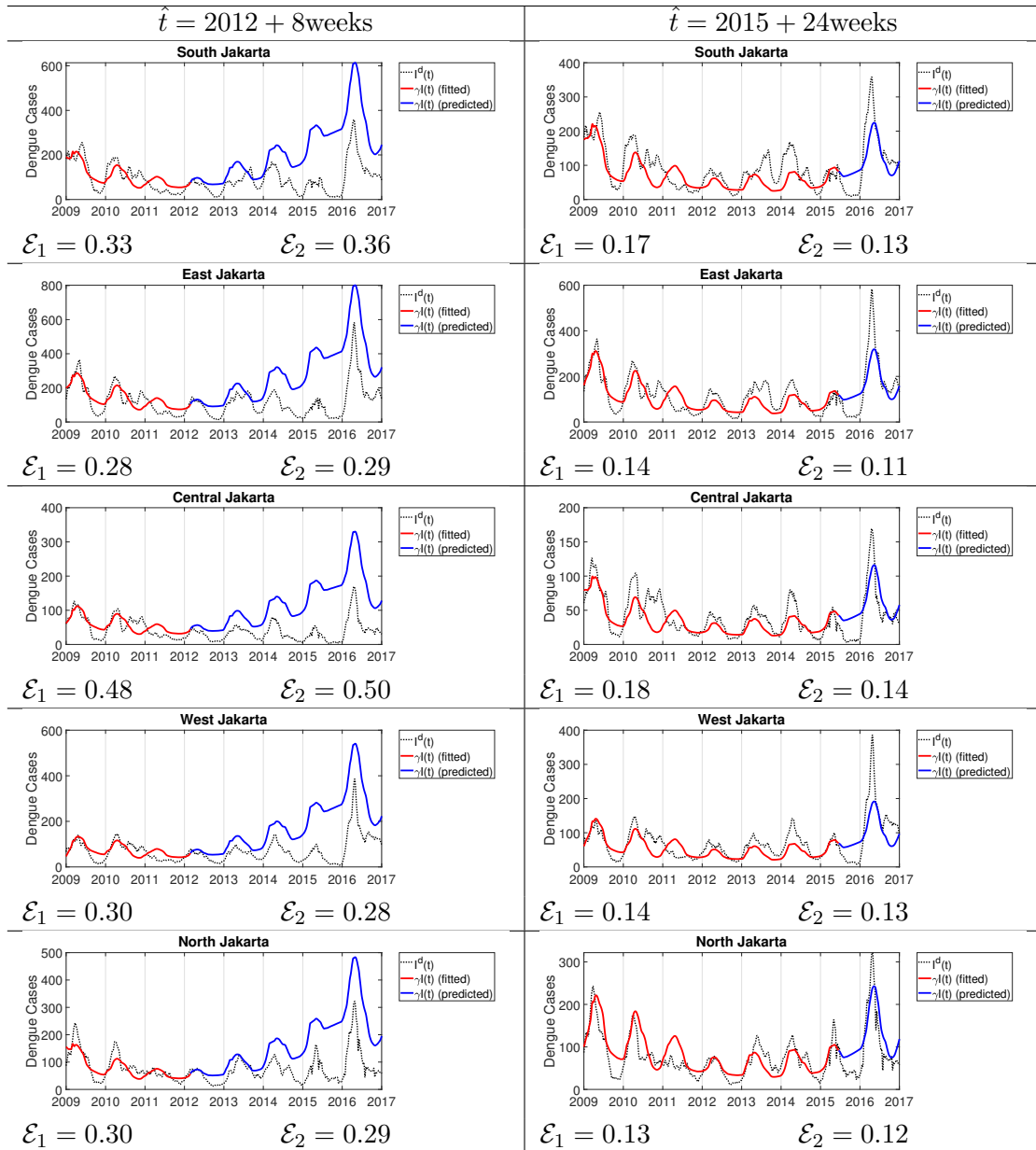
Table 7.10: Results of Simulation 3. The parameter fit (red) is executed in the interval $[2009; \hat{t}]$. The forecast (blue) based on this is carried out with the actual rain data for the period $[\hat{t}; 2017]$.



7.C Appendix C: Numerical findings and predictions with the two models

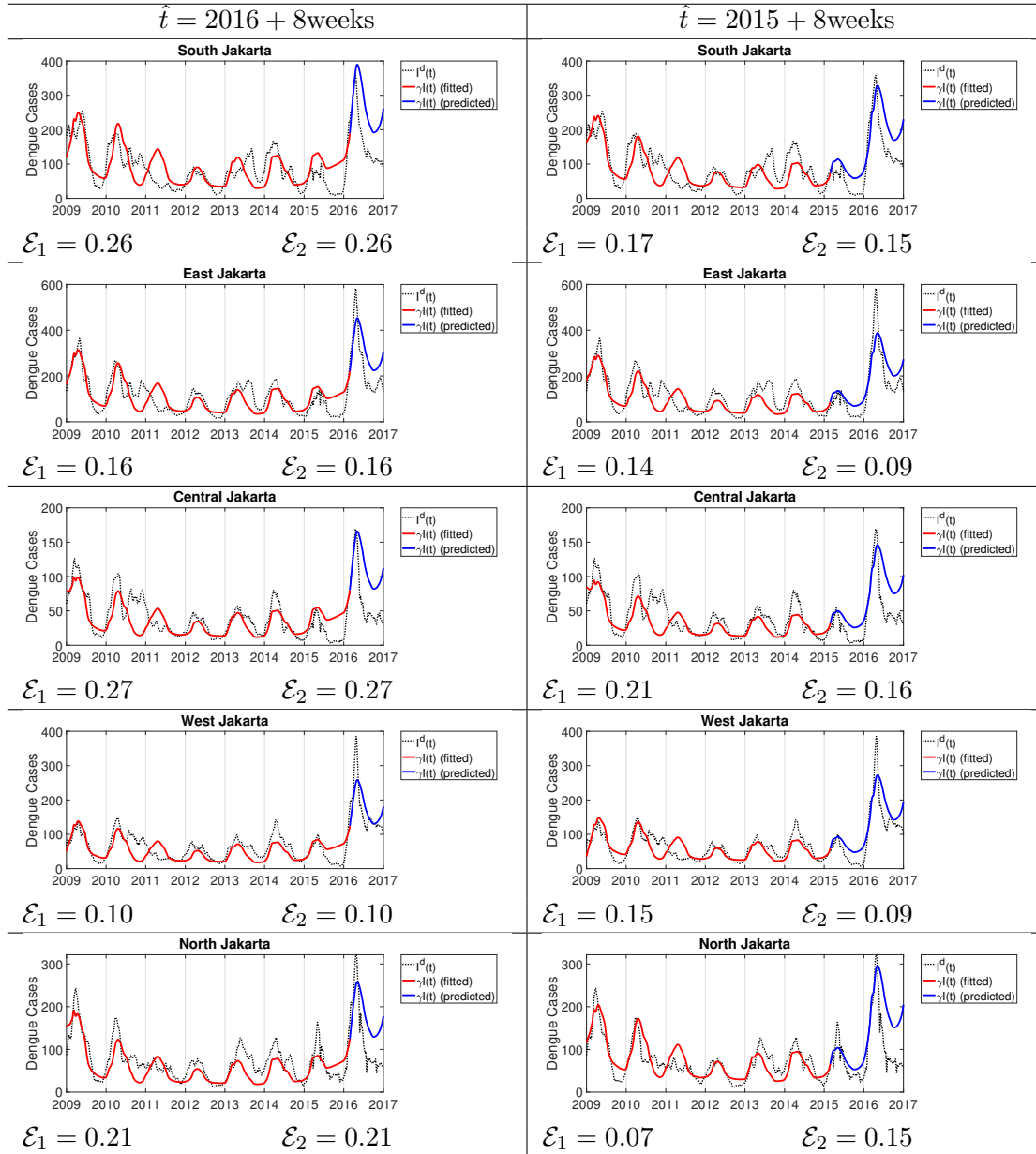


7 Appendix

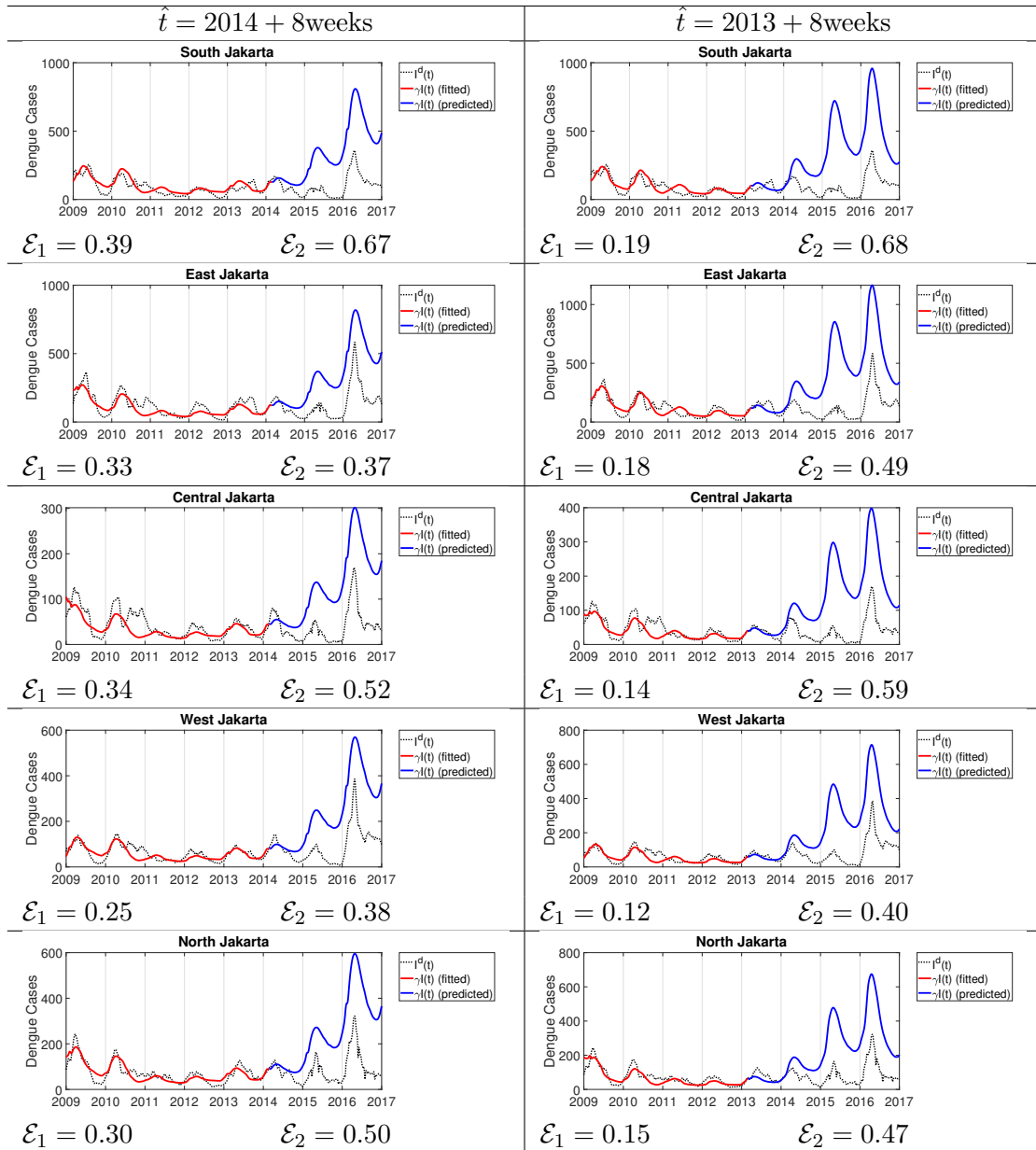


7.C Appendix C: Numerical findings and predictions with the two models

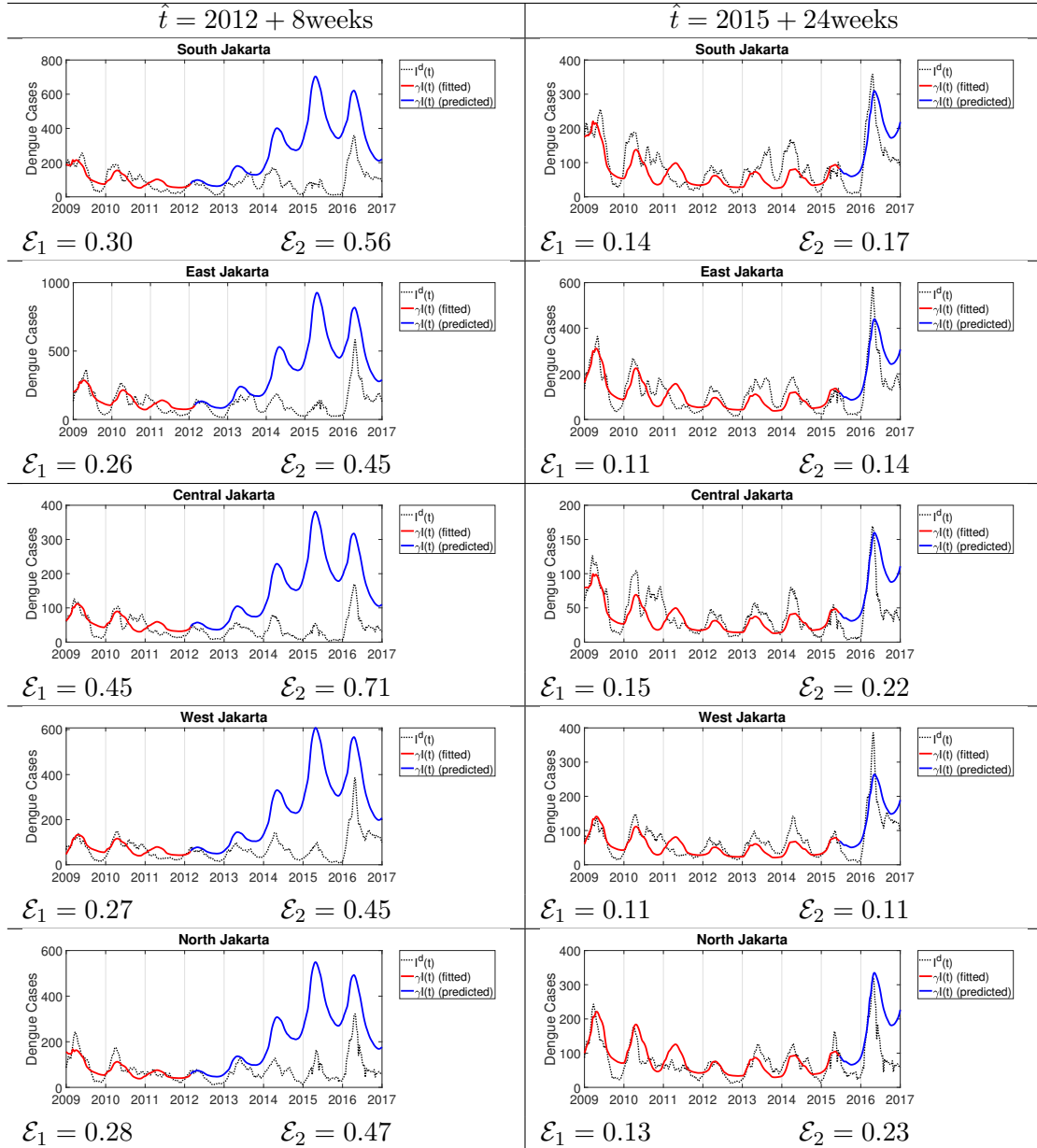
Table 7.11: Results of Simulation 4. The forecast (blue) in $[\hat{t}; 2017]$ is done with the average rain data from the period $[2009; \hat{t}]$ in which the parameter fit (red) is also carried out.



7 Appendix



7.C Appendix C: Numerical findings and predictions with the two models



Bibliography

- [1] Adams, L.V.; Butterly, J.R.: *Diseases of Poverty: Epidemiology, Infectious Diseases, and Modern Plagues*. Dartmouth College Press, 2015
- [2] Aguiar, M.; Ballesteros, S.; Kooi, B.W.; Stollenwerk, N.: *The role of seasonality and import in a minimalistic multi-strain Dengue model capturing differences between primary and secondary infections: complex dynamics and its implications for data analysis*. Journal of Theoretical Biology, Vol. 289, pp 181–196, 2011
<https://doi.org/10.1016/j.jtbi.2011.08.043>
- [3] Aguiar, M.; Kooi, B.W.; Martins, J.; Stollenwerk, N.: *Scaling of stochasticity in Dengue hemorrhagic fever epidemics*. Mathematical Modelling of Natural Phenomena, Vol. 7, No. 3, pp 1–11, 2012
<https://doi.org/10.1051/mmnp/201273013>
- [4] Aldila, D.; Götz, T.; Soewono, E.: *An optimal control problem arising from a Dengue disease transmission model*. Mathematical Biosciences, Vol. 242, No. 1, pp 9–16, 2012
<https://doi.org/10.1016/j.mbs.2012.11.014>
- [5] Ball, J.W.; Bindler, R.C.; Cowen, K.J.; Shaw, M.S.: *Child Health Nursing, Partnering with Children and Families*. Cram101, 2016
- [6] Bock, W.; Jayathunga, Y.: *Optimal control and basic reproduction numbers for a compartmental spatial multipatch Dengue model*. Mathematical Methods in the Applied Sciences, Vol. 41, No. 9, pp 3231–3245, 2018
<https://doi.org/10.1002/mma.4812>
- [7] Brockmann, D.: *Money Circulation Science – Fractional Dynamics in Human Mobility*. John Wiley and Sons, Ltd, pp 459–483, 2008
<https://doi.org/10.1002/9783527622979.ch16>
- [8] Caetano, M.A.L.; Yoneyama, T.: *Optimal and sub-optimal control in Dengue epidemics*. Optimal Control Applications and Methods, Vol. 22, No. 2, pp 63–73, 2001
<https://doi.org/10.1002/oca.683>
- [9] Chavez, J.; Götz, T.; Siegmund, S.; Wijaya, K.P.: *An SIR–Dengue transmission model with seasonal effects and impulsive control*. Mathematical Biosciences, Vol. 289, pp 29–39, 2017
<https://doi.org/10.1016/j.mbs.2017.04.005>
- [10] Ernst, K.; Walker, K. et al.: *Aedes aegypti (Diptera: Culicidae) Longevity and Differential Emergence of Dengue Fever in Two Cities in Sonora, Mexico*. Journal of medical entomology, Vol. 54, No.1, pp 204–211, 2017
<https://doi.org/10.1093/jme/tjw141>
- [11] Faber, W.; Hay, R.; Naafs, B.: *Imported skin diseases*. Wiley, 2012

Bibliography

- [12] Fletcher, R.: *A new approach to variable metric algorithms*. The Computer Journal, Vol. 13, No. 3, pp 317–322, 1970
- [13] Götz, T.; Altmeier, N.; Bock, W.; Rockenfeller, R.; Sutimin, S.; Wijaya, K.P.: *Modeling Dengue data from Semarang, Indonesia*. Ecological Complexity, Vol. 30, pp 57–62, 2017
<https://doi.org/10.1016/j.ecocom.2016.12.010>
- [14] Götz, T.; Nuraini, N.; Soewono, E.; Wijaya, K.P.: *Temephos spraying and thermal fogging efficacy on aedes aegypti in homogeneous urban residences*. ScienceAsia, Vol. 39, pp 48–56, 2013
<http://dx.doi.org/10.2306/scienceasia1513-1874.2013.39S.048>
- [15] Götz, T.; Rockenfeller, R.; Wijaya, K.P.: *Optimization problems in epidemiology, biomechanics and medicine*. International Journal of Advances in Engineering Sciences and Applied Mathematics, Vol. 7, pp 25–32, 2015
<https://doi.org/10.1007/s12572-015-0130-5>
- [16] Götz, T.; Soewono, E.; Wijaya, K.P.: *Advances in mosquito dynamics modeling*. Mathematical Methods in the Applied Sciences, Vol. 39, No. 16, 2015
<https://doi.org/10.1002/mma.3517>
- [17] Götz, T.; Soewono, E.; Wijaya, K.P.: *An optimal control model of mosquito reduction management in a Dengue endemic region*. International Journal of Biomathematics, Vol. 7, No. 5, 2014
<https://doi.org/10.1142/S1793524514500569>
- [18] Gubler, D.J.: *Dengue, Urbanization and Globalization: The Unholy Trinity of the 21 Century*. Tropical Medicine and Health, Vol. 39, pp 3–11, 2011
<https://doi.org/10.2149/tmh.2011-S05>
- [19] Gubler, D.J.: *The global emergence/resurgence of arboviral diseases as public health problems*. Archives of Medical Research, Vol. 33, No. 4, pp 330–342, 2002
[https://doi.org/10.1016/S0188-4409\(02\)00378-8](https://doi.org/10.1016/S0188-4409(02)00378-8)
- [20] Hansen, G.: *Mosquitoes*. ABDO Publishing Company, 2015
- [21] Hayes, C.G.; Phillips, I.A.; Callahan, J.D.; Griebenow, W.F.; Hyams, K.C.; Wu, S.J.; Watts, D.M.: *The epidemiology of Dengue virus infection among urban, jungle, and rural populations in the amazon region of Peru*. The American Journal of Tropical Medicine and Hygiene, Vol. 55, No. 4, pp 459–63, 1996
<https://doi.org/10.4269/ajtmh.1996.55.459>
- [22] Heidrich, P.; Götz, T.: *Modelling Dengue with the SIR Model*. In: Faragó I.; Izsák F.; Simon P. (eds), Progress in Industrial Mathematics at ECMI 2018. Mathematics in Industry, Vol. 30. Springer, pp 175–182, 2019
https://doi.org/10.1007/978-3-030-27550-1_22
- [23] Jones, J.A.: *Mosquito Facts and Information*. Lulu.com, Accessed 15 Aug 2020
<https://www.lulu.com>
- [24] Kooi, B.W.; Aguiar, M.; Stollenwerk, N.: *Analysis of an asymmetric two-strain Dengue model*. Mathematical Biosciences, Vol. 248, pp 128–139, 2014
<https://doi.org/10.1016/j.mbs.2013.12.009>

- [25] Lee, S.; Castillo–Chavez, C.: *The role of residence times in two–patch Dengue transmission dynamics and optimal strategies*. Journal of Theoretical Biology, Vol. 374, pp 152–164, 2015
<https://doi.org/10.1016/j.jtbi.2015.03.005>
- [26] Lenhart, S.; Workman, J.T.: *Optimal control applied to biological models*. CRC Press, 2007
- [27] Martcheva, M.: *An introduction to mathematical epidemiology*. Springer US, 2015
- [28] Morlan, H.B.; Hayes., R.O.: *Urban dispersal and activity of aedes aegypti*. Mosquito News, Vol. 18, No. 2, pp 137–144, 1958
- [29] Muir, L.E.; Kay, B.H.: *Aedes aegypti survival and dispersal estimated by mark–release–recapture in northern australia*. The American Journal of Tropical Medicine and Hygiene, Vol. 58, No. 3, pp 277–282, 1998
<https://doi.org/10.4269/ajtmh.1998.58.277>
- [30] Nocedal, J.; Wright, S.: *Numerical Optimization*. Springer New York, 2006
- [31] Polak, E.; Ribiere, G.: *Note sur la convergence de méthodes de directions conjuguées*. ESAIM: Mathematical Modelling and Numerical Analysis – Modélisation Mathématique et Analyse Numérique, Vol. 3, pp 35–43, 1969
- [32] Pontryagin, L.: *Mathematical Theory of Optimal Processes*. CRC Press, 2018
- [33] Pyke, A.T.; Moore, P.R.; Taylor, C.T.; Hall–Mendelin, S.; Cameron, J.; Hewitson, G.R.; Pukallus, D.S.; Huang, B.; Warrilow, D.; Hurk, A.F.: *Highly divergent Dengue virus type 1 genotype sets a new distance record*. Scientific Reports, Vol. 6, 2016
<https://doi.org/10.1038/srep22356>
- [34] Rabiner, L.; Schafer, R.: *Theory and Applications of Digital Speech Processing*. Pearson, 2011
- [35] Rao, K.; Kim, N.; Stepanov, V.; Hwang, J.: *Fast Fourier Transform – Algorithms and Applications*. Springer Netherlands, 2011
- [36] Reiskind, M.; Baisley, K.J.; Calampa, C.; Sharp, T.W.; Watts, D.M.; Wilson, M.L.: *Epidemiological and ecological characteristics of past Dengue virus infection in santa clara, peru*. Tropical Medicine and International Health, Vol. 6, No. 3, pp 212–218, 2008
<https://doi.org/10.1046/j.1365-3156.2001.00703.x>
- [37] Rocha, F.; Aguiar, M.; Souza, M.; Stollenwerk, N.: *Time–scale separation and centre manifold analysis describing vector–borne disease dynamics*. International Journal of Computer Mathematics, Vol. 90, No. 10, pp 2105–2125, 2013
<https://doi.org/10.1080/00207160.2013.783208>
- [38] Rocha, F.; Mateus, L.; Skwara, U.; Aguiar, M.; Stollenwerk, N.: *Understanding Dengue fever dynamics: a study of seasonality in vector–borne disease models*. International Journal of Computer Mathematics, Vol. 93, No. 8, pp 1405–1422, 2016
<https://doi.org/10.1080/00207160.2015.1050961>

Bibliography

- [39] Rodrigues, H.S.; Teresa, M.; Monteiro, T.; Torres, D.F.M.: *Vaccination models and optimal control strategies to Dengue*. Mathematical Biosciences, Vol. 247, pp 12–12, 2014
<https://doi.org/10.1016/j.mbs.2013.10.006>
- [40] Royal, L.; McCoubrey, I.: *International spread of disease by air travel*. American Family Physician, Vol. 40, No. 5, pp 129–136, 1989
- [41] Ryan, K.; Ahmad, N.; Weissman, S.; Alspaugh, J.; Drew, W.; Lagunoff, M.; Pottinger, P.; Reller, L.; Reller, M.; Sterling, C.: *Sherris Medical Microbiology, Seventh Edition*. McGraw–Hill Education, 2018
- [42] Shi, P.: *Molecular virology and control of flaviviruses*. Academic Press, 2012
- [43] Taylor–Robinson, A.W.: *Dengue diagnosis, treatment and vaccine design: are efforts hampered by multiple serotypes and cross-reactivity with Zika?*. Journal of Clinical Diagnosis and Treatment, Vol. 1, No. 2, pp 50–52, 2018
- [44] Tikhonov, A.N.; Goncharsky, A.; Stepanov, V.V.; Yagola, A.G.: *Numerical Methods for the Solution of Ill-Posed Problems*. Springer Amsterdam, 2013
- [45] Torre, C.: *Deterministic and stochastic metapopulation models for Dengue fever*. Arizona State University, 2009
- [46] Vasilakis, N.; Cardoso, J.; Hanley, K. et al.: *Fever from the forest: prospects for the continued emergence of sylvatic Dengue virus and its impact on public health*. Nature Reviews Microbiology, Vol. 9, pp 532–541, 2011
<https://doi.org/10.1038/nrmicro2595>
- [47] WetterKontor. Accessed 15 Aug 2020
<https://www.wetterkontor.de>
- [48] World Health Organization (WHO). Accessed 15 Aug 2020
<http://who.int>
- [49] World Health Organization (WHO): *Dengue control*. Accessed 15 Aug 2020
<http://who.int>
- [50] World Life Expectancy. Accessed 15 Aug 2020
<https://www.worldlifeexpectancy.com/indonesia-life-expectancy>
- [51] World Meteorological Organization. Accessed 15 Aug 2020
<https://worldweather.wmo.int>

8 Research Paper IV: Early Stage COVID–19 Disease Dynamics in Germany: Models and Parameter Identification

Thomas Götz Peter Heidrich

The paper *Early Stage COVID–19 Disease Dynamics in Germany: Models and Parameter Identification* by Thomas Götz and Peter Heidrich was first published as a preprint on *medRxiv* (<https://doi.org/10.1101/2020.04.23.20076992>). The peer-reviewed version is published on *Journal of Mathematics in Industry, Vol. 10, Springer Open, 2020* (<https://doi.org/10.1186/s13362-020-00088-y>). The layout of the paper is adapted to the present thesis.

Idea and organization were initiated by Thomas Götz. He contributed the sections *Introduction*, *Mathematical model* and *A few analytical considerations*. Peter Heidrich did the numerical programming with the calculations and the presentation of these in the sections *Adjoint equations and optimization* and *Simulation results*. The two authors complemented each other in the respective sections.

8.1 Abstract

Since the end of 2019 an outbreak of a new strain of coronavirus, called SARS–CoV–2, is reported from China and later other parts of the world. Since January 21, World Health Organization (WHO) reports daily data on confirmed cases and deaths from both China and other countries [17]. The Johns Hopkins University [3] collects those data from various sources worldwide on a daily basis. For Germany, the Robert–Koch–Institute (RKI) also issues daily reports on the current number of infections and infection related fatal cases [12]. However, due to delays in the data collection, the data from RKI always lags behind those reported by Johns Hopkins. In this work we present an extended *SEIRD*–model to describe the disease dynamics in Germany. The parameter values are identified by matching the model output to the officially reported cases. An additional parameter to capture the influence of unidentified cases is also included in the model.

Keywords: COVID–19, Epidemiology, Disease dynamics, *SEIRD*–model

8.2 Introduction

In December 2019, first cases of a novel *pneumonia of unknown cause* were reported from Wuhan, the seventh–largest city in China. In the meantime, these cases have been identified as infections with a novel strain of coronavirus, called SARS–CoV–2 and the disease it causes is called coronavirus disease 2019 (COVID–19). At the beginning of January 2020, the virus spread over mainland China and reached other provinces. Increased travel activities due to the Chinese new year festivities supported the expansion of the infection.

Since 21 January, WHO’s daily situation reports contain the latest figures on confirmed cases and deaths, see [17]. The first COVID–19 case in Germany was reported in late January 2020 in a company close to Munich, Bavaria. Later cases were imported by travelers from China, Iran or Italy as well as tourists returning from ski holidays in the Austria and Italy. By 1 March 2020 more than 100 cases were reported in Germany and since then the number of cases began to rise exponentially. The first deaths were reported on 9 March 2020 [12, 16]. By 16 March 2020 the federal government introduced first measures to reduce the spread of the disease: Schools, kindergartens and universities were closed. On 22 March these measures were tightened by implementing a national curfew and contact ban. People are advised to stay at home, leaving only for work related activities, necessary shopping, medical treatment or sports. All this should not be done in groups of more than two persons if they do not belong to the same household [1].

Our work is based on the data reported by Johns Hopkins University [3]. We refrain from using the official data from the Robert–Koch–Institute [12], since they suffer from a delay by several days due to the more complicated way of aggregating those data. For a detailed explanation of the difference between the data reported by Johns Hopkins and the Robert–Koch Institute we refer to the information given on the webpage of the Robert–Koch–Institute, see [13]. Johns Hopkins University continuously collects the data from internet queries at various sources (local health authorities, newspapers, etc.) whereas the Robert–Koch–Institute collects the data that are reported for the local health authorities to the district level, then state level and finally aggregates them to the federal statistics. Hence these data lag several days behind the ones collected by Johns Hopkins University.

The paper is organized as follows: In Section 8.3 we describe the model and the parameter identification problem. Our model consists of three variants of a five compartment *SEIRD*–system without demographic terms, where the transmission rate is either fixed (8.1) or time–dependent (8.3) and (8.4). The fatalities are either described by an ODE, see models (8.1) and (8.3), or via a delay term in model (8.4). In the parameter estimation problem, we determine the transmission rate, detection rate and lethality together with the initial values for the exposed and infected compartment. In Section 8.4 we discuss the sensitivity of our model with respect to detection rate. Section 8.5 is devoted to the adjoint equations used for solving the optimization problem. The simulation results are presented in Section 8.6. Here we do compare the results obtained from the three models presented in Section 8.3.

8.3 Mathematical model

To model the dynamics of the spread of COVID–19 incidences, we propose a hierarchy of *SEIRD* models. For details regarding the original *SIR*– and *SEIR*–model we refer to classical works on mathematical epidemiology, e.g [7]. For our basic *SEIRD*–model, the total population of Germany with $N \sim 83.000.000$ individuals is subdivided into *susceptibles* S , *exposed* E , *infected* I , *recovered* R and *deaths* D . The susceptibles constitute the reservoir of persons that are not yet infected with SARS–CoV–2. After infection susceptible become exposed meaning that they already carry the virus but are not yet infectious. With a rate ϑ exposed individuals become infectious and transmit the virus with rate β to susceptibles. An infected individual loses infectivity with γ and has a probability μ of dying due to the disease [18]. Figure 8.2 shows the transmission structure. By C we denote all infected cases, independent of their current status. This artificial compartment is later on used to compare with the total number of registered cases reported by Johns Hopkins or RKI.

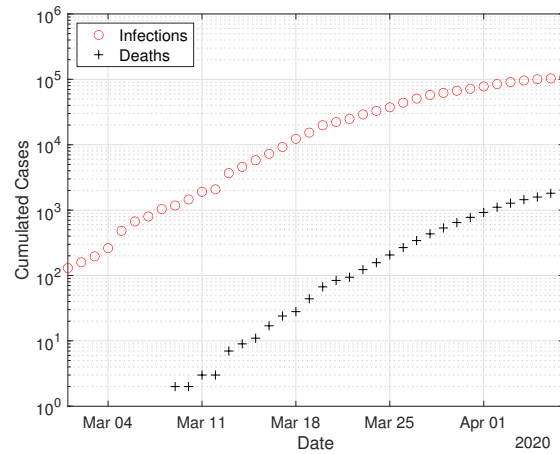


Figure 8.1: Case numbers in Germany from 1 March until 7 April 2020, as reported by Johns Hopkins University [3]. The initial time point is chosen as 1 March, since then the number of registered infections exceeds 100 cases.

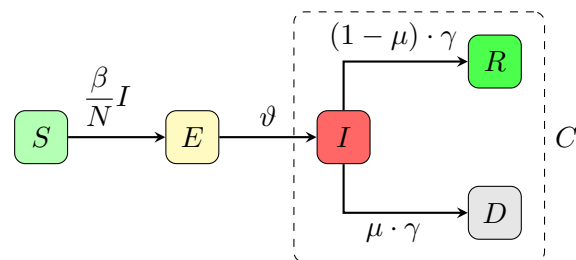


Figure 8.2: Transmission diagram for the basic *SEIRD*-model (8.1). The artificial compartment *C* contains all infected cases, i.e. current active infections, recovered and deaths.

The resulting system of ordinary differential equations (ODE) for the above described *SEIRD*-model reads as

$$\frac{dS}{dt} = -\frac{\beta}{N}SI, \quad S(t_0) = S_0 := N - E_0 - I_0, \quad (8.1a)$$

$$\frac{dE}{dt} = \frac{\beta}{N}SI - \vartheta E, \quad E(t_0) = E_0, \quad (8.1b)$$

$$\frac{dI}{dt} = \vartheta E - \gamma I, \quad I(t_0) = I_0, \quad (8.1c)$$

$$\frac{dR}{dt} = (1 - \mu) \cdot \gamma I, \quad R(t_0) = 0, \quad (8.1d)$$

$$\frac{dD}{dt} = \mu \cdot \gamma I, \quad D(t_0) = 0. \quad (8.1e)$$

The starting time t_0 is chosen as 1 March and the initial conditions for the recovered and dead compartment are assumed to be zero, since in Germany the first COVID-19 related death was recorded on 9 March. Also we may assume that the number of recovered individuals by 1 March is negligible. In the sequel, we will also consider two refined versions of the above basic model. At the onset of the disease, the numbers of exposed, infected, recovered and dead are still small and the number of susceptibles is approximately equal to the entire population N . In this setting, the *EI*-part of the model reduces to

$$\begin{pmatrix} E \\ I \end{pmatrix}' = \begin{pmatrix} -\vartheta & \beta \\ \vartheta & -\gamma \end{pmatrix} \cdot \begin{pmatrix} E \\ I \end{pmatrix}.$$

The maximal eigenvalue λ of this linear system determines the initial growth rate and is given by

$$\lambda = \frac{1}{2} \left(-(\vartheta + \gamma) + \sqrt{(\vartheta - \gamma)^2 + 4\vartheta\beta} \right)$$

and the *doubling time* T_2 equals

$$T_2 = \frac{\ln 2}{\lambda}.$$

Figure 8.3 depicts the dependence of the doubling time on the transmission rate β . As of mid April, the doubling time in Germany is approximately 14 days compared to 2.5 days by mid March.

In the basic model (8.1), the transmission rate β is assumed to be fixed. The German state and federal governments introduced several measures to slow down the spread of the disease. Similar measures are nowadays taken in almost every country worldwide. As of 16 March schools, kindergartens and universities were closed and on 22 March a general contact ban was enforced in Germany. Both measures aim at reducing the transmission rate β . To include this into the basic model (8.1), we also consider an alternative model for the transmission rate β : We assume β as a piecewise constant function on the time intervals prior to any measures, (until 15 March), after school closings (between 16 and 22 March) and after the contact ban (after March 22)

$$\beta(t) = \begin{cases} \beta_0 & : t < 16 \text{ March} \\ \beta_1 & : 16 \text{ March} \leq t \leq 22 \text{ March} \\ \beta_2 & : t > 22 \text{ March} \end{cases} \quad (8.2)$$

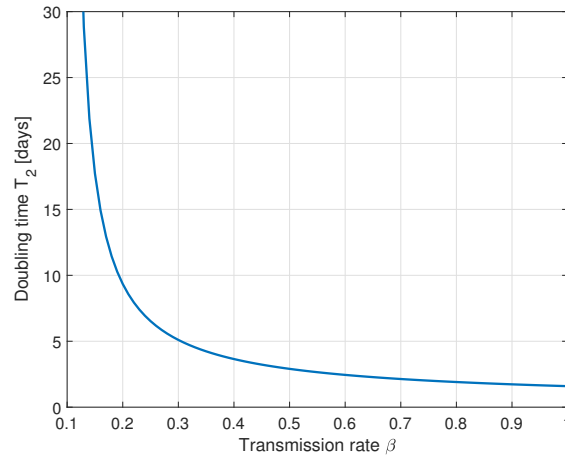


Figure 8.3: Plot of the doubling time T_2 in days versus the transmission rate β for fixed values $\vartheta = 1/2$ and $\gamma = 1/10$. A reduction of the transmission rate from $\beta = 0.8$ to $\beta = 0.2$ accounts for a slow down of the infection from doubling time 2 days to 10 days.

The resulting time-dependent *SEIRD*-model reads as

$$\frac{dS}{dt} = -\frac{\beta(t)}{N}SI, \quad S(t_0) = S_0 := N - E_0 - I_0, \quad (8.3a)$$

$$\frac{dE}{dt} = \frac{\beta(t)}{N}SI - \vartheta E, \quad E(t_0) = E_0, \quad (8.3b)$$

$$\frac{dI}{dt} = \vartheta E - \gamma I, \quad I(t_0) = I_0, \quad (8.3c)$$

$$\frac{dR}{dt} = (1 - \mu) \cdot \gamma I, \quad R(t_0) = 0, \quad (8.3d)$$

$$\frac{dD}{dt} = \mu \cdot \gamma I, \quad D(t_0) = 0. \quad (8.3e)$$

Setting $\beta := \beta_0 = \beta_1 = \beta_2$, the time-dependent model reduces to the basic one.

In order to validate our models and to identify the parameters involved therein, both the registered number of infections and the registered number of COVID-19 related deaths are important indications. The number of registered deaths is probably considerably more reliable, since the number of registered infections depends on the number of tests conducted and the dark figure of undetected, mostly asymptomatic cases, is assumed to be remarkably large [6]. We will discuss this point later in more detail. In the previous basic or time-dependent *SEIRD*-model, the actual increase of the disease related deaths $\frac{dD}{dt}$ is assumed to be proportional to the current number of infected persons. The Robert-Koch-Institute specifies an average of 10 days between the onset of symptoms and admission to the intensive care unit [11]. Therefore, we assume $\tau = 14$ for the time between the onset of infectiousness and death. In order to include this time lag into our model, we introduce a delay-term into the time-dependent model and obtain the final delayed time-dependent

model:

$$\frac{dS}{dt} = -\frac{\beta(t)}{N}SI, \quad S(t_0) = S_0 := N - E_0 - I_0, \quad (8.4a)$$

$$\frac{dE}{dt} = \frac{\beta(t)}{N}SI - \vartheta E, \quad E(t_0) = E_0, \quad (8.4b)$$

$$\frac{dI}{dt} = \vartheta E - \gamma[(1 - \mu)I + \mu I(t - \tau)], \quad I(s) = I_0(s) \quad \text{for } s \leq t_0, \quad (8.4c)$$

$$\frac{dR}{dt} = (1 - \mu) \cdot \gamma I, \quad R(t_0) = 0, \quad (8.4d)$$

$$\frac{dD}{dt} = \mu \cdot \gamma I(t - \tau), \quad D(t_0) = 0. \quad (8.4e)$$

Note, that for solving this delay differential equation (DDE) we need an initial history of the infected compartment, i.e. values $I_0(s)$ for $t_0 - \tau \leq s \leq t_0$. In all the three models, the parameters $\vartheta = 1/2$ [days⁻¹], $\gamma = 1/10$ [days⁻¹] are assume to be fixed and resemble a latency period of 2 days and a recovery period of 10 days, see [12, Situation report 31 March 2020]. The parameters in the transmission rate, i.e. β , or $\beta_0, \beta_1, \beta_2$ the lethality μ and the initial values E_0, I_0 resp. the initial history $I_0(s)$ for the exposed and infected compartment are yet unknown to us. We will identify them together with the *detection rate* δ by matching the model output to the given data. The detection rate δ corresponds to the fraction of infected individuals which are positively tested for SARS-CoV-2 and hence appear in the official recordings. Various sources speculate that this detection rate is in the order of magnitude of 10–20% meaning that the true number of infected 5 – 10 times larger than the number published in the official statistics, see [6].

To match the model output and the reported data we use a least squares approach. Let $u = (\beta, \delta, \mu, E_0, I_0)$ resp. $u = (\beta_0, \beta_1, \beta_2, \delta, \mu, E_0, I_0)$ denote the unknown model parameters to be determined. Furthermore, let $Y(t)$ and $Z(t)$ denote the data for the cumulated infected and dead cases at time t reported by Johns Hopkins University. The deviation between the model and the data is measured by the cost functional

$$\begin{aligned} J(u) &:= \frac{\|\delta(I + R) + D - Y\|_{L^2}^2}{\|Y\|_{L^2}^2} + c_1 \frac{\|D - Z\|_{L^2}^2}{\|Z\|_{L^2}^2} + c_2 \|u\|^2 \\ &= \frac{1}{\|Y\|_{L^2}^2} \left(\|\delta(I + R) + D - Y\|_{L^2}^2 + \omega_1 \|D - Z\|_{L^2}^2 + \omega_2 \|u\|^2 \right), \end{aligned} \quad (8.5)$$

where $\|f\|_{L^2}^2 := \int_{t_0}^{T_{\text{Fit}}} f(t)^2 dt$ denotes the square of the L^2 -norm of the function f on the interval $[t_0, T_{\text{Fit}}]$ and $\omega_1 = c_1 \frac{\|Y\|_{L^2}^2}{\|Z\|_{L^2}^2}$ as well as $\omega_2 = c_2 \|Y\|_{L^2}^2$. For the given data we have $\|Y\|_{L^2}^2 \simeq 1.2 \cdot 10^{11}$ and $\|Z\|_{L^2}^2 \simeq 6.5 \cdot 10^8$, hence $\omega_1 \simeq c_1 \cdot 185$. The cumulated infected Y , i.e. total positive tests, are to be matched in the *SEIRD*-model to those individuals who had been infected until time t , i.e. the sum of the infected I , recovered R and deaths D . To account for the uncertainty in the *true* number of infected and recovered cases, we multiply both compartments by the detection rate δ , which is itself part of the parameters to be identified. For the deaths we assume no undetected cases. By T_{Fit} we denote the time horizon used for the comparison between the model and the data. The regularization term $\omega_2 \|u\|^2$ is included to ensure the convexity of the cost-functional. The weighting parameters c_1, c_2 and hence $\omega_1, \omega_2 > 0$ allow to balance the contributions from the least squares error in the fatalities and from the size of the parameter values themselves to the least squares error in the infected cases. The weight c_1 for the fatal cases allows to compensate the different order of magnitude between the infected cases and the fatal cases,

typically $c_1 \simeq 2\text{--}3$ leading to $\omega_1 \simeq 500$. The weight c_2 is chosen small, such that the overall cost functional is still dominated by the least square fit between the model output and the given data.

The parameters u^* themselves are obtained from minimization problem

$$\min_u J(u) \text{ subject to one of the ODE-systems (8.1),(8.3) or (8.4),} \quad (8.6a)$$

$$u^* = \operatorname{argmin}_u J(u). \quad (8.6b)$$

8.4 A few analytical considerations

Due to the absence of demographic terms, our basic model (8.1) does not allow other equilibria besides the trivial disease free equilibrium $X^0 = (N, 0, 0, 0, 0)$. Since we focus only on the short-time behavior of the epidemics, demographic terms are excluded and equilibria do not play any important role.

An important issue is the question of whether we can identify the detection rate and lethality during the take-off period of the epidemics? The only data available for parameter identification are the total number of registered cases $C = I + R + D$ and the deaths D . The total registered cases heavily depend on the number of tests conducted. If a person is infected, but not tested, this person will not appear in the official statistics. Hence, there is a presumably large dark figure in the officially recorded data. Our model parameter δ takes this into account. The other, maybe more reliable, available data are the recorded deaths. Here we may assume that *all* COVID-19 related deaths are diagnosed and hence there is no dark figure in the D -compartment. A recent analysis by the Federal Statistical Office on the excess mortality in Germany for March and April 2020 confirms this assumption, see [2]. For other countries this assumption might be questionable, since they suffered from major COVID-19 outbreaks in care homes that did not enter the official statistics, e.g. in the UK, see [14]. However, one scenario could be possible. A large dark figure in the entire cases, i.e. a small detection rate δ and a very small lethality could result in the same or at least similar observed data as a moderate or even small dark figure and hence large detection rate δ combined with a higher lethality rate. In that setting a simultaneous identification of both, the detection rate δ and the lethality μ could be difficult due to their counteracting effects.

In order to investigate this scenario, we consider the simultaneous effect of the detection rate δ scaling both the initial values of the E and I compartment to account for undetected cases together with a lethality $\delta\mu$. Removing the S -compartment by setting $S = N - E - I - R - D$, the basic $SEIRD$ -system (8.1) reads as

$$\begin{aligned} \frac{dE}{dt} &= \frac{\beta}{N}(N - E - I - R - D)I - \vartheta E, & E(t_0) &= E_0/\delta, \\ \frac{dI}{dt} &= \vartheta E - \gamma I, & I(t_0) &= I_0/\delta, \\ \frac{dR}{dt} &= (1 - \delta\mu) \cdot \gamma I, & R(t_0) &= 0, \\ \frac{dD}{dt} &= \delta\mu \cdot \gamma I, & D(t_0) &= 0. \end{aligned}$$

The sensitivities $\Sigma_E := \partial_\delta E$ and $\Sigma_I, \Sigma_R, \Sigma_D$ of the solution with respect to the detection

rate satisfy the system

$$\Sigma'_E = \frac{\beta}{N}(N - E - 2I - R - D)\Sigma_I - \vartheta\Sigma_E - \frac{\beta}{N}I(\Sigma_E + \Sigma_R + \Sigma_D), \quad \Sigma_E(t_0) = -E_0/\delta^2, \quad (8.7a)$$

$$\Sigma'_I = \vartheta\Sigma_E - \gamma\Sigma_I, \quad \Sigma_I(t_0) = -I_0/\delta^2, \quad (8.7b)$$

$$\Sigma'_R = (1 - \delta\mu)\gamma\Sigma_I - \mu\gamma I, \quad \Sigma_R(t_0) = 0, \quad (8.7c)$$

$$\Sigma'_D = \delta\mu\gamma\Sigma_I + \mu\gamma I, \quad \Sigma_D(t_0) = 0. \quad (8.7d)$$

In Figure 8.4 we show the relative sensitivities Σ_C/C and Σ_D/D for detection rates $\delta = 0.1, 0.2$ and 0.33 .

The chosen initial values are $E_0 = 150$ and $I_0 = 100$ (detected) cases at day 0. All other parameters resemble the assumed values for Germany. Note, that at the onset of the epidemics, i.e. in case of $\delta = 0.1$ for $t \lesssim 30$ and for $\delta = 0.2, 0.33$ even for $t \lesssim 40$, the sensitivities are very small and hence the solution of the *SEIR*-model is almost *independent* of the particular value of the detection rate δ . Hence δ cannot be identified from the observed data in a reliable manner. To illustrate these findings, we consider a linearization of a simplified *SIR*-model during the initial phase of the epidemics. We neglect the exposed compartment and assume that at the initial phase, the number of susceptibles is approximately equal to the entire population. Hence we get the linear system

$$\begin{aligned} \hat{I}' &= (\beta - \gamma)\hat{I}, & \hat{I}(0) &= \frac{1}{\delta}I_0, \\ \hat{D}' &= \delta\mu\gamma\hat{I}, & \hat{D}(0) &= 0, \end{aligned}$$

with the solution

$$\hat{D}(t; \delta) = \frac{\mu\gamma}{\beta - \gamma} \left(e^{(\beta - \gamma)t} - 1 \right) I_0.$$

In this linearized setting, the approximation \hat{D} for the dead compartment is independent of the detection rate δ . From the graphs in Figure 8.4 one can conclude, the a significant dependence of the detected or dead compartment C resp. D is given only after the initial take-off period of the epidemic. In the setting of Germany, this implies, that during the month of March a reliable identification to the detection rate might not be possible.

8.5 Adjoint equations and optimization

In order to solve the minimization problem (8.6), we use the adjoint equations, for details see [4, 15]. We introduce the Lagrangian

$$\mathcal{L}(t, x, u, z) = J(u) + \int_{t_0}^{T_{Fit}} z(t)^T \left(g(t, x, u) - \frac{dx}{dt} \right) dt.$$

Here $z = (z_S, z_E, z_I, z_R, z_D)$ denotes the adjoint functions to the state variable $x = (S, E, I, R, D)$ and $g(t, x, u)$ denotes the right hand side of the ODE resp. DDE system.

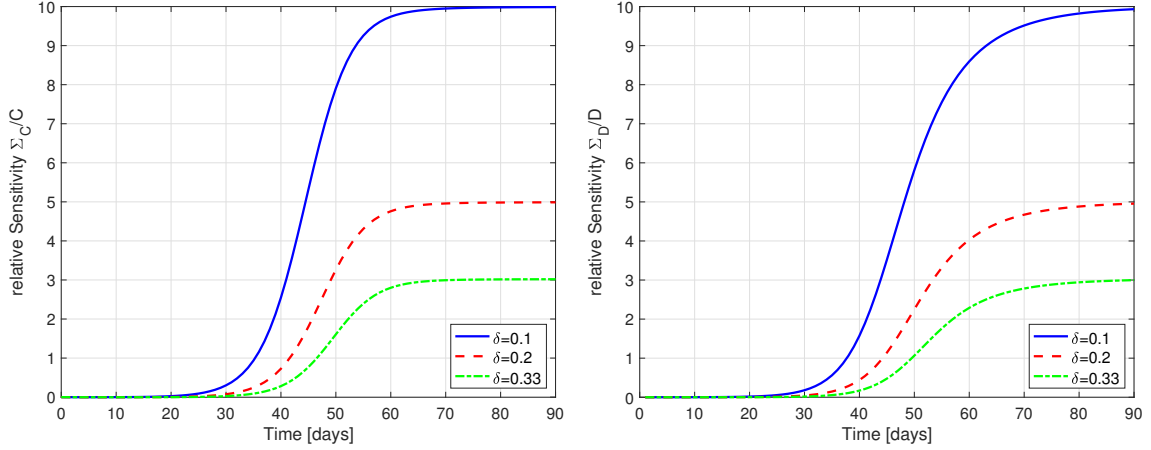


Figure 8.4: Relative sensitivities of C (left) and D (right) with respect to the detection rate δ for $\delta = 0.1$ (blue solid), $\delta = 0.2$ (red dashed) and $\delta = 0.33$ (green dash-dotted). At the onset of the epidemics, the sensitivities are extremely small, hence no reliable identification of δ is possible.

The gradient of \mathcal{L} with respect to the unknown parameters u is given by

$$\begin{aligned} \frac{\partial \mathcal{L}}{\partial \beta_i} &= 2c_2 \beta_i + \frac{1}{N} \int_{t_0}^{T_{Fit}} \frac{\partial \beta(t)}{\partial \beta_i} SI(z_E - z_S) dt, & i = 0, 1, 2, \\ \frac{\partial \mathcal{L}}{\partial \delta} &= 2c_2 \delta + \frac{2}{\|Y\|_{L^2}^2} \int_{t_0}^{T_{Fit}} (I + R) [\delta(I + R) + D - Y] dt, \\ \frac{\partial \mathcal{L}}{\partial \mu} &= 2c_2 \mu + \int_{t_0}^{T_{Fit}} \gamma I (z_D - z_I) dt, \\ \frac{\partial \mathcal{L}}{\partial E_0} &= 2c_2 E_0 + z_E(t_0) - z_S(t_0), \\ \frac{\partial \mathcal{L}}{\partial I_0} &= 2c_2 I_0 + z_I(t_0) - z_S(t_0). \end{aligned}$$

Note, that in the case $\beta = \beta_0 = \beta_1 = \beta_2$ we have $\frac{\partial \beta(t)}{\partial \beta} = 1$. By adding the time delay, we obtain

$$\frac{\partial \mathcal{L}}{\partial \mu} = 2c_2 \mu + \int_{t_0}^{T_{Fit}} \gamma I (z_I - z_R) + \gamma I (t - \tau) (z_D - z_I) dt.$$

The adjoint system reads as

$$\begin{aligned} \frac{dz_S}{dt} &= \frac{\beta(t)}{N} I (z_S - z_E), \\ \frac{dz_E}{dt} &= \vartheta (z_E - z_I), \\ \frac{dz_I}{dt} &= \frac{\beta(t)}{N} S (z_S - z_E) + \gamma [z_I - z_R + \mu (z_R - z_D)] - \frac{2\delta}{\|Y\|_{L^2}^2} [\delta(I + R) + D - Y], \\ \frac{dz_R}{dt} &= -\frac{2\delta}{\|Y\|_{L^2}^2} [\delta(I + R) + D - Y], \\ \frac{dz_D}{dt} &= -\frac{2}{\|Y\|_{L^2}^2} [\delta(I + R) + D - Y] - \frac{2c_1}{\|Z\|_{L^2}^2} (D - Z), \end{aligned}$$

supplemented by the terminal condition $(z_S, z_E, z_I, z_R, z_D)(T_{Fit}) = 0$. In the case of the time delay we receive

$$\begin{aligned} \frac{dz_I}{dt} = & \frac{\beta(t)}{N} S (z_S - z_E) + (1 - \mu) \gamma (z_I - z_R) - \frac{2\delta}{\|Y\|_{L^2}^2} [\delta(I + R) + D - Y] \\ & + \mu \gamma [z_I(t + \tau) - z_D(t + \tau)] \cdot \chi_{[t_0, T_{Fit} - \tau]}(t). \end{aligned}$$

Here $\chi_{[a,b]}(t)$ denotes the characteristic function of the interval $[a, b]$, i.e. we define $\chi_{[a,b]}(t) = 1$ for $t \in [a, b]$ and $= 0$ otherwise.

To solve the optimization problem (8.6) numerically, we apply the Forward–Backward Sweep method [4] combined with a Quasi–Newton method (*BFGS*) [9].

In each iteration step the ODEs and DDEs of the state variables and adjoint equations are solved with Runge–Kutta methods before the corresponding gradient and direction of descent can be determined. The algorithm stops as soon as the termination condition $\|J(u_{k+1}) - J(u_k)\| < \text{TOL}$ is fulfilled.

As initial values we use $\beta = \beta_0 = \beta_1 = \beta_2 = 0.3$ for the transmission rate. This is justified by the fact that an average Basic Reproduction Number of about $\mathcal{R}_0 = 3$ is assumed and in our basic model we have

$$\mathcal{R}_0 = \frac{\beta}{\gamma}.$$

Epidemiologically, \mathcal{R}_0 indicates the number of new infections an infected individual causes during the infectious period in an otherwise susceptible population. For the sake of simplicity, we assume the same starting value for I_0 and E_0 . This corresponds to the value at the first data point of our measurement, i.e. 130 registered infected persons on 1st March. As already mentioned, we assume that for the recovered and deaths at this time $R_0 = D_0 = 0$ holds. The possible problems with the optimization of δ and μ were already mentioned in the previous section. To increase the probability of generating a global minimum, we use $n = 1000$ normally distributed start values for both parameters fulfilling $\delta \sim \mathcal{N}(0.25, 0.25^2)$ and $\mu \sim \mathcal{N}(0.03, 0.03^2)$ with $\delta, \mu > 0$. The algorithm selects the best result of these n data fits. The reason for this is the assumption that the proportion of detected cases is between 1 – 50% and the lethality below 6%. For the case fatality rate μ we have

$$\frac{Z}{Y} \leq \mu \leq \frac{Z}{R_{\text{reported}}/\delta + Z}, \quad (8.8)$$

where R_{reported} stands for the reported recovered at time T_{Fit} . The approach for this estimation can be found in [11]. The smaller the detection rate δ , the lower the upper bound for the case fatality gets.

In case of the time delay we choose as initial history for $s \in [t_0 - \tau, t_0]$

$$I(s) = I_0 \exp\left(-\frac{\ln(0.1)}{\tau}(s - t_0)\right).$$

This is justified by the fact that the number of registered cases has increased tenfold during this period and we assume an exponential growth in this time span.

8.6 Simulation results

To estimate the unknown parameters u , we match the data reported on a daily basis by Johns Hopkins [3] to our simulation results for a time period starting on 1 March.

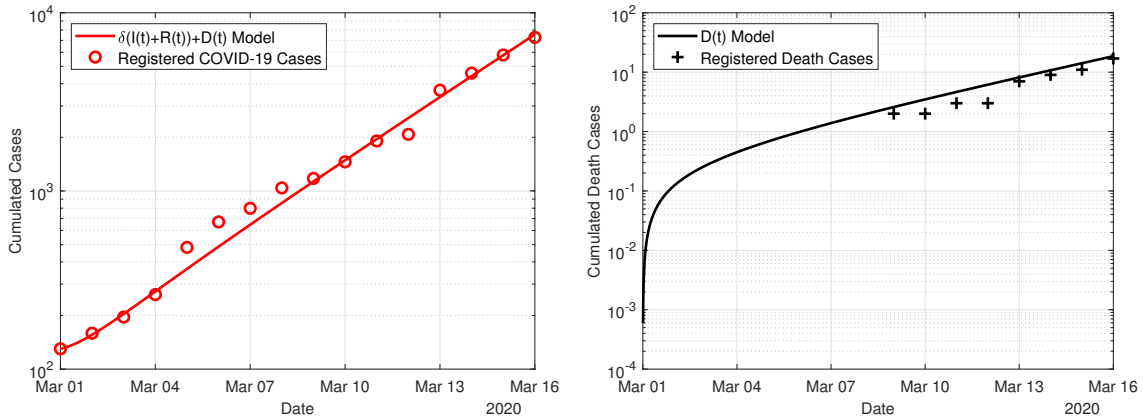


Figure 8.5: Fit of the basic model (8.1) to the data for the period 1 March to 16 March, i.e. before the onset of containment measures.

The first results in Figure 8.5 show a parameter estimation using the basic model (8.1) and the time period before the onset of any containment measures, i.e. before the closing of schools on 16 March. We fitted the parameters β , δ and μ along with the initial values E_0 and I_0 over the time period 1 March to 16 March. The initial values E_0 and I_0 are also subject to fitting, since the official data does not provide information about the active infections at a given day. The weight $\omega_2 = 1$ to keep the cost functional dominated by the two least square errors. The other weight is chosen as $\omega_1 = 500$ to compensate the significantly smaller value of the least square error in the fatal cases.

For the given time period of the fit, the model prediction and the observed data are in good accordance. The estimated parameter values are given in Table 8.1. The detection rate was estimated as $\delta = 0.37$ implying that the *true* number of infections exceeds the registered cases by a factor 3. The transmission rate $\beta = 0.57$ accounts for a doubling time of 2.6 days at the initial, uncontrolled phase of the epidemic in Germany.

In Figure 8.6 we show the results obtained with the time-dependent model (8.3). In this case, the fitting period equals to the entire simulation period starting from 1 March to 7 April. The weights ω_1, ω_2 are identical to the previous simulation. The obtained transmission rate and according doubling times change from $\beta_0 = 0.5232$ and $T_2(\beta_0) = 2.8$ days at the initial uncontrolled phase to $\beta_2 = 0.18$ and $t_2(\beta_2) = 11.4$ days after the contact ban has been introduced. The effect of the contact ban effectively reduces the transmission rate by a factor of about 3 and significantly slows down the speed of the epidemics by increasing the doubling time by a factor 4.

In Figure 8.7 we show the result obtained with the delay model (8.4). For the delay model, we assume a delay of 14 days between entering the class of infected and death. Again, we show the simulation results compared to the reported cases for the infections and deaths. Quite good agreement is found between the model and the simulation for both, infections and deaths. Compared to the time-dependent model, shown in Figure 8.6, the delay model agrees better in particular for the fatal cases. In Table 8.1 we have listed the estimated parameter values in for the three models. We have also included the normalized L^2 -difference between the simulation outcome and the given data, i.e. the first two summands from the cost functional (8.5). A t -test revealed that the deviations of the simulation to the reported data is not normal distributed at a significance level of 5%.

In the simulations the detection rate is found to be 20 – 40%, indicating that the *true* number of SARS-CoV-2 infections might be 3 – 5 times higher that the officially recorded data suggest. The lethality rate is found to be rather small, taking into account the large

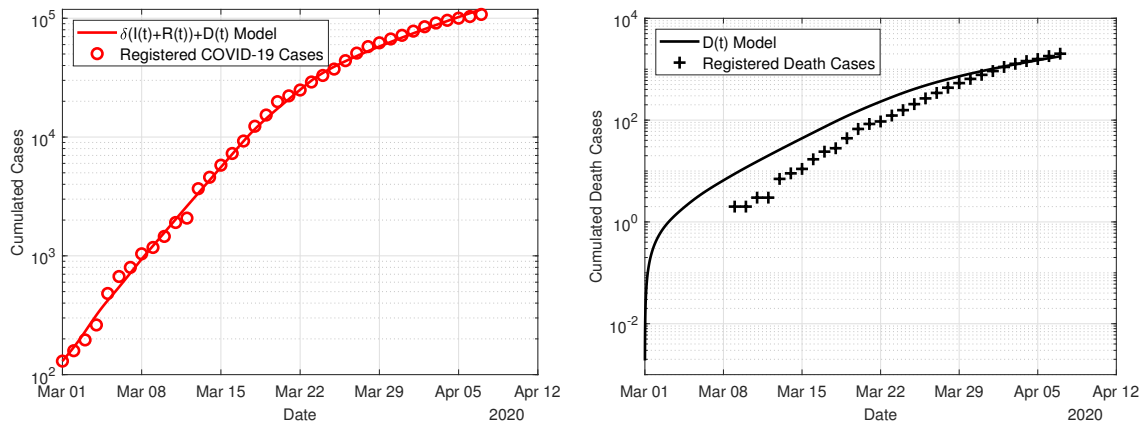


Figure 8.6: Fit of the time–dependent model (8.3) to the data for the period 1 March to 7 April.

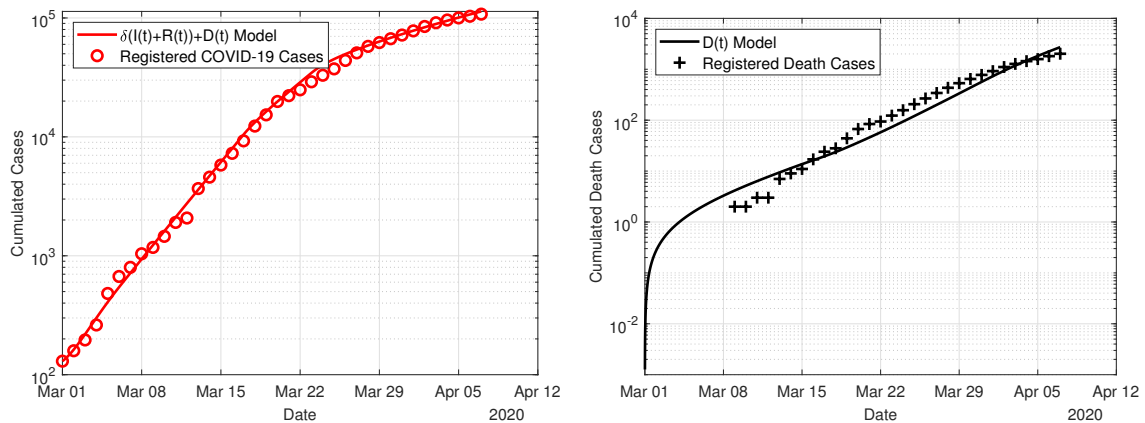


Figure 8.7: Fit of the delay model (8.4) to the data for the period 1 March to 7 April.

Table 8.1: Optimal parameter values for the three models (8.1), (8.3) and (8.4) obtained from the minimization problem (8.6).

Fit until	Parameter Model	β_0	δ	μ	$E_0 + I_0$	β_1	β_2	L^2 -diff
16.03.20	basic	0.566	0.372	0.0034	418	—	—	0.3771
07.04.20	time–dep	0.523	0.308	0.0087	659	0.3561	0.1788	0.2721
07.04.20	delay	0.553	0.202	0.0389	930	0.3578	0.1415	0.2242

number of *true cases*.

Comparing the obtained values for the lethality, the value for the delay–model seems to be most realistic, since in this model we compare the fatal cases today to the infections that occurred two weeks ago. The two other models related the fatal cases of today to the infected cases *today*, hence to a significantly larger number. Therefore in these two models, the lethality rate seems to be smaller.

8.7 Conclusions and outlook

We present three *SIR*–based models for describing the outbreak of the SARS–CoV–2 outbreak in Germany. Besides a standard *SEIR*–model, we consider an extension taking into account the effect of social distancing by a time–dependent reduction of the transmission rate. The third model introduces a delay–term to accurately describe the deaths depending on infected cases that occurred several days in the past. Comparing the simulation results to the data published by Johns Hopkins University allows an estimation of the unknown model parameters. Best results are obtained using the delay equation model. In this setting, we find a detection rate of about 20% and a lethality of about 4%. The social distancing measures were leading to an effective reduction of the transmission rate by a factor 4. That is, after the introduction of the measures roughly just 25% of the social contact compared to the initial period were leading to infections.

Declaration

Availability of data and materials: The used data on registered COVID–19 cases from Johns Hopkins university is available, see [3].

Competing interests: Not applicable.

Funding: Not applicable.

Authors’ contributions: Both authors contributed equally.

Acknowledgements: The authors would like to thank the MOCOS (MOdeling COrona Spread) International Group consisting of research groups at the universities in Kaiserslautern, Koblenz, Trier and Wrocław for valuable discussions on this urgent and internationally highly relevant issue. We also express our gratitude to the unknown referees for helping with their comments to improve the manuscript.

Authors’ information: Not applicable.

Bibliography

- [1] Federal Government of Germany: *Guidelines for reducing social contacts*. Accessed 23 Apr 2020
www.bundesregierung.de/breg-de/themen/coronavirus/besprechung-der-bundeskanzlerin-mit-den-regierungschefinnen-und-regierungschefs-der-laender-1733248 (in German)
- [2] Federal Statistical Office: *Press release No. 179 of 22 May 2020*. Accessed 23 Apr 2020
https://www.destatis.de/EN/Press/2020/05/PE20_179_12621.html
- [3] Johns Hopkins University: *Time series of confirmed COVID-19 cases globally*. Accessed 23 Apr 2020
github.com/CSSEGISandData/COVID-19/blob/master/csse_COVID_19_data/csse_COVID_19_time_series/time_series_COVID19_confirmed_global.csv
- [4] Lenhart, S.; Workman, J.T.: *Optimal control applied to biological models*, CRC Press, 2007
- [5] Leung, Gabriel; Wu, Joseph: *Real-time nowcast and forecast on the extent of the Wuhan CoV outbreak, domestic and international spread*. Accessed 23 Apr 2020
https://www.med.hku.hk/f/news/3543/7403/presentation_wuhan%20Coronavirus_20200121_final_1033.pdf (27 Jan 2020)
- [6] Magal, P.; Webb, G.: *Predicting the number of reported and unreported cases for the COVID-19 epidemic in South Korea, Italy, France and Germany*. Accessed 23 Apr 2020
[medRxiv doi.org/10.1101/2020.03.21.20040154](https://doi.org/10.1101/2020.03.21.20040154)
- [7] Martcheva, M.: *An introduction to mathematical epidemiology*, Springer US, 2015
- [8] National Health Commission of the People's Republic of China. Accessed 23 Apr 2020
<http://www.nhc.gov.cn> (in Chinese)
- [9] Nocedal, J.; Wright, S.: *Numerical Optimization*, Springer New York, 2006
- [10] Read, J.M.; Bridgen, J.R.E.; Cummings, D.A.T.; Ho, A.; Jewell, C.P.: *Novel coronavirus 2019-nCoV: early estimation of epidemiological parameters and epidemic predictions*. Accessed 23 Apr 2020
www.medrxiv.org/content/10.1101/2020.01.23.20018549v2
(28 Jan 2020)
- [11] Robert-Koch-Institute: *Corona fact sheet*. Accessed 23 Apr 2020
https://www.rki.de/DE/Content/InfAZ/N/Neuartiges_Coronavirus/Steckbrief.html
- [12] Robert-Koch-Institute: *Daily situation reports*. Accessed 23 Apr 2020
www.rki.de/DE/Content/InfAZ/N/Neuartiges_Coronavirus/Situationsberichte/Gesamt.html

Bibliography

- [13] Robert–Koch–Institute: *Why differ the information reported by RKI and Johns Hopkins University? (in German)*. Accessed 23 Apr 2020
<https://www.rki.de/SharedDocs/FAQ/NCOV2019/gesamt.html>
- [14] The Guardian: *UK care home Covid–19 deaths ‘may be five times government estimate’*. Accessed 23 Apr 2020
<https://www.theguardian.com/world/2020/apr/18/uk-care-home-covid-19-deaths-may-be-five-times-government-estimate>
(18 Apr 2020)
- [15] Vinter, R.: *Optimal Control*, Springer Basel, 2010
- [16] Wikipedia: *2020 coronavirus pandemic in Germany*. Accessed 23 Apr 2020
https://en.wikipedia.org/wiki/2020_coronavirus_pandemic_in_Germany#Statistics
- [17] World Health Organization (WHO): *Novel Coronavirus (2019–nCoV) situation reports*. Accessed 23 Apr 2020
www.who.int/emergencies/diseases/novel-coronavirus-2019/situation-reports
- [18] World Health Organization (WHO): *Q&A on coronaviruses*. Accessed 23 Apr 2020
www.who.int/news-room/q-a-detail/q-a-coronaviruses

9 Research Paper V: The COVID–19 Outbreak in Germany — Models and Parameter Estimation

Peter Heidrich Moritz Schäfer Mostafa Nikouei Thomas Götz

The paper *The COVID–19 Outbreak in Germany — Models and Parameter Estimation* by Peter Heidrich, Moritz Schäfer, Mostafa Nikouei and Thomas Götz is published in the journal *Communication in Biomathematical Sciences*, Vol. 3, No. 1, 2020 (<https://dx.doi.org/10.5614%2Fcbms.2020.3.1.5>). The layout of the paper is adapted to the present thesis.

The sections on the *Adjoint based approach* with its theoretical elaboration, calculation and evaluation are by Peter Heidrich. Moritz Schäfer delivered the corresponding sections on the *Metropolis algorithm*. Thomas Götz provided the idea for the article and took over the organization and the sections *Introduction* and *Model*. The authors complemented each other in corresponding sections. Mostafa Nikouei was involved in numerous consultative sessions and provided alternative programming methods via PYTHON, while the results of the present paper are calculated with MATLAB.

9.1 Abstract

Since the end of 2019 an outbreak of a new strain of coronavirus, called SARS–CoV–2, is reported from China and later also from other parts of the world. Since 21 January 2020, World Health Organization (WHO) reports daily data on confirmed cases and deaths from both China and other countries [21]. The Johns Hopkins University [8] collects those data from various sources worldwide on a daily basis. For Germany, the Robert–Koch–Institute (RKI) also issues daily reports on the current number of infections and infection related fatal cases and also provides estimates of several disease–related parameters [16]. In this work we present an extended *SEIRD*–model to describe these disease dynamics in Germany. The model takes into account the susceptible, exposed, infected, recovered and deceased fractions of the population. Epidemiological parameters like the transmission rate, lethality or the detection rate of infected individuals are estimated by fitting the model output to available data. For the parameter estimation itself we compare two methods: an adjoint based approach and a Monte–Carlo based Metropolis algorithm.

Keywords: COVID–19, Epidemiology, Disease dynamics, *SEIRD*–model, Parameter estimation, Adjoint equations, Metropolis algorithm.

9.2 Introduction

In December 2019, first cases of a pneumonia of unknown cause were reported from Wuhan, China. In the meantime, these cases were identified as infections with a novel strain of

coronavirus, called SARS-CoV-2, and the disease it causes was called Coronavirus Disease 2019 (COVID-19). At the beginning of January 2020, the virus spread over mainland China and reached other provinces. From 21 January onwards, WHO's daily situation reports [21] or Johns Hopkins University [8] (JHU) contain the latest figures on confirmed cases and deaths for almost all countries. In this work we rely on the data published by the JHU due to their rapid updates and easy accessibility.

The first COVID-19 case in Germany was reported on 27 January 2020 in Bavaria. Later cases were imported by travelers from China, Iran or Italy as well as tourists returning from ski holidays in Austria and Italy. By 1 March 2020, more than 100 cases were reported in Germany; since then, the number of cases began to rise exponentially. The first deaths were reported on 9 March [16]. By 16 March, the federal government introduced first measures to reduce the spread of the disease: schools, kindergartens and universities were closed. On 22 March, these measures were tightened by implementing a national curfew and contact ban. People are advised to stay at home, leaving only for work related activities, necessary shopping, medical treatment or sports [4]. By mid of April, these mitigation measures showed some success with the number of new infections declining from its peak of 6,294 on 28 March to less than 1,000 from 2 May onwards. On 6 May, a relaxation of the imposed restrictions to social and economic life was announced. Since then, the federal states are progressing at an individual pace to "normality".

Asking the population to remain cautious and not to cause a second wave, local governments of cities or districts are in charge to reinforce restrictions in case the number of new infections surpasses the limit of 50 per 100,000 inhabitants within 7 days as of 6 May [2, 3]. Already four days later five districts exceeded this limit; with no measures reported to alleviate it.

The pandemic continues to spread worldwide (as of June 2020) and the actual possibility of a second wave demands for models to predict epidemic scenarios for the near and mid future. The quality of those models heavily relies on the parameters used. In this study we present *SEIRD*-models which are some sort of quasi standard in epidemiological simulations and estimate their parameters by using the available data from the JHU. The estimation itself is based on a least squares fit between the model output and the reported data. Here, both the reported infections and the reported fatalities are taken into account.

9.3 Model

Following the classical *SIR*-models introduced by McKendrick [9] and its every-growing number of variants (cf. [11] for an overview), we chose an *SEIRD*-model to describe the COVID-19 outbreak in Germany. The entire population N is subdivided into five compartments: susceptibles S , exposed E , infected I , recovered R , and deceased D . The virus is transmitted from infected persons to susceptible persons at a time-dependent rate $\beta(t)$ and after an incubation phase of duration κ^{-1} exposed individuals get infectious. Loss of infectivity is gained after γ^{-1} days and with a probability μ , a patient dies from

the disease. This leads us to the following five-dimensional ODE system:

$$S' = -\frac{\beta(t)}{N}SI, \quad S(t_0) = S_0 = N - E_0 - I_0 - R_0 - D_0 > 0, \quad (9.1a)$$

$$E' = \frac{\beta(t)}{N}SI - \kappa E, \quad E(t_0) = E_0 \geq 0, \quad (9.1b)$$

$$I' = \kappa E - \gamma I, \quad I(t_0) = I_0 > 0, \quad (9.1c)$$

$$R' = (1 - \mu)\gamma I, \quad R(t_0) = R_0 \geq 0, \quad (9.1d)$$

$$D' = \mu\gamma I, \quad D(t_0) = D_0 \geq 0. \quad (9.1e)$$

The starting point t_0 is chosen as 1 March as on that date number of reported cases exceeded 100 cases for the first time, see Figure 9.1.

It is immediate to see that the model (9.1) has non-negative solutions, provided the initial values are all non-negative. Due to the absence of demographic terms, there is just the trivial disease-free equilibrium $S = N$ and $E = I = R = D = 0$. Since the intention of our model is to provide short- and mid-term simulations, we are not interested in its long-term behavior and hence possible endemic equilibria are of no concern.

As a variant of the above basic model, we also consider a delayed differential equation (DDE) version where we introduce a time lag τ between the infected and the deceased state so that the fraction of people who recover or die from the disease is not attained from the amount of infectives on the same day, but from the infectives data τ days earlier. The previous ODE model can thus be seen as a special case of the DDE model with $\tau = 0$.

$$S' = -\frac{\beta(t)}{N}SI, \quad S(t_0) = S_0 > 0, \quad (9.2a)$$

$$E' = \frac{\beta(t)}{N}SI - \kappa E, \quad E(t_0) = E_0 \geq 0, \quad (9.2b)$$

$$I' = \kappa E - \gamma((1 - \mu)I + \mu I(t - \tau)), \quad I(t) = \varphi(t) > 0, \quad (9.2c)$$

$$R' = (1 - \mu)\gamma I, \quad R(t_0) = R_0 \geq 0, \quad (9.2d)$$

$$D' = \mu\gamma I(t - \tau), \quad D(t_0) = D_0 \geq 0. \quad (9.2e)$$

Here, $\varphi : [t_0 - \tau, t_0] \rightarrow \mathbb{R}_+$ denotes the initial history of the infected required for the well-posedness of the above delay differential equation. Since the initial value I_0 of the infected at the starting date 1 March is later on subject of the estimation procedure, we assume the initial history to show some exponential behavior

$$\varphi(t) := I_0 \exp\left(-\frac{\ln(0.1)}{\tau}(t - t_0)\right)$$

for $t_0 - \tau \leq t \leq t_0$.

The transmission rate $\beta(t)$ can be related to the Basic Reproduction Number \mathcal{R}_0 via

$$\mathcal{R}_0(t) = \frac{\beta(t)}{\gamma}.$$

At the onset of the epidemic, the Basic Reproduction Number \mathcal{R}_0 in Germany was estimated to be $\mathcal{R}_0 \simeq 2.4$ – 4.1 , see [14]. To take the different levels of restriction imposed on the social and economic life, we assume $\beta(t)$ as a step function in time:

$$\beta(t) := \begin{cases} \beta_0, & t < 16 \text{ March} \\ \beta_1, & 16 \text{ March} \leq t < 22 \text{ March} \\ \beta_2, & 22 \text{ March} \leq t < 20 \text{ April} \\ \beta_3, & 20 \text{ April} \leq t. \end{cases} \quad (9.3)$$

Before the first restrictions were imposed on 16 March, the disease was allowed to spread almost uncontrolled. After kindergarden, school and university closings on 16 March, the measures were tightened on 22 March by introducing a contact ban and closing of a large number of shops and businesses. On 20 April, first relaxations were announced and public life began to re-increase, but along with compulsory wearing of masks which has been introduced in late April. For each of these stages we assume an specific contact rate between individuals and hence different transmission rates β_i . The values for the fixed model parameters are given in Table 9.1.

Table 9.1: Used parameter values.

Parameter	Value	Unit	Reference
N	83,019,213	–	[20]
κ	1/3	d ⁻¹	[17]
γ	1/10	d ⁻¹	[17]
τ	> 7	d	[17]

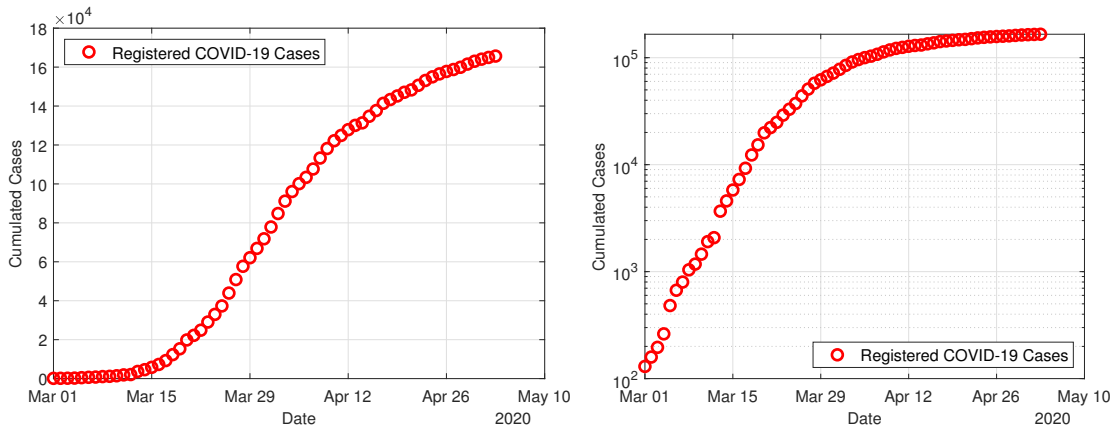


Figure 9.1: Graphs of cumulative infections in Germany according to Johns Hopkins University from March 1st to May 3rd. On the left side with normal scaling and on the right side in a semi-logarithmic scale.

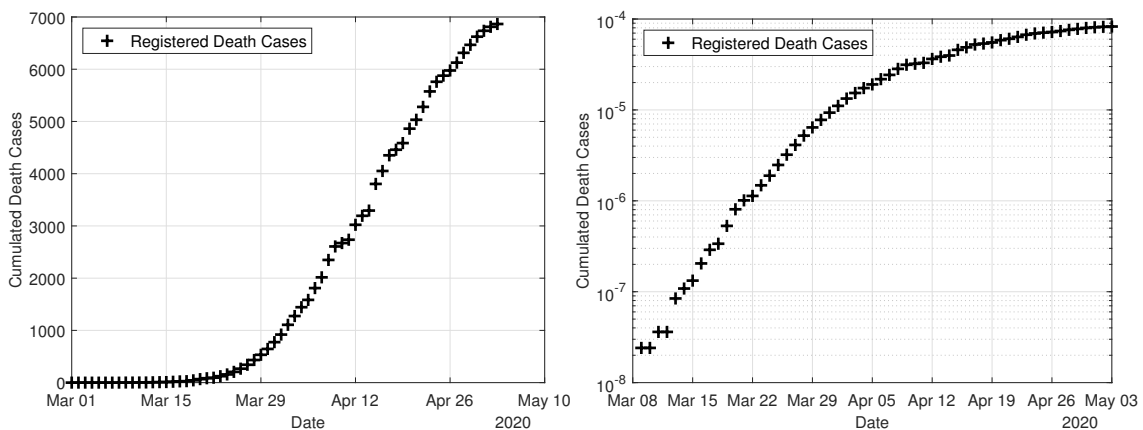


Figure 9.2: Graphs of cumulative death cases in Germany according to Johns Hopkins University from March 1st to May 3rd. The scaling is chosen as in Figure 9.1.

9.4 Parameter estimation

The unknown model parameter set u is estimated from a least squares fit of the model output to the given data. Let Y and Z denote the accumulated registered COVID–19 cases or the accumulated COVID–19 deaths in Germany as reported by Johns Hopkins University, see [8]. The reported cases Y consist of the currently infected cases, the recovered and the deceased cases. Since by the very nature of the matter, not all infections are detected, we introduce a detection rate δ . For the currently infected and the recovered ones, we assume that only this proportion δ is tested and detected and hence appears in the statistics; however, we assume no undetected deceased cases. Hence we compare the data Y to $\delta \cdot (I + R) + D$ from the model output. To put special emphasis on the fatalities, we add a term which just compared the reported and the simulated deaths to the cost functional. As a third contribution we add a regularization term proportional to the norm of the estimated parameters to attain a convex function and prevent unrealistic outliers. With this in mind we arrive at the following cost functional:

$$J(u) := \frac{\|\delta(I + R) + D - Y\|_{L^2}^2}{\|Y\|_{L^2}^2} + \frac{\|D - Z\|_{L^2}^2}{\|Z\|_{L^2}^2} + \omega \|u\|_2^2, \quad (9.4)$$

where $\omega > 0$ denotes some small weight allowing us to adjust the contribution between the normalized least squares terms and the regularization term and $\|f(t)\|_{L^2}^2 = \int_{t_0}^T f(t)^2 dt$ denotes the square of the L^2 -norm of a function f resp. $\|u\|_2^2 = \sum_i u_i^2$ for the square of the Euclidean norm of a vector u .

The parameters to be estimated in model (9.1) are the transmission rate, the detection rate, lethality and the numbers of exposed on 1 March 2020, i.e.

$$u = (\beta_0, \beta_1, \beta_2, \beta_3, \delta, \mu, E_0) \in \mathbb{R}^7$$

which is the same parameter set as in model (9.2) with added but fixed time lag τ . For the model with free and to-be-optimized time lag τ , we have the parameter set

$$u = (\beta_0, \beta_1, \beta_2, \beta_3, \delta, \mu, \tau, E_0, I_0) \in \mathbb{R}^9.$$

Here, we also estimate the initial number of infected on 1 March to allow for more flexibility of the model. The optimal parameters u^* are determined by solving the following minimization problem:

$$\min_u J(u) \quad \text{subject to ODE (9.1) resp. (9.2),} \quad (9.5a)$$

$$u^* = \operatorname{argmin}_u J(u). \quad (9.5b)$$

Table 9.2 shows the planned simulations including constraints for the optimized parameters in u .

Previous investigations in [7] already give us orders of magnitude for the initial values of the optimization for β_i and δ . For the lethality rate μ we assume the upper limit

$$\mu \leq \frac{Z(T)}{R(T)/\delta + Z(T)},$$

whereby $Z(T)$ denotes for the death cases and $R(T)$ denotes the registered recovered individuals at end time T [15]. This upper limit becomes smaller the fewer COVID cases are registered, since δ becomes smaller. For our data set we find

$$\mu \leq \frac{6866}{130600 + 6866} \approx 0.05 \quad (9.6)$$

Table 9.2: Simulations with the respective constraints of the fitted parameters. In Simulation 1 no time lag τ is included in the model. The starting values for I_0 and R_0 are only updated in the first two simulations by division with δ in each iteration. In Simulation 2 the time lag $\tau = 11.5$ is fixed as a mean value within the assumed interval. The parameter τ is also fitted in Simulation 3, just like I_0 . All other unknown parameters in this table are adjusted in each simulation.

Sim.	Model	β_i	δ	μ	τ	E_0	I_0	R_0
1	1	> 0.05	$0.05 - 0.5$	≤ 0.05	0	> 0	$114/\delta$	$16/\delta$
2	2	> 0.05	$0.05 - 0.5$	≤ 0.05	11.5	> 0	$114/\delta$	$16/\delta$
3	2	> 0.05	$0.05 - 0.5$	≤ 0.05	> 7	> 0	> 0	$16/\delta$

based on the registered cases, i.e. this upper limit would match, if $\delta = 1$. Building on the assumption that less than 50% of cases are detected, we also assume a starting value for the lethality rate that is less than half of the calculated upper limit of 5%. The order of magnitude of the time interval between the onset of infectiousness and death is derived from the investigations in [17]. From the timelines available there we derive $\tau \in (7, 17)$. In individual cases this period can be considerably longer, so that τ only represents an average value in the model. The starting values for I_0 and R_0 can be taken from the statistics. Depending on the value of the detection rate, the actual number is calculated by dividing the measured values for the infected and recovered cases by δ . Regarding an estimate of the exposed individuals E_0 at time t_0 , we use a derivation using the Basic Reproduction Number \mathcal{R}_0 , which indicates how many new infections an infected individual causes on average during its illness in an otherwise susceptible population. In our model, the infected persons I_0 are at different time stages during their infectiousness. As a mean value we assume the middle of this time interval. Thus, up to this point in time they could infect about $I_0 \mathcal{R}_0 / 2$ persons on average. Depending on the assumed Basic Reproduction Number, this results in different starting values for E_0 . The model adaptations are carried out in the simulations with the values $\mathcal{R}_0 \in \{3, 4, 5\}$ and it is checked if significant effects on the other parameters can be found. The selected start values can be seen in Table 9.3.

Table 9.3: Orders of magnitude of the initial values for adapting the model to the available data.

Param.	β_0	β_1	β_2, β_3	δ	μ	τ	E_0	I_0	R_0
Init. val.	0.6	0.4	0.1	0.25	0.02	11.5	$I_0 \mathcal{R}_0 / 2$	$114/\delta$	$16/\delta$

9.4.1 Adjoint based approach

To solve the minimization problem using adjoint functions we introduce the Lagrangian function

$$\mathcal{L}(u, x, z) = J(u) + \int_{t_0}^T z(t) \cdot \left(g(t, x, u) - \frac{dx}{dt} \right) dt,$$

whereby $z = (z_S, z_E, z_I, z_R, z_D)$ denotes the adjoint function regarding the state variable $x = (S, E, I, R, D)$ and $g(t, x, u)$ denotes the right side of the ODE resp. DDE system. It should be noted that within the integral, a scalar product of vectors is calculated. A critical point (u^*, x^*, z^*) needs to fulfill the necessary optimality condition

$$\nabla \mathcal{L}(u^*, x^*, z^*) = 0.$$

For precise details of the following procedure, please refer to [10]. Thus we find the gradient $\nabla_u \mathcal{L}$ regarding the parameters in u

$$\frac{\partial \mathcal{L}}{\partial \beta_i} = 2\omega\beta_i + \frac{1}{N} \int_{t_0}^T \frac{\partial \beta(t)}{\partial \beta_i} SI(z_E - z_S) dt, \quad i = 0, 1, 2, 3, \quad (9.7a)$$

$$\frac{\partial \mathcal{L}}{\partial \delta} = 2\omega\delta + 2 \int_{t_0}^T (I + R) (\delta(I + R) + D - Y) dt, \quad (9.7b)$$

$$\frac{\partial \mathcal{L}}{\partial \mu} = 2\omega\mu + \gamma \int_{t_0}^T I(z_D - z_I) dt, \quad (9.7c)$$

$$\frac{\partial \mathcal{L}}{\partial E_0} = 2\omega E_0 + z_E(t_0) - z_S(t_0), \quad (9.7d)$$

$$\frac{\partial \mathcal{L}}{\partial I_0} = 2\omega I_0 + z_I(t_0) - z_S(t_0), \quad (9.7e)$$

resp. in model (9.2) we obtain, due to the time delay τ ,

$$\frac{\partial \mathcal{L}}{\partial \mu} = 2\omega\mu + \gamma \int_{t_0}^T I(z_I - z_R) + I(t - \tau)(z_D - z_I) dt, \quad (9.7f)$$

$$\frac{\partial \mathcal{L}}{\partial \tau} = 2\omega\tau + \gamma\mu \int_{t_0}^T (z_I - z_D) \frac{dI}{dt} \Big|_{t=t-\tau} dt. \quad (9.7g)$$

The adjoint system is given by the equations

$$\frac{dz_S}{dt} = \frac{\beta(t)}{N} I(z_S - z_E), \quad (9.8a)$$

$$\frac{dz_E}{dt} = \kappa(z_E - z_I), \quad (9.8b)$$

$$\frac{dz_I}{dt} = \frac{\beta(t)}{N} S(z_S - z_E) + \gamma(z_I - z_R + \mu(z_R - z_D)) - \frac{2\delta(\delta(I + R) + D - Y)}{\|Y\|_{L^2}^2}, \quad (9.8c)$$

$$\frac{dz_R}{dt} = -\frac{2\delta}{\|Y\|_{L^2}^2} (\delta(I + R) + D - Y), \quad (9.8d)$$

$$\frac{dz_D}{dt} = -\frac{2}{\|Y\|_{L^2}^2} (\delta(I + R) + D - Y) - \frac{2}{\|Z\|_{L^2}^2} (D - Z), \quad (9.8e)$$

with the terminal condition $(z_S, z_E, z_I, z_R, z_D)(T) = 0$. By adding the time delay in model (9.2) we receive

$$\begin{aligned} \frac{dz_I}{dt} = & \frac{\beta(t)}{N} S(z_S - z_E) + (1 - \mu)\gamma(z_I - z_R) - \frac{2\delta}{\|Y\|_{L^2}^2} (\delta(I + R) + D - Y) \\ & + \mu\gamma(z_I(t + \tau) - z_D(t + \tau)) \cdot \chi_{[t_0, T - \tau]}(t). \end{aligned} \quad (9.8f)$$

Here χ denotes the characteristic function

$$\chi_{[t_0, T - \tau]}(t) = \begin{cases} 1, & t \in [t_0, T - \tau] \\ 0, & \text{else.} \end{cases}$$

Algorithm 4 Pseudocode for the approach including adjoint functions.

```

1:  $u, Y, Z \leftarrow$  load initial values for  $u$  and data
2:  $x, z \leftarrow$  solve ODE resp. DDE for state variable and adjoint function
3:  $J, \nabla J \leftarrow$  compute objective function and gradient regarding  $u$ 
4:  $s \leftarrow$  compute search direction
5: repeat
6:    $J_{old} \leftarrow J$ 
7:    $\vartheta \leftarrow \operatorname{argmin}_{\vartheta > 0} \psi(\vartheta)$  with  $\psi(\vartheta) := J(u + \vartheta s)$ 
8:    $u \leftarrow u + \vartheta s$ 
9:    $x, z, J, \nabla J, s \leftarrow$  update depending on  $u$ 
10: until  $\|J - J_{old}\|_2 < \text{TOL}$ 
11:  $u^*, x^*, z^*, J^* \leftarrow u, x, z, J$ 

```

Algorithm 4 represents the basic framework of the iterative optimization via adjoint functions. To find a preferably global minimum, n multivariate normally distributed start values for u can be created before step 1. These are then tested one after the other with the presented procedure and the best result is chosen. The mean values of this distribution are then the values in Table 9.3, and the variances can be selected according to the restrictions in Table 9.2. In step 2 the ODE or DDE are solved using Runge–Kutta methods. Since the state variable is solved forward and the adjoint function backward regarding the time scale due to the initial and end values, this is also called the forward–backward sweep method [10]. In MATLAB the ode45 and dde23 solvers are suitable for this purpose. The search direction s in steps 4 and 9 is selected as Quasi–Newton method (BFGS). Useful alternative search directions are (conjugated) gradient methods [13]. The line search procedure in step 7 cannot be solved analytically in our case. A common method for an appropriate step size ϑ^* would be a backtracking procedure considering the Armijo rule [1]. In the present simulation the procedure in Algorithm 5 is applied. It is based on a Taylor series of $\psi(\vartheta) := J(u + \vartheta s)$ developed around ϑ_0

$$\psi(\vartheta_0 + h) = \psi(\vartheta_0) + \psi'(\vartheta_0)h + \frac{1}{2}\psi''(\vartheta_0)h^2 + \dots$$

where ψ', ψ'', \dots stand for the respective derivatives of ψ regarding ϑ . Based on this, we assume that ψ for $\vartheta_0 = 0$ and sufficiently small values for $h = \vartheta$ can be approximated by a parabola with

$$\begin{aligned} \psi(\vartheta) &\simeq a\vartheta^2 + b\vartheta + c, \\ \psi'(\vartheta) &\simeq 2a\vartheta + b. \end{aligned} \tag{9.9}$$

Using the information $\psi(0) = J(u)$ and $\psi'(0) = \nabla J(u) \cdot s$ associated with a calculated value $\psi(\vartheta_1) = J(u + \vartheta_1 s)$ for small and fixed ϑ_1 allows to derive the parameters

$$\begin{aligned} c &= \psi(0), \\ b &= \psi'(0), \\ a &= (\psi(\vartheta_1) - \psi'(0)\vartheta_1 - \psi(0))/\vartheta_1^2, \end{aligned}$$

and, by using the necessary condition $\psi'(\vartheta^*) = 0$, find the optimum of the parabola in (9.9)

$$\vartheta^* = -b/(2a) = -0.5\psi'(0)\vartheta_1^2/(\psi(\vartheta_1) - \psi'(0)\vartheta_1 - \psi(0)).$$

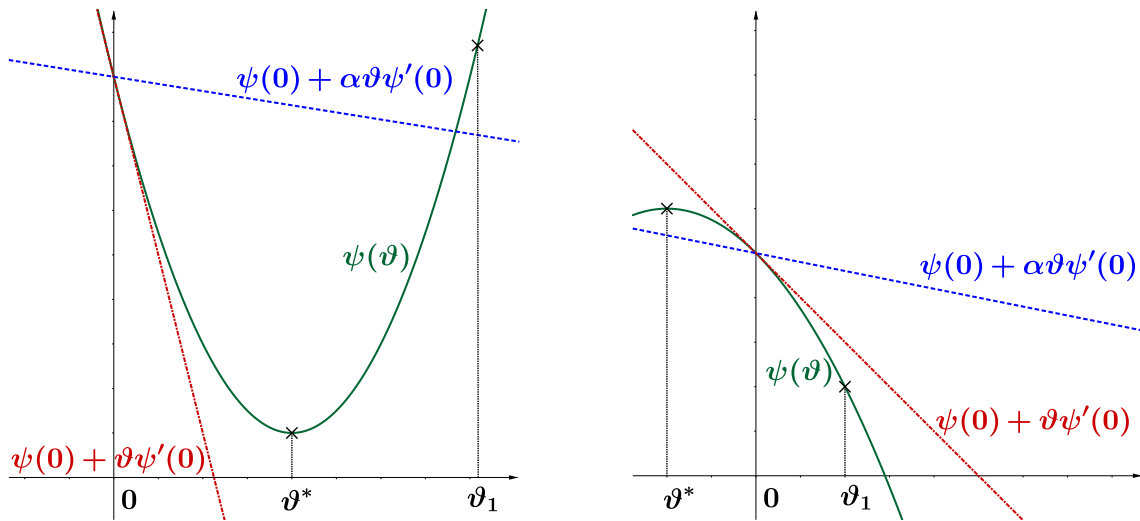


Figure 9.3: Graphical example to approximate the optimal value for ϑ^* with parabola linesearch. The left figure shows that the Armijo rule $\psi(\vartheta) \leq \psi(0) + \alpha\vartheta\psi'(0)$ is not fulfilled for ϑ_1 and the new step size is determined using the parabola minimum ϑ^* . To make sure that the possible minimum of the parabola is below that line, one chooses a small value for $\alpha \in (0, 0.5)$, e.g. $\alpha = 1e-4$. In the right figure the Armijo rule is already fulfilled with the fixed increment ϑ_1 which can be adopted. There can also be a parabola maximum, so that ϑ^* takes a negative value. However, this is circumvented because in this case, there is no optimization of the step size.

Algorithm 5 Pseudocode for line search in step 7 of Algorithm 4.

```

1:  $u, J(u), \nabla J(u), s \leftarrow$  input
2:  $\vartheta \leftarrow 1$ 
3:  $\psi(0) \leftarrow J(u)$ 
4:  $x \leftarrow$  compute state variable depending on  $u + \vartheta s$ 
5:  $\psi(\vartheta) \leftarrow J(u + \vartheta s)$ 
6:  $\psi'(0) \leftarrow \nabla J(u) \cdot s$ 
7:  $\alpha \leftarrow$  value in  $(0, 0.5)$ 
8: if  $\psi(\vartheta) > \psi(0) + \alpha\vartheta\psi'(0)$  then
9:   repeat
10:     $\vartheta \leftarrow -0.5\psi'(0)\vartheta^2 / (\psi(\vartheta) - \psi'(0)\vartheta - \psi(0))$ 
11:     $x \leftarrow$  update depending on  $u + \vartheta s$ 
12:     $\psi(\vartheta) \leftarrow J(u + \vartheta s)$ 
13:  until  $\psi(\vartheta) \leq \psi(0) + \alpha\vartheta\psi'(0)$  (Armijo rule)
14: end if
15:  $\vartheta^* = \vartheta$ 

```

The effect of the weight ω can be seen on the diagonal of the Hessian matrix in model (9.1)

$$\nabla_u^2 \mathcal{L} = 2 \operatorname{diag} \left(\omega, \omega, \omega, \omega, \omega + \int_{t_0}^T (I + R)^2 dt, \omega, \omega, \omega \right),$$

whereby all other entries in $\nabla_u^2 \mathcal{L}$ are 0. The value of ω directly influences the definiteness of the Hessian matrix and thus the convexity of the objective function. For this reason, different values for ω are tested in the simulations.

9.4.2 Metropolis algorithm

According to the procedure described in [19], a Metropolis algorithm (cf. [5, 6, 12]) for model (9.2) can be set up using the initial history and initial values for the to-be-estimated parameter set u . Using the parameter set u_0 as of Table 9.3 as starting conditions, we assign random draws u_{new} from a normally distributed (and thus symmetric) proposal function q , i.e. $u_{new} \sim q(u_{new}|u_{i-1})$, in every iteration i .

Using the previously defined $J(u)$ as the target distribution, we calculate the approximative distribution by

$$\pi(u) = c \cdot \exp \left(-\frac{J(u)^2}{2\sigma^2} \right), \quad (9.10)$$

whereby c is an arbitrary value in \mathbb{R} . For the acceptance probability, it follows

$$\alpha(u_{new}|u_{i-1}) = \min \left\{ 1, \frac{\pi(u_{new}) \cdot q(u_{i-1}|u_i)}{\pi(u_i) \cdot q(u_i|u_{i-1})} \right\} = \min \left\{ 1, \frac{\pi(u_{new})}{\pi(u_i)} \right\}. \quad (9.11)$$

In Eq.(9.11) we can see that the value of c is redundant as it cancels out in the division.

If the sample is accepted with the probability α , we set $u_i = u_{new}$; with the probability $1 - \alpha$, the sample is declined, meaning $u = u_{i-1}$ [18, 19].

Algorithm 6 Pseudocode for the Metropolis algorithm.

- 1: $u, Y, Z \leftarrow$ load initial values for u and data
 - 2: $x, z \leftarrow$ solve ODE resp. DDE for state variable
 - 3: $J \leftarrow$ compute objective function regarding u
 - 4: $\sigma \leftarrow$ standard distribution of the solution, i.e. $I + R + D$ over time
 - 5: $s \leftarrow$ set step size (standard deviation) for the algorithm, e.g. $s := u/100$
 - 6: **repeat**
 - 7: $u_{old} \leftarrow u$ from previous draw
 - 8: $\hat{u}_{new} \leftarrow u \sim \mathcal{N}(u_{old}, s)$
 - 9: $x, z, J(\hat{u}_{new}) \leftarrow$ update depending on u
 - 10: $\alpha \leftarrow \min \{ 1, \exp (J(u_{old})^2 - J(u_{new})^2 / 2\sigma^2) \}$
 - 11: $u_{new} \leftarrow \hat{u}_{new}$ with probability α and $u_{new} := u$ with probability $1 - \alpha$
 - 12: **until** maximum value of draws is reached
 - 13: $u^*, x^*, J^* \leftarrow$ means of all u, x, J
-

Algorithm 6 represents the basic framework of the iterative optimization via the Metropolis algorithm. In step 1, the mean values of this distribution as of Table 9.3 are loaded as well as the variances according to the restrictions in Table 9.2. In step 2 the ODE or DDE are again solved using Runge–Kutta methods via MATLAB’s ode45 and dde23 solvers. The step size s in step 5 is selected as a fraction of the initial guess for the parameter set u so that the parameters are allowed move with an individual ”speed” through the

search space. In steps 6 to 12, the process is repeated for all draws, the number of draws in our case is set to $2e + 4$. Alternatively, you can think about termination conditions, but we avoided this due to the random nature of the system. Firstly, the update of the parameter set u is done by taking a random value out of the normal distribution with mean u and standard deviation s . After solving the system in step 9, the cost functional $J(u)$ is compared to the previous cost functional with the function α in step 10 and the new parameter set is accepted or rejected according to 9.11 in step 11. The estimation parameter set can then be computed out of the mean value of the draws in step 13. Alternatively, in case of non-convergence, you can compute the best fitting u of the set and use this as initial value as of step 1 again, to attain better results. Choosing the weights ω for the target function $J(u)$ was done under two purposes. The first purpose was to create a convex target function so that the algorithm does not converge to local minima (see also the previous subsection for this). The Metropolis algorithm allows steps into parameter sets having a "worse" target distribution with a certain probability, but it is still possible that it runs into local but not global minima after a *final* amount of steps which justifies the usage of the term $\omega \|u\|^2$. The other purpose is to not have a too large ω so that the model-related terms still have a major impact on the outcome of $J(u)$. For these two regards, we found that a range for ω between $\omega := 10^{-9}$ and $\omega := 10^{-7}$ is decent, but we will also present the results if we neglect the term with ω , i.e. $\omega = 0$. For values $\omega \in (0, 10^{-9})$ no significant changes in the outcomes to $\omega = 0$ were detected, while for $\omega > 10^{-7}$ the model-related terms are negligible and the results are quite unrealistic.

9.5 Numerical results and comparison of the algorithms

Table 9.4: Numerical results.

Algorithm Simulation	Adjoint			Metropolis		
	1	2	3	1	2	3
β_0	0.60	0.64	0.62	0.55	0.70	0.64
β_1	0.50	0.48	0.51	0.49	0.40	0.64
β_2	0.101	0.082	0.092	0.113	0.085	0.086
β_3	0.099	0.050	0.058	0.054	0.055	0.055
δ	0.31	0.27	0.18	0.29	0.20	0.19
μ	0.015	0.018	0.011	0.013	0.013	0.011
τ	0	11.5	9.0	0	11.5	7.3
$E_0 + I_0 + R_0$	831	1,105	1,512	1,255	854	1,090
$(J(u) - \omega \ u\ _2^2) \cdot 10^3$	23.0	9.1	6.1	18.1	8.2	3.2
Iterations	23	22	31	20000	20000	20000

Table 9.4 shows the respectively best numerical results of the two algorithms. The values for the transmission parameters β_i are of similar magnitudes in almost all simulations and algorithms. In isolated cases there are more significant deviations, such as $\beta_1 = 0.64$ in Simulation 3 of the Metropolis approach or the value $\beta_3 = 0.099$ in Simulation 1 of the adjoint approach. The values show that the dynamics of the model at the beginning of the measurement period with $\beta_0 \simeq 0.6$ suggest a much higher \mathcal{R}_0 than assumed. The first measures lead to a small to moderate reduction of the transmission rate to $\beta_1 \simeq 0.5$, whereas the following lockdown causes a significant decrease of the transmission rate to $\beta_2 \simeq 0.1$. This also fits with the estimates of the RKI that the Basic Reproduction Number

is said to have dropped to a value of around $\mathcal{R}_0 \simeq 1$ due to the extensive restrictions [16]. In the last phase of the data adaptation the transfer rate drops to $\beta_3 \simeq 0.06$. Here, due to the loosening of the measurements, one would expect an increase of the transmission rate. However, these were introduced very slowly and under very strict hygiene measures, combined with a mask requirement in public spaces, which apparently has decreased the β value. Regarding the detection rate δ we find values of around 20 – 30% in all cases. This means that according to the simulations, the actual number of infected people is 3–5 times higher than the official reports. The computed lethality is between 1–2% and is therefore roughly a third of 5% which was calculated in (9.6) regarding the registered cases at the end time point T . The average time interval τ between the onset of infectivity and death in Simulation 3 is between 7 and 10 days. The influence of τ is also evident with regard to the normalized least squares terms $J(u) - \omega \|u\|_2^2$. By adding a fixed time lag in Simulation 2 and then adjusting it in the third simulation, a significant improvement is shown in all algorithms as $J(u)$ is considerably smaller. Regarding the magnitudes of the least squares terms, the algorithms show similar values in comparison to each other and lead to useful adjustments with minor deviations of the model from the available data sets. This is also illustrated by the graphical results which are shown in Appendices 9.A and 9.B. The sum of the initial values $E_0 + I_0 + R_0$ lies within a realistic range at $\simeq 1000$. Thus, the unknown initial value for the exposed individuals E_0 is approximately in the order of magnitude of the infected I_0 with an upward tendency, as expected. The variation regarding the initial value for $E_0 = I_0 \mathcal{R}_0 / 2$ in the optimization does not lead to significant differences in the results when $\mathcal{R}_0 \in \{3, 4, 5\}$ is changed. For this reason, the results are presented here only for initial estimations of $\mathcal{R}_0 = 3$. In the case of the Metropolis algorithm, the number of iterations is much higher than in the adjoint approach. This is due to the fact that the Metropolis approach relies on random draws and thus a large amount of draws is needed to obtain convergence and to diminish the effect of outliers. This seemingly disadvantageous property of the Metropolis algorithm is partly counter-balanced when using n multivariate normally distributed values for u as starting guesses for the adjoint-based optimization. This also increases the iteration number by a factor n . On the other hand, this would have the consequence that the probability of reaching a global minimum for $J(u)$ would increase significantly. This aspect is already been cared for in the Metropolis algorithm so no additional computations are required unless the chain statistics (as to be seen in the following sections). The value for $J(u)$, especially in Simulation 3 are slightly more accurate using the Metropolis algorithm. The comparison of the runtimes in Simulation 3 on an Intel Core i5–6400 with 2.7 GHz and 16 MB–RAM also reflects this. Due to the higher number of iterations, the Metropolis algorithm also has a longer runtime, see Table 9.5.

Table 9.5: Average required runtime of the algorithms on an Intel i5–6400 with 2.7 GHz and 16 MB–RAM.

Algorithm	Average runtime [s]
Adjoint approach	10
Metropolis	140

Additionally, the influence of the weight ω on the optimization is tested. Table 9.6 shows the results of the least squares term $J(u) - \omega \|u\|_2^2$ for Simulation 3 with the two algorithms and different weights.

Table 9.6: Values for the normalized least squares terms $(J(u) - \omega \|u\|_2^2) \cdot 10^3$ for the optimization with different weights ω regarding the algorithms in Simulation 3.

Algorithm	$\omega = 0$	$\omega = 10^{-9}$	$\omega = 10^{-8}$	$\omega = 10^{-7}$
Adjoint approach	8.9	8.8	6.1	12.0
Metropolis	3.8	3.2	3.4	4.1

The results show that an appropriate weight value is $\omega \simeq 10^{-8}$ resp. 10^{-9} , depending on the chosen algorithm. If the weight is too large, the value of the least squares term also deteriorates. This makes sense since the disturbance caused by $\omega \|u\|_2^2$ on the objective function becomes too large. On the other hand, however, a sufficiently small value for ω leads to better optimization performance, since a weight of $\omega = 0$ on the other hand gives a worse result.

9.5.1 Specific results for the adjoint approach

As shown in Table 9.4, the approach with adjoint functions leads to similar numerical results as the other tested routine. The graphical results of Simulation 3 are shown in Figure 9.4.

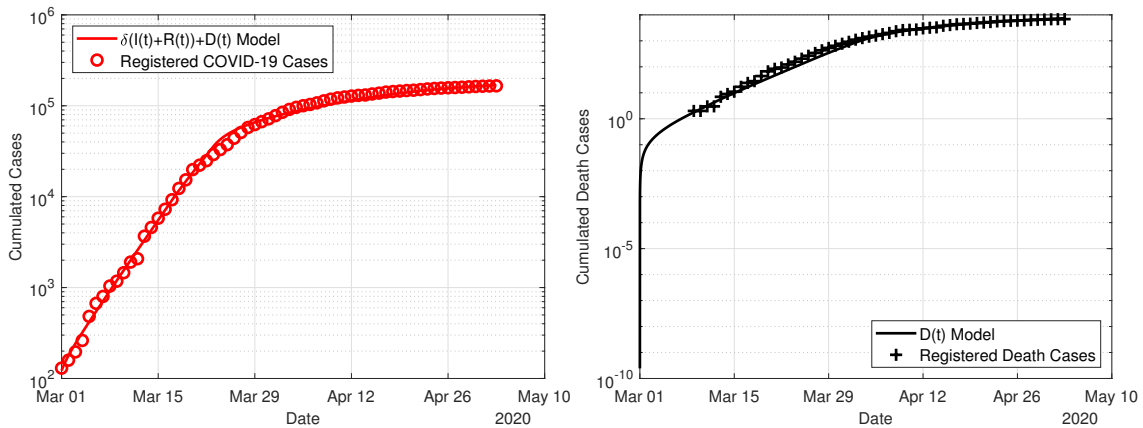


Figure 9.4: Plots for $\tau := \text{free}$, $E_0 = \text{free}$, $I_0 = \text{free}$, $\mathcal{R}_0 = 3$ and $\omega = 10^{-8}$.

The necessary number of iterations until the convergence of the algorithm shows that the algorithm moves quickly to the corresponding minima, see Figure 9.5. The process clarifies that the algorithm is very close to the optimal objective function value already after 15 iterations and needs the remaining calculation steps to reach the given tolerance limit $\text{TOL} = 10^{-12}$. However, the prerequisite for rapid convergence is a good starting value for u .

In addition to the presented simulations with restrictions, the algorithm was performed without limitations for the searched parameters, see Table 9.7 and Figure 9.6.

Table 9.7: Numerical results of Simulation 3 without restrictions concerning the estimated parameters.

β_0	β_1	β_2	β_3	δ	μ	τ	$E_0 + I_0 + R_0$	$J(u) - \ u\ _2^2$
0.77	0.46	0.27	0.41	0.002	0.0001	7	65046	$7 \cdot 10^{-4}$

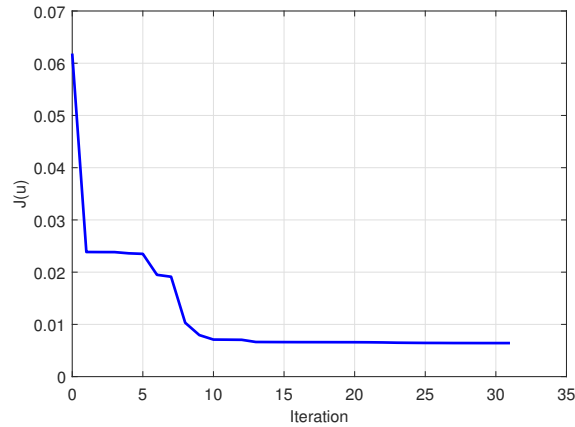


Figure 9.5: Development of the objective function J depending on the corresponding iteration step.

The results show that the normalized least squares term $J(u) - \|u\|_2^2$ can be reduced significantly compared to the restricted variants. It is noticeable, however, that the fitted value for the detection rate δ is very small at about 0.02%. This would mean that only every 500th infected person would be registered. This seems unrealistic, even if the dark figure is unknown. The values for transmission rate, lethality and actual number of exposed, infected and recovered at the beginning of the measurement period are changed accordingly. Due to the very low detection rate in this simulation, the spread of the disease would have been much more intense than expected.

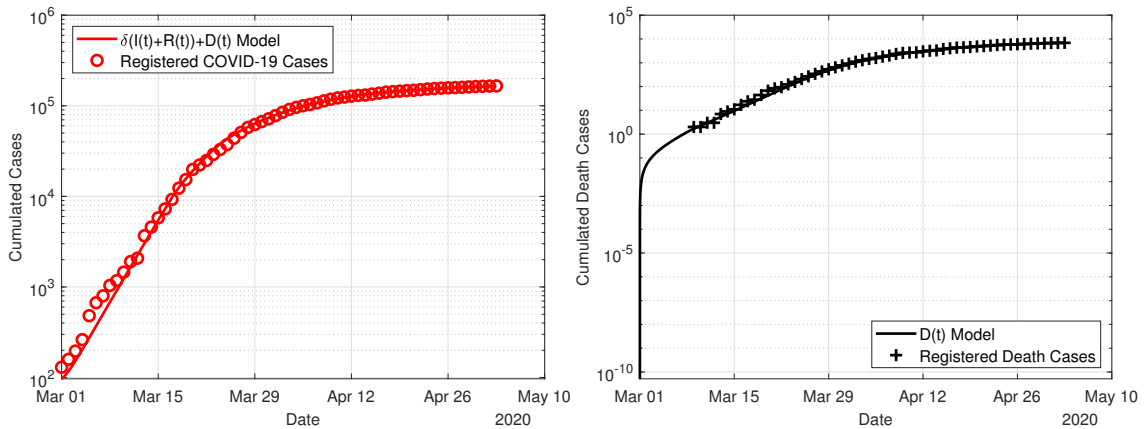


Figure 9.6: Graphical results of Simulation 3 without restrictions concerning the estimated parameters.

9.5.2 Specific results for the Metropolis algorithm approach

We now consider the value for

$$J(u) - \omega \|u\|_2^2 = \frac{\|\delta(I + R) + D - Y\|_{L^2}^2}{\|Y\|_{L^2}^2} + \frac{\|D - Z\|_{L^2}^2}{\|Z\|_{L^2}^2},$$

i.e. the cost functional $J(u)$ without the last term including the weight ω . This way we can compare the simulations with different weights ω in terms of $J(u)$ because the last term trivially raises along with ω .

Table 9.8: $(J(u) - \omega \|u\|_2^2) \cdot 10^3$ for the different weights ω .

Simulation	$\omega = 0$	$\omega = 10^{-9}$	$\omega = 10^{-8}$	$\omega = 10^{-7}$
1	18.6	18.1	18.6	21.7
2	8.7	8.2	9.2	9.6
3	3.8	3.3	3.4	4.1

Table 9.8 shows that the weight $\omega = 10^{-9}$ always yields the best, i.e. smallest values for the given cost functional $J(u)$. Moreover, what you can also see in Tables 9.10, 9.12 and 9.14 in Appendix 9.B, the value $J(u)$ for the weight $\omega = 10^{-9}$ is larger than the value $J(u)$ with the weight $\omega = 0$, even when the term $10^{-9} \cdot \|u\|_2^2$ is *not* subtracted, which means that interestingly, the simulation with $\omega = 10^{-9}$ provides a better result for a different cost functional.

The plots for the infected and dead cases in Simulation 3 with $\omega = 1e-9$, thus the best simulation, are shown in Figure 9.7.

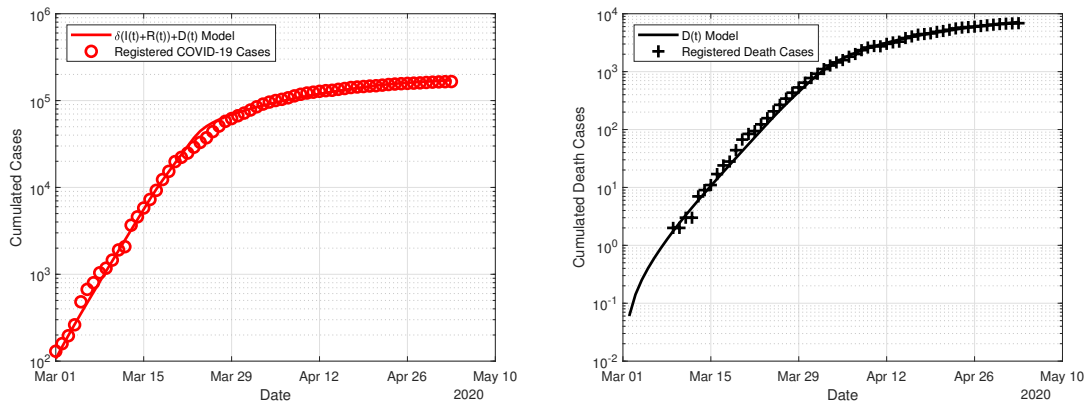


Figure 9.7: Plots for $\tau = \text{free}$, $E_0 = \text{free}$, $I_0 = \text{free}$, $\mathcal{R}_0 := 3$ and $\omega = 10^{-9}$.

The chain statistics done with the optimal results in Simulation 3 for $\omega = 10^{-9}$ as of Figure 9.8 show that for most parameters a normal distribution is visible and thus the Metropolis algorithm appears to have converged. The parameter τ does not appear to be normally distributed, but still remains in the range from 7–8 days. This also affects some smaller side peaks regarding the other parameters. As the infection data has the step size of 1 day, we assume that no further optimization within that range is possible, so an estimation of $\tau \approx 7-8$ days is decent enough.

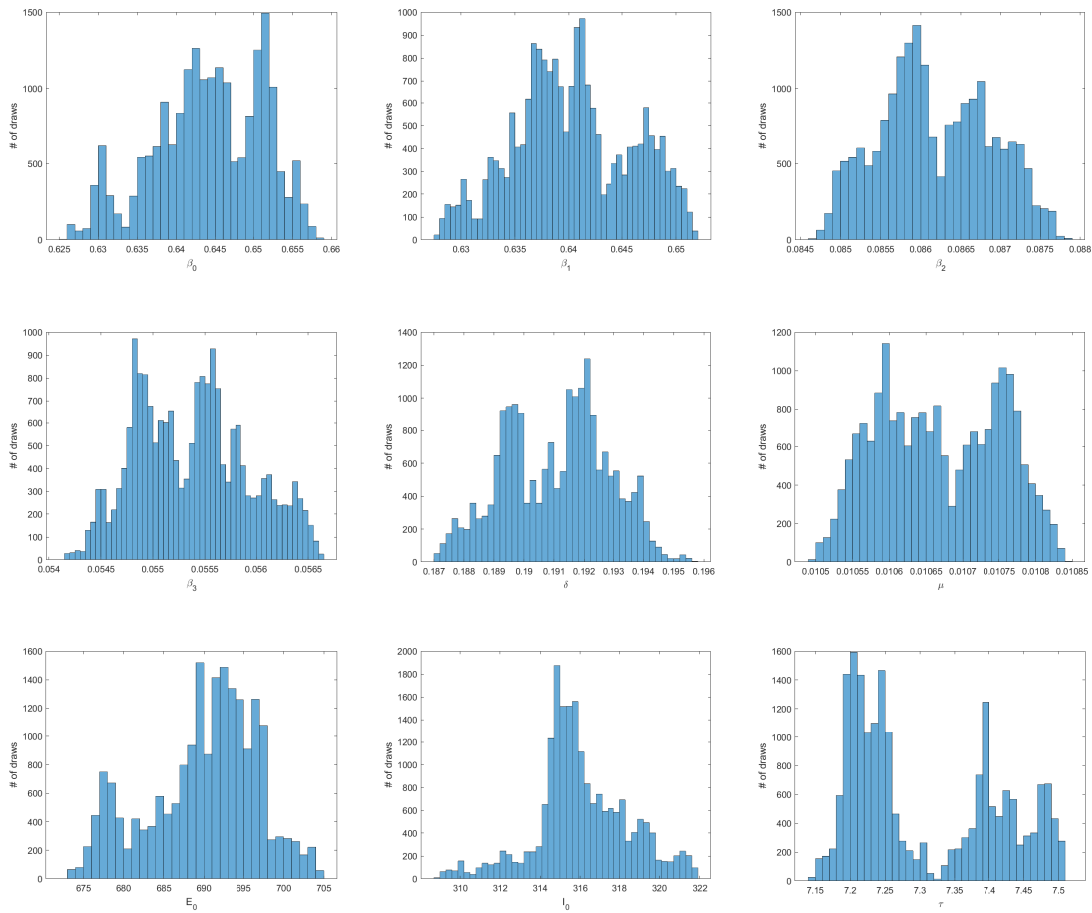


Figure 9.8: Parameter statistics for Simulation 2 and $\omega = 10^{-9}$, using the best approximation with respect to $J(u) - \omega \|u\|_2^2$ as starting value and a step size of $u_0/1000$. Except of τ , most histograms appear roughly normally distributed around their mean values.

A detailed numerical analysis as well as figures for all relevant plots can be found in Appendix 9.B. In the figures it is also visible that with fixed values $\tau = 0$ or $\tau = 11.5$ the estimated death cases run after resp. run ahead of the data.

9.6 Conclusion

In the present work, two *SEIRD*-models for modelling the COVID-19 outbreak in Germany were adapted to existing data from 1st of March to 3rd of May. Two different approaches for the estimation of parameters and approximation of the infection data were used and their results and performance were compared. Regarding the graphical and numerical results, all routines have provided similar meaningful results. Each approach has advantages and disadvantages and should be selected depending on the application needs, time, possible analytical and programming effort. The Corona outbreak results show that the restrictions taken by the authorities have had a major impact on the dynamics of spread. The Basic Reproduction Number could be reduced from a presumably much higher value than the assumed $\mathcal{R}_0 \simeq 3$ to the epidemiologically important limit $\mathcal{R}_0 \simeq 1$. Adding a time lag τ between the onset of infectiousness and death significantly increases

the accuracy of the tested model. This time delay is estimated by the data adjustment to an average of 8 days, although in reality there may be very different values depending on how long life-support measures are maintained in intensive care units. The adjustment regarding the detection rate and lethality showed that, according to the model, the actual number of infected people is approximately 3–5 times higher than registered and at $\mu \approx 1\text{--}2\%$, the lethality is lower than assumed.

Conceivable extensions of the present work would be the application to other countries, the integration of travel or commuting after the relaxation of exit restrictions or the integration of control variables to mathematically derive the optimal time intervals for future lockdowns. With respect to the latter, in order to detect a new increase in infections early on – before it returns to exponential growth – a measure within the model of the possible increase in transmission rate is required.

Appendix

9.A Appendix A: Plots for the adjoint approach

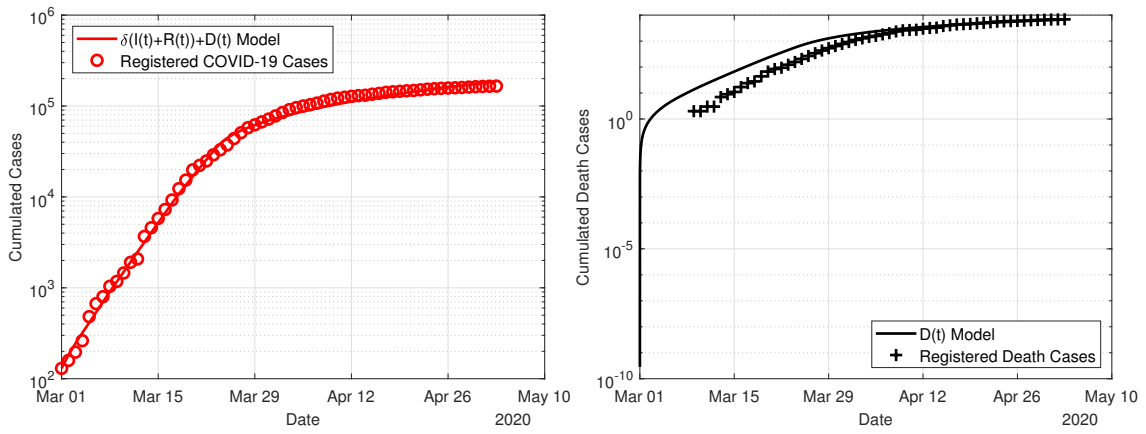


Figure 9.9: Plots for $\tau = 0$, $E_0 = \text{free}$, $I_0 = 114/\delta$, $\mathcal{R}_0 = 3$ and $\omega = 10^{-8}$.

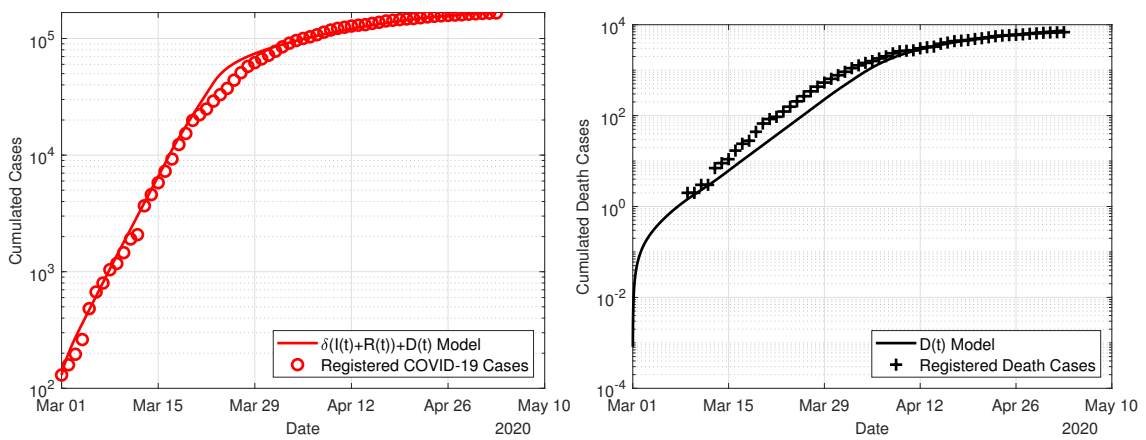


Figure 9.10: Plots for $\tau = 11.5$, $E_0 = \text{free}$, $I_0 = 114/\delta$, $\mathcal{R}_0 = 3$ and $\omega = 10^{-8}$.

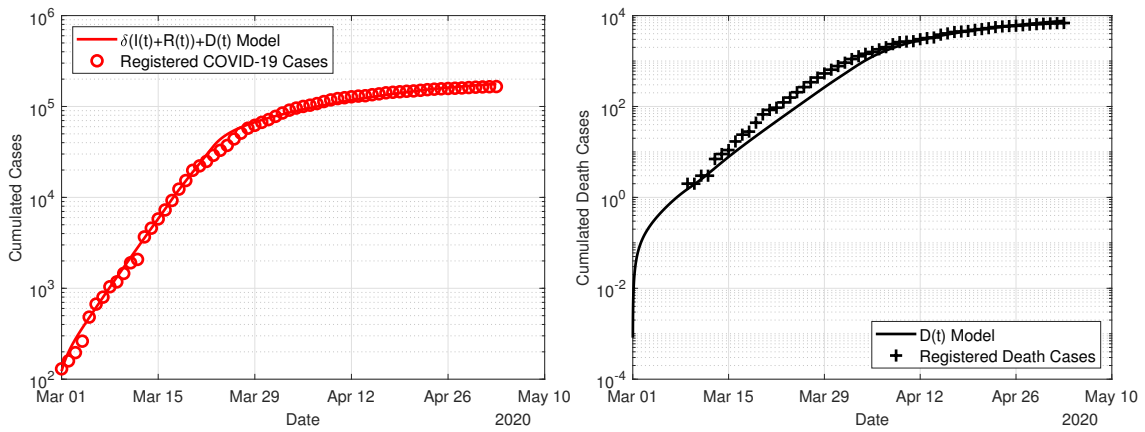


Figure 9.11: Plots for $\tau = \text{free}$, $E_0 = \text{free}$, $I_0 = \text{free}$, $\mathcal{R}_0 = 3$ and $\omega = 0$.

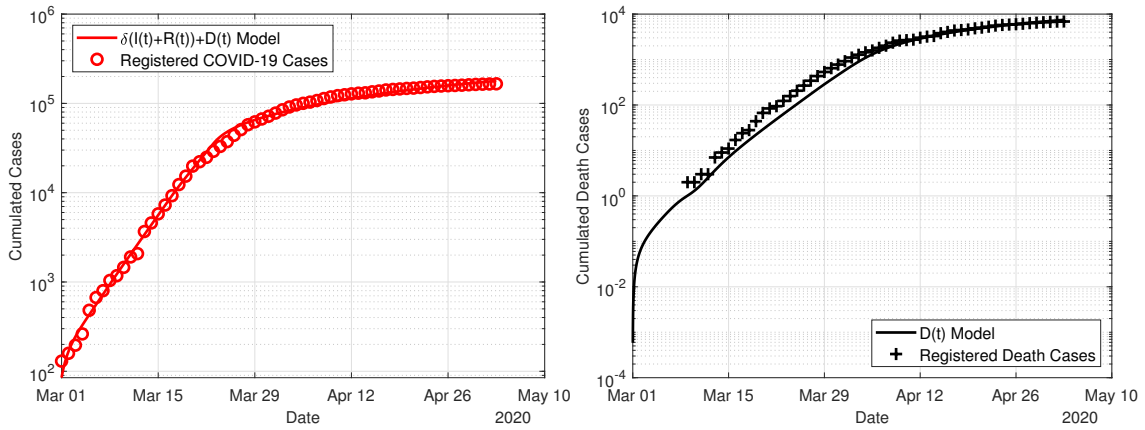


Figure 9.12: Plots for $\tau = \text{free}$, $E_0 = \text{free}$, $I_0 = \text{free}$, $\mathcal{R}_0 = 3$ and $\omega = 10^{-9}$.

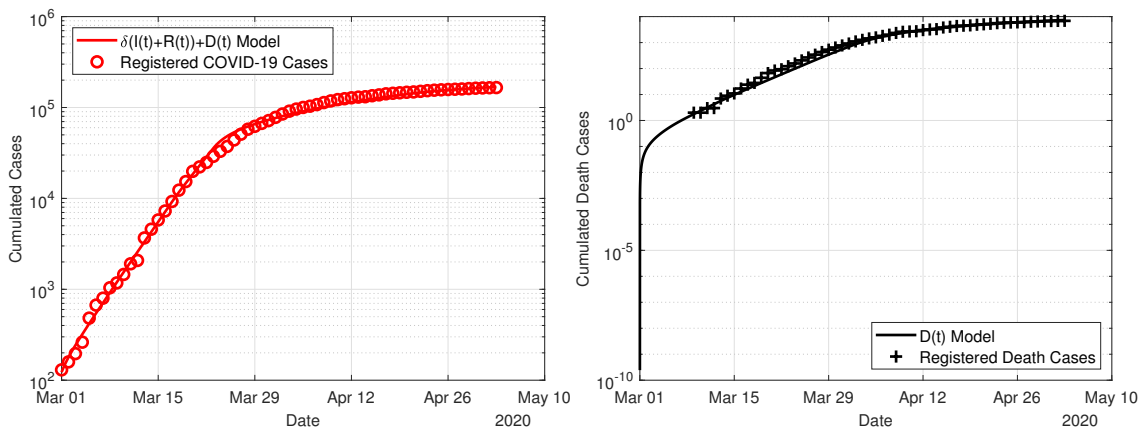


Figure 9.13: Plots for $\tau := \text{free}$, $E_0 = \text{free}$, $I_0 = \text{free}$, $\mathcal{R}_0 = 3$ and $\omega = 10^{-8}$.

9.B Appendix B: Results and plots for Metropolis algorithm

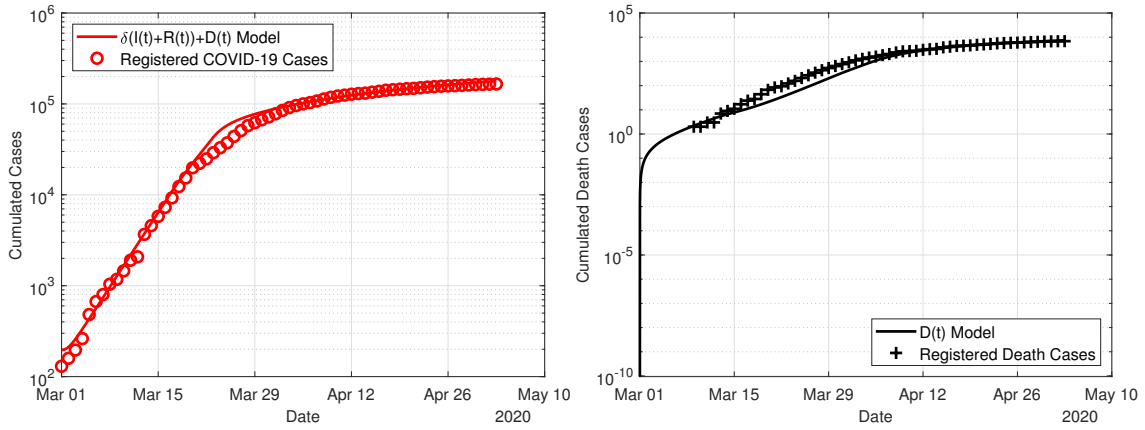


Figure 9.14: Plots for $\tau = \text{free}$, $E_0 = \text{free}$, $I_0 = \text{free}$, $\mathcal{R}_0 = 3$ and $\omega = 10^{-7}$.

9.B Appendix B: Results and plots for Metropolis algorithm

Simulation 1 – No delay and fixed initial infectives

Table 9.9: Estimates for $\tau = 0$, $E_0 = \text{free}$, $I_0 = 114/\delta$, $R_0 = 16/\delta$, $\mathcal{R}_0 = 3$ after $r = 20000$ draws and using a step size of $s = u_0/100$.

Parameter	$\omega = 0$		$\omega = 10^{-9}$		$\omega = 10^{-8}$		$\omega = 10^{-7}$	
	mean	std.	mean	std.	mean	std.	mean	std.
β_1	.5822	.0353	.5525	.0439	.5935	.0177	.6381	.0227
β_2	.5378	.0169	.4936	.0350	.4828	.0160	.4645	.0348
β_3	.1140	.0111	.1130	.0067	.10940	.0048	.1014	.0130
β_4	.0671	.0032	.0538	.0033	.0502	.0027	.0510	.0056
δ	.2307	.0089	.2933	.0116	.2137	.0104	.3142	.0309
μ	.0105	.0010	.0131	.0016	.0095	.0007	.0137	.0011
E_0	540.7	22.5	811.4	41.5	819.8	52.9	440.8	16.1

Table 9.10: $J(u) \cdot 1000$ for the different weights in Simulation 1. The column represents the weight that is used for $J(u)$ in the Metropolis algorithm and the row shows the value of $J(u)$ for all four ω .

w.r.t. ω	weight ω			
	0	10^{-9}	10^{-8}	10^{-7}
0	18.6	18.1	18.6	21.7
10^{-9}	19.2	18.9	19.5	22.1
10^{-8}	24.0	26.2	28.1	25.0
10^{-7}	72.3	99.1	114.2	54.3

9 Appendix

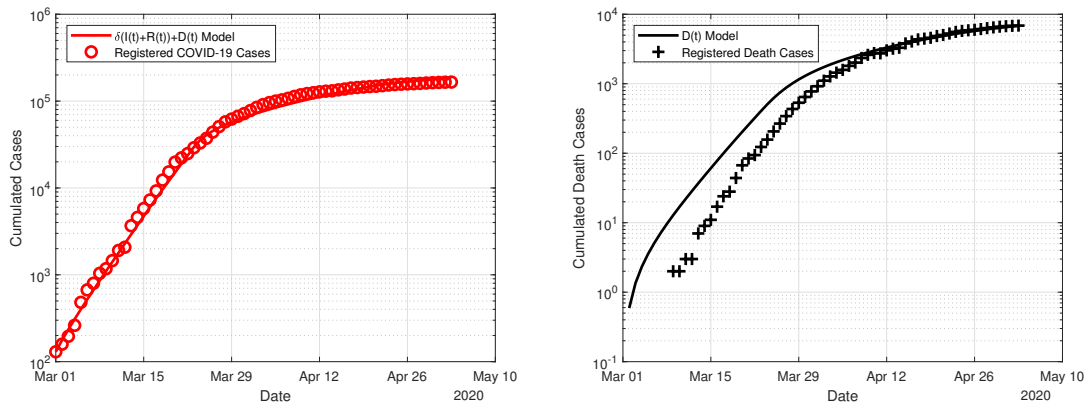


Figure 9.15: Plots for $\tau = 0$, $E_0 = \text{free}$, $I_0 = \frac{114}{\delta}$, $\mathcal{R}_0 = 3$ and $\omega = 0$.

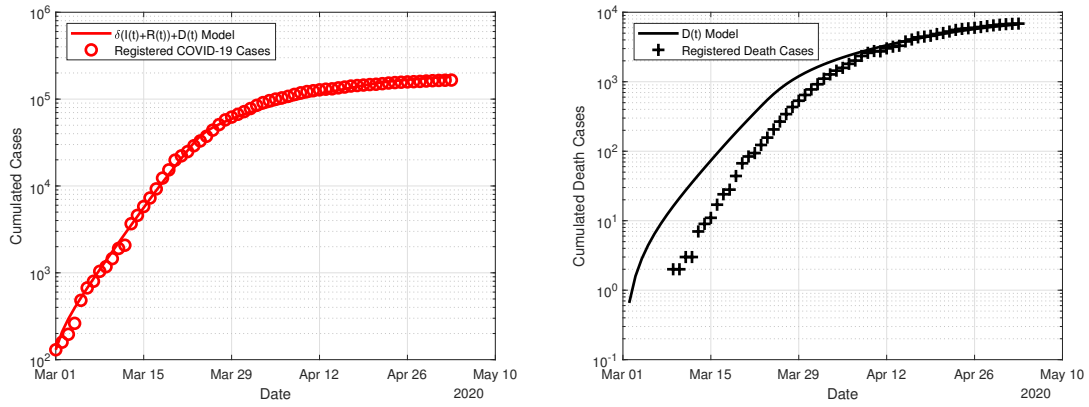


Figure 9.16: Plots for $\tau = 0$, $E_0 = \text{free}$, $I_0 = \frac{114}{\delta}$, $\mathcal{R}_0 = 3$ and $\omega = 0$.

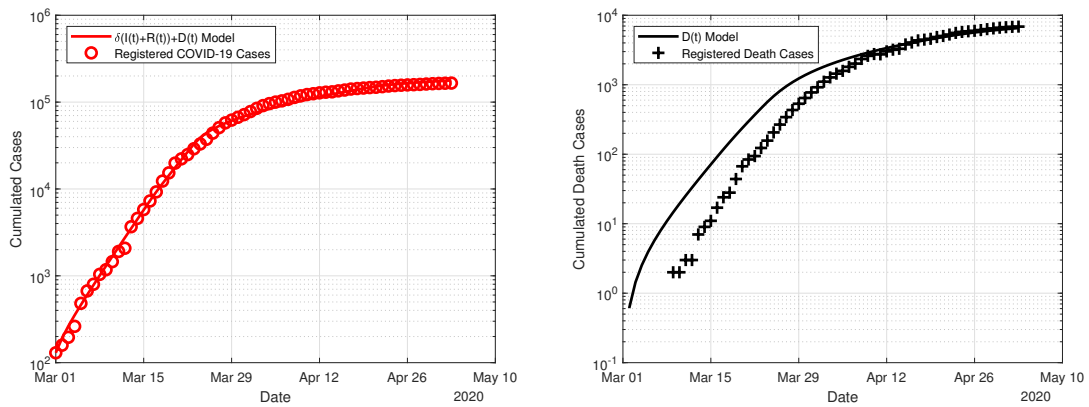


Figure 9.17: Plots for $\tau = 0$, $E_0 = \text{free}$, $I_0 = \frac{114}{\delta}$, $\mathcal{R}_0 = 3$ and $\omega = 0$.

9.B Appendix B: Results and plots for Metropolis algorithm

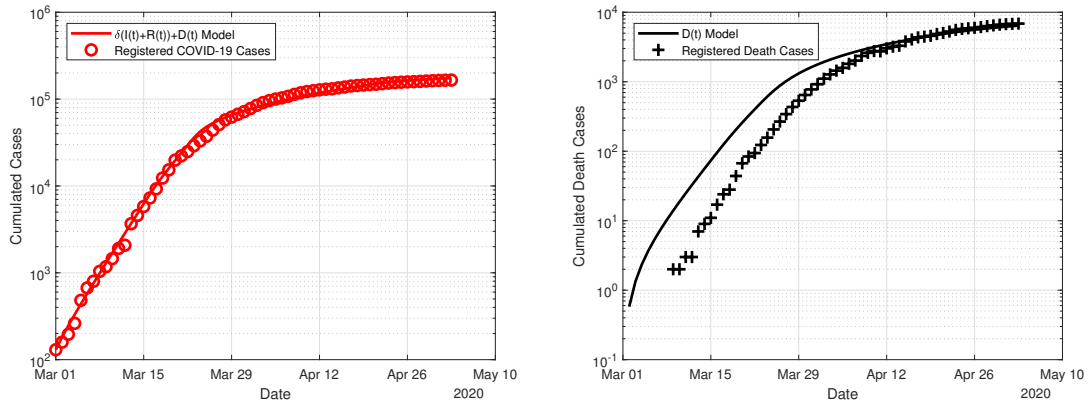


Figure 9.18: Plots for $\tau = 0$, $E_0 = \text{free}$, $I_0 = \frac{114}{\delta}$, $\mathcal{R}_0 = 3$ and $\omega = 0$.

Simulation 2 – Fixed delay and initial infectives

Table 9.11: Estimates for $\tau = 11.5$, $E_0 = \text{free}$, $I_0 = 114/\delta$, $R_0 = 16/\delta$, $\mathcal{R}_0 = 3$ after $r = 20000$ draws and using a step size of $s = u_0/100$.

Parameter	$\omega = 0$		$\omega = 10^{-9}$		$\omega = 10^{-8}$		$\omega = 10^{-7}$	
	mean	std.	mean	std.	mean	std.	mean	std.
β_1	.6735	.0538	.7045	.0600	.6391	.0411	.6678	.0508
β_2	.4414	.0250	.3951	.0336	.4823	.0323	.5011	.0323
β_3	.0810	.0073	.0846	.0075	.0820	.0059	.0790	.0090
β_4	.0672	.0042	.0552	.0073	.0520	.0027	.0605	.0091
δ	.2055	.0228	.2050	.0161	.2761	.0217	.2871	.0214
μ	.0132	.0009	.0131	.0013	.0178	.0011	.0179	.0013
E_0	737.0	62.8	661.2	31.3	620.6	70.5	409.2	18.7

Table 9.12: $J(u) \cdot 1000$ for the different weights in Simulation 2. The column represents the weight that is used for $J(u)$ in the Metropolis algorithm and the row shows the value of $J(u)$ for all four ω .

w.r.t. ω	weight ω			
	0	10^{-9}	10^{-8}	10^{-7}
0	8.7	8.2	9.2	9.6
10^{-9}	9.6	9.0	9.7	9.9
10^{-8}	17.2	15.7	14.7	12.8
10^{-7}	93.8	82.9	64.8	42.1

9 Appendix

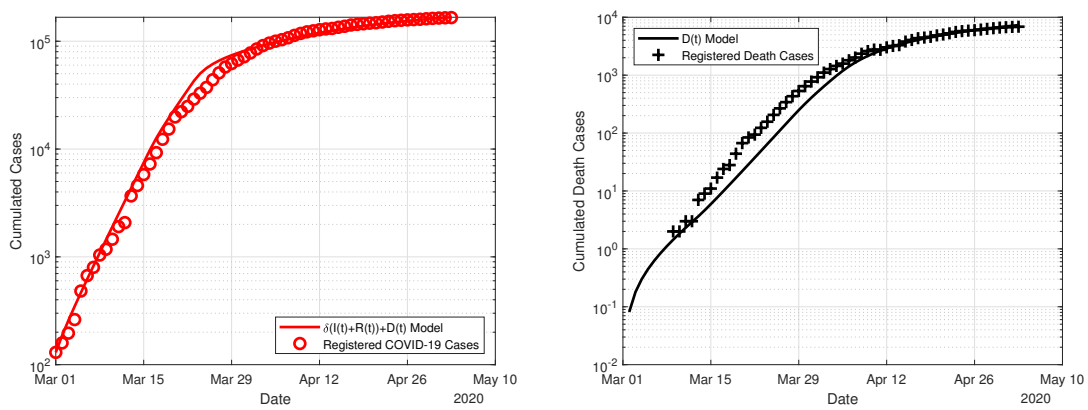


Figure 9.19: Plots for $\tau = 11.5$, $E_0 = \text{free}$, $I_0 = 114/\delta$, $\mathcal{R}_0 = 3$ and $\omega = 0$.

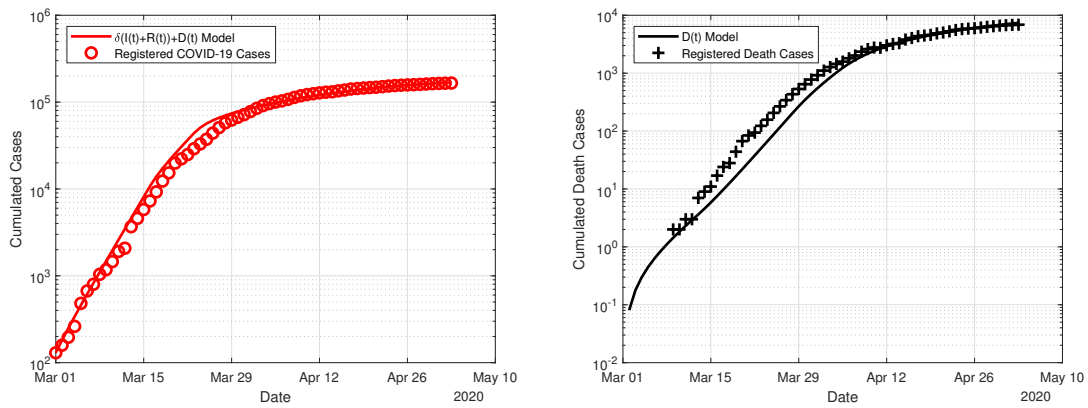


Figure 9.20: Plots for $\tau = 11.5$, $E_0 = \text{free}$, $I_0 = 114/\delta$, $\mathcal{R}_0 = 3$ and $\omega = 10^{-9}$.

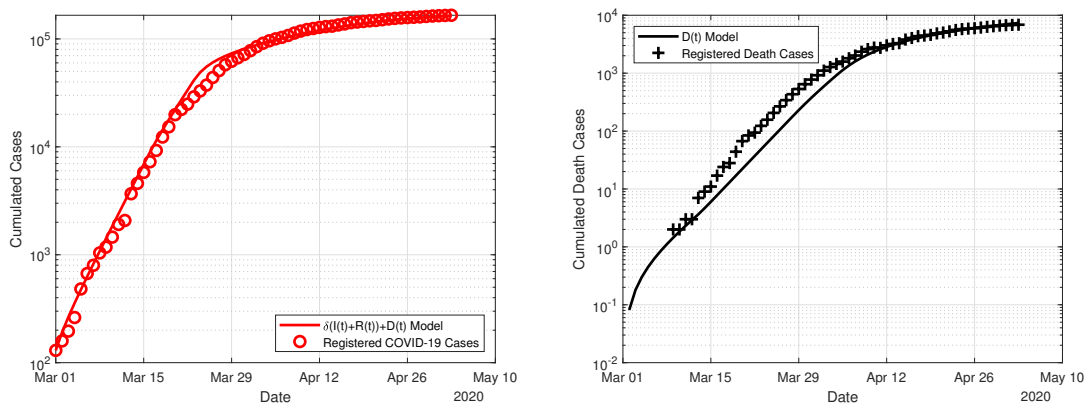


Figure 9.21: Plots for $\tau = 11.5$, $E_0 = \text{free}$, $I_0 = 114/\delta$, $\mathcal{R}_0 := 3$ and $\omega := 10^{-8}$.

9.B Appendix B: Results and plots for Metropolis algorithm

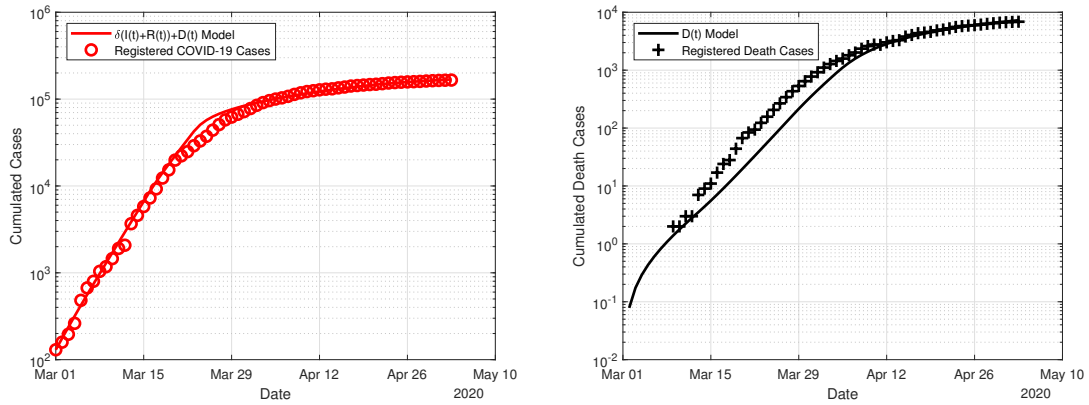


Figure 9.22: Plots for $\tau = 11.5$, $E_0 = \text{free}$, $I_0 = 114/\delta$, $\mathcal{R}_0 = 3$ and $\omega = 10^{-7}$

Simulation 3 – Free delay and initial infectives

Table 9.13: Estimates for $\tau = \text{free}$, $E_0 = \text{free}$, $I_0 = \text{free}$, $R_0 = 16/\delta$, $\mathcal{R}_0 = 3$ after $r = 20000$ draws and using a step size of $s = u_0/100$.

Algorithm	$\omega = 0$		$\omega = 10^{-9}$		$\omega = 10^{-8}$		$\omega = 10^{-7}$	
	mean	std.	mean	std.	mean	std.	mean	std.
β_1	.5859	.0530	.6442	.0357	.6737	.0300	.7370	.0548
β_2	.4785	.0359	.6403	.0250	.5197	.0396	.4587	.0183
β_3	.0926	.0097	.0862	.0039	.0920	.0037	.0949	.0034
β_4	.0556	.0025	.0554	.0038	.0502	.0019	.0576	.0025
δ	.2768	.0295	.1911	.0115	.2063	.0135	.2237	.0155
μ	.0154	.0008	.0107	.0006	.0117	.0006	.0128	.0005
E_0	790.0	46.7	690.0	52.5	500.8	206.4	351.2	14.9
I_0	493.1	40.1	316.1	30.2	439.0	140.7	350.7	115.7
τ	7.3	.6	7.3	.4	7.4	.3	7.2	.6

Table 9.14: $J(u) \cdot 1000$ for the different weights in Simulation 3. The column represents the weight that is used for $J(u)$ in the Metropolis algorithm and the row shows the value of $J(u)$ for all four ω .

w.r.t. ω	weight ω			
	0	10^{-9}	10^{-8}	10^{-7}
0	3.8	3.3	3.4	4.1
10^{-9}	4.7	3.8	3.8	4.3
10^{-8}	12.5	9.0	7.8	6.5
10^{-7}	90.5	60.9	47.7	28.7

9 Appendix

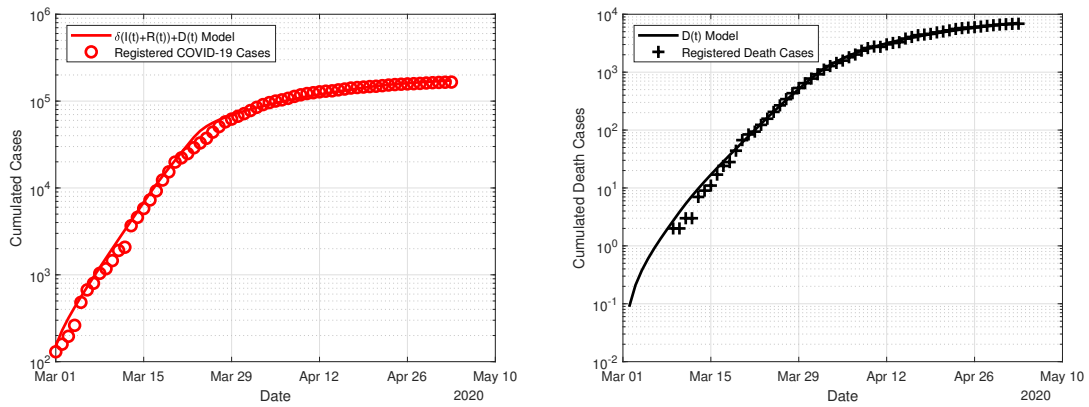


Figure 9.23: Plots for $\tau := \text{free}$, $E_0 = \text{free}$, $I_0 = \text{free}$, $\mathcal{R}_0 = 3$ and $\omega := 0$

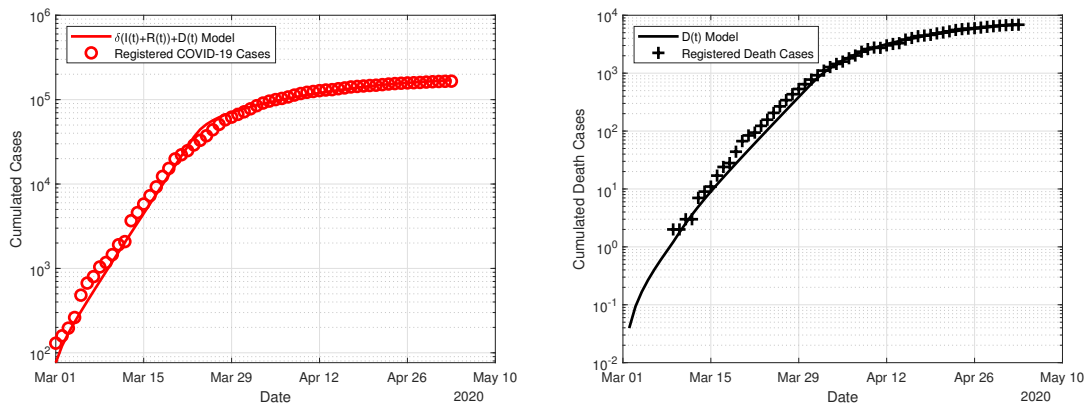


Figure 9.24: Plots for $\tau = \text{free}$, $E_0 = \text{free}$, $I_0 = \text{free}$, $\mathcal{R}_0 = 3$ and $\omega := 10^{-9}$.

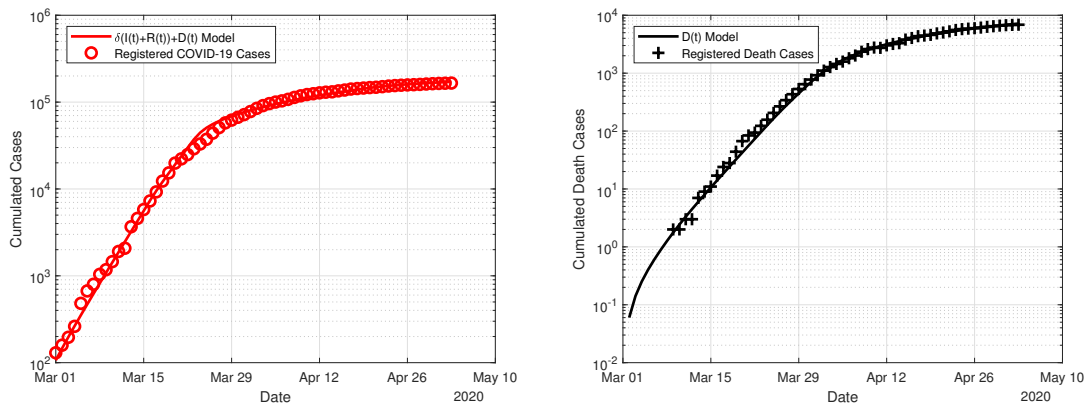


Figure 9.25: Plots for $\tau = \text{free}$, $E_0 = \text{free}$, $I_0 = \text{free}$, $\mathcal{R}_0 = 3$ and $\omega := 10^{-8}$.

9.B Appendix B: Results and plots for Metropolis algorithm

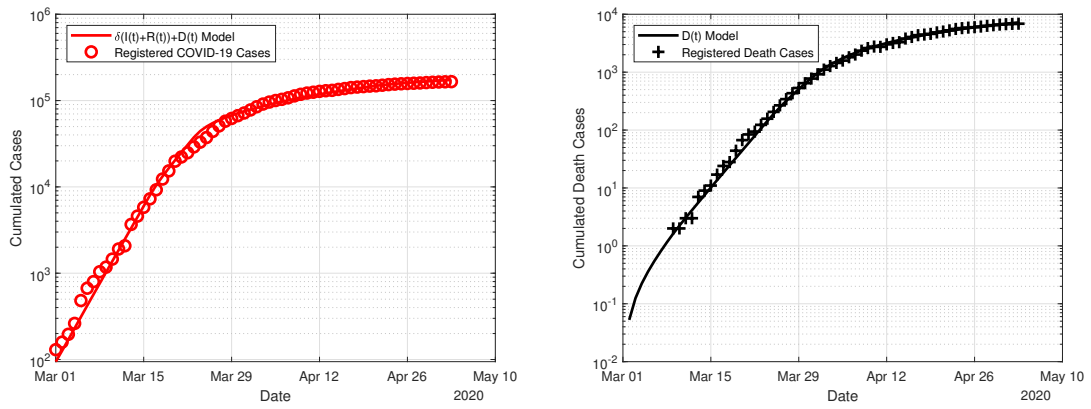


Figure 9.26: Plots for $\tau = \text{free}$, $E_0 = \text{free}$, $I_0 = \text{free}$, $\mathcal{R}_0 = 3$ and $\omega = 10^{-7}$.

Bibliography

- [1] Armijo, L.: *Minimization of functions having Lipschitz continuous first partial derivatives*. Pacific Journal of Mathematics, Vol. 16, No. 1, pp 1–3, 1966
- [2] Chambers, M.; Carrel, P.: *Germany eases lockdown, with 'emergency brake' on hand if needed*. Reuters, 6 May 2020. Accessed 18 June 2020
<https://www.reuters.com/article/us-health-coronavirus-merkel-idUSKBN22I24E>
- [3] Federal Government of Germany: *Contact Restrictions Extended*. Accessed 18 June 2020
<https://www.bundesregierung.de/breg-en/news/fahrplan-corona-pandemie-1744276>
- [4] Federal Government of Germany: *Guidelines for reducing social contacts*. Accessed 18 June 2020
www.bundesregierung.de/breg-de/themen/coronavirus/besprechung-der-bundeskanzlerin-mit-den-regierungschefinnen-und-regierungschefs-der-laender-1733248
- [5] Gelman, A.; Carlin, J.B.; Stern, H.S.; Rubin, D.B.: *Bayesian Data Analysis*. 2nd Edition, Chapman and Hall, London, 1996
- [6] Gilks, W.R.; Richardson, S.; Spiegelhalter, D.J.: *Markov chain Monte Carlo in Practice*. Chapman and Hall/CRC, 1996
- [7] Götz, T.; Heidrich, P.: *COVID-19 Disease Dynamics in Germany: First Models and Parameter Identification*. Accessed 18 June 2020
medRxiv <https://doi.org/10.1101/2020.04.23.20076992>
- [8] Johns Hopkins University: *Time series of confirmed COVID-19 cases globally*. Accessed 18 June 2020
github.com/CSSEGISandData/COVID-19/blob/master/csse_COVID_19_data/csse_COVID_19_time_series/time_series_COVID19_confirmed_global.csv
- [9] Kermack, W.O.; McKendrick, A.G.: *Contributions to the mathematical theory of epidemics-I*. Bulletin of Mathematical Biology, Vol. 53, pp 33–55, 1991
<https://doi.org/10.1007/BF02464423>
- [10] Lenhart, S.; Workman, J.T.: *Optimal control applied to biological models*. CRC Press, 2007
- [11] Martcheva, M.: *An introduction to mathematical epidemiology*. Springer US, 2015
- [12] Metropolis, N.; Rosenbluth, A.W.; Rosenbluth, M.W.; Teller, A.H.; Teller, E.: *Equation of State Calculations by Fast Computing Machines*. The Journal of Chemical Physics, Vol. 21, pp 1087–1092, 1953
<http://link.aip.org/link/doi/10.1063/1.1699114?ver=pdfcov>

Bibliography

- [13] Nocedal, J.; Wright, S.: *Numerical Optimization*. Springer New York, 2006
- [14] Read, J.M.; Bridgen, J.R.E.; Cummings, D.A.T.; Ho, A.; Jewell, C.P.: *Novel coronavirus 2019-nCoV: early estimation of epidemiological parameters and epidemic predictions*. Accessed 18 June 2020
medRxiv www.medrxiv.org/content/10.1101/2020.01.23.20018549v2
- [15] Robert-Koch-Institute: *Corona fact sheet*. Accessed 18 June 2020
https://www.rki.de/DE/Content/InfAZ/N/Neuartiges_Coronavirus/Steckbrief.html
- [16] Robert-Koch-Institute: *Daily situation reports*. Accessed 18 June 2020
www.rki.de/DE/Content/InfAZ/N/Neuartiges_Coronavirus/Situationsberichte/Gesamt.html
- [17] Robert-Koch-Institute: *Modellierung von Beispielszenarien der SARS-CoV-2-Epidemie 2020 in Deutschland*. Accessed 22 June 2020
https://www.rki.de/DE/Content/InfAZ/N/Neuartiges_Coronavirus/Modellierung_Deutschland.pdf?__blob=publicationFile
- [18] Rusatsi, D.N.: *Bayesian analysis of SEIR epidemic models*. Dissertation, Lappeenranta University of Technology. Accessed 18 June 2020
<http://lutpub.lut.fi/>
- [19] Schäfer, M., Götz, T.: *Modelling Dengue Fever Epidemics in Jakarta*. International Journal of Applied and Computational Mathematics, Vol. 6, No. 84, 2020
<https://doi.org/10.1007/s40819-020-00834-1>
- [20] Statistisches Bundesamt (Germany): *Bevölkerungsstand (31.12.2018)*. Accessed 18 June 2020
https://www.destatis.de/DE/Home/_inhalt.html
- [21] World Health Organization (WHO): *Novel Coronavirus (2019-nCoV) situation reports*. Accessed 18 June 2020
www.who.int/emergencies/diseases/novel-coronavirus-2019/situation-reports

Part III
Closing

10 Conclusions and Outlook

10.1 Summary

In the present thesis, the author's motivation for researching the epidemiological topic treated was revealed at the beginning. Subsequently, the fundamental theory for the investigation and solution of ordinary differential equations, the use of these for epidemiological mathematical modelling and fundamentals for static and dynamical optimization were presented. The combination of static and dynamical optimization to solve a L^2 norm based least squares problem for parameter fitting of models to real data sets was introduced and performed using adjoint functions.

In the case of dengue, a model reduction of an *SIRUV* to an *SIR* model with time-dependent transmission rate via time-scale separation was initially necessary in order to work practically with real data sets from Colombo and Jakarta. This enabled us to perform a useful and realistic parameter estimation with the adjoint approach. Furthermore, this could be used to study the direct impact of seasonal meteorological conditions on the disease. In addition, the data was used to test the extent to which the dengue model can be utilized to predict future peaks and their intensity and duration. The results show that both short and long-term forecasts are possible with a certain quality of the data sets. Especially in the case of Jakarta this could be shown impressively which was also examined via multipatch model with daily commuter movements. In this case, realistic and useful results could be obtained regarding the parameter fitting and also regarding the predictive power of this model, forecasts matching the real data sets could be made.

Regarding the spread of the neurogenic Coronavirus with the disease COVID-19 a *SEIRD* model with and without time delay was used. This model was applied to the initial spread in Germany. The results show that the model with time delay and the presented parameter estimation provided very realistic values, especially with respect to the detection rate and lethality rate which were hardly valid at that time. Subsequently, the time delay *SEIRD* model was applied to a more advanced data set in Germany and this time the adjoint approach was compared with a Metropolis algorithm regarding the parameter estimation. It became clear that the former requires a higher analytical effort but converges much faster with suitable initial values and is therefore less computationally demanding. This refers only to local minima since the Metropolis algorithm has proven to be more effective on a global level.

10.2 Outlook

Based on this research, a versatile application for parameter estimation using adjoint functions is now conceivable, both with regard to other epidemiological contexts and in other areas of mathematical modelling including ordinary or partial differential equations. In principle, of course this requires numerous, usable data sets in order to further test and apply the method. As already demonstrated here in relation to Metropolis algorithm, this kind of parameter fitting should be compared with other common methods by means of practical examples.

10 Conclusions and Outlook

Regarding vector-borne diseases, it is worth using the reduced *SIR* system applied in the present thesis to simulate other diseases of this type and make possible predictions. Especially in the case of dengue, a refinement of the approach to a multistrain model should be considered. Also a differentiated modelling with regard to external influences like the entire meteorology is desirable.

Regarding the COVID-19 models, we are currently still in a learning process as the disease itself still needs further research. Accordingly, the models can be adapted and refined in future, of course as practical as possible. So far, our research has been limited mainly to Germany. Here it is desirable to use the presented models also for data sets of different countries and regions. Similar to the dengue model, the mobility component should also be included in this study and its significance for the dynamics of disease should be better investigated with the models.

In principle, the mathematical models should be examined with regard to their predictive power and, in the case of a positive evaluation, with the help of optimal control theory, the use of possible control variables should be optimized for disease containment.

Bibliography

- [1] Ableitinger, C.: *Biomathematische Modelle im Unterricht – Fachwissenschaftliche und didaktische Grundlagen mit Unterrichtsmaterialien*. Springer Fachmedien Wiesbaden, 2010
- [2] Amann, H.: *Gewöhnliche Differentialgleichungen*. Walter de Gruyther GmbH Berlin/New York, 1995
- [3] Armijo, L.: *Minimization of functions having Lipschitz continuous first partial derivatives*. Pacific Journal of Mathematics, Vol. 16, No. 1, pp 1–3, 1966
- [4] Broyden, C.G.: *The Convergence of a Class of Double–rank Minimization Algorithms 1. General Considerations*. IMA Journal of Applied Mathematics, Vol. 6, No. 1, pp 76–90, 1970
<https://doi.org/10.1093/imamat/6.1.76>
- [5] Elstrodt, J.: *Maß– und Integrationstheorie*. Springer Berlin Heidelberg, 1996
- [6] Fischer, Gerd: *Lineare Algebra: Eine Einführung für Studienanfänger*. Springer DE, 2014
- [7] Fletcher, R.; Reeves, C.: *Function minimization by conjugate gradients*. The Computer Journal, Vol. 7, No. 2, pp 149–154, 1964
- [8] Forster, Otto: *Analysis 1: Differential– und Integralrechnung einer Veränderlichen*. Springer DE, 2016
- [9] Forster, Otto: *Analysis 2: Differentialrechnung im \mathbb{R}^n , gewöhnliche Differentialgleichungen*. Vieweg+Teubner, 2008
- [10] Forster, Otto: *Analysis 3: Maß– und Integrationstheorie, Integralsätze im \mathbb{R}^n und Anwendungen*. Vieweg+Teubner, 2012
- [11] Gâteaux, R.: *Fonctions d’une infinité de variables indépendantes*. Bulletin de la Société Mathématique de France, Vol. 47, pp 70–96, 1919
- [12] Gelfand, I.M.; Fomin, S.V.: *Calculus of Variations*. Dover Publications Mineola New York, 2012
- [13] Georgii, H.–O.: *Stochastik: Einführung in die Wahrscheinlichkeitstheorie und Statistik*. Walter de Gruyther GmbH Berlin/Boston, 2015
- [14] Goldfarb, D.: *A Family of Variable Metric Updates Derived by Variational Means*. Mathematics of Computation, Vol. 24, No. 109, pp 23–26, 1970
- [15] Hanke–Bourgeois, H.: *Grundlagen der Numerischen Mathematik und des Wissenschaftlichen Rechnens*. Vieweg+Teubner, 2009

Bibliography

- [16] Heuser, H.: *Gewöhnliche Differentialgleichungen: Einführung in Lehre und Gebrauch*. Vieweg+Teubner, 2009
- [17] Heuser, H.: *Lehrbuch der Analysis: Teil 2*. B.G. Teubner Verlag Wiesbaden, 2004
- [18] Jost, J.; Li–Jost, X.: *Calculus of Variations*. Cambridge University Press, 1998
- [19] Keeling, M.J.; Rohani, P.: *Modeling Infectious Diseases in Humans and Animals*. Princeton University Press, 2011
- [20] Lenhart, S.; Workman, J.T.: *Optimal control applied to biological models*. CRC Press, 2007
- [21] Liu, X.; Stechlin, P.: *Infectious Disease Modeling: A Hybrid System Approach*. Springer International, 2017
- [22] Martcheva, M.: *An introduction to mathematical epidemiology*. Springer US, 2015
- [23] Nocedal, J.; Wright, S.: *Numerical Optimization*. Springer New York, 2006
- [24] Polak, E.; Ribiere, G.: *Note sur la convergence de méthodes de directions conjuguées*. ESAIM: Mathematical Modelling and Numerical Analysis – Modélisation Mathématique et Analyse Numérique, Vol. 3, pp 35–43, 1969
- [25] Pontryagin, L.: *Mathematical Theory of Optimal Processes*. CRC Press, 2018
- [26] Querenburg, B.v.: *Mengentheoretische Topologie*. Springer Berlin Heidelberg New York, 2001
- [27] Robert–Koch–Institute (RKI): *COVID–19 und Impfen*. Accessed 10 Jan 2021
<https://www.rki.de/DE/Content/Infekt/Impfen/ImpfungenAZ/COVID-19/COVID-19.html>
- [28] Robert–Koch–Institute (RKI): *Infektionsschutz und Infektionsepidemiologie: Fachwörter – Definitionen – Interpretationen*. Berlin, 2015
https://www.rki.de/DE/Content/Service/Publikationen/Fachwoerterbuch_Infektionsschutz.pdf?__blob=publicationFile
- [29] Robert–Koch–Institute (RKI): *SARS–CoV–2 Steckbrief zur Coronavirus–Krankheit–2019 (COVID–19)*. Accessed 27 Oct 2020
https://www.rki.de/DE/Content/InfAZ/N/Neuartiges_Coronavirus/Steckbrief.html
- [30] Shanno, D.: *Conditioning of Quasi–Newton Methods for Function Minimization*. Mathematics of Computation, Vol. 24, No. 111, pp 647–656, 1970
- [31] Souza, M.: *Multiscale analysis for a vector–borne epidemic model*. Journal of Mathematical Biology, Vol. 68, pp 1269–1293, 2014
<https://doi.org/10.1007/s00285-013-0666-6>
- [32] Tikhonov, A.N.; Goncharsky, A.; Stepanov, V.V.; Yagola, A.G.: *Numerical Methods for the Solution of Ill–Posed Problems*. Springer Amsterdam, 2013
- [33] Walter, W.: *Gewöhnliche Differentialgleichungen: Eine Einführung*. Springer Berlin Heidelberg New York, 1976

- [34] Werner, D.: *Funktionalanalysis*. Springer Berlin Heidelberg, 2005
- [35] World Health Organisation (WHO): *Dengue and severe dengue*. Accessed 27 Oct 2020
<https://www.who.int/news-room/fact-sheets/detail/dengue-and-severe-dengue>
- [36] World Health Organisation (WHO): *Dengue control*. Accessed 10 Jan 2021
https://www.who.int/denguecontrol/control_strategies/en/
- [37] World Health Organisation (WHO): *Disease outbreaks*. Accessed 25 Oct 2020
<https://www.who.int/>

